UNIVERSITY OF SOUTHAMPTON

Proton and Metal Ion Interactions of Fulvic Acid solutions and of Alumina and Alumina/Fulvic Acid suspensions.

Thesis submitted in accordance with the requirements of the University of Southampton for the degree of Doctor of Philosophy.

by

Alexander Roberts Baker

Department of Oceanography

UNIVERSITY OF SOUTHAMPTON

ABSTRACT

FACULTY OF SCIENCE

OCEANOGRAPHY

Doctor of Philosophy

PROTON AND METAL ION INTERACTIONS OF FULVIC ACID SOLUTIONS AND OF ALUMINA AND ALUMINA/FULVIC ACID SUSPENSIONS

by Alexander Roberts Baker

Four generally applicable ion – substrate adsorption models were selected from the literature. These (the Gouy Chapman, constant capacitance, triple layer and polyelectrolyte gel models) were examined with the aim of identifying those best suited to modelling the interactions of natural organic matter and organic coated particles in aquatic, and particularly estuarine, systems.

In order to aid this investigation, data on the proton exchange behaviour of a natural fulvic acid sample (in solutions containing the major ions of seawater and in an artificial seawater solution), a model particulate (γ–alumina) and mixtures of these two (in NaCl solutions) were obtained by potentiometric titration.

Modelling of the fulvic acid data was most successful with the Gouy Chapman and constant capacitance models. The use of an iterative speciation modelling procedure provided stability constant values for surface complexation reactions of the carboxylic acid site of the fulvic acid. These values were obtained from high ionic strength data and, although they gave a good prediction of fulvic acid surface charge in artificial seawater, they are unlikely to be useful under estuarine conditions as lower ionic strength data was not well modelled. The effect of solution ionic strength on fulvic acid surface charge development could only be reproduced by taking the non–planar surface geometry of the fulvic acid into account using the spherical Gouy Chapman model. The triple layer and polyelectrolyte gel models were not able to describe the behaviour of the fulvic acid successfully.

Using the constant capacitance model intrinsic stability constant values were obtained for the interactions of alumina when negatively charged. Stability constants were also obtained for the interactions of the fulvic acid / alumina mixture, although the effect of fulvic acid adsorption and desorption reactions were not considered explicitly by the model. These reactions are pH dependent and contribute to the overall proton balance during titration. Polyelectrolyte gel analysis indicated that the organic coating of the mixture was impermeable to electrolyte ions.

ACKNOWLEDGEMENTS

I am deeply grateful to my supervisors, Dr. D. R. Turner and Dr M. S. Varney, for much patient assistance and valuable constructive criticism throughout my work at the Plymouth Marine Laboratory and the Oceanography Department of Southampton University.

I am also indebted to a large number of the members of staff at PML for their assistance. In particular, the technical help given by Susan Knox, John Wood and Malcolm Liddicoat is gratefully acknowledged. I would also like to thank the members of NCS Local Support, Plymouth and the librarians of both libraries at PML for their help, and David Turner and Sean Nicholson for allowing me access to the excellent facilities at PML.

The friendship and support of numerous people in Plymouth, Southampton, Swansea and elsewhere has been greatly valued. Those most worthy of special thanks (for general silliness and food) include Becky, Vince, Pete, Dave, Duncan, Malc and Doris. Thanks to Jane, Nigel, Jackie and Phil for their help and hospitality on my frequent returns to Plymouth.

I must also thank the NERC for providing me with a weekly income lower than the recommended minimum wage (Grant GT4/87/AAPS/47).

Very special thanks goes to my parents for their moral support and for providing financial support which others had far more obligation to give.

TABLE OF CONTENTS

LIST OF FIGURES

LIST OF TABLES

LIST OF SYMBOLS

a	activity	
A	surface area of solid	$m^2.kg^{-1}$
c	concentration of electrolyte	$mol.l^{-1}$
C	capacitance	$F.m^{-2}$
D_s	total site density	$mol.m^{-2}$
e	elementary electron charge	1.60×10^{-19} C
E	electrode potential	V
E^0	standard electrode potential	V
F	Faraday constant	9.648×10^4 $C.mol^{-1}$
H_{init}	residual acid concentration before titration began	$mol.l^{-1}$
I	ionic strength	$mol.l^{-1}$
j_H	acid region liquid junction potential	V
j_{OH}	base region liquid junction potential	V
k	Boltzmann constant	1.38×10^{23} $J.K^{-1}$
k_e	electrode slope	mV per decade
K^{app}	apparent dissociation contant	
K_H	intrinsic affinity constant	
K^{int}	intrinsic dissociation contant	
K_W	dissociation constant of water	$mol^2.l^{-2}$
m_s	mass of substrate titrated	g
N	Avogadro's number	6.023×10^{23} mol^{-1}
N_A	number of moles of protons added	mol
N_s	total number of surface sites	$C.m^{-2}$
q_0	reduced diffuse layer thickness	
R	molar gas constant	8.31 $J.mol^{-1}.K^{-1}$
T	temperature	K
V	volume of titrant added	l
V_p	volume of gel	$l.kg^{-1}$
V_x	partial molar volume of diffusible component (x) in a gel	
V_0	initial volume	l
y_0	reduced surface potential	
z	charge on ion	
α	degree of dissociation (fraction of dissociated sites)	
γ	activity coefficient	
Γ_H	proton adsorption density	$mol.m^{-2}$
δn_{OH}	formation function	$mmol.g^{-1}$
ε	relative permittivity of water at 25°C	
ε_0	permittivity of free space	8.85×10^{-12} $F.m^{-1}$

κ	inverse diffuse layer thickness	m^{-1}
θ	fraction of undissociated sites	
ν	number of ionizible groups on a gel	$mol.kg^{-1}$
π	osmotic pressure of water in a gel	
ρ	density	$g.cm^{-3}$
σ_0	surface charge	$C.m^{-2}$
ψ_0	surface potential	V
ψ_β	potential at layer of adsorbed counter ions	V

1. INTRODUCTION

1.1 Background

1.1.1 Introduction

Discharge of heavy metals into natural aquatic systems as a result of anthropogenic activities often leads to problems of pollution. Toxic elements, such as copper and lead, are borne into the aquatic environment by industrial effluent, sewage sludge, mining wastes and rain out of atmospheric pollution. Concern over the general effects of pollutants on water quality (as regards human use of waterways, health of aquatic ecosystems and the consumption of their produce) is reflected in, for instance, European Community minimum bathing water standards and periodic bans on sales of catches of fish (especially shellfish) from stressed environments.

Controls on metal inputs to the environment are an obvious necessity if water quality standards are to be maintained and a balance achieved between man's demands on the environment and its ability to cope with those demands. However, controls cannot be implemented without an understanding of the behaviour of the pollutant metals in the environment, or the ability to predict this behaviour using models (Turner, 1990).

1.1.1.1 Metal Speciation

Natural aquatic systems are extremely complex mixtures, containing simple inorganic and organic ligands, mineral particles and large organic macromolecules. Seawater, for example, contains most of the stable elements of the periodic table, although most are present at very low concentrations (Turner & Whitfield, 1983). In such mixtures, a given metal ion may potentially bind to any of the inorganic, organic or particulate ligands present. Its distribution among the available ligands (its chemical speciation) is governed by their concentrations and the relative strengths of its interactions with them, as well as the strength of their interactions with, and the concentrations of, other metals.

Metal speciation provides a key to many geochemical and biological processes occurring in aquatic systems (Buffle *et al.*, 1990), including:

Cycling and residence times – removal of metal ions may be brought about by precipitation or uptake onto suspended particles and subsequent sedimentation, while residence times may be increased by complexation with dissolved species (e.g. Zamuda & Sunda, 1982; Suffet & MacCarthy, 1989).

Biological availability and toxicity – free metal ions are generally more readily available to organisms, as they are relatively easily transported across cell walls or membranes, although transport rates are increased when metal complexes are lipid soluble (Florence, 1983).

However, the complexity and diversity of species present in aquatic environments can cause great difficulties in determining metal speciation. Organic coatings on mineral

particles in natural aquatic systems confer negative charges (and therefore, the potential for interaction with metal ions) on them (Neihof & Loeb, 1972; Hunter & Liss, 1979; Gibbs, 1983). It has also been shown that the negative charge of riverine particles decreases when they come into contact with high concentrations of Ca^{2+} and Mg^{2+} in seawater (Hunter & Liss, 1979). Also, reduction in biological availability does not necessarily require removal from solution, since complexation of metal ions by dissolved species can prevent their uptake by biota (Florence, 1983; Winner, 1985).

1.1.1.2 Study Techniques

Understanding of the environmental behaviour of metal ions can be gained in two ways (Turner, 1990):

i) studies of metal distributions and interactions in natural systems or slightly perturbed natural systems

ii) laboratory studies of simplified model systems related to the environment of interest.

Approach *i)* has the advantage of showing the actual response of the system under study and has been used to great effect in the estuarine mixing studies of Sholkovitz and co–workers (Sholkovitz, 1976; Sholkovitz & Copland, 1981). However, the results of such experiments are, necessarily, specific to the system under study and are of limited use when considering other environments. Also, a consequence of working on natural samples is that assessment of the roles of the individual components of the systems is extremely difficult (if not impossible), due to the complexity of the sample.

Laboratory experiments on model systems (*ii)* above) allow the interactions of specific components of natural systems to be investigated with as many, or as few, constraints on sample complexity and physical conditions as required. Extremely simple model systems have the advantage of being relatively easy to interpret, while increased complexity (i.e. increased number of components) is necessary in order to provide more realistic models. The systematic variation in chemical and physical parameters in laboratory studies on a model system can reveal the major influences on a system's environmental behaviour far more readily than studies on more varied and complex natural systems (Buffle *et al.*, 1990). Laboratory studies on specific components of natural systems often require that those components are isolated, fractionated or concentrated from environmental samples (Shuman *et al.*, 1990). Isolation, fractionation and concentration procedures may cause modification of the component of interest and it is desirable that, as well as studies on the isolates alone, they are re–combined in order to confirm that the properties of the original sample can be reproduced (Shuman *et al.*, 1990).

Experiments on model systems provide indications of the strengths of interaction between the components of interest (i.e. metal – ligand stability constants), which can be used as inputs to computer based chemical speciation models such as HALTAFALL (Ingri

et al., 1967) or MINEQL (Westall *et al.*, 1976). These models can then be used to predict the distribution of the metal of interest through any environment for which ligand concentrations have been determined.

The interactions of simple ligands with metal ions are relatively easily studied (and incorporated into speciation models), through the techniques of classical chemistry. The study of macromolecular organic matter and inorganic particles however, is complicated by their size and heterogeneity, which necessitate the use of electrostatic and other corrections.

1.1.2 Natural Organic Matter (Humic Substances)

Humic substances often account for a large proportion of the total dissolved organic carbon (DOC) (Reuter & Perdue, 1977) and are ubiquitous in the environment. They are the products of degradation of plant and animal tissue and are found in all environments where such degradation occurs (Suffet & MacCarthy, 1989).

They have been divided into three subsets on an operational basis according to their solubilities in aqueous solution (Hayes *et al.*, 1989).

Humic acid – the fraction of humic substances which is soluble in alkaline solution, but which is precipitated when the solution pH is lowered below 2.

Fulvic acid – humic substances soluble in aqueous solution at all pH values.

Humin – completely insoluble in aqueous solution.

As each fraction is an extremely complex mixture, these definitions correspond to broad classes of compounds with similar properties, rather than unique chemicals. Humic substances are also rather large (average molecular weights for aquatic fulvic and humic acids are 700 – 1000 daltons and 1000 – 3000 daltons respectively (Hayes *et al.*, 1989)), although they are generally smaller than proteins (>10,000 daltons – Buffle, 1988) or synthetic polymers (>5,000 daltons – Travers & Marinsky, 1974; Anspach & Marinsky, 1975).

As a consequence of their size and heterogeneity they have not been well characterised structurally. Commonly they contain both aliphatic and aromatic carbon groups together with oxygen, nitrogen and (small amounts of) sulphur containing functional groups.

Over the pH range of natural systems some of the oxygen containing functional groups (carboxylic acids and phenolic and alcoholic hydroxides) are dissociated, giving humic substances negative charges. They are reported to interact strongly with di– and tri–valent metals (Benes *et al.*, 1976) and to decrease metal bioavailability by complexation (Winner, 1985; Suffet & MacCarthy, 1989).

1.1.3 Natural Inorganic Particles

The inorganic particles in natural systems can be divided into two classes, clays and amphoteric oxyhydroxides.

Clays interact with cations in solution by ion exchange with cations held between their aluminosilicate layers at constant particle charge (Davis & Hayes, 1986). The oxyhydroxides of iron, aluminium, manganese and silicon are effective sorbents in natural systems (Dzombak & Morel, 1990) (a role which is enhanced by their ability to coat other particles). Their interactions with cations are driven by pH dependent surface reactions, which determine the charge on the particles (and thus their affinity for cations).

1.1.4 Previous Work

1.1.4.1 Interactions of Humic Substances

The proton and metal ion interactions of humic substances have been extensively studied in a variety of electrolyte media and using a number of analytical techniques. Several workers (e.g. Wilson & Kinney, 1977; Turner *et al.*, 1986) have chosen to conduct metal binding experiments at constant hydrogen ion concentrations (either by use of pH buffers or readjustment of pH following metal ion addition), thus enabling relatively simple models to be used for the determination of metal binding stability constants.

The need to provide stability constant data with a wider application has led other workers to study the acid – base chemistry of humic substances at different ionic strengths (Marinsky *et al.*, 1980; Marinsky *et al.*, 1982a; Dempsey & O'Melia, 1983; Ephraim *et al.*, 1986; Tipping *et al.*, 1988; Ephraim *et al.*, 1989; Cabaniss, 1991), as the essential precursor to studying metal – humic interactions over wider ranges of experimental conditions (Marinsky *et al.*, 1982b; Ephraim & Marinsky, 1986) and in systems where competition effects may occur (Tipping *et al.*, 1988).

Metal ion interactions with humic substances have been reported to occur through chelation reactions with functional groups in arrangements resembling those of salicylic and phthalic acids, e.g. Eqn. 1.1.1, (Stevenson, 1976; Marinsky *et al.*, 1982; De Wit *et al.*, 1989).

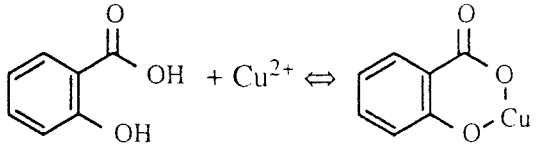

(1.1.1)

1.1.4.2 Interactions of Particulate Matter

A large volume of data has also been acquired on metal interactions with suspended particulates. Metal binding on oxyhydroxides has been found to be highly dependent on both pH and ionic strength, and a number of binding reactions (e.g. mono– and bi–dentate complexes) have been proposed (Eqns. 1.1.2 – 1.1.4; Westall, 1987; De Wit *et al.*, 1989).

$$SOH + M^{2+} \Leftrightarrow SOM^{+} + H^{+} \qquad (1.1.2)$$

$$\begin{matrix} SOH \\ | \\ SOH \end{matrix} + M^{2+} \Leftrightarrow \begin{matrix} SO \diagdown \\ | \quad M \\ SO \diagup \end{matrix} + 2H^{+} \qquad (1.1.3)$$

$$SOH + M^{2+} + OH^{-} \Leftrightarrow SOMOH + H^{+} \qquad (1.1.4)$$

The surface chemistries of alumina and hydrous ferric oxides have been comprehensively reviewed by Davis & Hem (1989) and Dzombak & Morel (1990) respectively.

1.1.4.3 Adsorption of Organics on Particulate Matter

The adsorption of natural organic matter onto aqueous oxide surfaces is extremely common in the environment (Tomaic & Zutic, 1988), and is responsible for altering the character of the particle – solution interface (e.g. conferring negative charge on it (Hunter & Liss, 1979)) and thus altering the environmental behaviour of the particle (Raspor, 1989).

Uptake of simple and natural, macromolecular organics on a variety of surfaces (iron oxides and oxyhydroxides (Parfitt *et al.*, 1977; Tipping, 1981; Ho & Miller, 1985), aluminium oxides (Parfitt *et al.*, 1977; Kummert & Stumm, 1980; Davis, 1980; Davis & Gloor, 1981; Zutic & Tomaic, 1988) and manganese oxides (Tipping, 1990)) has shown adsorption to be pH dependent, generally decreasing with increasing pH.

Adsorption reactions have been ascribed to ligand exchange with surface hydroxyl and protonated hydroxyl groups (SOH and SOH_2^{+}), both for simple organic acids (Kummert & Stumm, 1980) and for humic substances (Parfitt *et al.*, 1977; Tipping, 1981), e.g. Eqn. 1.1.5.

$$SOH + FA^{-} \Leftrightarrow S\text{–}FA + OH^{-} \qquad (1.1.5)$$

The decrease in adsorption with increasing pH therefore reflects the decreasing numbers of SOH^{+} and SOH groups on the particle surface, as well as the increasing repulsion of the negatively charged surface for the like–charged humics (Raspor, 1989).

Repulsive forces between organics at high adsorption loadings (Raspor, 1989) may be reduced by protonation of humic functional groups not directly involved in adsorption (Tipping, 1981) or coadsorption (charge neutralisation or ternery complex formation) of divalent cations such as Ca^{2+} and Mg^{2+} (Davis, 1982; Tipping, 1990).

Diprotic organic acids possessing functional groups in *ortho* arrangements have been found to adsorb to a greater extent than do monoprotic acids (Kummert & Stumm, 1980). The inability of a portion of a lake sediment organic extract to adsorb to alumina (Davis, 1980) has been related to its relatively low weak acidity content, which was taken to imply a low proportion of functional groups in *ortho* arrangements (Davis, 1982).

Adsorption of natural organics has been shown to be rapid (Davis, 1980) and greatest for the higher molecular weight fractions of the organics studied (Davis & Gloor, 1981; Zutic & Tomaic, 1988).

Adsorption at the charged siloxane surfaces of clays is also pH dependent (Slavek & Pickering, 1981) and, at constant pH, increases with increasing charge on the cations associated with the clay (Tipping, 1990).

1.1.4.4 Interactions of Organic – Particulate Mixtures

Studies on model mixed organic – particle systems have shown that complexation of copper by bipyridyl enhances its adsorption on SiO_2 (Bourg *et al.*, 1979), that copper uptake on α–Al_2O_3 is also enhanced by the presence of glutamic and benzoic acids (the former by complexation with the adsorbed organic, the latter by formation of surface – Cu – organic bridging bonds) (Ballion & Jaffrezic–Renault, 1985), but that EDTA does not enhance Cu uptake from seawater onto γ–Al_2O_3, as neither EDTA nor Cu–EDTA are adsorbed (Plavsic *et al.*, 1980).

The uptake of metals by particulates (U – hematite (Ho & Miller, 1985), Cu, Cd – alumina (Davis, 1984; Xu *et al.*, 1989), Pb, Cu, Zn, Cd, Cr, Hg – clay (Slavek & Pickering, 1981; Wu *et al.*, 1985)) in the presence of natural organics is generally enhanced at low pH and inhibited at high pH. At low pH metal ions bind to adsorbed organic matter more readily than to the organic free surface, while at higher pH metal ion uptake is suppressed by the formation of soluble metal – organic species (Davis, 1984).

The extent of the influence of the organic matter is dependent on the strength of its interaction with the metal. Davis (1984) found very little influence on Cd uptake on γ–alumina of a natural organic extract for which it had little affinity. Adsorbed humic and fulvic acids have also been shown to have little effect on the reduction of cadmium at a mercury electrode (Cosovic & Kozarac, 1984). Groundwater fulvic acid, on the other hand, had a significant effect on Cd uptake on α–Al_2O_3 (Xu *et al.*, 1989).

Mercury uptake on illite in the presence of humic and fulvic acids showed a rather different pattern, being greatly enhanced at all pH values (Wu *et al.*, 1985).

1.2 Study Aims

Previous studies of the metal ion interactions of humic substances, particulates and various mixtures of the two have been extensive (Section 1.1.4). However, the model systems used (particularly for humic substances) have frequently been restricted (in terms of pH and ionic strength) in order to simplify the process of determining metal binding stability constants. As a consequence of this, the results obtained are of limited value when considering metal interactions in natural systems.

The principal aim of this research work is therefore, to identify a model (or models) capable of describing the interactions of natural organic matter and organic coated

inorganic particles in solutions relevant to estuarine systems. In order to be effective, such a model must be able to take explicit account of changes in both ionic strength and pH.

A number of models describing metal adsorption on humic substances and mineral particles have been reported in the literature, and a cross–section of these are discussed in Sections 1.3 & 1.4.

In order to facilitate the identification of an appropriate model, experimental work will be conducted to obtain a data set showing the ionic strength dependence of the cation exchange chemistry of a natural fulvic acid sample (in solutions containing the major ions of seawater) and of a model particulate and mixtures of natural organic and model particulate (in NaCl solutions).

1.3 Modelling of Adsorption on Humic Substances

1.3.1 Introduction

The modelling of humic substance interactions is complicated by the heterogeneity of their functional groups and their polyelectrolytic (see Section 1.3.1.1) and polymeric nature. Aquatic humic substances have been found to closely resemble soil derived humics (Reuter & Perdue, 1977), and a number of models have been developed from soil science to describe their proton and metal ion interactions.

The Continuous Distribution models (Section 1.3.2) assume that fulvic acid (FA) consists of a continuum of binding sites. The distribution function may be assumed (Normal Distribution model) or unknown (Affinity Spectrum and Site Occupation Distribution Function models).

The N–Site models (Section 1.3.3) assume there to be a small number (i.e. <10) of distinct binding sites on the FA. Only one binding site is assumed in the Multidentate (uni– and bi– dentate complexes formed) and Electrostatic (binding controlled by the net charge on the FA) models. The Multisite model assumes that there is a small number of different binding sites on the FA.

Modelling of fulvic acid interactions has also been attempted by representing them as mixtures of well defined simple ligands (Mixture model) and by analogy to electrolyte permeable synthetic polymeric gels (Polyelectrolyte Gel model).

The Gouy Chapman diffuse layer theory has also been used to model adsorption on humic substances (De Wit *et al.*, 1988), but since this theory has its roots in particle interaction modelling it is included in Section 1.4.

1.3.1.1 Polyelectrolyte Effect

Substances, such as humic and fulvic acids and particulate oxides, which possess several active functional groups per structural unit (organic macromolecule or oxide particle) are said to be *polyelectrolytic* (Tanford, 1961).

The deprotonation behaviour of, for instance, a polymer of a simple mono–protic monomer will differ markedly from that of the monomer, because of the interactions between the charged sites on the polymeric molecule. Deprotonated (i.e. charged) monomer molecules in solution repel one another and, being free to move, become dispersed throughout the solution, thus reducing the electrostatic interactions between them to a minimum. When, however, the acidic sites of the polymer become charged, they are unable to move apart, because they are part of the same molecule.

Successive deprotonations of the polymer functional groups lead to an increasing net charge on the macromolecule, the effect of which is to make further deprotonations increasingly more difficult.

A titration curve of the polymeric material will not, therefore, show the distinct sigmoidal curve of the monomer, but will be skewed, with greater amounts of titrant being required to reach a given degree of dissociation of the polymer than for the equivalent fractional dissociation of monomer functional groups (see Figure 1.1).

In cases where the polyelectrolyte is suspended in a solution of a simple electrolyte, the polyelectrolyte effect is reduced by the counterion action of the electrolyte. Ions of opposite charge are attracted to the polyelectrolyte from solution and stabilise the charge on the macromolecule. Charge development (e.g. deprotonation) is therefore easier in solutions containing electrolyte ions than in solutions where counterions are not present, and is also easier in high ionic strength solutions than in low, by virtue of more counterions being present (Healy & White, 1978).

Apparent stability constants determined for a polyelectrolyte in solutions of different ionic strength will differ as a result of the polyelectrolyte effect (De Wit *et al.*, 1988).

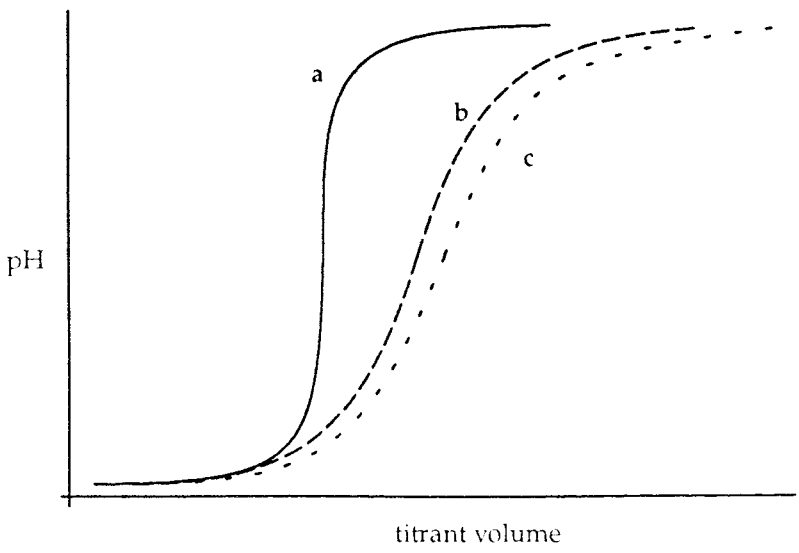

Figure 1.1 Schematic representation of the titration curves of a simple mono–protic monomer (**a**), and its polymer in high (**b**) and low (**c**) ionic strength solutions.

1.3.2 Continuous Distribution Models

The Affinity Spectrum model transforms the titration curve into a frequency distribution of $\log_{10} K$ (Thakur *et al.*, 1980) by the equation –

$$N(K) = \left(f_1 - (f_2 - f_1)\frac{a}{(a-1)^2}\right)\frac{1}{2\log_{10} a} \qquad (1.3.1)$$

where

$$f_1 = C(a/K) - C(1/aK) \qquad (1.3.2)$$

$$f_2 = C(a^2/K) - C(1/a^2K) \qquad (1.3.3)$$

$$C(x) = [ML] \text{ at } [M] = x \qquad (1.3.4)$$

a is an arbitrary constant (optimum value 0.2, Thakur *et al.*, 1980).

Buffle and co–workers (1990) state that the Site Affinity Distribution Function (SADF) is the only rigorous distribution function applicable to the interactions of natural organic matter, but that it is prone to severe artifacts due to experimental error. They propose the use of an alternative, the Site Occupation Distribution Function (SODF), plotting $\log_{10} \omega^*$ against $\log_{10} K^*$ to determine stability constant distributions. ω^* is determined from Eqn. 1.3.5 and K^* is the weighted mean of the thermodynamic equilibrium constants.

$$\omega^* = -\frac{d([ML]/[L]_T)}{d \log_{10} K^*} \qquad (1.3.5)$$

The Normal Distribution model assumes the FA binding sites to be normally distributed about a mean (μ) of $\log_{10} K$ values (Perdue & Lytle, 1983). The concentration of bound metal is given by Equation 1.3.6.

$$[ML] = \frac{[N]}{\sigma\sqrt{\pi}} \int_{-\infty}^{+\infty} \exp - \left(\frac{\mu - \log_{10} K}{\sigma\sqrt{2}}\right)^2 d \log_{10} K \qquad (1.3.6)$$

where σ is the standard deviation of the distribution and [N] is the total concentration of ligand.

1.3.3 N–Site Models

According to the Multidentate model binding occurs at only one type of site on the FA, but a bidentate complex (ML_2) is formed in addition to the 1:1 complex, ML, when the ligand concentration is much higher than that of the metal (Buffle *et al.*, 1977). The total bound metal concentration for this model is –

$$[ML]_T = \frac{K_1[M]([N] - 2[ML_2])}{1 + K_1[M]} \qquad (1.3.7)$$

where $[ML_2]$ is obtained from –

$$[ML_2]^2 + \left([N] + \frac{1 + K_1[M]^2}{4K_2[M]}\right) [ML_2] + \frac{[N]^2}{4} = 0 \qquad (1.3.8)$$

K_1 and K_2 are the stability constants of the uni– and bi– dentate complexes respectively.

The Electrostatic model assumes that the stability constant of the one binding site is dependent on the charge density at the surface of the FA and thus changes with the extent of binding of the ligand (Wilson & Kinney, 1977; Cabaniss *et al.*, 1984). The bound metal concentration is therefore –

$$[ML] = [N] \frac{K^*[M]}{1 + K^*[M]} \qquad (1.3.9)$$

$$K^* = K^{int} \exp - \left(2zw \frac{[M]_T - [M]}{[N]}\right) \qquad (1.3.10)$$

where $[M]_T$ is the total metal concentration, z is the charge of the metal ion and w is an electrostatic factor.

In the case of the Multisite model, binding takes place at a small number (m) of single binding sites, each with a stability constant (K_i) and total ligand concentration ($[N_i]$) (Rodbard, 1973; Hunston, 1975; Paxéus & Wedborg, 1985).

$$[ML]_T = \sum_{i=1}^{m} \frac{K_i[M][N_i]}{1 + K_i[M]} \qquad (1.3.11)$$

This model has been adapted to take account of competition for fulvic acid binding sites (Cabaniss & Shuman, 1988). For example, the equilibrium between protonated and metal bound ligand (Eqn. 1.3.12) (assuming the concentration of protonated ligand is much greater than that of the unprotonated ligand) is described by Equation 1.3.13.

$$HL + M^{n+} \Leftrightarrow ML^{(n-1)+} + H^+ \quad , \; K_{MH}^{app} \qquad (1.3.12)$$

$$[ML] = [N] \frac{K_{MH}^{app}[M]}{[H] + K_{MH}^{app}[M]} \qquad (1.3.13)$$

Similar equations can be written to account for competition of the metal with another cation (e.g. Ca^{2+} or Mg^{2+}) or for the formation of a ternary complex (e.g. FA–M–OH).

1.3.4 Mixture Model

The fulvic acid sample is represented by a large number of random (computer–generated) model structures containing simple (characterised) functional groups (Linder & Murray, 1987). The structures generated by the computer are tailored to match the known properties of a particular sample, e.g. elemental composition, percentage aromatic carbon.

Statistical means are then used to attempt to mimic the behaviour of the sample by varying the relative contributions of each of the model structures.

1.3.5 Polyelectrolyte Gel Model

Marinsky and co–workers have developed a means of quantifying the effect of simple salt concentration on the potentiometric properties of weakly acidic polymeric gels (Marinsky, 1985; Marinsky *et al.*, 1985).

The model compensates for interactions between the simple salt ions and the charged polymer, by adding a Donnan Potential term to the apparent dissociation constant, pK^{app}. This term takes into account the progressive invasion of simple salt ions into the matrix of a permeable gel as a titration proceeds. The dependence of pK^{app} on the ionic strength of the electrolyte can indicate whether the gel is flexible or rigid.

$$pH - pNa - \log_{10}\{\alpha^2/(1-\alpha)\} - \log_{10}(v/V_p) = p\overline{K}_{HA}{}^{app} \qquad (1.3.14)$$

The model has been applied to the protonation and metal ion equilibria of fulvic acids (Ephraim *et al.*, 1986, Ephraim & Marinsky, 1986) and humic acids (Marinsky *et al.*, 1982a & b). The three fulvic acid samples studied were found to behave similarly to impermeable polyelectrolyte gels, i.e. pK^{app} was a function of pH. Two of the FA's appeared to be rigid while the third was more flexible.

1.3.6 Summary

Of the models outlined above, the Affinity Spectrum, Normal Distribution, Multidentate, Electrostatic and Multisite models (Sections 1.3.2 & 1.3.3) have been examined critically by Turner and co–workers (Turner *et al.*, 1986). Statistical means were used to assess the models' treatment of M^{2+} – FA binding data at constant pH, using both experimental data and synthetic data obtained from a six ligand system (from Fish & Morel, 1984).

The Affinity Spectrum model was found to be highly susceptible to random errors. The changes produced in the $\log_{10}$ K frequency distributions by small random errors in the test data were so large that it was not considered possible to apply the model to experimental data sets with confidence.

Fitting with the Electrostatic and Normal Distribution models was initially only possible after a value for [N] had been fixed, either arbitrarily or by separate experiments. Subsequent analysis of the data sets with the NAG non–linear regression routine did fit values of [N], but the results were statistically poor (Turner, pers. comm., 1989).

The Multidentate model was only able to fit the synthetic data sets and one experimental data set satisfactorily.

The Multisite model gave significant fits to all the experimental and synthetic data sets and residual sum of squares and F–ratio tests also showed it to be statistically the best of the models.

Cabaniss and co-workers (Cabaniss *et al.*, 1984) have also examined a number of models, including those above, and concluded that goodness of fit alone did not provide sufficient validation of a model. They found that several models could provide 'good' fits to a data set, even though they may have been founded on contradictory assumptions, and thus the statistical analysis of a fit cannot provide a validation of a model's assumptions.

The majority of these models are unable to take account of changes in more than one experimental variable (e.g. pH, ionic strength, [M]) simultaneously. These (the Affinity Spectrum, Normal Distribution, Multidentate, Electrostatic and (unmodified) Multisite models) cannot therefore, be expected to provide adequate descriptions of humic substance interactions in estuarine systems.

1.4 Modelling of Adsorption on Particle Surfaces

1.4.1 Introduction

The surface (S) of a particulate oxide or oxyhydroxide can be considered to be a two dimensional array of immobile S–OH groups (Dzombak & Morel, 1990). Complexation can occur at these sites as a result of their protonation / deprotonation in an aqueous medium. These reactions at the substrate surface give rise to a charge (σ), which is smeared out over the surface, and an associated surface potential (ψ).

In solution the surface charge is counter balanced (and stabilised) by oppositely charged ions clustering at the surface–solution boundary. The structure of this boundary layer and the reactions which occur at the particle surface are the subjects of the surface complexation models.

(There is a degree of confusion in the literature regarding the naming of different surface–solution boundary layers. Some authors refer to the case of an adsorbed layer of counterions in combination with a diffuse layer as the constant capacitance model (Davis & Hem, 1989), here however, this will be referred to as the Gouy Chapman – Stern model, and the definition of the constant capacitance model will be taken from Westall & Hohl (1980)).

1.4.2 Gouy Chapman Model

The charge on the solid surface is counter balanced by a diffuse layer of charge in the solution (Bockris & Reddy, 1970). The density of this charge decreases exponentially with distance from the surface (similarly to the Debye–Hückel theory describing potential decay away from a charged ion in solution) (Figure 1.2a – solid line).

Adsorption of counterions may occur at the solid surface, forming a Stern layer (Westall & Hohl, 1980) (Figure 1.2a – dashed line).

1.4.3 Constant Capacitance Model

Acid–base and complexation reactions occur in a plane adjacent to the particle surface characterised by a surface potential (ψ) and a fixed capacitance (C) (Morel *et al.*,

1981; Westall, 1987) (Figure 1.2b). This can be considered to be a high ionic strength limiting case of the Gouy Chapman – Stern model, in which the surface charge is completely balanced by counterions in the Stern layer (Westall & Hohl, 1980).

1.4.4 Triple Layer Model

The region of solution adjacent to the particle surface is divided into three layers (Davis *et al.*, 1978, Davis & Leckie, 1978). Adsorption occurs at the two inner layers. Reactions involving the small protons and hydroxyl ions occur at the inner–most layer (ψ_0, C_1) and complexation reactions of the larger cations and anions at the outer (ψ_β, C_2). The third layer again contains a diffuse layer (Figure 1.2c).

1.4.5 Surface Reactions

Protonation / deprotonation reactions at oxyhydroxide surfaces have been considered to be one or two step processes. The one step process (Eqn. 1.4.1) enables the acid–base chemistry of the surface to be described by only one stability constant (Van Riemsdijk *et al.*, 1986), while the two step process (Eqns. 1.4.2 & 1.4.3) requires two pK values (Davis *et al.*, 1978; Morel *et al.*, 1981).

$$SOH_2^{0.5+} \Leftrightarrow SOH^{0.5-} + H_s^+ \,, \quad K_H = [SOH^{0.5-}][H_s^+]/[SOH_2^{0.5+}] \qquad (1.4.1)$$

$$SOH_2^+ \Leftrightarrow SOH + H_s^+ \,, \quad K_1^{int} = [SOH][H_s^+]/[SOH_2^+] \qquad (1.4.2)$$

$$SOH \Leftrightarrow SO^- + H_s^+ \,, \quad K_2^{int} = [SO^-][H_s^+]/[SOH] \qquad (1.4.3)$$

1.4.6 Summary

The ability of the Gouy Chapman – Stern, Gouy Chapman, constant capacitance and triple layer models to describe the acid – base chemistry of γ–Al_2O_3 at a single ionic strength and of TiO_2 at several ionic strengths (constant capacitance and triple layer only) has been examined by Westall & Hohl (1980). They concluded that the models were able to produce practically identical fits to the data at one ionic strength, although derived stability constant values were different for different models. The constant capacitance and triple layer models also provided good fits to the TiO_2 data, the constant capacitance model even performing well for ionic strengths well below those for which it is theoretically justified.

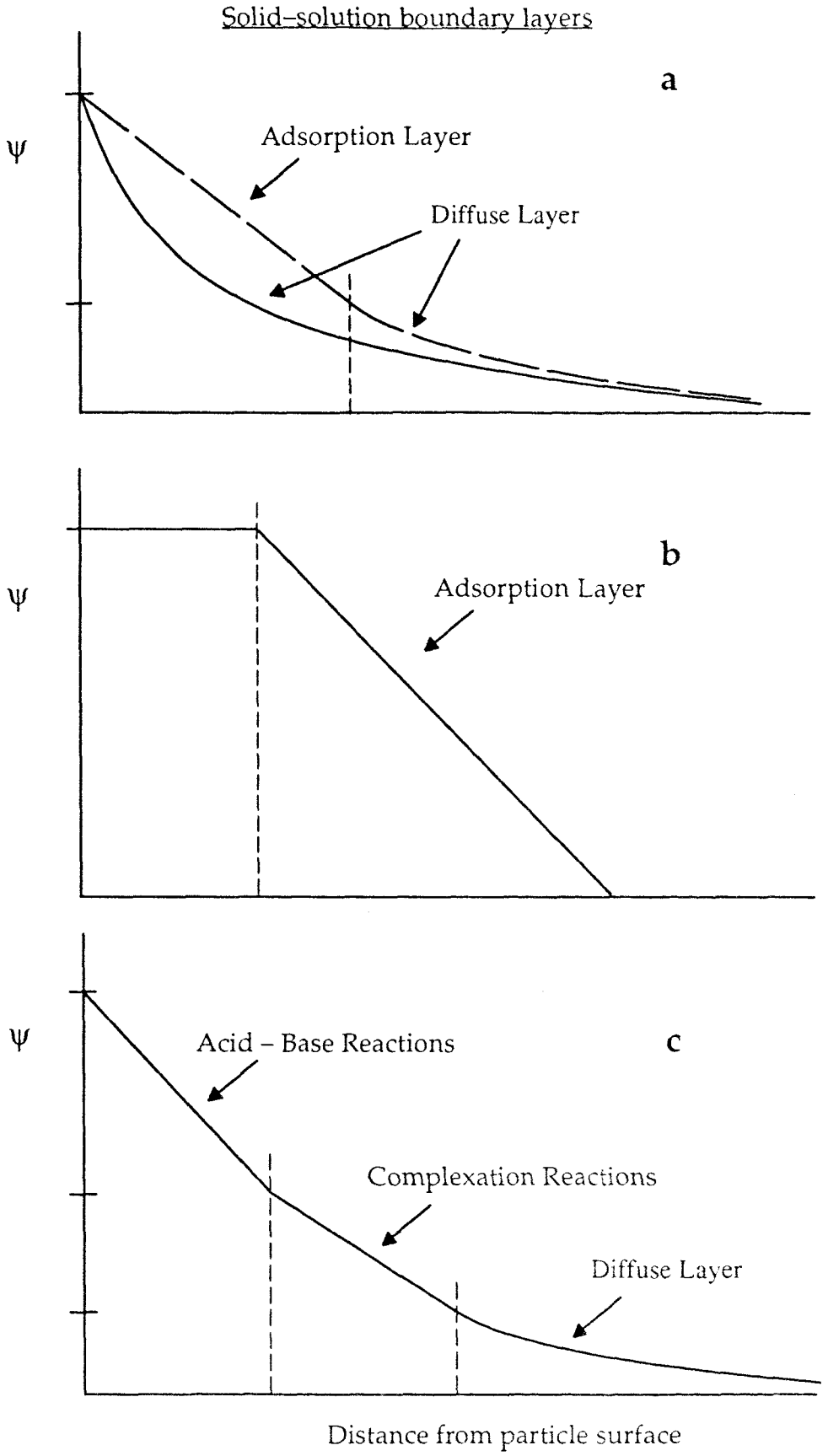

Figure 1.2 Schematic representations of the decay of potential (ψ) away from a charged particle according to (**a**) the Gouy Chapman / Gouy Chapman – Stern, (**b**) the constant capacitance and (**c**) the triple layer models.

1.5 System under study

1.5.1 Organic material

A sample of aquatic fulvic acid (FA) has been obtained from the Tamar River, UK (Varney, 1982).

The sample was extracted from 1700l of filtered river water by hydrophobic adsorption on Amberlite XAD–7 resin. The initial chemical parameters of the water sample are listed in Table 1.1. After desorption from the extraction resin the FA was passed over a cation exchange resin (Amberlite IR–120, H^+ form) to reduce metal ion impurities before freeze drying and storage under nitrogen.

The sample was then characterised by a variety of analytical techniques, including elemental analysis, gel filtration chromatography, IR and UV–Vis spectroscopy and pyrolysis GC–MS. The results of some of these analyses are summarised in Tables 1.2 & 1.3. The molecular weight of the sample (M_W) has been estimated, from its weight average Stokes' radius at pH 1.15 (Table 1.3), as 825 daltons.

In addition to this, the proton and lead and copper ion exchange behaviour of the FA was studied in 0.1M $NaClO_4$ solution by a number of methods (ion selective electrode, anodic stripping voltammetry, differential pulse anodic stripping voltammetry) (Varney, 1982; Varney *et al.*, 1983; Turner *et al.*, 1986; Turner *et al.*, 1987b).

1.5.2 Particulate material

Aluminium oxides have point of zero charges in the neutral pH range (Tipping, 1990), and this has prompted other investigators to study their interactions with natural organic matter (Parfitt *et al.*, 1977; Davis, 1980).

The particulate sample chosen for this study was γ–Al_2O_3. Although this is not the most common form of aluminium oxide in the environment (gibbsite – Davis & Hem, 1989), it is readily available commercially and has been studied quite extensively as a result of its use as a catalyst support phase. The point of zero charge pH (pH_{PZC}) of this material has been reported to be ~8.5 (Huang & Stumm, 1972), so that over the pH range of most natural systems the particles carry positive charges. Thus under the pH conditions of natural aquatic systems γ–Al_2O_3 can be expected to interact with negatively charged humic substances (Davis, 1980; Davis & Gloor, 1981).

Table 1.1 Initial chemical parameters of Tamar River water from which fulvic acid was extracted (Varney, 1982).

Volume	1700	l
Particulates	6.44	$mg.l^{-1}$
DOC	3.50	$mg.l^{-1}$
Dissolved Phosphate	0.032	mg P l^{-1}
Dissolved Nitrate	>2.65	mg N l^{-1}
Dissolved Nitrite	0.019	mg N l^{-1}
Dissolved Silicate	2.81	mg Si l^{-1}
Chlorophyll	0.57	µg (chl a) l^{-1}
Phaeophytins	0.59	$\mu g.l^{-1}$

Table 1.2 Results of elemental analysis of Tamar River fulvic acid sample and of the residue remaining after the fulvic acid had been ashed.

Fulvic acid analysis (Weight percent)

C	H	N	Ash	O
41.4%	5.1%	2.8%	1.18%	49.4%

Ash analysis ($\mu mol.g^{-1}$ of fulvic acid*)

Cu	Zn	Fe	Al	Pb	Cd
6	4	8	55	<0.5	<10

* Metal concentrations are erroneously reported in $nmol.g^{-1}$ in Varney, 1982.

Table 1.3 Results of gel filtration chromatography (weight average Stokes' radii (R_W)) of Tamar River fulvic acid at various pH values.

pH	R_W (nm)
1.15	0.658
2.15	0.691
4.00	0.906
6.89	0.949
7.44	1.052
9.26	1.321

1.5.3 Adsorption Models

As stated in Section 1.3.6, the majority of the adsorption models reported for humic substances are unsuitable for application to metal ion binding in non pH buffered solutions. The modified multisite model of Cabaniss & Shuman (Section 1.3.3), while including proton concentration explicitly (Eqn. 1.3.13), is unable to take account of ionic strength changes and is therefore, also unsuitable for use under estuarine conditions. The mixture model (Section 1.3.4) is unable to include electrostatic correction terms and is also discounted.

The remaining models (Gouy Chapman, constant capacitance, triple layer and polyelectrolyte gel) are of general application (including terms describing pH and ionic strength) and are selected for investigation in this study.

The polyelectrolyte gel model (Section 1.3.5) treats the substrate – solution interface as a three dimensional matrix, in contrast to the models of Section 1.4, which consider a two dimensional plane. The interactions of a mineral particle whose organic coating was permeable to simple salt ions may therefore be best described by this model.

The models selected are described in detail in Chapter 2.

2. ADSORPTION MODELS

2.1 Overview

2.1.1 Introduction

The Gouy Chapman (GC), constant capacitance (CC), triple layer (TL) and polyelectrolyte gel (PG) models have been selected from the literature for comparison in this study (see Section 1.5.3).

The basis of all these models is that a localised charge develops on a substrate as a result of ionisation of its active functional groups. This charge attracts counterions from solution to the substrate, causing the formation of a boundary layer at the substrate – solution interface. The electrical properties of this boundary layer (which are different from those of the bulk of the solution) affect reactions at the substrate surface through their influence on transport of ions from the bulk solution to the substrate (Westall, 1987).

The differences between the models arise in their conceptions of the substrate surface and the structure of the electrical boundary layer at the substrate – solution interface.

i) **substrate surface geometry** (two dimensional substrate surfaces (GC, CC, TL) or three dimensional matrices (PG))

ii) **substrate–solution interface structure** (dissipation of surface charge through one (GC), two (CC) or three (TL) distinct layers of charge in solution or inclusion of electrolyte counterions within the substrate matrix (PG))

A number of reactions have also been proposed to account for the development of electric charge at the surface of, or within, the substrate. Protonation / deprotonation and complexation of surface groups on oxyhydroxide particles may occur through one step (one pK) or two step (two pK) reactions (Sections 2.1.3.1 & 2.1.3.2). These reactions are not specific to particular electrostatic models, e.g. "one pK" or "two pK" processes can be applied to the constant capacitance or triple layer models with equal freedom. Reactions occurring on organic macromolecules (humics) are more commonly described in terms of the functional groups of simple organic molecules, classically carboxylic acids and phenolic hydroxides (Schnitzer & Khan, 1972).

2.1.2 Surface Geometry and Interface Structure

Gel coatings on hydrous oxide particles or porous organic structures may allow invasion of electrolyte ions into the substrate (Westall, 1987, Marinsky, 1985). In this case charged "surface" sites and their associated counterions are confined within the three dimensional matrix of the substrate and there is little or no appreciable extension of the boundary layer beyond the substrate matrix and into the solution (Westall, 1987). The polyelectrolyte gel model describes the potential arising inside a charged three dimensional substrate (the Donnan potential).

Non–porous substrates may only support reactions in two dimensions, i.e. at the substrate surface. This gives rise to a plane of charge on the substrate surface and a

boundary layer of counterions extending into the solution (Westall, 1987). The Gouy Chapman, constant capacitance and triple layer models describe the boundary layers formed at the interfaces of two dimensional substrates. The different boundary layer structures of these models were illustrated in Figure 1.2 and are also shown in more detail in Figure 2.1 (GC), Figure 2.2 (CC) and Figure 2.4 (TL).

2.1.3 Surface Reactions

2.1.3.1 One pK model

Protonation / deprotonation of the surface sites (S) is described by a one step, one pK process (Van Riemsdijk *et al.*, 1986). ($[H_s^+]$ refers to the concentration of protons at the substrate surface.)

$$SOH_2^{0.5+} \Leftrightarrow SOH^{0.5-} + H_s^+ \;,\; K_H = [SOH^{0.5-}][H_s^+]/[SOH_2^{0.5+}] \qquad (2.1.1)$$

Charged surface sites may be complexed by major electrolyte ions in solution (Yates *et al.*, 1974), e.g. in NaCl solution

$$SOH^{0.5-} + Na_s^+ \Leftrightarrow SOH\text{–}Na^{0.5+} \;,\; K_{Na} = \frac{[SOH\text{–}Na^{0.5+}]}{[SOH^{0.5-}][Na_s^+]} \qquad (2.1.2)$$

$$SOH_2^{0.5+} + Cl_s^- \Leftrightarrow SOH_2\text{–}Cl^{0.5-} \;,\; K_{Cl} = \frac{[SOH_2\text{–}Cl^{0.5-}]}{[SOH_2^{0.5+}][Cl_s^-]} \qquad (2.1.3)$$

2.1.3.2 Two pK model

The reactions describing ionisation of the surface sites according to the two pK model are (Davis *et al.*, 1978) –

$$SOH_2^+ \Leftrightarrow SOH + H_s^+ \;,\; K_1^{int} = [SOH][H_s^+]/[SOH_2^+] \qquad (2.1.4)$$

$$SOH \Leftrightarrow SO^- + H_s^+ \;,\; K_2^{int} = [SO^-][H_s^+]/[SOH] \qquad (2.1.5)$$

Complexation of the charged species is described by Eqns 2.1.6 & 2.1.7.

$$SO^- + Na_s^+ \Leftrightarrow SO^-\text{–}Na^+ \;,\; K_{Na}^{int} = \frac{[SO^-\text{–}Na^+]}{[SO^-][Na_s^-]} \qquad (2.1.6)$$

$$SOH_2^+ + Cl_s^- \Leftrightarrow SOH_2^+\text{–}Cl^- \;,\; K_{Cl}^{int} = \frac{[SOH_2^+\text{–}Cl^-]}{[SOH_2^+][Cl_s^-]} \qquad (2.1.7)$$

2.1.3.3 Electrostatic Correction

The terms used in Equations 2.1.1 – 2.1.7 to describe proton and major ion concentrations refer to their free concentrations at the surface of the substrate. As these values are not normally available from experimental data, the GC, CC, TL and PG models incorporate equations to correct experimental bulk solution concentrations for the electrostatic effects of the substrate solution interface (e.g. Eqn. 2.1.8).

$$[H_s^+] = [H^+]\, E \qquad (2.1.8)$$

where E is the electrostatic correction term applicable to the model in use.

2.2 Gouy Chapman (colloidal particle) Model

2.2.1 Introduction

The proton and metal ion binding behaviour of humic substances has been described, in terms of the surface properties of colloidal particles, using the Gouy Chapman model (De Wit *et al.*, 1988; De Wit *et al.*, 1989). This represents the fulvic acid–solution interface as a double layer, consisting of localised surface charge surrounded by a 'cloud' of counter ions (diffuse layer) in the electrolyte solution (Bockris & Reddy, 1970). Figure 2.1 shows the decrease in potential with distance from the colloid surface.

The charge and potential conditions applying in the double layer are different from those of the bulk electrolyte, causing changes to the properties of the electrolyte (e.g. pH) in this region. The size of these changes in bulk properties is dependent on the surface potential of the colloid (ψ_0).

e.g.
$$pH_s = pH + \frac{F\psi_0}{RT} \qquad (2.2.1)$$

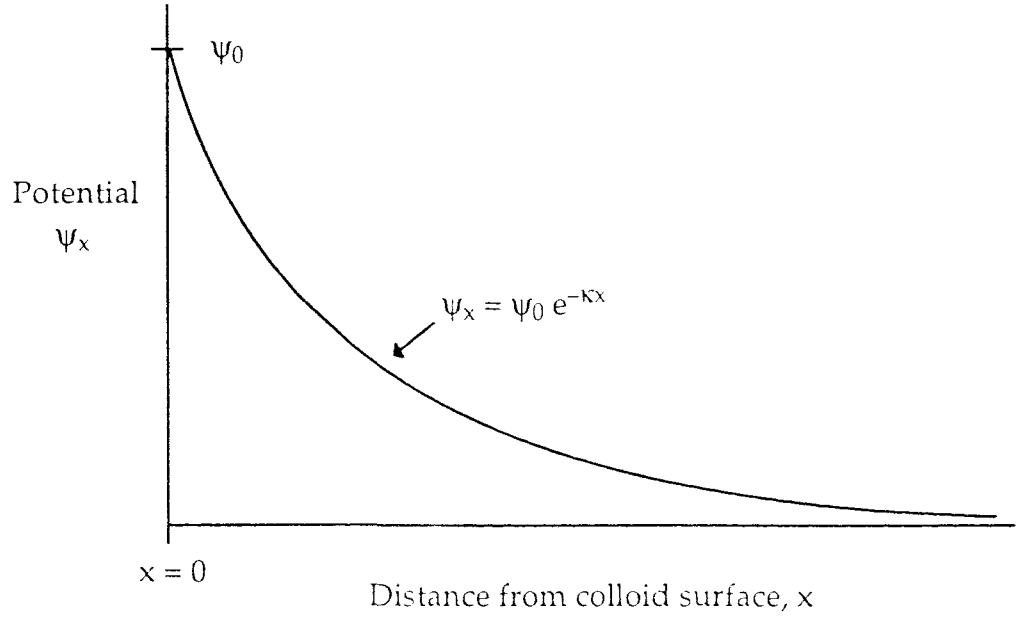

Figure 2.1 Potential decay away from the surface of a charged colloidal particle (Bockris & Reddy, 1970).

The magnitude of the surface potential is dependent on the ionic strength of the electrolyte. This causes plots of the fraction of undissociated functional groups (θ) of a substrate against pH obtained at different ionic strengths to diverge from one another. The adjusted parameter (pH_s) is independent of electrolyte ionic strength, and allows the divergent θ vs pH curves to be plotted as a single θ vs pH_s "master curve" (De Wit *et al.*, 1988).

The estimation of ψ_0 is dependent on the size of the colloidal particle. A large particle (>10nm, De Wit *et al.*, 1989) requires the calculation to be based on planar geometry, while for smaller particles spherical geometry can be employed.

2.2.2 Planar Colloid Surface

The surface potential – charge relationship for a planar surface of an inorganic particle is described by the Gouy Chapman – Stern model. Adsorption occurs at the Stern layer (capacitance, C_1) (Bockris & Reddy, 1970) and for 1:1 electrolytes (ionic strength, I) Eqn. 2.2.2 applies. (σ_0 is the surface charge, ε_0 and ε are the permittivity of free space and the relative permittivity of water respectively.)

$$\psi_0 = \frac{\sigma_0}{C_1} + \frac{2RT}{F} \operatorname{arcsinh}\left(\frac{\sigma_0}{\sqrt{(8\varepsilon\varepsilon_0 RTI)}}\right) \qquad (2.2.2)$$

For oxyhydroxide colloids C_1 can be taken in the range 1–5 $F.m^{-2}$ (De Wit *et al.*, 1988). In the case of organic colloids, such as humic and fulvic acids, hydrophilic parts of the molecule extend beyond the adsorbed layer and into the diffuse layer (De Wit *et al.*, 1988), so that $C_1 \rightarrow \infty$. Equation 2.2.2 can therefore be simplified –

$$\psi_0 = \frac{2RT}{F} \operatorname{arcsinh}\left(\frac{\sigma_0}{\sqrt{(8\varepsilon\varepsilon_0 RTI)}}\right) \qquad (2.2.3)$$

and pH_s can be calculated by combining Eqns. 2.2.1 and 2.2.3.

$$pH_s = pH + 2\operatorname{arcsinh}\left(\frac{\sigma_0}{\sqrt{(8\varepsilon\varepsilon_0 RTI)}}\right) \qquad (2.2.4)$$

2.2.3 Spherical Colloidal Particle

The spherical electric field arising from a small colloidal particle is described by the Poisson – Boltzmann Equation (Loeb *et al.*, 1961). This uses the dimensionless parameters y_0 ('reduced surface potential') and q_0 ('reduced distance'), which are related to surface potential (ψ_0) and particle radius (r) by equations 2.2.5 and 2.2.6.

$$y_0 = \frac{F\psi_0}{RT} \qquad (2.2.5)$$

$$q_0 = \kappa r \qquad (2.2.6)$$

where κ is determined from the concentration of the (1:1) electrolyte (c), the absolute temperature (T) and the charge on the counterion (z_+, for a negatively charged colloid).

$$\kappa^2 = \frac{2000F^2cz_+}{\varepsilon\varepsilon_0 RT} \qquad (2.2.7)$$

The behaviour of unsymmetric electrolytes may be described similarly by substituting solution ionic strength for concentration, as the diffuse layer charge is brought about by inclusion of counterions at the interface, rather than exclusion of coions (Hunter, 1981). Combination of equations 2.2.6 & 2.2.7 therefore gives Eqn. 2.2.8, which is valid for all electrolytes.

$$q_0 = \sqrt{\frac{2000F^2Iz_+}{\varepsilon\varepsilon_0 RT}}\ r \qquad (2.2.8)$$

The surface charge – potential relationship for this system is given in terms of the surface charge estimated from the Debye–Hückel approximation (σ_{DH}) (Stigter, 1972), since the spherical Poisson – Boltzmann equation cannot be solved analytically (Hunter, 1981).

$$\sigma_{DH} = D.y_0(1 + 1/q_0)\ ,\quad y_0 << 1 \qquad (2.2.9)$$

The limit of $y_0 << 1$ in Eqn. 2.2.9, although not strictly true for high ion concentrations, has been justified for proteins in concentrations of univalent ions up to ~0.1M (Tanford, 1961). The term D in Eqn. 2.2.9 is a correction factor giving σ_{DH} in units of $C.m^{-2}$ (Eqn. 2.2.10).

$$D = \frac{\varepsilon\varepsilon_0\kappa RT}{F} \qquad (2.2.10)$$

$$\frac{\sigma_0}{\sigma_{DH}} = 1 + \left\{ \frac{2}{y_0}\sinh\left(\frac{y_0}{2}\right) - 1 \right\} \sum_{k=0}^{7}\sum_{l=0}^{6} B_{kl}x^k z^l \qquad (2.2.11)$$

Table 2.1 Coefficients B_{kl} for Equation 2.2.11 (Stigter, 1972).

	l = 0	1	2	3	4	5	6
0	.388917	.070569	.016814	−.013557	−.005624	−.008658	.009627
1	.642050	.013094	−.037574	−.030964	.023083	.031695	−.023939
2	.104159	−.115093	−.020634	−.028683	.061791	.153012	−.142080
3	−.329087	.004369	.067834	.105858	−.087719	−.206741	.171248
k = 4	−.051492	.088811	−.003242	.148986	−.121085	−.423790	.365274
5	.148633	−.021655	−.037477	−.184967	.126408	.427771	−.353492
6	.012484	−.028032	.010308	−.110936	.066759	.283863	−.236144
7	−.032374	.011509	.002383	.105881	−.060958	−.252617	.206451

where the values of the constant B_{kl} are given in Table 2.1 and x and z are calculated from Equations 2.2.12 & 2.2.13.

$$x = \log_{10} q_0 \tag{2.2.12}$$

$$z = y_0/4 - 1 \tag{2.2.13}$$

2.2.4 Intrinsic Affinity Constants

2.2.4.1 Calculation of the Mastercurve

The molecular weight (M) of an organic colloid (e.g. fulvic acid) can be used as an adjustable parameter in the determination of a σ_0 (and θ) vs pH_s "mastercurve". Variation of M away from its true value causes displacement of the σ_0 (θ) vs pH_s curves from one another (De Wit *et al.*, 1991a), since the colloid surface area, and hence, the charge density (σ_0) is dependent on molecular weight. In the case of spherical colloids, where r may also be used as an adjustable parameter, more than one "mastercurve" may be found for different values of M and r. The range of r and M values which will produce a mastercurve can be restricted by use of Eqn. 2.2.14.

$$M = {}^4/_3\,\pi r^3 \rho N \tag{2.2.14}$$

Here ρ is the average density of the humic and can take values in the range 0.7 – 1.7 $g.cm^{-3}$ (De Wit *et al.*, 1991a) and N is Avogadro's number.

For inorganic colloids the total site density (D_s) is recommended as the adjustable parameter for mastercurve determination (De Wit *et al.*, 1989).

2.2.4.2 Determination of Affinity Constants

The proton adsorption density of the i th acidic site ($\Gamma_{i,H}$) is related to the total site density (D_s) and pH_s by Eqn. 2.2.15 (De Wit *et al.*, 1989).

$$\Gamma_{i,H} = \frac{D_s K_{i,H}[H_s]}{1 + K_{i,H}[H_s]} = D_s \theta_i \tag{2.2.15}$$

The intrinsic affinity constant for this site can thus be expressed as

$$\begin{aligned} \log_{10} K_{i,H} &= pH_s + \log_{10}\{\Gamma_{i,H}/(D_s - \Gamma_{i,H})\} \\ &= pH_s + \log_{10}\{\theta_i/(1 - \theta_i)\} \end{aligned} \tag{2.2.16}$$

and it can be seen that $\log_{10} K_{i,H} = pH_s$ ($\theta_i = 0.5$).

The overall degree of protonation of the colloid (θ) is given by Eqn. 2.2.17, where f_i represents the fractional abundance of the i th site, and this is related to the surface charge on the colloid by Eqn. 2.2.18.

$$\theta = \sum_{i=1}^{n} f_i \theta_i \tag{2.2.17}$$

$$1 - \theta = 1 - \sum_{i=1}^{n} f_i\theta_i = \frac{\sigma_0}{D_s F} \qquad (2.2.18)$$

If the number of different sites (n) and their fractional abundances (f_i) are known a set of $pK_{i,H}$ values can be obtained relatively easily from the equations above. Where these values are not known, De Wit and co-workers (1988, 1989, 1990 & 1991a) recommend the use of affinity distributions (the Condensation Approximation (Nederlof *et al.*, 1988), MUSIC (Hiemstra *et al.*, 1989), LOGA-1 (Nederlof *et al.*, 1990)) to extract intrinsic affinity constants from the mastercurve.

2.3 Surface Complexation Models

2.3.1 Introduction

Surface complexation models assume that the principal mechanism of surface charge development is reaction of major electrolyte ions with surface ionisable groups. Surface complexation reactions occur in addition to the association and dissociation reactions of protons and hydroxyls at the particle surface (Yates *et al.*, 1974; Davis *et al.*, 1978).

The potential at the solid – solution interface is affected by the surface charge on the solid, and different models for this relationship have been proposed. The constant capacitance model (CC) (Morel *et al.*, 1981; Westall, 1987) assumes that all reactions affecting surface charge occur in the same plane (Figures 2.2 & 2.3). The triple layer model (TL) (Davis *et al.*, 1978; Davis & Leckie, 1978) considers a three layer interface, in which association / dissociation reactions and complexation reactions occur at different distances from the surface (Figures 2.4 & 2.5). A total of seven parameters are required to describe the constant capacitance interface, while twelve are needed for the triple layer model (See Table 2.2).

Table 2.2 Parameters used to describe surface complexation model interfaces.

Parameter	Constant Capacitance	Triple Layer
Potential	ψ, ψ_1	ψ_0, $\psi\beta$, ψ_d
Charge	σ, σ_1	σ_0, $\sigma\beta$, σ_d
Capacitance	C	C_1, C_2
Permittivity	ε	ε_1, ε_2
Distance	d	β, γ

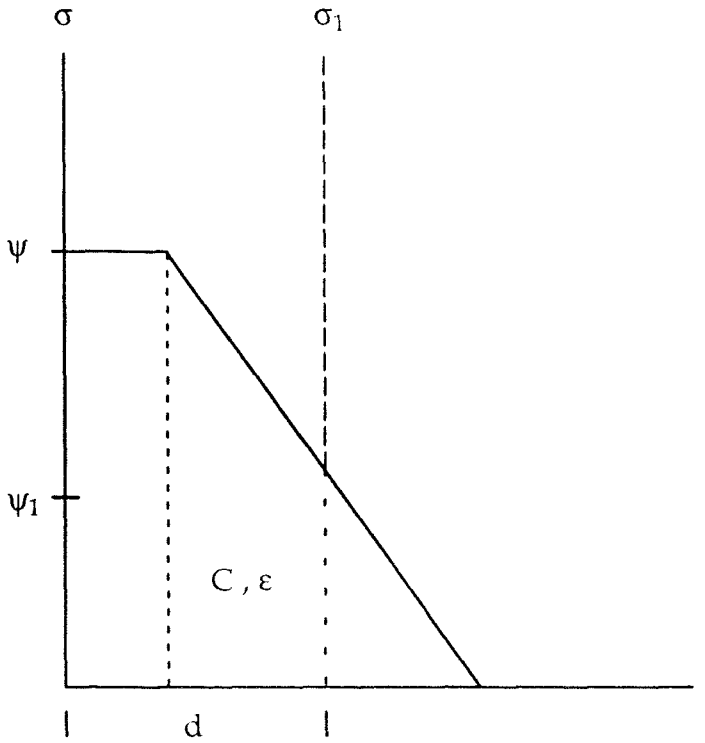

Figure 2.2 Potential and charge distributions at a planar surface according to the constant capacitance model (Westall, 1987).

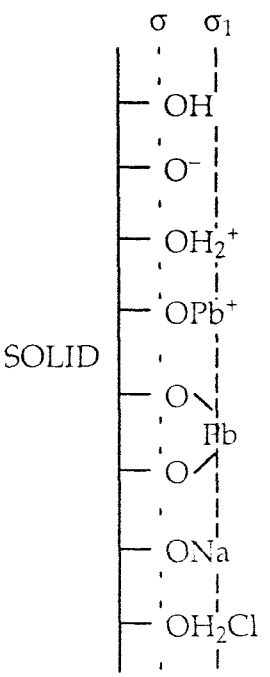

Figure 2.3 Locations of adsorbed species at the solid – solution interface as envisaged by the constant capacitance model (Morel *et al.*, 1981).

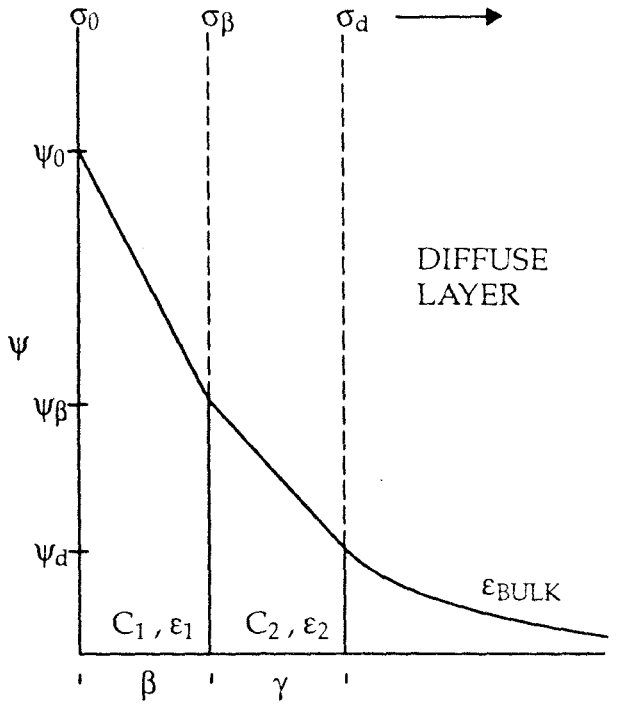

Figure 2.4 Schematic representation of the charge distribution at a planar surface and the potential decay away from the surface according to the triple layer model (Davis *et al.*, 1978).

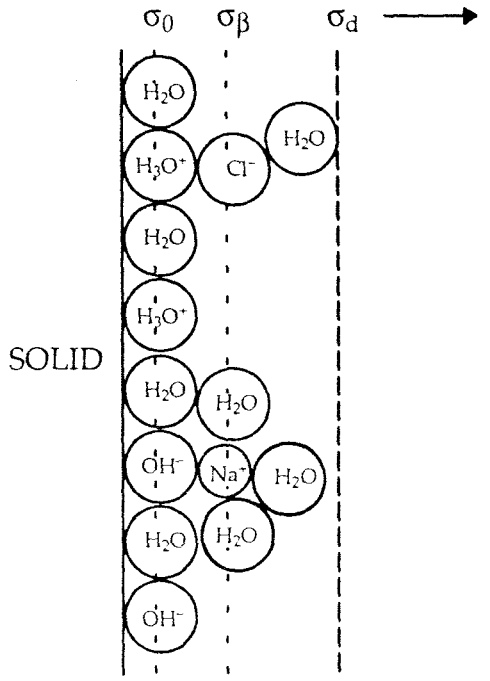

Figure 2.5 Possible locations of molecules at an oxide – solution interface and their relation to the planes of charge at the interface (Davis *et al.*, 1978).

2.3.2 Electrostatic Correction Terms

The "two pK" scheme (Section 2.1.3.2, Eqns. 2.1.4 – 2.1.7) describing surface reactions has been used in conjunction with the triple layer model (Davis *et al.*, 1978) and the constant capacitance model (Lövgren *et al.*, 1990).

The electrostatic correction terms (E of Eqn. 2.1.8) for protonation / deprotonation reactions (Eqns. 2.1.4 & 2.1.5) for these models are given by Eqns. 2.3.1 (CC) and 2.3.2 (TL), in which ψ and ψ_0 represent the potentials at the planes of proton adsorption.

$$E = \exp(-e\psi/kT) \qquad (2.3.1)$$

$$E = \exp(-e\psi_0/kT) \qquad (2.3.2)$$

Electrostatic correction terms must also be applied to electrolyte ion concentrations.

$$[Na_s^+] = [Na^+]\,E' \qquad (2.3.3)$$

$$[Cl_s^-] = [Cl^-]\,(E')^{-1} \qquad (2.3.4)$$

E′ is the electrostatic correction term applicable at the layer of adsorbed counter ions. (See Figures 2.3 (CC) and 2.5 (TL)). For the triple layer model E′ is given by Eqn. 2.3.5, while for the constant capacitance model E′ = E.

$$E' = \exp(-e\psi_\beta/kT) \qquad (2.3.5)$$

The reactions leading to ion pair formation can also be written as complex ionisations by combining Eqns. 2.1.5 & 2.1.6 and 2.1.4 & 2.1.7 –

$$SOH + Na_s^+ \Leftrightarrow SO^-\text{–}Na^+ + H_s^+ \quad , \; {}^*K_{Na}^{int} = K_2^{int}K_{Na}^{int} \qquad (2.3.6)$$

$$SOH_2^+\text{–}Cl^- \Leftrightarrow SOH + H_s^+ + Cl_s^- \quad , \; {}^*K_{Cl}^{int} = K_1^{int}/K_{Cl}^{int} \qquad (2.3.7)$$

The concentration of each type of surface site can be calculated from equations 2.3.8 – 2.3.11, which are derived from the acid–base and complex ionisation reactions (Eqns. 2.1.4, 2.1.5, 2.3.6 & 2.3.7) together with electrostatic correction terms (Eqns. 2.1.8, 2.3.3 & 2.3.4). These can be solved for any value of pH and electrolyte concentration with known values for N_s (the total number of surface sites), K_1^{int}, K_2^{int}, ${}^*K_{Na}^{int}$, ${}^*K_{Cl}^{int}$ and the capacitance(s) of the adsorption layer(s), after E, E′ and [SOH] are treated as independent variables.

$$[SOH_2^+] = \frac{[SOH][H^+]}{K_1^{int}}\,E \qquad (2.3.8)$$

$$[SO^-] = \frac{[SOH]K_2^{int}}{[H^+]}\,(E)^{-1} \qquad (2.3.9)$$

$$[SO^{-}\text{–}Na^{+}] = \frac{[SOH][Na^{+}]*K_{Na}^{int}}{[H^{+}]}\frac{E'}{E} \qquad (2.3.10)$$

$$[SOH_2^{+}\text{–}Cl^{-}] = \frac{[SOH][H^{+}][Cl^{-}]}{*K_{Cl}^{int}}\frac{E}{E'} \qquad (2.3.11)$$

E′/E is given by Eqn. 2.3.12 for the triple layer model, and is unity for the constant capacitance model.

$$E'/E = \exp((e\psi_0 - e\psi_\beta)/kT) \qquad (2.3.12)$$

2.3.3 Determination of Surface Ionisation Constants

Values for the surface ionisation constants (K_1^{int}, K_2^{int}, $*K_{Na}^{int}$ and $*K_{Cl}^{int}$) may be determined from experimental data according to the method of Davis and co–workers (Davis *et al.*, 1978).

2.3.3.1 Protonation / Deprotonation

In low ionic strength solutions, where electrolyte ions are not available for complexation, Eqns. 2.3.8 & 2.3.9 are sufficient to describe the development of surface charge (Davis *et al.*, 1978).

For a negatively charged surface, SOH_2^{+} can be ignored, and the concentrations of surface species and the fraction of charged sites (α) on the particle are related to the surface charge (σ_0) by Eqns. 2.3.13 – 2.3.15, where B is a correction factor (= F.V/A.m_s).

$$[SO^{-}] \approx -\sigma_0/B \qquad (2.3.13)$$

$$[SOH] \approx (N_s - |\sigma_0|)/B \qquad (2.3.14)$$

$$\alpha_- = -\sigma_0/N_s \qquad (2.3.15)$$

Eqn 2.3.9 can be rewritten in terms of surface charge using Eqns. 2.3.13 & 2.3.14

$$K_2^{int} = \frac{-\sigma_0\,[H^{+}]}{N_s - |\sigma_0|}E \qquad (2.3.16)$$

and in terms of the fraction of charged sites using Eqn 2.3.15

$$K_2^{int} = \frac{\alpha_-}{1-\alpha_-}[H^{+}]\,E \qquad (2.3.17)$$

Taking the logarithm of this leads to Eqn. 2.3.18

$$pK_2^{int} = pH - \log_{10}\{\alpha_-/(1-\alpha_-)\} - \log_{10} E$$

$$= pK_2^{app} - \log_{10} E \qquad (2.3.18)$$

When there is no charge on the particle $\log_{10} E = 0$ and it follows that $pK_2^{int} = pK_2^{app}$ at this point. pK_2^{int} can therefore be determined by plotting $[pH - \log_{10}\{\alpha_-/(1-\alpha_-)\}]$ versus α_- and extrapolating to $\alpha_- = 0$.

When the surface is positively charged SOH_2^+ and SOH are the dominant surface species and (by a similar argument) pK_1^{int} can be determined by plotting $[pH + \log_{10}\{\alpha_+/(1 - \alpha_+)\}]$ versus α_+.

2.3.3.2 Complex Ionisation

In high ionic strength solutions complexation reactions (Eqns. 2.3.10 & 2.3.11) are assumed to be primarily responsible for the development of surface charge. Examination of the electrostatic terms of the association / dissociation and complexation reactions, i.e. Eqns. 2.3.1, 2.3.2, 2.3.5 & 2.3.12, supports this assumption.

Considering a negatively charged surface, it can be seen from Eqn. 2.3.9 that as the dissociation reaction proceeds it is progressively inhibited by increased potential (Eqns. 2.3.1 or 2.3.2). The formation of the complex (Eqn. 2.3.10), however, is a more favourable process, being helped by the positive term in Eqn. 2.3.12 (TL), or by the fact that there is no electrostatic repulsion in the case of the constant capacitance model.

The surface charge is therefore a function of the concentration of the SO^-–Na^+ complex.

$$[SO^-–Na^+] \approx -\sigma_0/B \qquad (2.3.19)$$

Similarly to the low ionic strength case (for the triple layer model), Eqn. 2.3.10 can be rewritten using Eqns. 2.3.12, 2.3.14, 2.3.15 & 2.3.19.

$$*K_{Na}^{int} = \frac{\alpha_-}{1 - \alpha_-}\frac{[H^+]}{[Na^+]}\exp((e\psi_\beta - e\psi_0)/kT) \qquad (2.3.20)$$

and

$$p*K_{Na}^{int} = pH - \log_{10}\{\alpha_-/(1 - \alpha_-)\} + \log_{10}[Na^+] + (e\psi_0 - e\psi_\beta)/2.3kT$$

$$= p*K_{Na}^{app} + (e\psi_0 - e\psi_\beta)/2.3kT \qquad (2.3.21)$$

At $\sigma_0 = 0$, $\psi_0 = \psi_\beta$ and, therefore, $*K_{Na}^{int} = *K_{Na}^{app}$

$p*K_{Na}^{int}$ can be determined by plotting $\{pH - \log_{10}\{\alpha_-/(1 - \alpha_-)\} + \log_{10}[Na^+]\}$ against α_- and extrapolating to $\alpha_- = 0$. ($p*K_{Cl}^{int}$ can be found similarly, by a plot of $\{pH + \log_{10}\{\alpha_+/(1 - \alpha_+)\} - \log_{10}[Cl^-]\}$ against α_+.)

2.3.4 Charge – Potential Relationships

2.3.4.1 Constant Capacitance Model

The relationship between surface charge and potentials for the constant capacitance model is given by equation 2.3.22 (Westall & Hohl, 1980; Morel *et al.*, 1981).

$$\sigma/C = \psi \qquad (2.3.22)$$

The capacitance (C) is related to the permittivity (ε) and thickness (d) of the adsorbed layer (Eqn. 2.3.23) (Westall, 1987), while for electroneutrality to be preserved equation 2.3.24 must also be true.

$$C = \varepsilon\varepsilon_0/d \qquad (2.3.23)$$

$$\sigma + \sigma_1 = 0 \qquad (2.3.24)$$

2.3.4.2 Triple Layer Model

The charge – potential relationship for the triple layer model can be expressed by two equations similar to Eqn. 2.3.22 and a Gouy Chapman type equation (Eqn. 2.2.27, which gives σ_d in units of $\mu C.cm^{-2}$) (Davis *et al.*, 1978).

$$\sigma_0/C_1 = \psi_0 - \psi_\beta \qquad (2.3.25)$$

$$-\sigma_d/C_2 = \psi_\beta - \psi_d \qquad (2.3.26)$$

$$\sigma_d = -11.74\sqrt{C}\sinh\frac{ze\psi_d}{2kT} \qquad (2.3.27)$$

The outer layer capacitance (C_2) was taken as a constant value of 0.2 $F.m^{-2}$. The inner layer capacitance (C_1) was treated as an adjustable parameter and (at constant relative permittivity of the inner layer, ε_1) is thought to be inversely proportional to the distance of counter ion approach, β (Davis *et al.*, 1978). Equation 2.3.29 describes electroneutrality for this model.

$$C_1 = \varepsilon_1\varepsilon_0/\beta \qquad (2.3.28)$$

$$\sigma_0 + \sigma_\beta + \sigma_d = 0 \qquad (2.3.29)$$

2.3.5 Determination of N_s

Tritium exchange, surface geometry or infra–red determination of surface hydroxyl groups can be used to determine N_s (Davis *et al.*, 1978). These authors considered that potentiometric determination of N_s (e.g. through calculation of a formation function (δn_{OH}) (see Section 3.7.2)) was arbitrary, since the value obtained is dependent on the pH range of the titration and on solution ionic strength.

2.4 Polyelectrolyte Gel Model

2.4.1 Introduction

This model has been developed from studies of the proton and metal ion complexation properties of synthetic polyelectrolyte gels (Anspach & Marinsky, 1975; Marinsky & Anspach, 1975; Travers & Marinsky, 1974; Marinsky *et al.*, 1985) and colloidal and particulate suspensions (Marinsky *et al.*, 1983). Where a sample is permeable to the ions of its supporting electrolyte, the counterions associated with fixed charges on the sample are included within its three dimensional matrix (Marinsky, 1987). As a consequence of this the electrical influence of charge on the sample does not extend appreciably into the surrounding solution, as is the case with non–permeable samples.

The model consists of a qualitative investigation of the sample's permeability characteristics, together with a quantitative analysis of the invasion of electrolyte ions into the sample matrix (Marinsky, 1985; Marinsky & Ephraim, 1986).

2.4.2 Molecular Permeability Investigation

The ability of simple salt ions to invade a gel matrix can be judged by use of the apparent dissociation constant given by the Henderson–Hasselbalch Equation (pK_{HH}).

$$pK_{HH} = pH - \log_{10} \{\alpha/(1 - \alpha)\} \qquad (2.4.1)$$

Equation 2.4.2 describes the distribution of activities of a metal salt (MX) and its acid (HX) between gel (denoted by the overbar) and solution phases, in terms of their partial molar volumes (V) and the osmotic pressure of water in the gel (π)

$$\ln \frac{a_{HX}\bar{a}_{MX}}{a_{MX}\bar{a}_{HX}} = \frac{\pi}{RT} (V_{HX} - V_{MX}) \qquad (2.4.2)$$

Assuming that $\pi/RT\ (V_{HX} - V_{MX})$ is negligible, for a permeable gel we get –

$$pH + pX = p\overline{H} - p\overline{M} + pM + pX \qquad (2.4.3)$$

by including a term describing the ratio of dissociated to undissociated reactive sites on the gel $[-\log_{10} \{\alpha/(1 - \alpha)\}]$ a Henderson–Hasselbalch type equation is obtained.

$$pH - \log_{10} \{\alpha/(1 - \alpha)\} + pX = p\overline{H} - p\overline{M} + pM - \log_{10} \{\alpha/(1 - \alpha)\} + pX$$

$$= pK_{HH} + pX \qquad (2.4.4)$$

A plot of pK_{HH} against pH + pX will yield a common line for all ionic strengths if the gel is rigid. If the gel is flexible the activities of the diffusible components in the gel phase will no longer be controlled directly by α and the plots will diverge with changing ionic strength.

In the case of a salt impermeable gel the ratio of the charged species in the gel and solution phases (Eqn. 2.4.3) becomes –

$$pH = p\overline{H} - p\overline{M} + pM \qquad (2.4.5)$$

and, as before

$$pH - \log_{10} \{\alpha/(1 - \alpha)\} = p\overline{H} - p\overline{M} + pM - \log_{10} \{\alpha/(1 - \alpha)\}$$

$$= pK_{HH} \qquad (2.4.6)$$

Here pK_{HH} is a function of pH alone for a rigid gel, flexible gels again causing the lines to diverge with changing ionic strength.

Similar behaviour has been reported for the anion exchange properties of β–FeOOH (Paterson & Rahman, 1984). The chloride ion exchange capacity of β–FeOOH was found

to be a function of pH + pX when the electrolyte anion was Cl^-, but was dependent only on pH when the anion used was ClO_4^-. This was thought to arise because the large perchlorate ion was excluded from the small pores of the crystal structure (0.5 nm) and was therefore unable to replace the Cl^- ions present in them.

Investigation of several fulvic acid samples has shown them to be impermeable to salt ions and, generally, rigid (Ephraim *et al.*, 1986).

2.4.3 Gel Invasion Analysis

As dissociation of functional groups on a permeable gel (HA) proceeds, a Donnan Potential arises which forces invasion of simple salt ions into the gel in order to maintain electroneutrality. The effect of the counter ion, X, cancels from the mass balance equation (Eqn 2.4.2) to give –

$$pM - pH = p\overline{M} - p\overline{H} + 0.4343(\pi/RT)(V_H - V_M) \qquad (2.4.7)$$

The activities of the metal ions and protons in the gel phase ($p\overline{M}$ and $p\overline{H}$) can also be described by Equations 2.4.8 & 2.4.9. (where $p\overline{K}_{HA}^{int}$ is the intrinsic dissociation constant of the gel phase functional group and $\overline{C}_M$ refers to the concentration of the metal in the gel phase)

$$p\overline{H} = p\overline{K}_{HA}^{int} + \log_{10}\{\alpha/(1-\alpha)\} + \log_{10}\bar{\gamma}_A \qquad (2.4.8)$$

$$p\overline{M} = -\log_{10}\overline{C}_M - \log_{10}\bar{\gamma}_M \qquad (2.4.9)$$

However, $\overline{C}_M$ is not a measurable parameter and must be estimated from the number of ionisable groups on the gel (ν) and its volume (V_p) (Eqn. 2.4.10).

$$\overline{C}_M = \frac{\alpha\nu}{V_p} \qquad (2.4.10)$$

Combination of Eqns 2.4.7 – 2.4.10 gives –

$$pM - pH = -\log_{10}(\nu/V_p) - \log_{10}\bar{\gamma}_M - p\overline{K}_{HA}^{int} - \log_{10}\{\alpha^2/(1-\alpha)\}$$
$$- \log_{10}\bar{\gamma}_A + 0.4343(\pi/RT)(V_H - V_M) \qquad (2.4.11)$$

In most cases $0.4343(\pi/RT) \rightarrow 0$ and, if the electrolyte is a sodium salt, there is experimental evidence to suggest that $\bar{\gamma}_M = \bar{\gamma}_H$ (Marinsky, 1985), so –

$$pNa - pH = -\log_{10}(\nu/V_p) - \log_{10}\{\alpha^2/(1-\alpha)\} - p\overline{K}_{HA}^{int} - \log_{10}\bar{\gamma}_H$$
$$- \log_{10}\bar{\gamma}_A \qquad (2.4.12)$$

The apparent dissociation constant ($p\overline{K}_{HA}^{app}$) is related to $p\overline{K}_{HA}^{int}$ by Eqn. 2.4.13

$$p\overline{K}_{HA}^{int} + \log_{10}\bar{\gamma}_H + \log_{10}\bar{\gamma}_A = p\overline{K}_{HA}^{app} \qquad (2.4.13)$$

and so, can be calculated from experimentally accessible parameters according to Eqn. 2.4.14.

$$pH - pNa - \log_{10}\{\alpha^2/(1-\alpha)\} - \log_{10}(v/V_p) = p\bar{K}_{HA}^{app} \qquad (2.4.14)$$

As $\alpha \rightarrow 0$, $\{\log_{10}\bar{\gamma}_A + \log_{10}\bar{\gamma}_H\} \rightarrow 0$ and it follows that a plot of $[pH - pNa - \log_{10}\{\alpha^2 v/(1-\alpha)V_p\}]$ against α will have an intercept at $\alpha = 0$ of $p\bar{K}_{HA}^{int}$.

2.4.4 Determination of Parameters

2.4.4.1 Gel Volume

Two methods of determining the volume of a polyelectrolyte gel (V_p) are proposed. Where the polyelectrolyte is a synthetic polymer the gel volume can be calculated using the (known) distance between charged sites and structural charge density of the polymer (Marinsky *et al.*, 1985).

When the structural characteristics of the sample are not known (i.e. it is not a synthetic polymer) V_p can be measured experimentally (Marinsky *et al.*, 1983). The sample is removed from solution by centrifugation onto a glass frit, weighed and dried to constant mass. The volume of water expelled from the sample by drying is taken to be the volume of the gel.

2.4.4.2 Number of Ionisable Groups

In the case of synthetic polymers the number of ionisable groups on the gel is easily accessible from the number of repeating (monomer) units known to be present (Slota & Marinsky, 1980). However, no method of determining this parameter which is applicable to natural polyelectrolytes has been identified from this literature.

2.5 Summary

2.5.1 Differences Between Models

The models dealing with adsorption on two dimensional substrates (Gouy Chapman, constant capacitance, triple layer) differ from one another chiefly in the complexity of the substrate – solution boundary layer they describe. The Gouy Chapman and constant capacitance models are the simplest structurally, each having only one layer in the vicinity of the substrate surface. (The constant capacitance model is the simpler of the two from a computational point of view, having a linear charge – potential relationship). The Gouy Chapman – Stern and triple layer models each add layers of specifically adsorbed (immobile) ions immediately adjacent to the substrate surface (one layer for Gouy Chapman – Stern, two for triple layer) in addition to a diffuse layer.

The polyelectrolyte gel model differs substantially from the others in that it considers the substrate to be a three dimensional matrix containing both charged "surface" sites and counterions. Inclusion of the counterions within the substrate matrix results in little or no influence of the substrate charge on the electrical properties of the surrounding solution (Westall, 1987).

2.5.2 Applicability of Models

Assessment of the relative merits of the two dimensional substrate models must be based on a balance between their simplicity (and consequent ease of use) and the accuracy of their description of the boundary layer. E.g. the triple layer model, the most complicated, requires the most parameters to describe the boundary layer.

The constant capacitance and triple layer models have both been used successfully to describe adsorption processes on mineral particles (Lövgren *et al.*, 1990; Davis *et al.*, 1978). The presence of an organic coating may, however, change the adsorption behaviour of a particle surface. If hydrophilic parts of the organic coating cause disruption of the specific adsorption layers, as suggested by De Wit and co–workers (De Wit *et al.*, 1988), the Gouy Chapman model may prove to be the most effective. Alternatively, permeation of electrolyte ions into the organic coating may produce polyelectrolyte gel–type behaviour. However, the small size of the fulvic acid, relative to synthetic polymers, is likely to prevent electrolyte ions from being able to penetrate its molecules, and thus the polyelectrolyte gel model may not be applicable to this system.

3. EXPERIMENTAL METHODS AND DATA ANALYSIS

3.1 Reagents

3.1.1 Fulvic Acid

A sample of aquatic fulvic acid extracted from the Tamar River at Gunnislake Bridge (the limit of salt water intrusion up the river) (Varney, 1982) was used as a representation of natural organic matter throughout this work. Elemental and molecular size analyses for this sample are reproduced in Tables 1.2 & 1.3. This light brown, freeze–dried powder was stored in a dessicator.

Stock solutions of fulvic acid (1.05 $g.l^{-1}$) were prepared at least a week before required, to allow ageing of the solution, and stored in the dark.

3.1.2 Alumina

Highly pure γ–Al_2O_3 with an average particle size of 0.015μm was obtained commercially (BDH Ltd., Poole, Dorset). The alumina was washed with 0.01M NaOH, to remove any organics present on the particles, and then rinsed repeatedly with double distilled water until the suspension attained a constant pH. The alumina was separated from the liquid phase by centrifugation at 15,000 rpm for 30 minutes. The sample was then dried to constant mass (80°C, 2hr) and stored in a dessicator until required.

3.1.3 Reaction Solutions

All solutions were prepared with double distilled water, the secondary boiler of the still containing $KMnO_4$ to oxidise organics. The distilled water was collected directly from the still outlet after it had been boiling continuously for at least two hours. Care was taken to minimise contact with the air, in order to reduce uptake of CO_2 by the solutions.

3.1.3.1 Electrolyte Solutions

Titration solutions (NaCl, Na_2SO_4, $CaCl_2$, $MgCl_2$) were prepared from the highest available grade reagents (Aristar or Analytical Grade).

Artificial seawater was prepared from these reagents using the (slightly modified) recipe of Whitfield & Turner (1981). As pH buffering was undesirable, carbonate and borate were omitted. Other ions listed in this recipe, but whose effects on fulvic acid chemistry were not studied in this work (K^+, Sr^{2+}, F^-, Br^-), were also omitted. The ionic strength of the solution was adjusted by proportionally increasing the amounts of NaCl, Na_2SO_4, $CaCl_2$ and $MgCl_2$ used (Table 3.1).

Solutions of the hygroscopic salts $CaCl_2$ and $MgCl_2$, used in titrations and the preparation of artificial seawater, were calibrated by $AgNO_3$ titration (flourescein indicator) to determine their chloride content and, hence, their exact molarities.

Table 3.1 Quantities of NaCl and Na_2SO_4 (crystalline) and $CaCl_2$ and $MgCl_2$ stock solutions (0.971M & 1.004M respectively) used in the preparation of 1 litre of unbuffered artificial seawater (Whitfield & Turner, 1981).

Preparation method was as described in Whitfield & Turner, with the exception of the aeration step, which was omitted as this would have caused unnecessary CO_2 uptake by the solution.

	Mass solid (g)	Mass solution (g)	Concentration ($mol.kg^{-1}$)
NaCl	25.6967		0.43971
Na_2SO_4	4.1547		0.02925
$CaCl_2$		11.5891	0.01072
$MgCl_2$		58.9903	0.05530

3.1.3.2 Titrant Solutions

Solutions of HCl (0.1M and 1.0M) and NaOH (0.1M and 0.5M) were made up by diluting ampoules of the concentrated reagents (Volucon, May & Baker Ltd.). NaOH solutions were stored under a carbon dioxide absorbent (Carbosorb, BDH Ltd.) and titrated against the acid solutions at regular intervals to check their molarity.

3.1.3.3 Buffer Solutions

Buffer solutions were made up, according to the NBS system, from potassium phthalate (pH 4.008 @ 25°C) and Na_2HPO_4/KH_2PO_4 (pH 6.865 @ 25°C) (Eisenman, 1967). The pH of these solutions was held at the stated values by thermostatting them at 25°C when in use.

3.2 Apparatus and Experiment Control

3.2.1 Titration Apparatus

Acid–base titrations of the fulvic acid, alumina and mixed fulvic/alumina samples were carried out using microcomputer controlled titration systems. Each titration system consisted of an IBM XT or AT computer, a "Microlink" interface box (Biodata Ltd., Manchester), acid and base dosing autoburettes and appropriate electrodes, temperature probes, stirrers and N_2 delivery apparatus (Figures 3.1 & 3.2). A diagram of the reaction vessel is shown in Figure 3.3.

These systems were developed from an earlier titration apparatus, which was controlled by a Research Machines 380Z computer, running software written in FORTRAN IV (Turner *et al.*, 1987a; Turner *et al.*, 1991). As part of this work, the software was re–written in FORTRAN 77 and extensively revised to allow greater flexibility of

experimental design, to more easily accommodate changes in apparatus and to take account of the different data logging capabilities of the computers used.

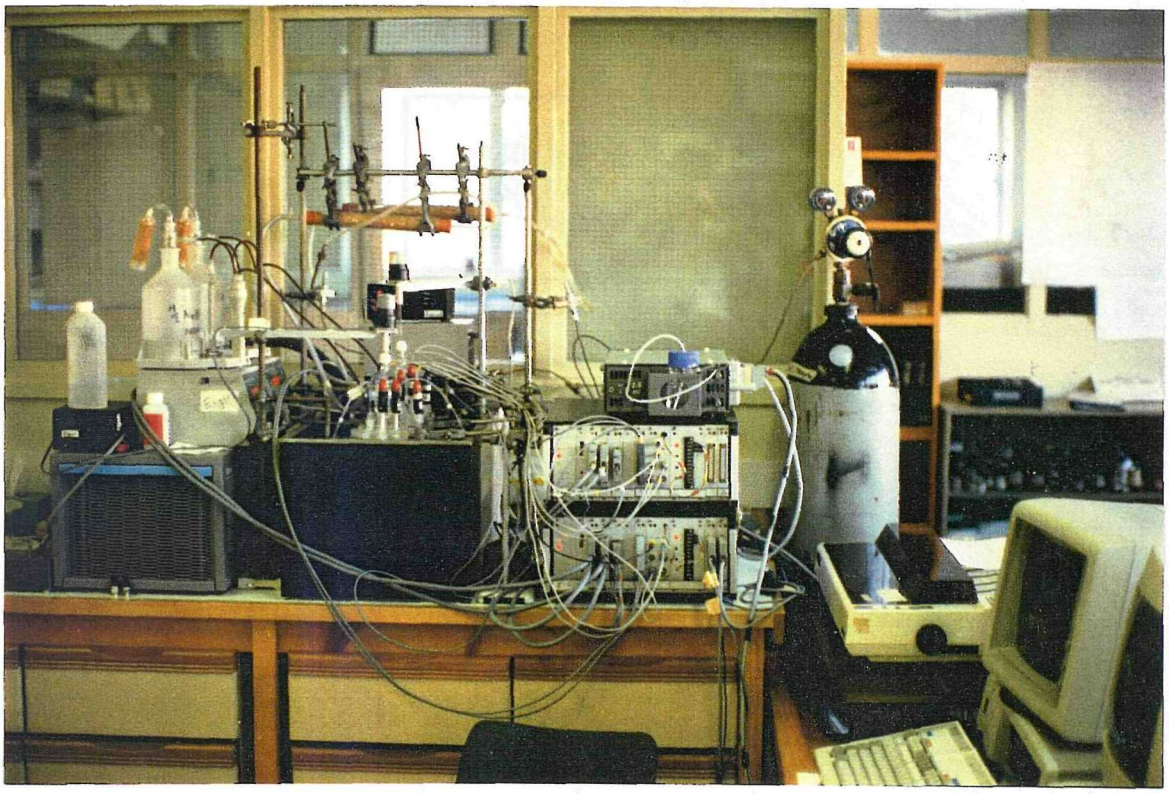

Figure 3.1 Photograph showing the potentiometric titration systems.

The Microlink interface boxes are in the centre of the picture, with the waterbath to the left and computers to the right. The waterbath houses both reaction vessels, into which electrodes, stirrers and nitrogen delivery tubes have been placed. Tubes of Carbosorb CO_2 absorbent are mounted above the waterbath to remove CO_2 from the nitrogen supply before it enters the reaction vessels.

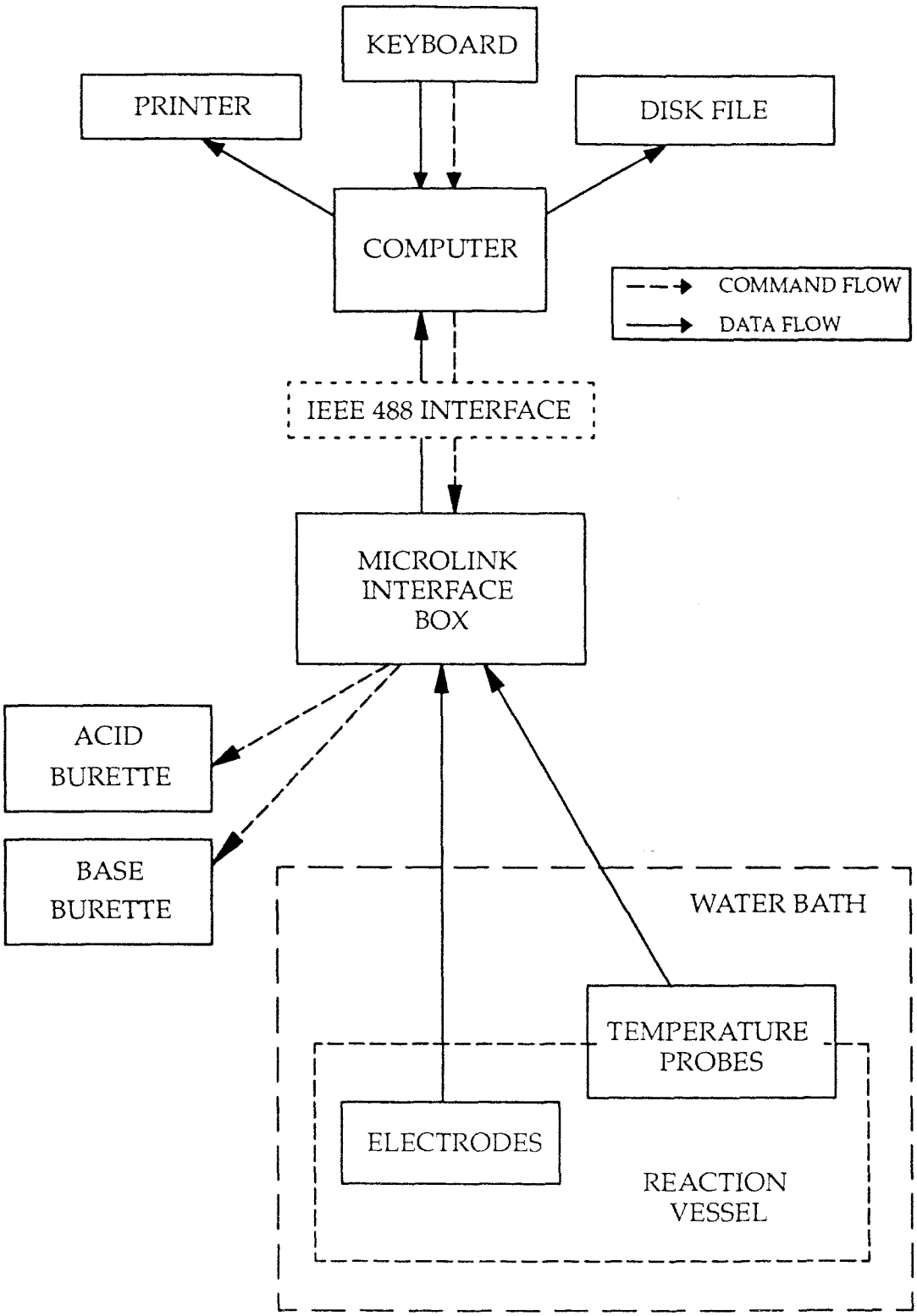

Figure 3.2 Schematic representation of the titration apparatus showing the flow of control commands and data through the system.

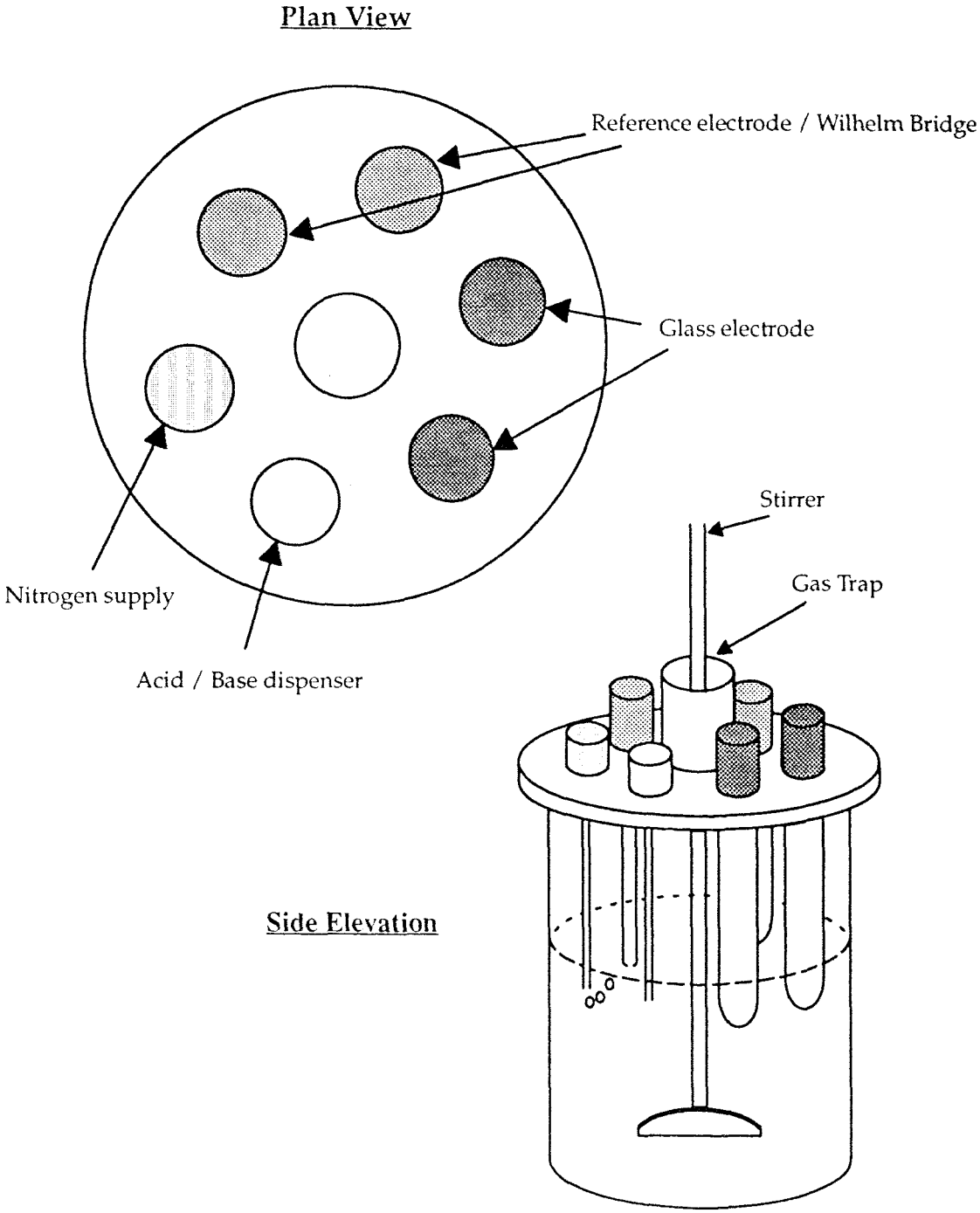

Figure 3.3 Diagram showing plan and side views of the reaction vessel used for potentiometric titrations. The gas trap surrounding the stirrer at the top of the reaction vessel contains distilled water, and allows nitrogen to leak out of the vessel while preventing other gases from entering.

3.2.1.1 Microlink System

The Microlink equipment is based on a modular design which allows several different pieces of equipment to be controlled by one computer through a standard IEEE 488 interface. Each component of the titration system is connected to a module in the Microlink box which can be addressed by the computer. The computer is then able to send commands to the burettes and receive data from the temperature probes and electrodes.

3.2.1.2 Burettes

A Radiometer ABU80 Autoburette was used for acid dosing. This was fitted with a 2.5ml exchange unit and was capable of delivering doses in increments of 0.001ml.

Base dosing was carried out by Metrohm 655 Dosimats. These had a dosing accuracy of ±0.001ml.

Solutions held in burette reservoirs were thoroughly mixed and the contents of each burette barrel refreshed before each titration.

3.2.1.3 Electrodes

Glass and single junction reference electrodes (Russell, UK.) were used to monitor pH changes during acid–base titrations. Before use these electrodes were conditioned by soaking in 0.1M HCl overnight, and then in an electrolyte solution of the appropriate ionic strength for several days. After this conditioning, and periodically thereafter, their response to pH change was checked in NBS buffers.

Micro–combination electrodes (Russell, UK.) were used to measure pH in small sample volumes (e.g. fulvic acid adsorption experiments, Section 3.4.1). These were calibrated with NBS buffers before use.

3.2.1.4 Wilhelm Bridges

Russell (frit type) reference electrodes used in potentiometric titrations were held in Wilhelm bridges. This arrangement (Figure 3.4) separates the electrode from particles in the reaction vessel, which may clog its frit, while maintaining electrical contact with the reaction solution (Forsling *et al.*, 1952).

3.2.1.5 Temperature Probes

Stainless steel shielded, platinum resistance temperature probes were used to measure the temperature of each reaction vessel and the water bath. These were connected to the Microlink system in a four–wire arrangement to give accurate readings and, in conjunction with the Analogue to Digital Converter used, they were capable of resolving temperature differences of 0.05°C.

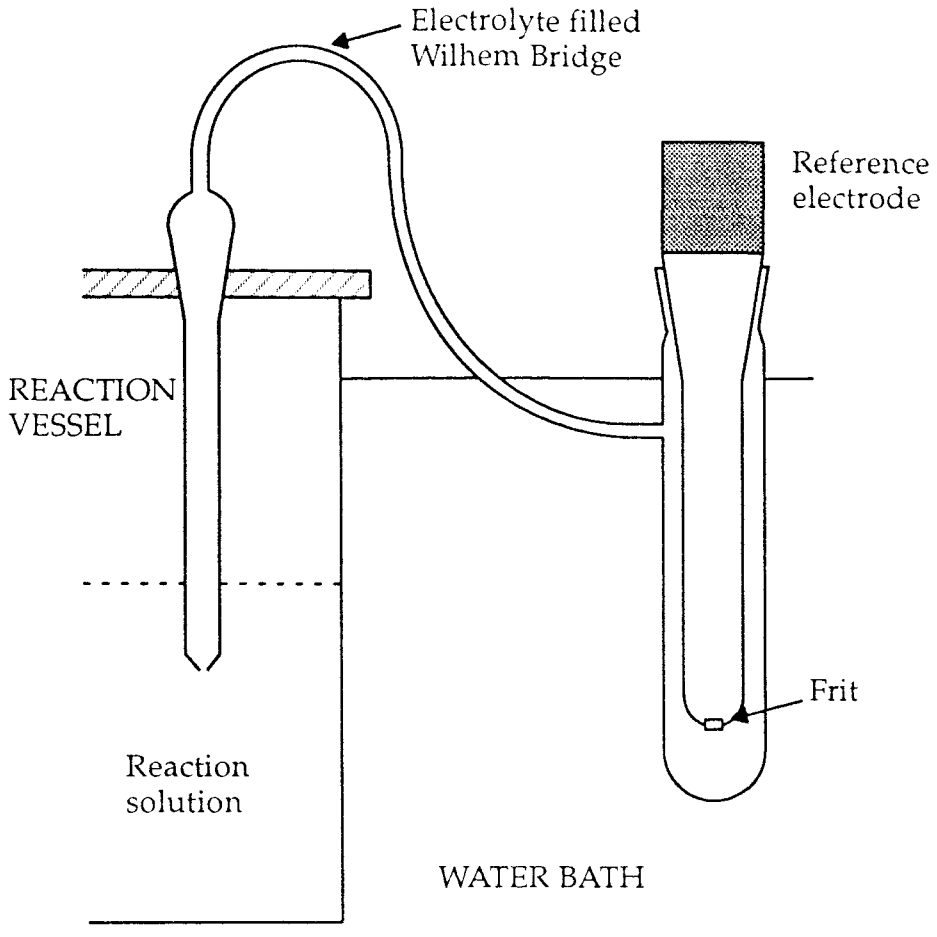

Figure 3.4 Diagram of the Wilhelm Bridge arrangement, showing how the Russell reference electrode frits are protected from clogging by particles in the reaction solution.

3.2.2 Control Software

A Fortran 77 computer program was used to control the Microlink interface box and, therefore, the titration.

Before titration began, the program prompted the user to enter details of the electrodes being used and the experimental conditions. The temperature of the reaction solution and the water bath were then measured by the computer.

The user was able to define potentials which required special action by the program. The well buffered regions of the titration curve (at low and high pH) could be titrated faster by specifying potentials at which multiple additions of base should be made. The titration could also be stopped (e.g. before the precipitation of the hydroxides of calcium or magnesium could occur) by defining a potential at which base addition should cease.

The experimental regime is outlined in Sections 3.3.1 & 3.3.3. After the expulsion of CO_2 by acidification described in Section 3.3.1 was completed, the titration was entirely controlled by the computer program.

3.3 Potentiometric Acid–Base Titrations

3.3.1 Titration Method

Reaction solutions (approx. 210ml) were made up from electrolyte solution with calibrated pipettes. The reaction substrate (fulvic acid stock solution, dry alumina powder or both) was added to bring the substrate concentration to 50 mg FA l^{-1}, 0.48 g Al_2O_3 l^{-1} or (50 mg FA + 0.48 g Al_2O_3) l^{-1}. The solution was then degassed with "white spot" high purity nitrogen for at least an hour before titration began.

The reaction vessel was immersed in a well mixed water bath which was thermostatted to approximately 25°C. Stirring of the reactants was carried out mechanically by a glass rod fitted with a Teflon fin. The use of a magnetic "flea" stirrer was avoided as it was felt that this would cause grinding of particulate samples on the base of the reaction vessel.

The initial pH of a solution of a humic substance is an important experimental parameter, as it provides a means of correcting the relative proton balance obtained from titration data to an absolute scale (De Wit *et al.*, 1990). Measurements of this parameter, however, were hampered by a persistent fault in one of the titration systems, in which measured electrode potentials were initially extremely high (> 250 mV). Although the source of this fault was not located, potentials rapidly returned to normal values on acidification of the titration solutions and the fault was never found to re–occur during a titration (blank or substrate).

Titrations were therefore started by acidification of the solution to pH 2 or 3 with standard 1.0M or 0.1M HCl and degassing was continued to ensure that any CO_2 in the solution was driven off. The completion of CO_2 expulsion was indicated by the attainment of a steady electrode potential after acid addition and generally took a further 20–30 minutes.

The degassed solution was then titrated, by stepwise addition of 0.5M or 0.1M NaOH, to pH 11 (or pH 9.5 for $MgCl_2$ and artificial seawater solutions). An equilibration period, of 100 seconds for fulvic acid or alumina alone, and 10 minutes for the mixed fulvic/alumina system, was left between base addition and measurement of steady electrode potentials (Section 3.3.3).

A small, constant stream of nitrogen was maintained through the solution during the course of the titration to prevent carbon dioxide from leaking back into the reaction vessel.

3.3.2 Calibration of Electrodes

Electrodes used in acid–base titrations were calibrated by means of blank titrations prior to titration of the substrate. These titrations were carried out over the pH range to be used in the substrate titration, and in the same electrolyte solution.

Table 3.2 Example of part of a potentiometric titration output file. The top of the file shows the name of the data file and the time and date at which the experiment was started. The values for volume etc. below this were all entered by the user, with the exception of temperature, which was measured by the program. The initial electrode drift value and the identification numbers of the electrodes making up each of the electrode pairs is also recorded.

Where the acceptable rate of drift was increased in order to obtain steady potential readings the drift rate actually used for each electrode pair was recorded under the relevant potential reading.

SAMPLE NAME: NS7F1 TIME 13:43:56 DATE 1/11/1989

VOLUME	WT.SED	[ACID]	[ALK]	IONIC STRNGTH	TEMP
209.38	0.0105	1.000	0.100	0.700	25.00

[BURETTE NO:1=ACID,2=ALKALI] [DRIFT=3E-7]

VOLUME ADDED		POTENTIALS (V)			
BURETTE 1	BURETTE 2	35 46	35 60	36 46	36 60
1.580	0.000	0.2296	0.2417	0.2231	0.2352
1.580	0.500	0.2287	0.2409	0.2222	0.2344
1.580	1.000	0.2278	0.2400	0.2213	0.2335
1.580	1.500	0.2269	0.2391	0.2205	0.2326
1.580	2.000	0.2260	0.2382	0.2195	0.2317
1.580	2.500	0.2250	0.2372	0.2185	0.2307
1.580	3.000	0.2240	0.2361	0.2175	0.2296
1.580	3.500	0.2230	0.2350	0.2164	0.2285
1.580	4.000	0.2218	0.2339	0.2153	0.2274
*****	*****	0.0000003	0.0000006	0.0000003	0.0000003
1.580	4.500	0.2206	0.2327	0.2142	0.2262
1.580	5.000	0.2195	0.2315	0.2130	0.2250
1.580	5.500	0.2182	0.2302	0.2117	0.2237
1.580	6.000	0.2169	0.2289	0.2104	0.2224
1.580	6.500	0.2155	0.2274	0.2090	0.2210
*****	*****	0.0000006	0.0000003	0.0000003	0.0000003
1.580	7.000	0.2140	0.2260	0.2076	0.2195

Blank titrations were analysed by fitting the data to the Nernst Equation by non–linear least squares regression analysis to obtain various parameters such as electrode slope (k_e) for use in the analysis of the substrate titration. (See Section 3.6 for a detailed description of this analysis.)

3.3.3 Electrode Pairs and Potential Drift Rate

Four electrodes, two glass and two reference, were used for each titration. Thus, switching glass and reference electrodes gave four measurable (glass – reference) electrode pairs. Any failure of one of the electrodes was easily detectable by comparison with other potential readings.

Electrode potentials were recorded as the means of 82 measurements of the electrodes and the rate of drift of each pair was calculated using the difference between consecutive mean potentials and the time taken per electrode reading (0.4 seconds).

The controlling computer program initially accepted a potential reading as stable if it was changing by less than 3×10^{-7} volts/second. If a steady reading had not been reached after five consecutive comparisons of means, the acceptable drift value was doubled and potential measurement continued. The process of doubling the drift value continued until a steady reading was obtained.

If the drift value of one or more of the electrode pairs had increased during measurement, the actual drift values at which steady potentials had been obtained were recorded for all the electrode pairs (Table 3.2).

3.4 Fulvic Acid Adsorption Experiments

3.4.1 Method

The pH and ionic strength dependence of fulvic acid adsorption on alumina was examined by a series of batch experiments.

A portion of alumina (5 mg) was suspended in 10ml of NaCl solution of the appropriate ionic strength and left to equilibrate for 30 minutes. After equilibration the pH of the suspension was adjusted by addition of 0.1M HCl or NaOH.

Fulvic acid stock solution (0.5 ml) was then added to bring the fulvic acid concentration to 50 $mg.l^{-1}$. The fulvic/alumina ratio used (1 mg FA : 9.5 mg Al_2O_3) was, therefore, the same as that used in mixed fulvic/alumina potentiometric titrations. The suspensions were then agitated overnight to allow equilibrium to be attained. The pH and ionic strength values at which experiments were carried out are shown in Table 3.3.

The final pH of each batch was measured before the supernatant liquid was centrifuged off and the amount of fulvic acid remaining in solution was determined by dissolved organic carbon (DOC) analysis (Section 3.4.2).

Table 3.3 Ionic strength (I) and approximate pH values used for fulvic acid adsorption experiments.

	pH =	3	4	5	6	7	8	9	10
	0.7M	√*	√	√*•	√	√	√	√	√*
I =	0.1M	√	√	√*•			√		√
	0.01M	√		√*•			√		√

√ indicates experiments carried out, * indicates "alumina blank", • indicates "fulvic acid blank"

Blank analyses were carried out by suspending alumina in NaCl solutions to which no fulvic acid had been added ("alumina blank"), and by adding fulvic acid to NaCl solutions containing no alumina ("fulvic acid blank").

3.4.2 Dissolved Organic Carbon Analysis

The amount of fulvic acid remaining in solution after equilibration with alumina was determined by DOC analysis, using a method similar to that of Sugimura and Suzuki (Sugimura & Suzuki, 1988).

Prior to analysis each sample was acidified with 10% phosphoric acid and degassed with oxygen, to expel inorganic carbon as CO_2. A portion of the degassed solution (200µl) was then injected onto the oxidation column of the instrument (3% Pt on Al_2O_3 catalyst) at 680°C under a stream of oxygen. Quantitative oxidation of the organic carbon produced carbon dioxide, which was dried with magnesium perchlorate. Detection of the CO_2 was by infra–red gas analyser connected to a computing integrator. The amount of carbon in the sample was then calculated from the area under the CO_2 curve.

Replicate injections were made for each sample and the instrument was calibrated before and after analysis by injection of standard solutions of caffeine (300, 200, 150, 100, 50 & 0 µMC in 0.7M, 0.1M and 0.01M NaCl). (Thanks to Axel Miller for carrying out this analysis.)

3.5 BET Adsorption Experiments

3.5.1 Method

Specific surface areas of the particulate samples used in this study were determined by BET adsorption (Brunauer *et al.*, 1938), using a Micromeritics 'FlowSorb II 3200' BET apparatus.

A known mass of sample was placed in a sample vial and heated to 120°C for 5 minutes under a stream of 30% nitrogen in helium gas to expel atmospheric moisture. Residual moisture was removed from the sample by subjecting it to an adsorption / desorption cycle (immersion in liquid nitrogen followed by immersion in water) before surface area measurement began.

Nitrogen adsorption on the sample was induced by immersing the sample vial in liquid nitrogen, while desorption occurred when the sample vial was immersed in a beaker containing water at room temperature. Through integration of adsorption and desorption peaks the instrument gave a value of surface area in square metres. The (slightly higher) value obtained from the desorption peak was considered by the instrument manufacturers to be the more reliable.

The instrument was calibrated (with appropriate corrections for atmospheric pressure and temperature) before use.

3.6 Blank Titration Analysis

3.6.1 Introduction

Blank acid–base titrations (Section 3.3.2) were analysed using Gran functions, and by non–linear fitting of a modified Nernst Equation, in order to calibrate the electrodes and to quantify the effect of the background electrolyte (Turner *et al.*, 1991).

Non–linear fitting of the titration data (electrode potential, E, and titrant volume, V) was carried out by a Fortran 77 computer program. E was chosen as the dependent variable as the errors in potential measurement were larger than those of V (the independent variable) and were also constant over most of the titration range. The fitting parameters were weighted by the program before being passed to the NAG subroutine E04FCF, so that iterations were carried out on parameters of the same magnitude.

3.6.2 Gran Function

The acid and base region proton balances (Eqn 3.6.1 & 3.6.2) can be written in terms of the number of moles of protons added (N_A), the residual proton concentration in the reaction solution (H_{init}) and the initial volume of reactants (V_0).

$$N_A = -H_{init}V_0 + (V_0 + V)[H^+] \qquad (3.6.1)$$

$$N_A = -H_{init}V_0 - (V_0 + V)[OH^-] \qquad (3.6.2)$$

These equations can be used together with the Nernst Equation (Eqn. 3.6.3) and the ionic product of water (Eqn. 3.6.4) to derive Gran functions (Gran, 1952) applicable in the acid (Eqn. 3.6.5) and base (Eqn. 3.6.6) regions of the titration curve.

$$E = E^0 + (RT/F) \ln [H^+] \qquad (3.6.3)$$

$$K_W = [H^+] [OH^-] \qquad (3.6.4)$$

$$(V_0 + V) \exp\left(\frac{FE}{RT}\right) = N_A \exp\left(\frac{FE^0}{RT}\right) + H_{init} V_0 \exp\left(\frac{FE^0}{RT}\right) \qquad (3.6.5)$$

$$(V_0 + V) \exp\left(-\frac{FE}{RT}\right) = -\frac{N_A}{K_W} \exp\left(-\frac{FE^0}{RT}\right) - \frac{H_{init} V_0}{K_W} \exp\left(-\frac{FE^0}{RT}\right) \qquad (3.6.6)$$

3.6.3 Nernst Equation

3.6.3.1 Acid Region

In the acid region of the titration curve (where $[OH^-]$ can be ignored) the simple Nernst equation (Eqn. 3.6.3) can be re–written to include a term representing the residual proton concentration of the reaction solution (Eqn. 3.6.7 – k_e is the electrode slope, $[H^+]$ is defined by Eqn. 3.6.1).

$$E = E^0 + k_e \ln \{N_A / (V_0 + V) + H_{init} V_0 / (V_0 + V)\} \qquad (3.6.7)$$

In low ionic strength solutions a pH dependent liquid junction potential develops, due to the increasing contribution of H^+ ions to the total ionic mobility of the solution with increasing acidity. The analysis program is therefore able to include an additional term in the expanded Nernst equation (Eqn. 3.6.7), to account for the development of a liquid junction potential.

$$E = E^0 + k_e \ln \{N_A / (V_0 + V) + H_{init} V_0 / (V_0 + V)\} + j_H[H^+] \qquad (3.6.8)$$

As j_H is a fitted parameter, this option forces the value for electrode slope (k_e) to be fixed at its theoretical value ($k_e = RT/F$) in order to avoid increasing the number of fitted parameters.

Non–linear regression thus yields values of E^0, k_e, and H_{init} (Eqn. 3.6.7) or E^0, H_{init}, and j_H (Eqn. 3.6.8).

3.6.3.2 Base Region

In the base region (where $[H^+]$ is negligible) the Nernst equation can be written –

$$E = E^0 + k_e \ln K_W - k_e \ln \{- N_A / (V_0 + V)\} \qquad (3.6.9)$$

Similarly to Section 3.6.3, a base region liquid junction potential ($j_{OH}[OH^-]$) is also included.

$$E = E^0 + k_e \ln K_W - k_e \ln \{- N_A / (V_0 + V)\} + j_{OH}[OH^-] \qquad (3.6.10)$$

Equation 3.6.10 is used for all ionic strength solutions, since the exclusion of the liquid junction term at high ionic strengths would provide the analysis program with only one parameter for non–linear fitting (K_W). The inclusion of the base region liquid junction term at high ionic strengths thus improves the fitting conditions.

Non–linear regression of equation 3.6.10 yields values of $\{E^0 + k_e \ln K_W\}$ (from which K_W can be calculated, using the values of E^0 and k_e obtained in the acid region) and j_{OH}.

3.6.4 Analysis Procedure

The use of Gran functions and the modified Nernst equations to analyse blank titrations is illustrated by taking three experiments carried out in NaCl solutions as examples. Untreated titration data for one electrode pair from each of these experiments (ionic strengths 0.01M (Expt. NA0B21), 0.1M (Expt. NA1B28), 0.7M (Expt. NA7B43)) are shown in Figure 3.5.

Plots of the Gran functions (the left hand sides of Eqns. 3.6.5 & 3.6.6) against the net number of moles of base added to the reaction solution provided qualitative analysis of blank titrations. The (acid and base region) linear plots converge at the neutralisation point of the titration, giving an indication of the magnitude of H_{init} (by the displacement of the convergence point from zero net moles of base added). Also, the presence of a pH dependent liquid junction potential could be judged by the curvature of the plots. A straight line indicated that the liquid junction potential was not pH dependent (i.e. j_H and j_{OH} were very small), while the curvature increased with increasing pH dependence (and decreasing ionic strength) (Figure 3.6).

Quantitative analysis was achieved by non–linear fitting of the modified Nernst equations (Eqns. 3.6.7, 3.6.8 & 3.6.10).

Fitting of the acid region was carried out first, since parameters obtained from this region (E^0 and k_e) were required in the calculation of the base region parameters. In practice, it was found that removing a few data points from the neutralisation region of the titration curve improved the fit. These points were subject to large errors, due to the poor buffering of the reaction solution in this region. The liquid junction potential term (j_H) was included in the fitting procedure (i.e. Eqn. 3.6.8 was used) if there was a discernible curvature of the acid region Gran plot for the experiment in question, otherwise j_H was set to zero and Eqn. 3.6.7 was fitted.

Once the acid region parameters had been obtained, the base region parameters (K_W and j_{OH}) were fitted, again removing points from the neutralisation region if necessary.

Where fitting of the base region parameters was unsatisfactory (especially for $MgCl_2$ solutions, due to a lack of data points (see Sections 3.2.2 & 3.3.1)) a theoretical value for K_W was calculated from Pitzer parameters (Harvie *et al.*, 1984) (Table 3.4) and the base region liquid junction parameter was set to zero.

The goodness of the fit obtained was assessed by plotting residual potentials (the difference between the observed electrode potential and that calculated from the fitted parameters) against net number of moles of base added (Figure 3.7). A good fit was considered to be one whose residuals were small ($\leq \pm 0.20$ mV) and randomly distributed about 0 mV (i.e. no systematic difference between experiment and calculation).

Upon completion of the analysis the values of E^0, H_{init}, k_e, pK_W, j_H and j_{OH} obtained for each pair were written to a disk file for use in the calculation of pH (Section 3.7.1).

Table 3.4 Theoretical values of pK_W calculated for titration solutions from Pitzer parameters. (Thanks to Dr Simon Clegg for Pitzer calculations.)

Solution	Ionic Strength ($mol.l^{-1}$)		
	0.7	**0.1**	**0.01**
NaCl	13.68	13.77	13.89
Na_2SO_4	12.92	13.39	13.78
$CaCl_2$	13.41	13.69	13.87
$MgCl_2$	12.78	13.30	13.76
Artificial Seawater	13.15	(Ionic strength 0.726 $mol.l^{-1}$)	

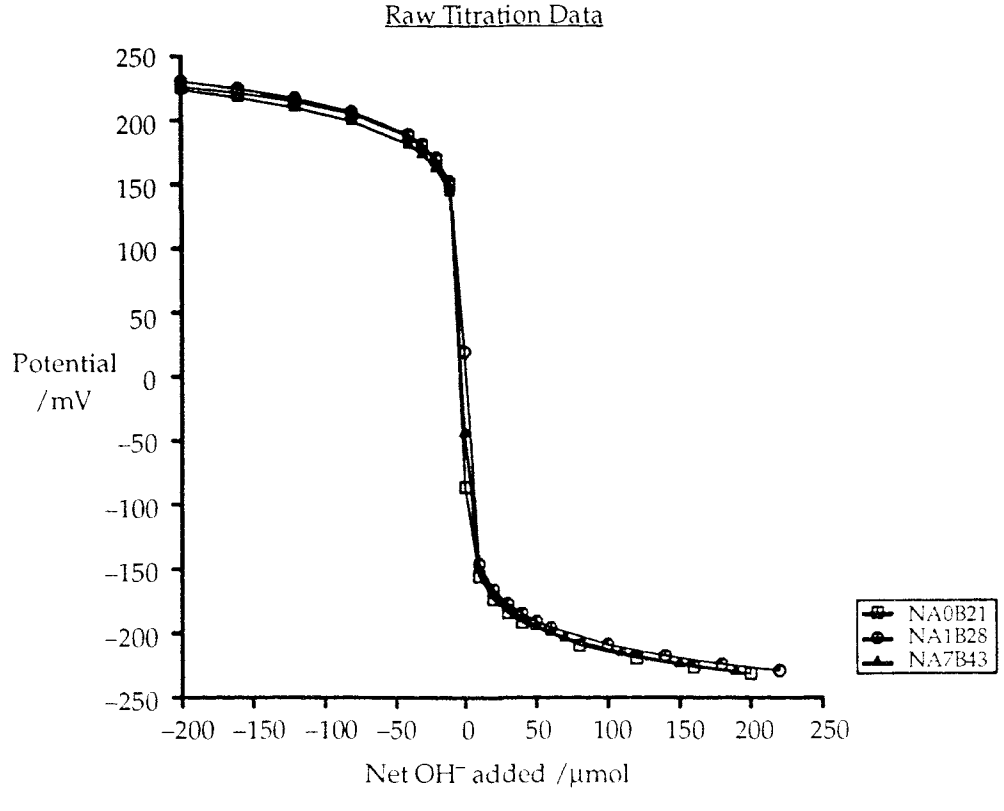

Figure 3.5 Plots of electrode potential against net amount of base added to reaction solution for blank titrations in NaCl solutions of various ionic strengths.

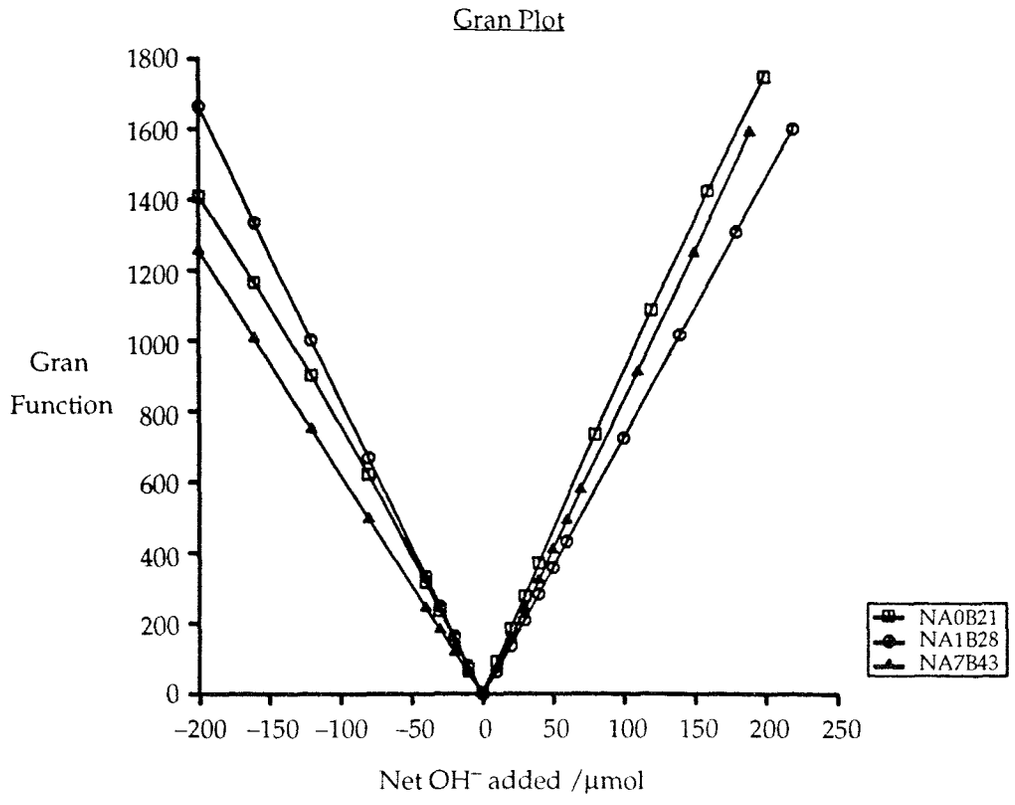

Figure 3.6 Acid and base region Gran functions plotted against net amount of base added.

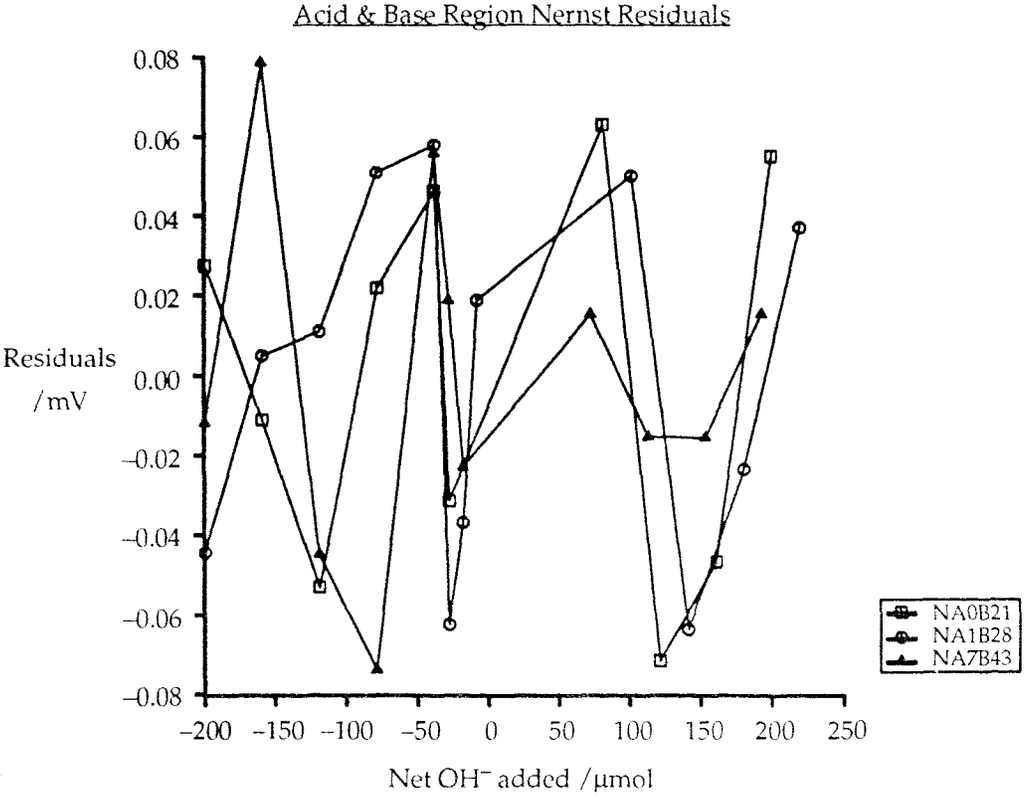

Figure 3.7 Residual potentials from Nernst Equation fitting procedure plotted against net amount of base added for NaCl solutions.

The results of the analyses of samples NA0B21, NA1B28 and NA7B43 are shown in Table 3.5 (in which K_H and K_{OH} refer to the number of points removed from the acid and base sides of the neutralisation region respectively, and GLASS and REF identify the electrodes used).

The standard errors for the Nernst equation parameters and pK_W are extremely small (E^0 <0.25%, k_e <0.5%, pK_W <0.05%), as are the standard deviations of the acid and base region fits. Standard errors for the other fitted parameters however, are somewhat higher (H_{init} 1 – 23%, j_H 0.3 – 15%, j_{OH} 5 – 40%). Their inclusion in the fitting procedure is justified by the decrease in the number of degrees of freedom of the fit and the consequent improvement in the quality of the fitting.

3.7 Substrate Titration Analysis

3.7.1 Determination of pH

The pH measured by each electrode pair in a titration of fulvic acid, alumina or fulvic acid / alumina mixture was calculated using the results of the preceding blank titration (Section 3.6.4).

Electrode potential and titrant addition data from the substrate titration were matched with the appropriate calibration parameters, according to electrode pair, by a computer program. The hydrogen ion concentration corresponding to each potential reading (E) was then calculated by the NAG subroutine C05ADF (by finding the root of Equation 3.7.1).

$$ff = -E + E^0 + k_e \ln [H^*] + j_H[H^*] + j_{OH}K_W/[H^*] \qquad (3.7.1)$$

where $[H^+] = [H^*]$ (ff=0).

3.7.2 Formation Function

The formation function (δn) provides a convenient means of assessing the proton exchange capacity of a titrated substrate (Varney *et al.*, 1983). The number of protons exchanged per unit mass of substrate can be plotted against pH, for either forward (base) or backwards (acid) titrations, to give a clear representation of the progress of the titration.

The amount of OH^- (or H^+) consumed during an acid–base titration can be calculated as the difference between the net amount of base or acid added (subscript a) and the equilibrium OH^- or H^+ concentration. A formation function, whose zero point will be the start of the titration (superscript 0), is then calculated from Equation 3.7.2 (Sposito & Holtzclaw, 1977; Stumm & Morgan, 1970), which is written as a forward titration formation function (δn_{OH}). (Charges are omitted for clarity; m_s is the mass of titrated substrate.)

$$\delta n_{OH} = \{OH_a - OH - (H^0 - H)\}/m_s \qquad (3.7.2)$$

Table 3.5 Fitted Nernst equation parameters, their standard errors and standard deviations of acid (σ_A) and base (σ_B) region fits for experiments NA0B21, NA1B28 and NA7B43.

NA0B21 $K_H = 2$ $K_{OH} = 5$ $V_0 = 209.29$ $RT/F = 59.15$ mV

GLASS	REF	E^0/mV	k_e/mV	H_{init}/μM	j_H/V.M^{-1}	σ_A/mV
34	66	410.03±0.13	not fitted	−7.65±0.75	−5.09±0.15	0.049
34	64	410.10±0.13	not fitted	−6.16±0.76	−4.75±0.16	0.050
17	66	409.40±0.18	not fitted	−7.09±0.99	−4.85±0.20	0.065
17	64	409.71±0.01	not fitted	−6.76±0.07	−4.85±0.02	0.005

pK_W	j_{OH}/V.M^{-1}	σ_B/mV
13.90±0.002	1.80±0.20	0.085
13.89±0.001	1.74±0.12	0.049
13.89±0.002	1.84±0.20	0.082
13.89±0.002	1.86±0.19	0.080

NA1B28 $K_H = 1$ $K_{OH} = 6$ $V_0 = 209.29$ $RT/F = 59.13$ mV

GLASS	REF	E^0/mV	k_e/mV	H_{init}/μM	j_H/V.M^{-1}	σ_A/mV
33	61	406.73±0.03	not fitted	−2.63±0.08	−0.37±0.45	0.027
33	67	409.71±0.04	not fitted	−2.60±0.11	−0.46±0.06	0.035
38	61	397.54±0.04	not fitted	−2.65±0.12	−0.42±0.06	0.039
38	67	400.51±0.04	not fitted	−2.60±0.11	−0.46±0.06	0.035

pK_W	j_{OH}/V.M^{-1}	σ_B/mV
13.78±0.002	−0.29±0.13	0.053
13.79±0.002	−0.29±0.13	0.053
13.78±0.002	−0.51±0.12	0.050
13.79±0.002	−0.29±0.13	0.053

NA7B43 $K_H = 1$ $K_{OH} = 7$ $V_0 = 209.29$ $RT/F = 59.16$ mV

GLASS	REF	E^0/mV	k_e/mV	H_{init}/μM	j_H/V.M^{-1}	σ_A/mV
36	69	405.19±0.85	59.27±0.28	−4.89±1.14	not fitted	0.076
36	65	407.33±0.47	59.05±0.15	−5.01±0.63	not fitted	0.042
39	69	402.67±0.75	59.26±0.24	−5.51±0.99	not fitted	0.067
39	65	404.84±0.74	59.06±0.24	−5.45±0.98	not fitted	0.066

pK_W	j_{OH}/V.M^{-1}	σ_B/mV
13.69±0.001	−1.31±0.08	0.035
13.72±0.003	−1.01±0.31	0.132
13.69±0.001	−1.05±0.05	0.022
13.72±0.004	−1.04±0.32	0.135

The formation function can, however, be calculated relative to any desired reference point by the inclusion of terms representing the added and observed amounts of OH^- (or H^+) at that point.

$$\delta n_{OH} = \{(OH_a - OH_a^0) - (OH - OH^0) - (H^0 - H)\}/m_s \qquad (3.7.3)$$

Superscript 0 in Equation 3.7.3 refers to the chosen reference point, not necessarily to the start of the titration.

3.7.3 Analysis Software

Data from the titrations of fulvic acid, alumina and fulvic acid / alumina mixtures were analysed on an IBM 9377 mainframe computer. Additions were made to an existing FORTRAN 77 program (Turner *et al.*, 1991), which carried out surface charge and pK extrapolation calculations (Section 2.3.3).

Subroutines were added to this program so that it was also able to solve the Henderson–Hasselbalch equation (Section 2.4.2), the polyelectrolyte gel model equations (Section 2.4.3) and the planar and spherical Gouy Chapman equations (Sections 2.2.2 & 2.2.3).

4. FULVIC ACID: FORMATION FUNCTIONS

4.1 Introduction

The results of potentiometric acid–base titrations of the Tamar River fulvic acid are shown in Figures 4.1 – 4.5 (pH vs net base added) and Figures 4.9 – 4.13 (δn_{OH} vs pH – see Section 3.7.2). These titrations were carried out at a fulvic acid concentration of 50 $mg.l^{-1}$ in solutions containing the major ions of seawater (NaCl, Na_2SO_4, $CaCl_2$ & $MgCl_2$) and an artificial seawater solution containing only those ions.

The concentration of fulvic acid used is rather lower than those used in other, similar studies (e.g. 1 $g.l^{-1}$ (Varney, 1982), 53 – 666 mg (TOC).l^{-1} (Dempsey & O'Melia, 1983), 1.85 $g.l^{-1}$ (Paxéus *et al.*, 1983)). This was made necessary by the relatively small quantity of sample available for the study (<400 mg). This concentration does correspond to the levels of dissolved organic carbon (DOC) found in organic – rich aquatic environments (e.g. swamp waters (Suffet & MacCarthy, 1989)), but a direct consequence of the low concentration is that formation functions cannot be determined accurately for pH values much below 4 or above 10 (Perdue, 1990).

4.2 pH Plots

The potentials recorded by the electrodes during each experiment have been converted into pH values using calibration data obtained from prior blank titrations (see Sections 3.6 & 3.7.1). The calibration data for these experiments are included in Appendix 1.A.

4.2.1 Ionic Strength Effects

Figures 4.1 – 4.4 illustrate the effects of changing solution ionic strength on the acid–base reactions of the fulvic acid sample in each of the simple salt solutions studied.

The polyelectrolyte effect (as well as the adsorption models described in Chapter 2) predicts that electrolyte ions stabilise charge on a macromolecular or particulate sample by acting as counterions to the charge (see Section 1.3.1.1). High ionic strength solutions should allow a higher charge to develop on the fulvic acid than that which is attainable in low ionic strength solutions by virtue of having a greater capacity to stabilise charge (i.e. more counterions). Close examination of Figures 4.1 – 4.4 shows that this is indeed the case. In each of the salts the number of moles of base required to increase the solution pH by one unit increases with increasing ionic strength. (This effect is clearer in the plots shown in Section 4.3.4 (Figures 4.9 – 4.12)).

The stabilising effect of electrolyte ions on fulvic acid charge may also be expected to displace these pH curves from one another along the x–axis (Net OH^- added) of the plots (Section 1.3.1.1). (Higher ionic strength solutions require more base to be added to reach a given pH than do low ionic strength ones, causing plots of the type shown in Figures 4.1 – 4.4 to diverge. If the starting point of each titration corresponds to the same state of charge

of the fulvic acid, the pH curves will spread out along the x–axis, with higher ionic strength displaced to higher values of base added.)

Of the experiments carried out, only the Na_2SO_4 results (Figure 4.2) exhibit this pattern. Although the pH curves obtained for the other salts (Figures 4.1, 4.3 & 4.4) are displaced from one another, they are not arranged in the 0.01M – 0.1M – 0.7M order expected, nor is the spacing between curves regular. This irregularity is probably caused by the difficulty in starting the titrations at the same state of charge of the fulvic acid (a problem which is compounded by the low concentration of fulvic acid in use). The most obvious way to achieve this would have been to start all the titrations from the pH of zero point charge (pH_{PZC}) of the fulvic acid (pH_{PZC} 1.15 (Varney, 1982)). Attainment of this pH was not practical, however, since it would have required addition of very large quantities of acid and base, and may have resulted in the coagulation of the fulvic acid.

The large displacement of the 0.7M NaCl curve (Figure 4.1) from the other NaCl experiments may also be partly due to the pretreatment of the fulvic acid used in this experiment. (This fulvic acid sample was dissolved in 0.7M NaCl solution prior to titration, all other samples were pretreated by dissolution in double distilled water).

4.2.2 Initial pH of Fulvic Acid Solutions

The pH at which the fulvic acid titration curves of Figures 4.1 – 4.5 pass through the point of zero net added base can be taken as an indication of the initial pH of each experimental solution. (Direct measurements of this parameter are, unfortunately, not available for these experiments due to operational difficulties, see Section 3.3.1).

With the exception of the titration curve in artificial seawater (Figure 4.5), these experiments indicate that the fulvic acid solutions were alkaline prior to titrant addition. (It is unclear why the fulvic acid – seawater solution alone appears to be acidic). The sample in use is reported to have been de–salted and is also reported to contain relatively low levels of several metals (Varney, 1982, see Section 1.5.1). As such its solution should be acidic rather than alkaline.

Investigation of the acidity of the fulvic acid stock solutions used for these experiments (when diluted to the experimental concentration, 50 $mg.l^{-1}$) and of a freshly prepared and aged 50 $mg.l^{-1}$ FA solution also shows them to be alkaline (see Table 4.1). (The higher pH of stock solution A than solution B (Table 4.1) probably accounts for the large displacement of the 0.7M NaCl titration curve from the other curves in Figure 4.1, which was noted in Section 4.2.1).

Table 4.1 Fulvic acid stock solution pH values.

pH values for double distilled water (DDW) are for water used to dilute stock solutions A and B to 50 $mg.l^{-1}$, and to prepare solution C.

Stock Solution	pH FA	pH DDW	Experiment
A	7.98	5.75	0.7M NaCl (NA7F5)
B	7.14	5.75	all others
C	7.05	5.78	none

Table 4.2 Metal content of Tamar River fulvic acid determined by semi–quantitative ICP–MS analysis. Figures in parentheses are metal contents reported previously for this sample (Varney, 1982).

Element	Concentration $\mu mol.g^{-1}$ FA	
Mg	76	
Al	3	(55)
Ca*	1300	
Ti	4	
Fe*	39	(8)
Cu	11	(6)
Zn	5	(4)
Sr	3	
Ba	1	

* Peak subject to interferences

Table 4.3 Sodium and calcium content of Tamar River fulvic acid determined by flame – AAS.

Element	Concentration $mmol.g^{-1}$ FA
Na	1.3±0.1
Ca	1.73±0.04

In the light of these pH measurements, the metal content of stock solution C was examined by inductively coupled plasma – mass spectrometry (ICP–MS) in semi – quantitative mode and flame atomic adsorption spectroscopy (AAS). ICP–MS results (Table 4.2) have been obtained by subtracting the mass spectrum of the double distilled water used to prepare the stock solution from that of the fulvic acid solution. (Concentrations obtained in semi–quantitative mode are accurate to within a factor of three).

The major isotope peaks of calcium are subject to interferences in the ICP–MS technique, the concentration quoted in Table 4.2 has been obtained from the minor isotope ^{44}Ca. The ICP–MS signal of sodium is obscured by carrier gas (Ar) peaks. Sodium and calcium analyses were therefore also carried out by AAS (Table 4.3). (There is good agreement between the values obtained for calcium concentration by ICP–MS and AAS, despite the interference involved in the ICP–MS measurement).

The concentrations of Cu, Zn, Fe and Al found for the fulvic acid by ICP–MS are in broad agreement with those previously reported by Varney. However, the high concentrations of sodium and calcium found by AAS suggest that the hydrogen ion exchange step of the fulvic acid purification procedure was rather inefficient. These concentrations would be expected to give a higher ash content for the fulvic acid (13.7%, as Na_2O and CaO) than was previously reported (Varney, 1982).

The high pH of the fulvic acid solutions may therefore be attributed to the significant quantities of sodium and calcium in the sample, and the dissociation of these metals from the fulvic acid in solution. Complete dissociation of Na^+ and Ca^{2+} from the fulvic acid would raise the total Na^+ and Ca^{2+} ion concentrations by 65 μM and 85 μM respectively (i.e. 0.7% and 2.6% in I = 0.01M solutions of these ions) at the fulvic acid concentration in use.

4.2.3 Sample Precipitation

Figure 4.4 shows that there is a slight discontinuity in the titration curve of the 0.01M $MgCl_2$ experiment at ~pH 10. The sample was found to have precipitated and, since precipitation did not occur at this pH in any other fulvic acid titration, or in the corresponding blank titrations in 0.01M $MgCl_2$, the precipitate was presumed to be a Mg–fulvate complex.

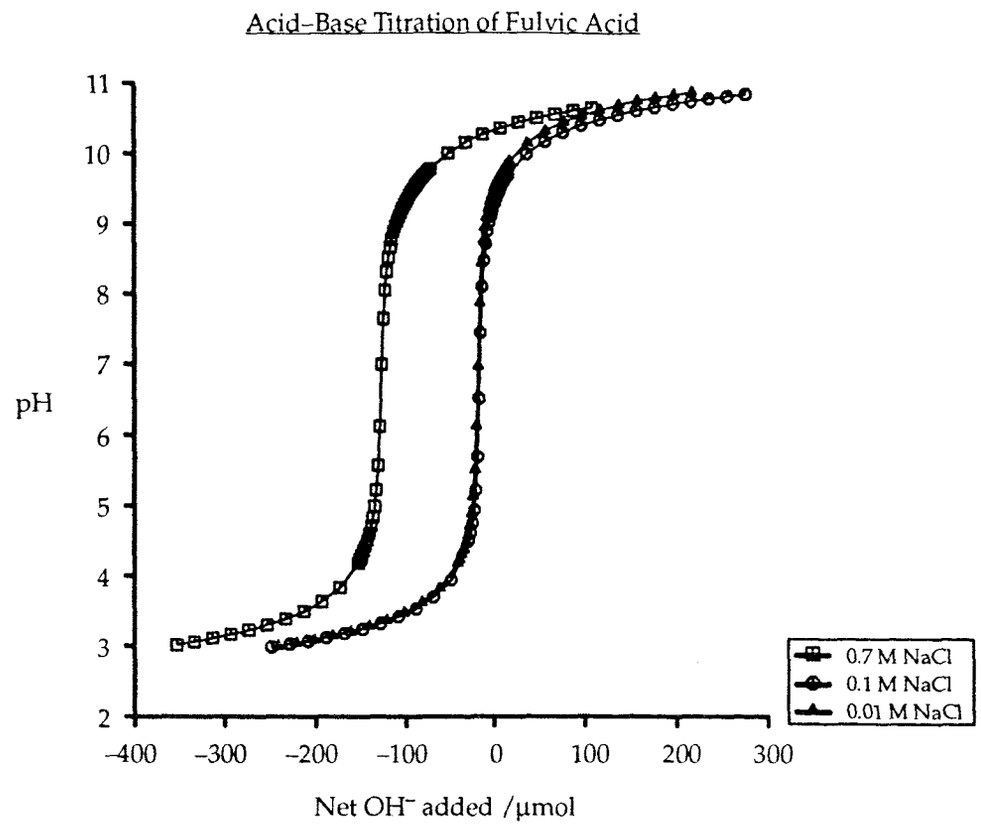

Figure 4.1 Titration data (pH vs net base added) for Tamar River fulvic acid in NaCl solutions of various ionic strengths.

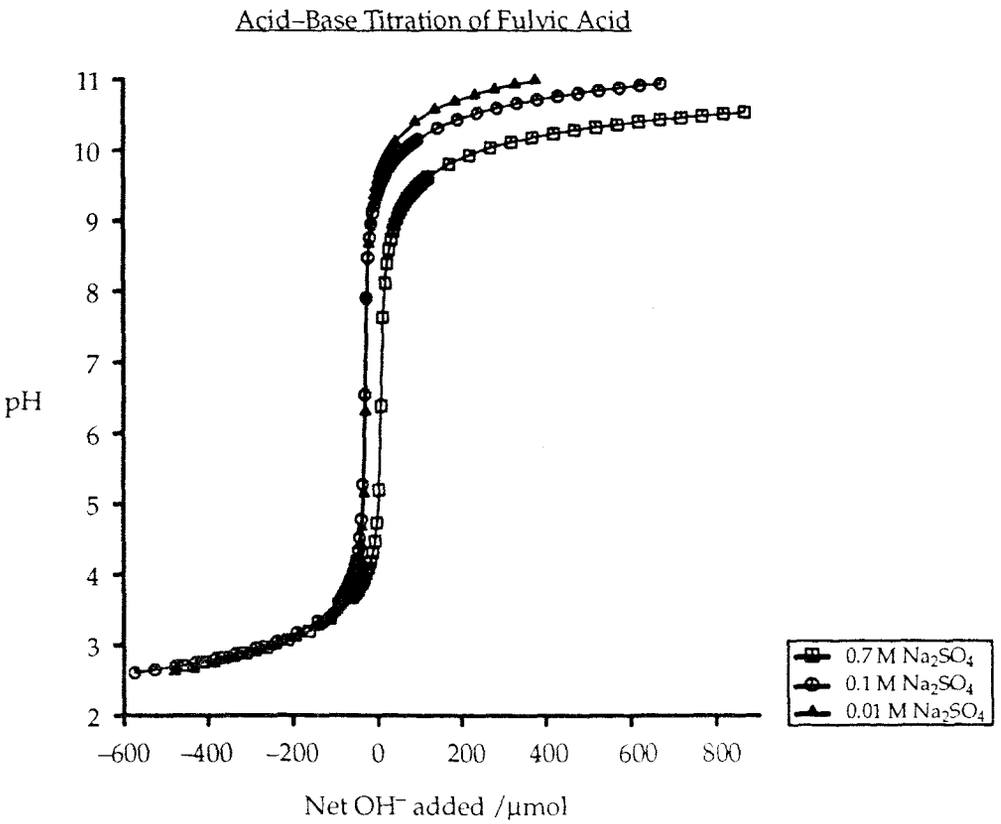

Figure 4.2 Titration data (pH vs net base added) for Tamar River fulvic acid in Na_2SO_4 solutions of various ionic strengths.

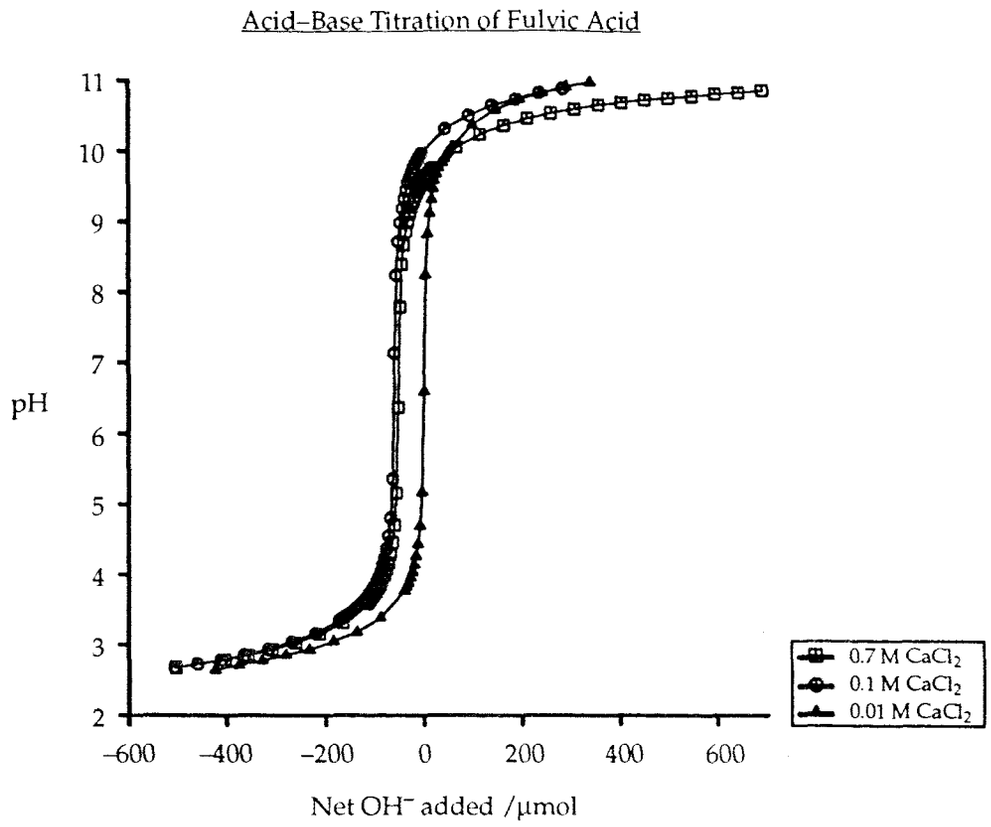

Figure 4.3 Titration data (pH vs net base added) for Tamar River fulvic acid in $CaCl_2$ solutions of various ionic strengths.

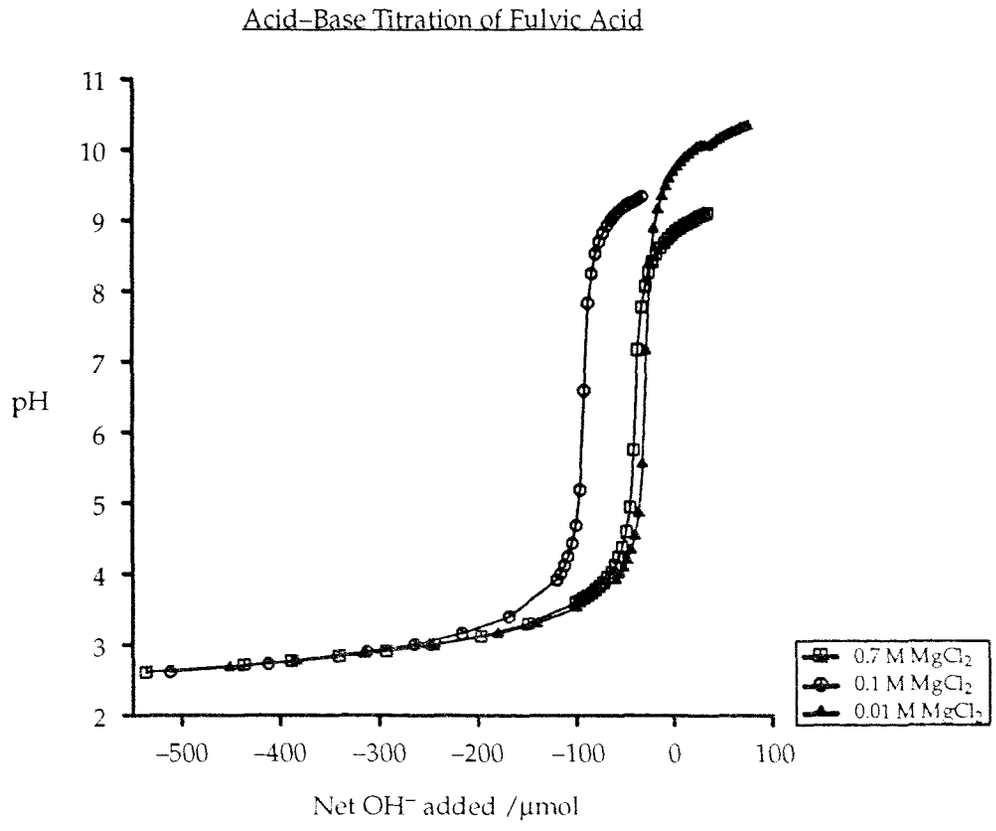

Figure 4.4 Titration data (pH vs net base added) for Tamar River fulvic acid in $MgCl_2$ solutions of various ionic strengths.

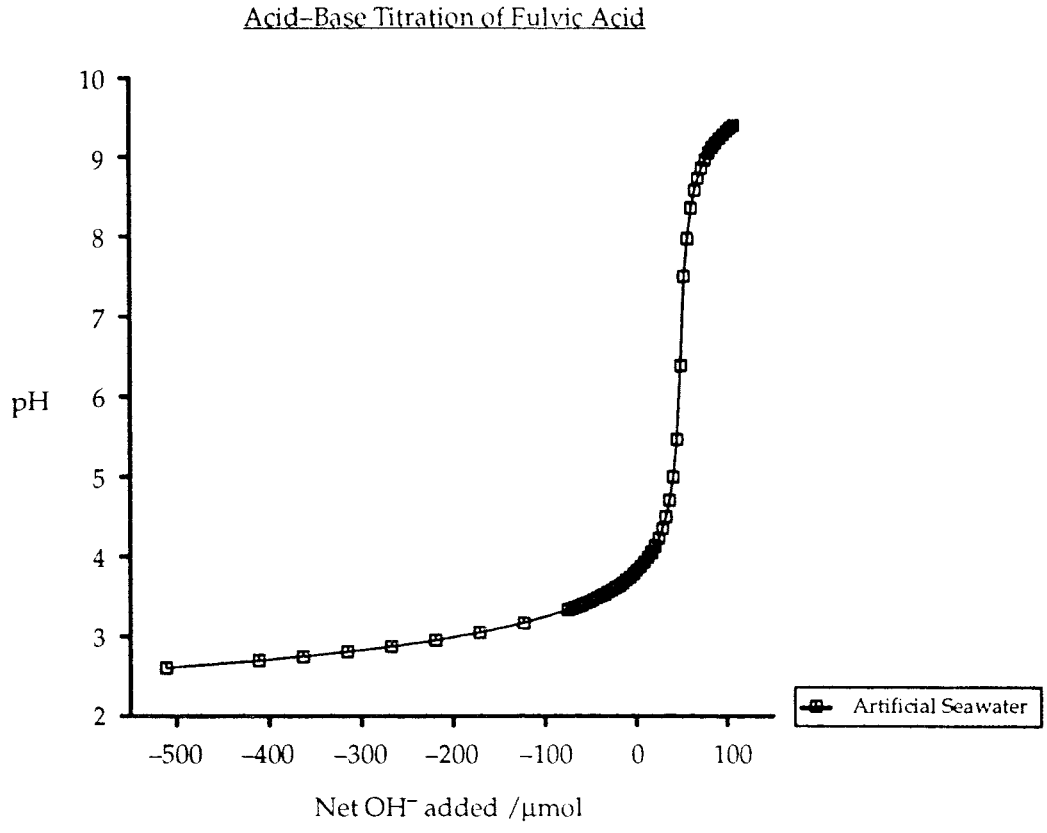

Figure 4.5 Titration data (pH vs net base added) for Tamar River fulvic acid in artificial seawater solution.

4.3 Formation Function

4.3.1 Introduction

The titration data presented in Section 4.2 were transformed into relative formation functions (δn_{OH}') using Eqn. 3.8.3 of Section 3.7.2. (The use of a titration data point to provide a zero for the formation function results in a relative function only and δn_{OH}' does not necessarily reflect the absolute charge on the substrate). Initially a data point from the neutralisation region of each titration was selected to be the reference point (i.e. δn_{OH}' = 0) of the plots.

This approach, however, causes problems when comparing formation function plots from different experiments. The fact that no two experiments had data points with exactly the same pH value (and hence δn_{OH}') compounded the problem of no point of the titration curves being linked to a defined state of the fulvic acid (i.e. pH_{PZC}, Section 4.2.1), so that the values of δn_{OH}' for a given experiment bore little relation to those of any other experiment. Comparisons of the formation functions of different experiments are best achieved using absolute values rather than relative ones.

Despite the relative nature of the curves, it was found that the forms of the formation function plots were constant irrespective of which data point was chosen as the reference.

Also, all of the formation function plots had an inflection point within the pH range 6.0 – 7.5 (See Figures 4.9 – 4.13).

4.3.2 Calculation of Absolute Formation Functions

The pH of fulvic acid solutions to which no acid or base have been added can be used to calculate an absolute formation function for that pH (De Wit *et al.*, 1990). This is accomplished by assuming that charge develops on the fulvic acid as a result of the dissociation of protonated and metal–bound functional groups. (In this case protons, sodium and calcium are assumed to make a significant contribution to charge development (Section 4.2.2)).

Thus, the concentration of fulvic acid charge at this pH ($[FA^-]$) can be calculated using Eqn. 4.3.1.

$$[FA^-] = [H^+] + [Na^+] + 2[Ca^{2+}] - [OH^-] - [X^-] \qquad (4.3.1)$$

where the proton and hydroxyl ion concentrations ($[H^+]$ & $[OH^-]$) are calculated from the initial solution pH (pH_i) and $[X^-]$ is the residual acid concentration of the solution (H_{init}). $[Na^+]$ and $[Ca^{2+}]$ are calculated from the sodium and calcium contents of the fulvic acid and $[FA^-]$ is related to the formation function by Eqn. 4.3.2.

$$\delta n_{OH}(pH_i) = [FA^-]V_0 / m_s \qquad (4.3.2)$$

Although initial pH values are not available for the titrations examined in this section, such data is available for a replicate fulvic acid titration (NA7F1CD). Diluted stock solution pH values may also be used to provide an estimate of titration solution initial pH values.

Figures 4.6 & 4.7 show formation functions for fulvic acid titrations carried out in 0.7M NaCl solutions. These have been calculated using Eqn. 3.8.3 and corrected using Eqns. 4.3.1 & 4.3.2. Figure 4.6 shows the formation function for experiment NA7F1CD corrected using its initial solution pH, while Figure 4.7 shows formation functions for all of the experiments using diluted stock solution pH values to calculate $[H^+]$ and $[OH^-]$ in Eqn. 4.3.1.

The curves of Figures 4.6 & 4.7 are quite similar in form and magnitude, although δn_{OH} for experiment NA7F5 is approximately 0.5 $mmol.g^{-1}$ greater than for the other experiments over most of the pH range of Figure 4.7. The magnitude of δn_{OH} for experiment NA7F1CD is very similar in both of the plots (δn_{OH} values for corresponding data points being offset from one another by 0.042 $mmol.g^{-1}$).

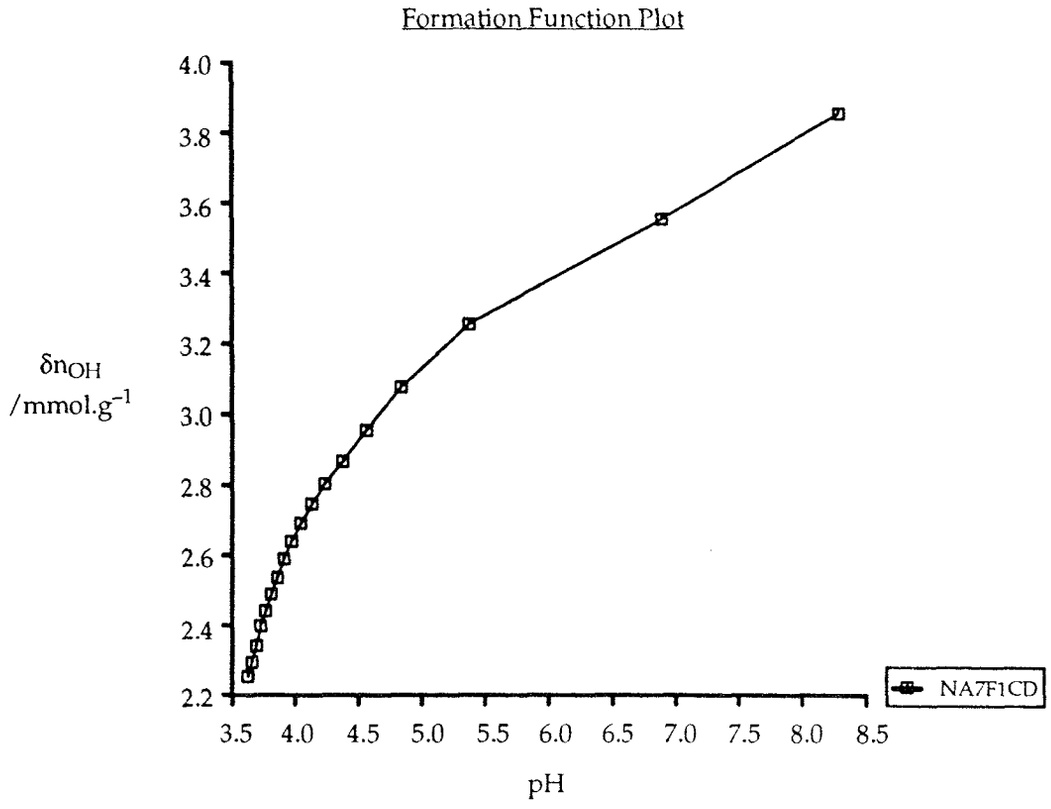

Figure 4.6 Formation function plot for experiment NA7F1CD, corrected to absolute values using its initial solution pH.

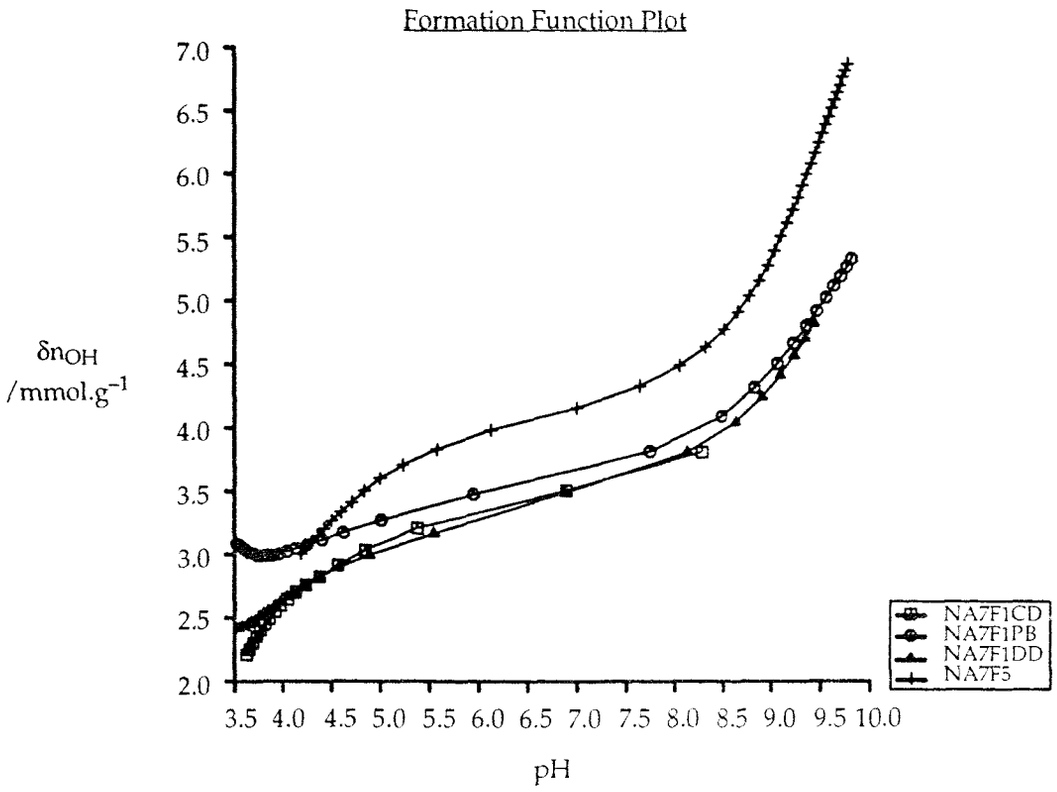

Figure 4.7 Formation function plot for titrations of Tamar River fulvic acid in 0.7M NaCl solutions, corrected to absolute values using diluted stock solution pH values.

4.3.3 Inflection Point

The inflection point on the formation function curves, noted in Section 4.3.1, can be thought of as marking the boundary between the titration of two distinct sets of fulvic acid functional groups. These are probably the (strongly acidic) carboxylic acid and (weakly acidic) phenolic hydroxyl groups proposed for humic substances (Schnitzer & Khan, 1972). As such, the inflection point of each curve should mark a point of common charge among the titrations, i.e. where carboxylic acid sites are deprotonated and phenolic hydroxyl sites are not.

In practice there may be a small amount of dissociation of non – carboxylic acid groups below the inflection point if this is located much above pH 6 (Cabaniss, 1991). However, the use of separate experiments to determine carboxyl acidity (e.g. CaOAc titrations, ^{13}C – NMR) also leads to problems of interference (Dempsey, 1981; Perdue, 1985).

This then provides a means of adjusting all of the formation function curves for fulvic acid to absolute values, by calculation of an absolute charge for the inflection point and determination of the pH at which it occurs in each experiment.

The use of the inflection point in this way also avoids the arbitrary assignment of some pH value to mark the carboxylic – phenolic boundary which has been attempted by some other workers (e.g. Davis, 1982). A formation function differentiation technique has been found to be the least error prone of a number of means of determining carboxyl acidity from potentiometric data (Cabaniss, 1991).

4.3.3.1 Determination of Inflection Point pH

In order to use the inflection point as the reference point for the formation function it was necessary to determine the pH at which it occurred (pH_{infl}) in each experiment. This was achieved by use of NAG subroutines to fit a spline to each of the δn_{OH} vs pH curves (subroutine E01BAF) and then to calculate the first and second derivatives of this spline (subroutine E02BCF). The inflection point in the δn_{OH} curve appears as a minimum in a plot of its first derivative and is identified by the point at which the second derivative is equal to zero. Figure 4.8 shows the spline fitted to the formation function calculated for the 0.7M NaCl experiment and its first and second derivatives.

The values of pH_{infl} determined for the fulvic acid titrations are shown in Table 4.4. As expected for a polyelectrolyte (Section 1.3.1.1), pH_{infl} increases with decreasing ionic strength for all of the salts studied.

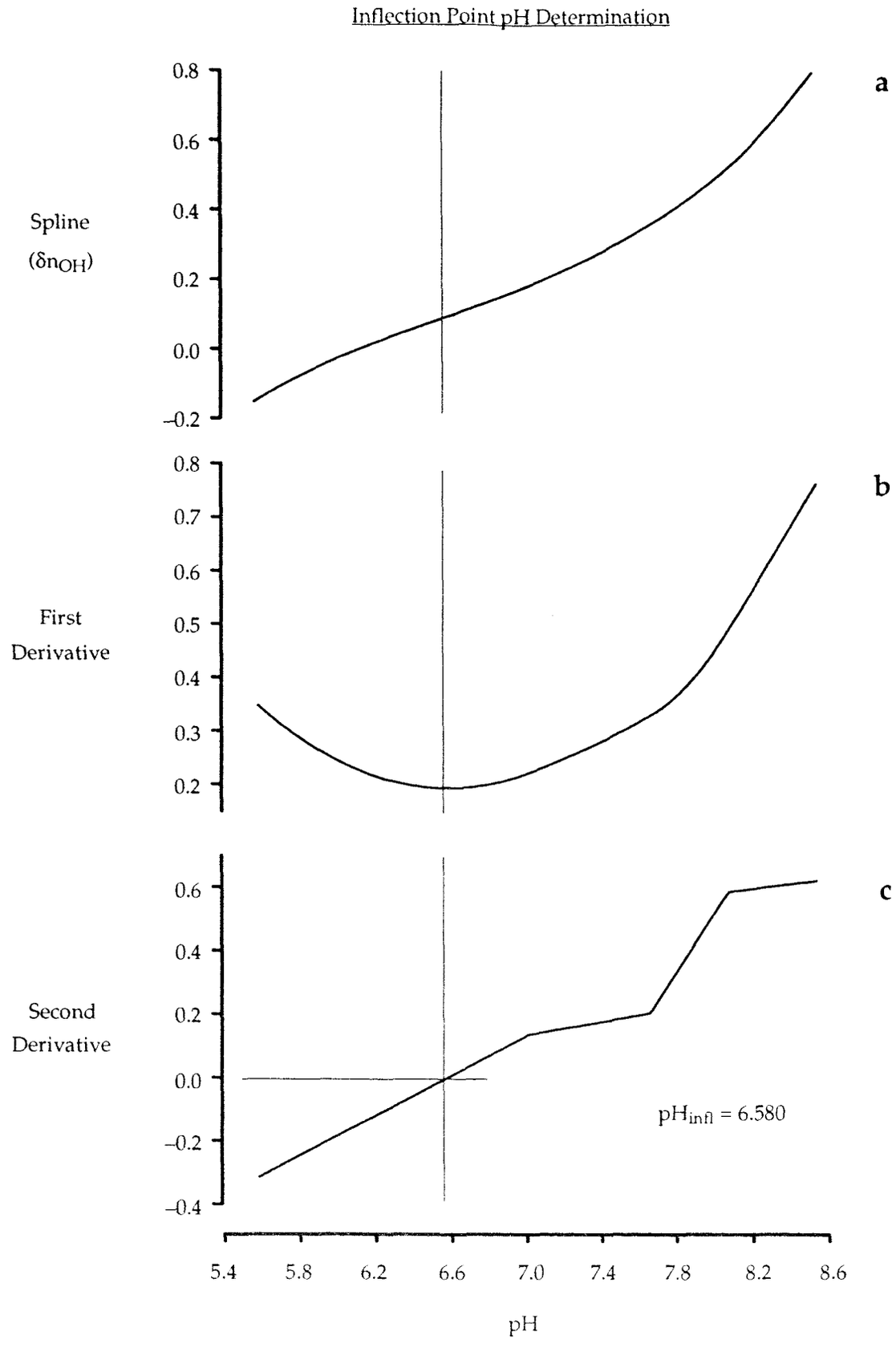

Figure 4.8 Determination of pH_{infl} for fulvic acid titration carried out in 0.7M NaCl solution. A spline function (**a**) has been fitted to the formation function curve and its first (**b**) and second (**c**) derivatives calculated.

Table 4.4 Inflection point pH values (pH_{infl}) for fulvic acid titrations carried out in simple salt solutions at various ionic strengths and artificial seawater.

Solution	Ionic Strength ($mol.l^{-1}$)		
	0.7	**0.1**	**0.01**
NaCl	6.580	6.934	7.321
Na_2SO_4	6.368	6.584	6.671
$CaCl_2$	6.259	6.379	6.762
$MgCl_2$	6.012	6.422	6.869
Artificial Seawater	6.185	(Ionic strength 0.726 $mol.l^{-1}$)	

4.3.3.2 Determination of Inflection Point Charge

It has been reported that the titration curves of fulvic acid in high ionic strength solutions (1M and 5M $NaNO_3$) vary little from one another (Ephraim *et al.*, 1986), 1M solutions being suggested as the upper limit of ionic strength effects on titration curves (Ephraim *et al.*, 1989). This implies that the charge on the fulvic acid at the inflection point of the formation function is best determined from titration curves in the highest available ionic strength solution.

This parameter has therefore been determined from the absolute formation function plots obtained for titrations in 0.7M NaCl solutions (Figures 4.6 & 4.7, Section 4.3.2). The value of the formation functions of experiments NA7F1CD, NA7F1PB and NA7F1DD at the inflection point pH for this solution (pH 6.580, Section 4.3.3.1) in Figures 4.6 & 4.7 is ~3.5 $mmol.g^{-1}$.

4.3.4 Corrected Formation Function

Formation functions referenced to their inflection points were calculated by a two stage process. Firstly a formation function was calculated using Eqn. 3.8.3 as before, choosing a reference point whose pH was as close to pH_{infl} as possible. A spline was then fitted to this formation function which was used to determine the value of δn_{OH} at pH_{infl} (subroutine E02BBF) and this value was used as an offset for the δn_{OH} curve so that $\delta n_{OH}(pH_{infl}) = 3.5$ $mmol.g^{-1}$. This correction procedure was made necessary by the lack of initial pH data for most of the fulvic acid titrations and by the alkaline form of the sample used.

Corrected formation function plots for NaCl, Na_2SO_4, $CaCl_2$, $MgCl_2$ and artificial seawater solutions are shown in Figures 4.9 – 4.13. As indicated in Section 4.2.1, these plots show that, for a given pH range, the greatest number of fulvic acid functional groups

are titrated in the highest ionic strength solutions. E.g. for NaCl solutions over the pH range 4.0 – 9.5 (Figure 4.9) the changes in formation function ($\Delta\delta n_{OH}$) are 4 mmol.g^{-1} (0.7M), 2.25 mmol.g^{-1} (0.1M) and 2 mmol.g^{-1} (0.01M).

The greatest value of the formation function in Figures 4.9 – 4.13 can be taken as an estimate of the total acidity of the Tamar River fulvic acid sample. Figure 4.9 shows this value to be ~6.5 mmol.g^{-1}, which is in very good agreement with the total acidity reported for this sample in 0.1M $NaClO_4$ solution (6.5 mmol.g^{-1}, Varney, 1982). It is also within the range of total acidities reported for other aquatic fulvic acid samples, e.g. 3.95 – 4.15 mmol.g^{-1} (Paxéus *et al.*, 1983) and 15 mmol.g^{-1} (TOC) (Dempsey & O'Melia, 1983).

Figure 4.14 shows formation function curves reported for an aquatic fulvic acid fraction at several ionic strengths of KCl (Dempsey & O'Melia, 1983). These curves are qualitatively similar to those of Figures 4.9 – 4.12, with curves at different ionic strengths displaced along the x–axis, except at very low and high pH values, where the Tamar River curves tend to overlap. This overlapping is presumably a consequence of the low fulvic acid concentration used in this study.

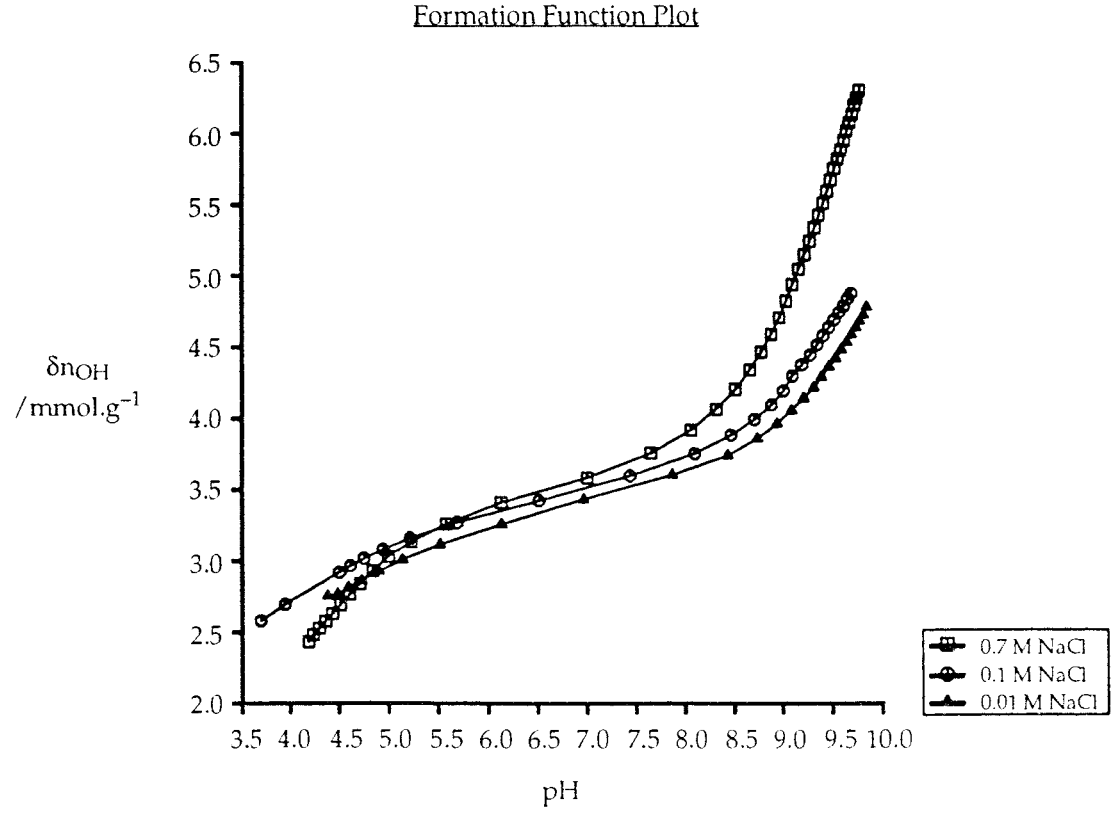

Figure 4.9 Plot of corrected formation function (δn_{OH}) against pH for Tamar River fulvic acid in NaCl solutions.

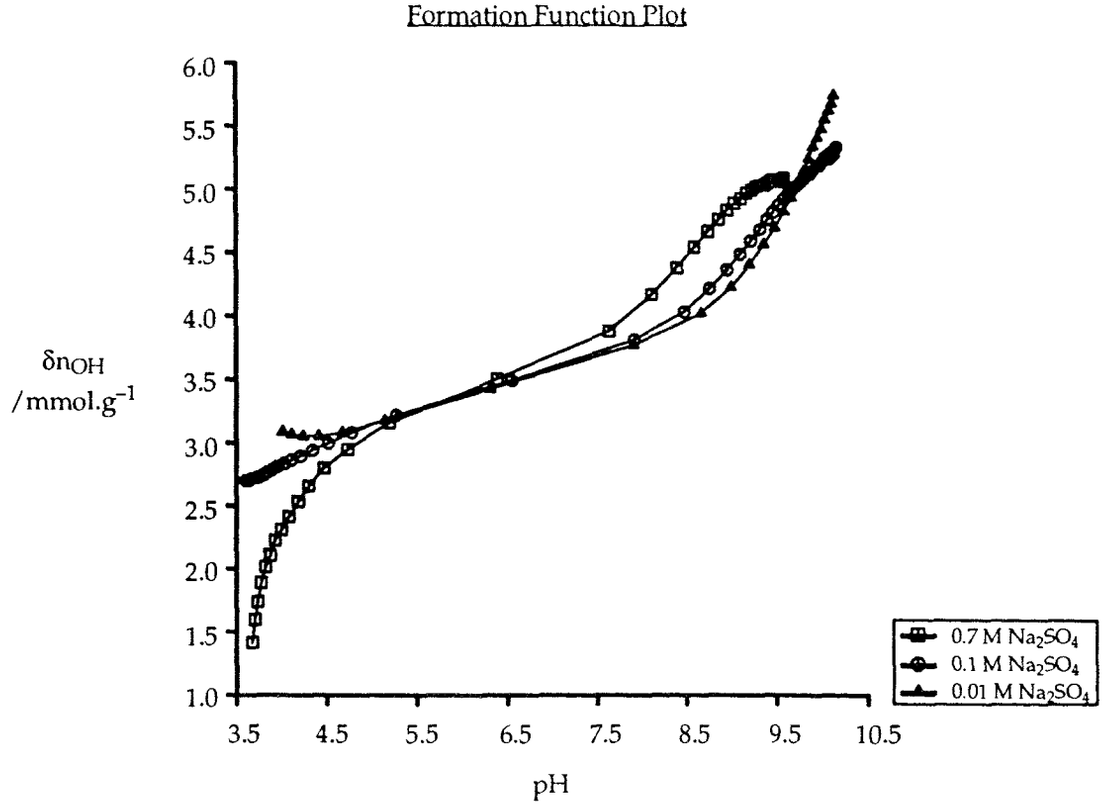

Figure 4.10 Plot of corrected formation function (δn_{OH}) against pH for Tamar River fulvic acid in Na_2SO_4 solutions.

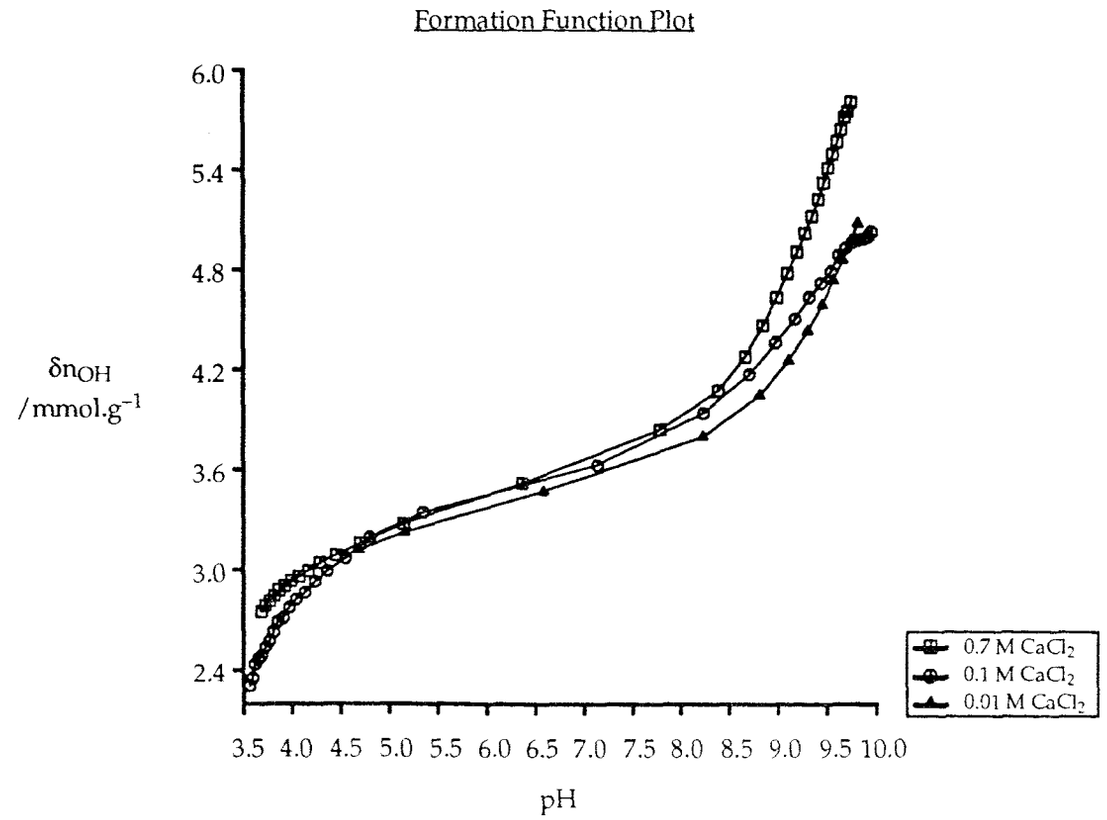

Figure 4.11 Plot of corrected formation function (δn_{OH}) against pH for Tamar River fulvic acid in $CaCl_2$ solutions.

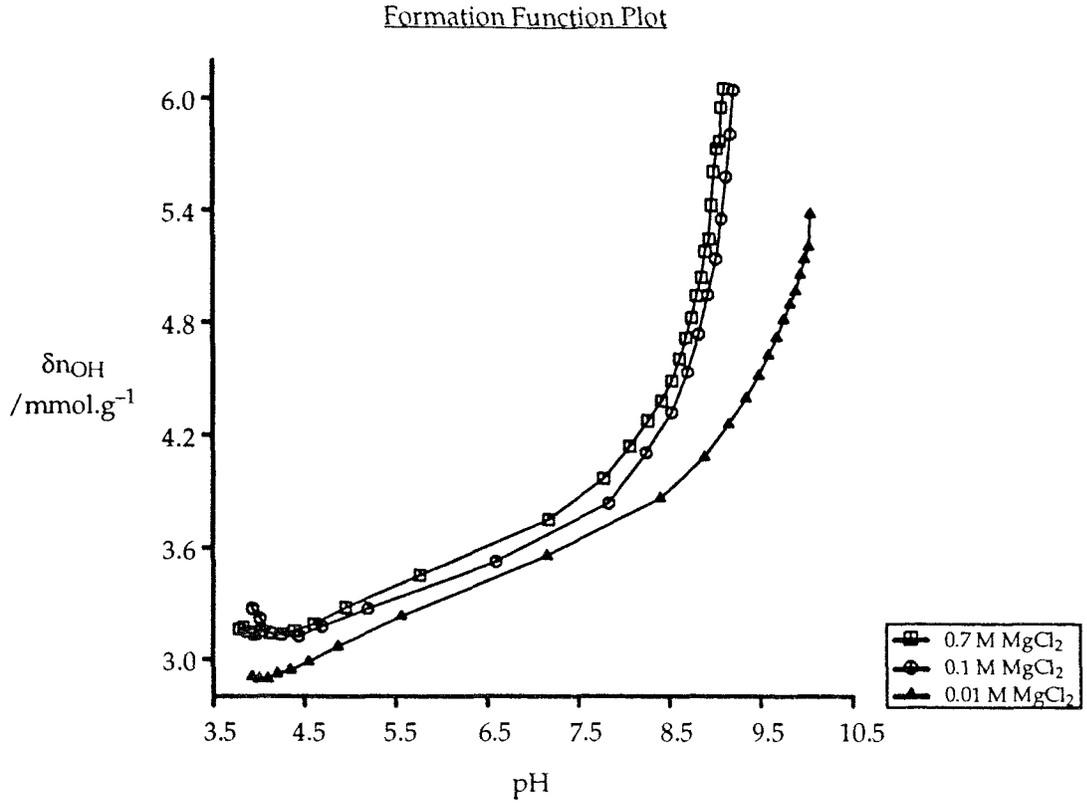

Figure 4.12 Plot of corrected formation function (δn_{OH}) against pH for Tamar River fulvic acid in $MgCl_2$ solutions.

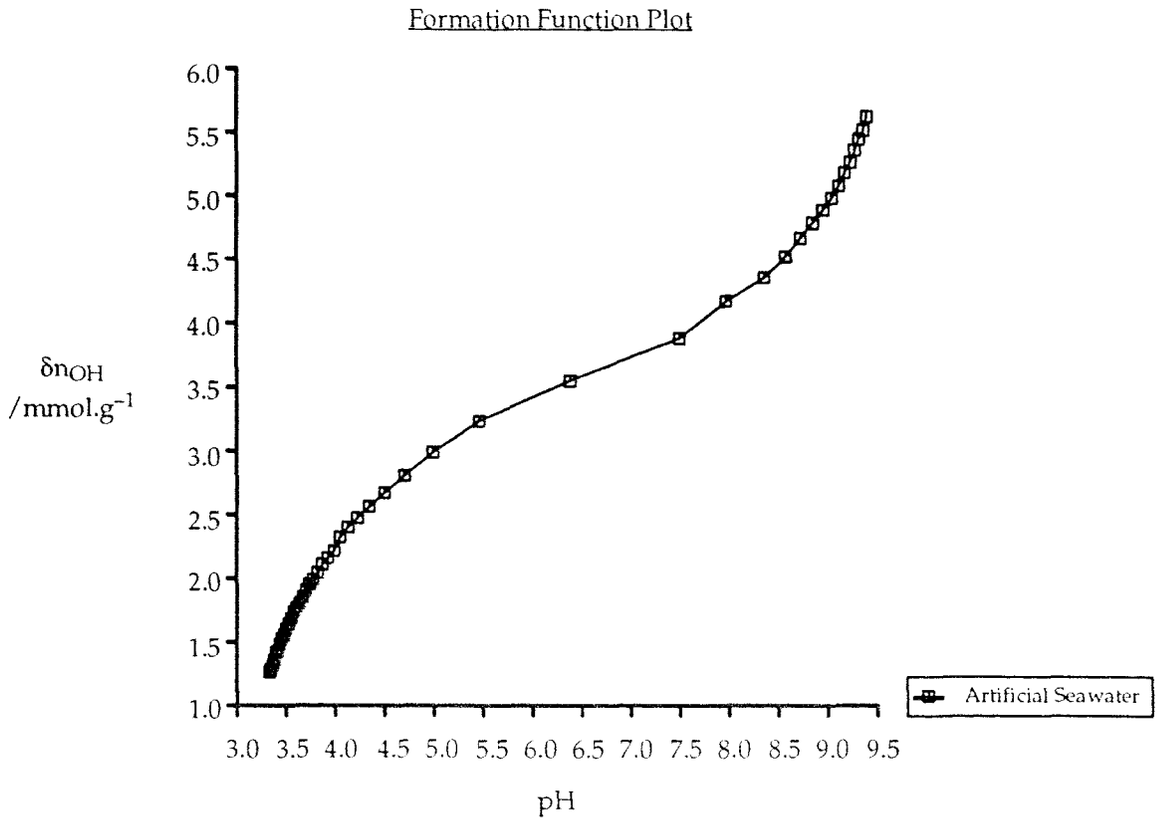

Figure 4.13 Plot of corrected formation function (δn_{OH}) against pH for Tamar River fulvic acid in artificial seawater solution.

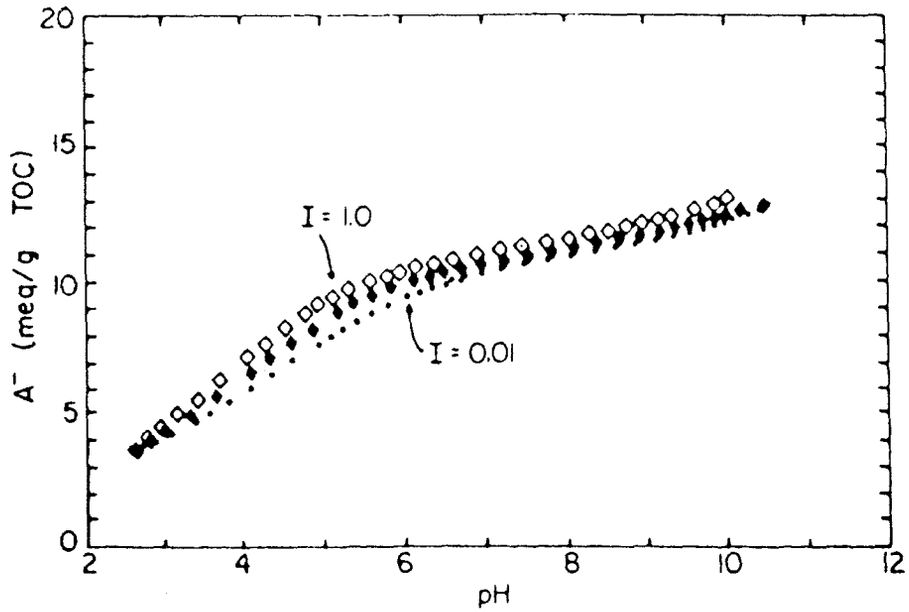

Figure 4.14 Formation function (A^-) for an aquatic fulvic acid fraction in KCl solutions at ionic strengths of 1.0M, 0.1M & 0.01M. (Reproduced with permission from Dempsey & O'Melia, 1983).

5. FULVIC ACID: POLYELECTROLYTE GEL ANALYSIS

5.1 Introduction

As stated in Section 2.4, the polyelectrolyte gel analysis of Marinsky and co–workers consists of a diagnostic test for the invasion of salt ions into a substrate matrix, together with a model capable of describing such salt ion invasion (Marinsky, 1985). The diagnostic section of this analysis (Section 2.4.2) is based on plots of the Henderson–Hasselbalch pK (pK_{HH}, Eqn. 2.4.1) against pH or against pH+pX (where X is the electrolyte anion). For salt ion permeable substrates, plots of pK_{HH} vs pH+pX at different ionic strengths coincide, while for salt ion impermeable substrates coincidence of different ionic strength data is achieved by plotting pK_{HH} vs pH (Marinsky, 1985). Thus, for a given electrolyte salt, Marinsky's analysis predicts that either the 'pK_{HH} vs pH' or 'pK_{HH} vs pH+pX' plots for different ionic strengths will produce a series of coincident lines, while the lines of the other plot will be displaced from one another by one log unit for every ten fold change in ionic strength.

Where invasion of salt ions into the substrate matrix occurs (as indicated by the Henderson–Hasselbalch plots), a means of accounting for the effects of the resultant Donnan potential is proposed (Marinsky, 1985). Plots of the apparent stability constant (Eqn. 2.4.14) against the degree of dissociation of the substrate (α) can be extrapolated to $\alpha = 0$ to provide (ionic strength independent) intrinsic stability constants ($p\overline{K}_{HA}^{int}$).

(The equations presented in Section 2.4 have been derived for 1:1 electrolytes only (and specifically sodium salts in the case of Eqns. 2.4.12 – 2.4.14). The validity of applying them to other electrolytes (i.e. Na_2SO_4, Section 5.2) is discussed in Section 5.3.)

5.1.1 Determination of α

The degree of dissociation (α) of the fulvic acid sample can be calculated using the absolute formation functions for the titrations obtained in Section 4.3.4.

$$\alpha = \frac{\delta n_{OH}}{\delta n_{OH}^{max}} \qquad (5.1.1)$$

By using the absolute formation function, the lower dissociation limit ($\alpha = 0$) is implicitly defined by $\delta n_{OH} = 0$. The upper limit ($\alpha = 1$) is therefore defined by the value of δn_{OH}^{max}. This can take one of two values.

When carboxyl acidity only is considered, δn_{OH}^{max} takes the value of the absolute formation function at the titration curve inflection point (i.e. $\delta n_{OH}^{max} = 3.5$ mmol.g^{-1}), while the overall degree of dissociation of the FA is described by setting δn_{OH}^{max} equal to its total acidity (6.5 mmol.g^{-1}, see Section 4.3.4).

5.2 Permeability of Fulvic Acid to Salt Ions

The susceptibility of the Tamar River fulvic acid sample to invasion by salt ions was investigated by plots of pK_{HH} vs pH and pK_{HH} vs pH+pX. pK_{HH} was calculated for the

carboxylic acid sites of the fulvic acid only, as Eqn. 2.4.1 is valid for a single functional group type only. The results are shown in Figures 5.1 & 5.2 (NaCl), Figures 5.3 & 5.4 (Na_2SO_4), Figures 5.5 & 5.6 ($CaCl_2$) and Figures 5.7 & 5.8 ($MgCl_2$). (The data in Figures 5.1 – 5.8 have been plotted to slightly lower pH values than have been used elsewhere in this work. This has been done to give a wider range of α values for the carboxylic acid sites, but these extra data points are rather less accurate than those at higher pH values (Perdue, 1990)).

Comparison of each pair of "Permeability Test" and "Impermeability Test" plots (e.g. Figures 5.1 & 5.2) shows that the fulvic acid exhibits the behaviour of a salt ion impermeable substrate when the reactions of its carboxylic acid sites are examined. The pK_{HH} vs pH curves for each salt (Figures 5.1, 5.3, 5.5 & 5.7) broadly coincide with one another, while the pK_{HH} vs pH+pX curves are widely separated.

This behaviour is shown even more distinctly when a corresponding set of curves is generated using the overall degree of dissociation of the fulvic acid to calculate pK_{HH} (although Eqn. 2.4.1 is not strictly valid in this case). Figures 5.9 & 5.10, which have been calculated for NaCl solutions, are representative of the plots obtained for all of the experiments, and show an almost complete coincidence of the pK_{HH} vs pH curves and a separation of pK_{HH} vs pH+pX curves proportional to solution ionic strength.

It is therefore concluded from Figures 5.1 – 5.10 that the Tamar River fulvic acid is impermeable to Na^+, Ca^{2+} and Mg^{2+} ions. Calculation of stability constants corrected for the Donnan Potential (Eqn. 2.4.14) has not been carried out, since there should be no Donnan effect arising in this system.

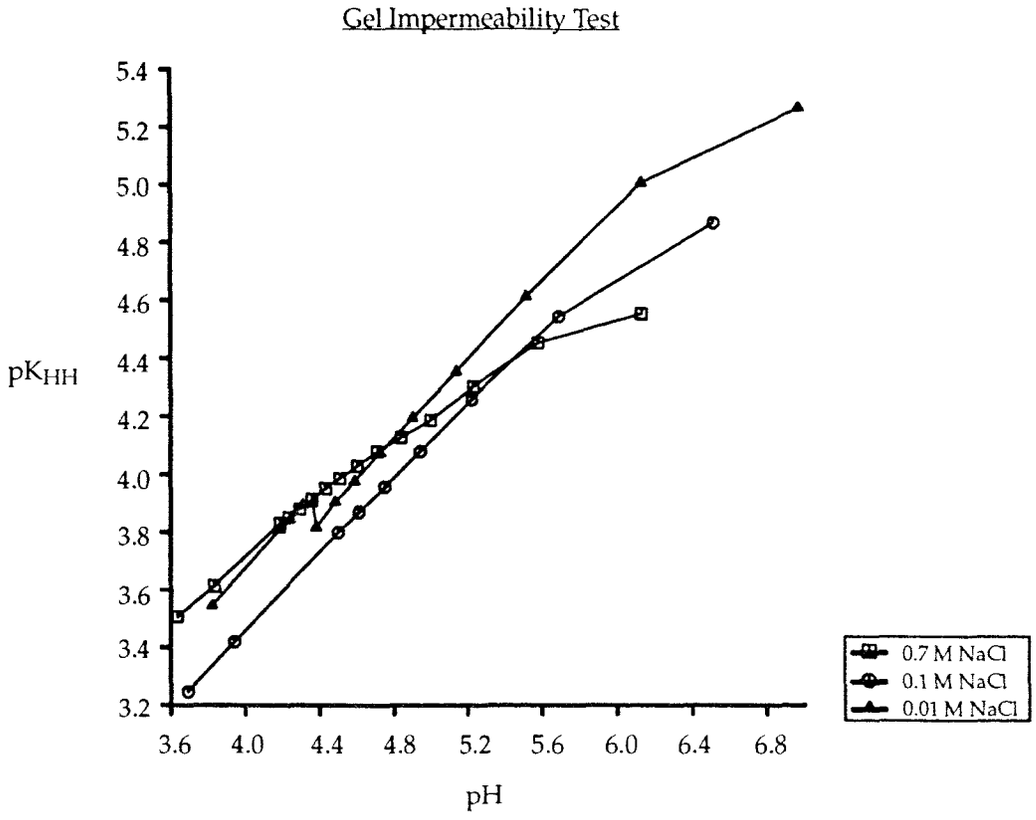

Figure 5.1 Plot to test for impermeability of Tamar River fulvic acid to Na^+ ions in NaCl solutions (carboxylic acid sites only).

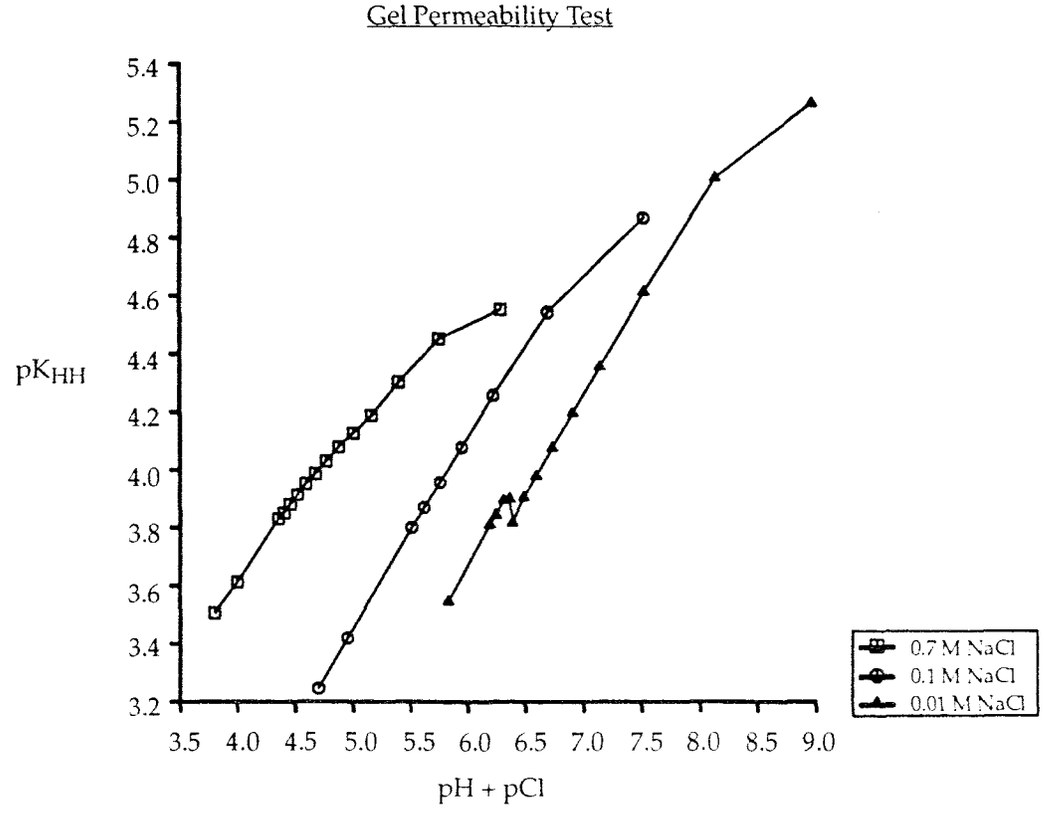

Figure 5.2 Plot to test for permeability of Tamar River fulvic acid to Na^+ ions in NaCl solutions (carboxylic acid sites only).

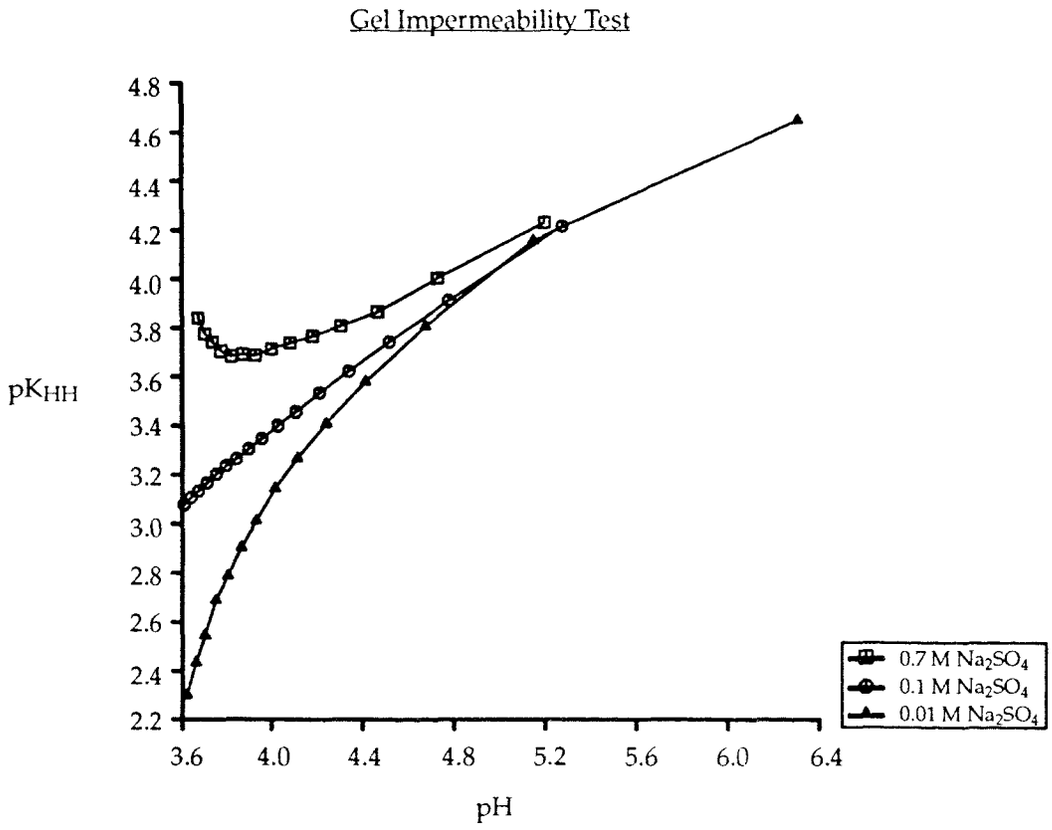

Figure 5.3 Plot to test for impermeability of Tamar River fulvic acid to Na^+ ions in Na_2SO_4 solutions (carboxylic acid sites only).

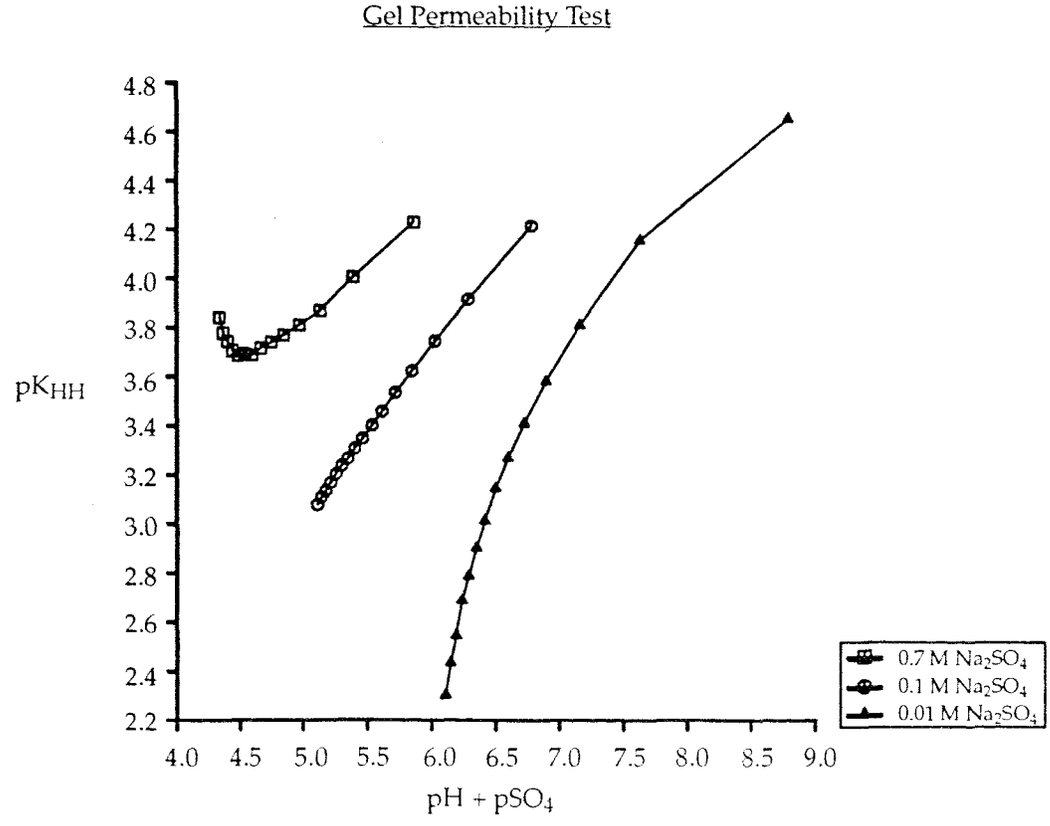

Figure 5.4 Plot to test for permeability of Tamar River fulvic acid to Na^+ ions in Na_2SO_4 solutions (carboxylic acid sites only).

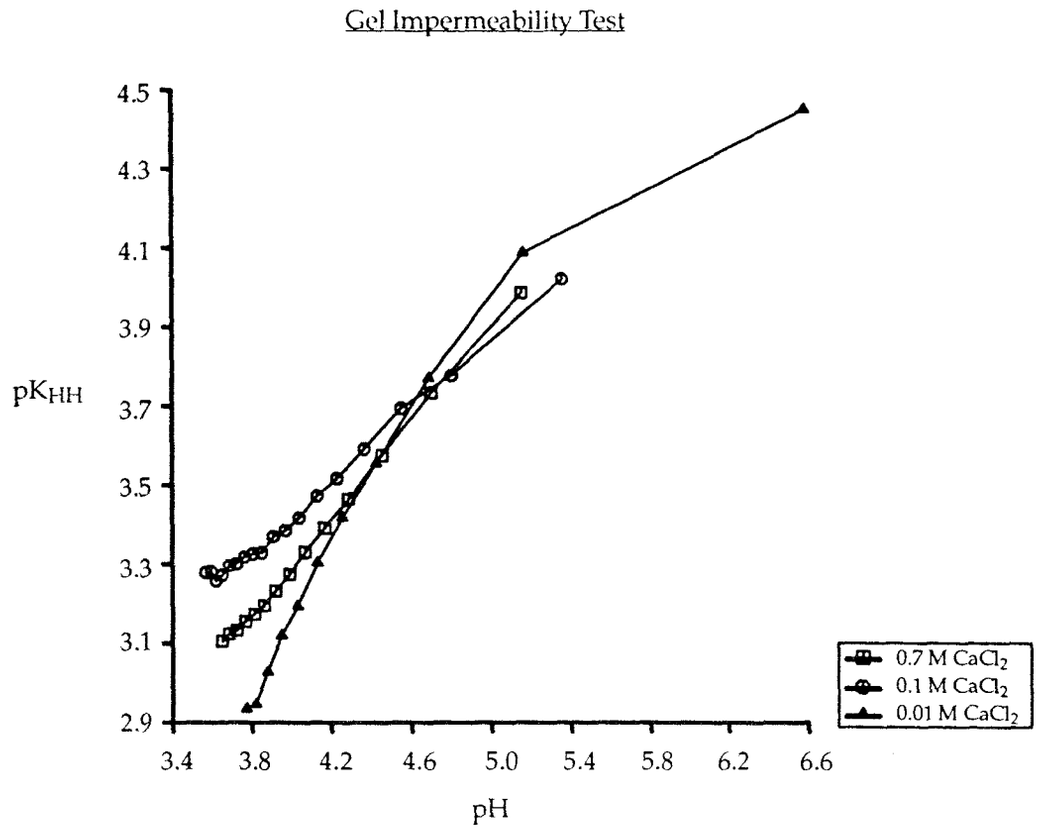

Figure 5.5 Plot to test for impermeability of Tamar River fulvic acid to Ca^{2+} ions in $CaCl_2$ solutions (carboxylic acid sites only).

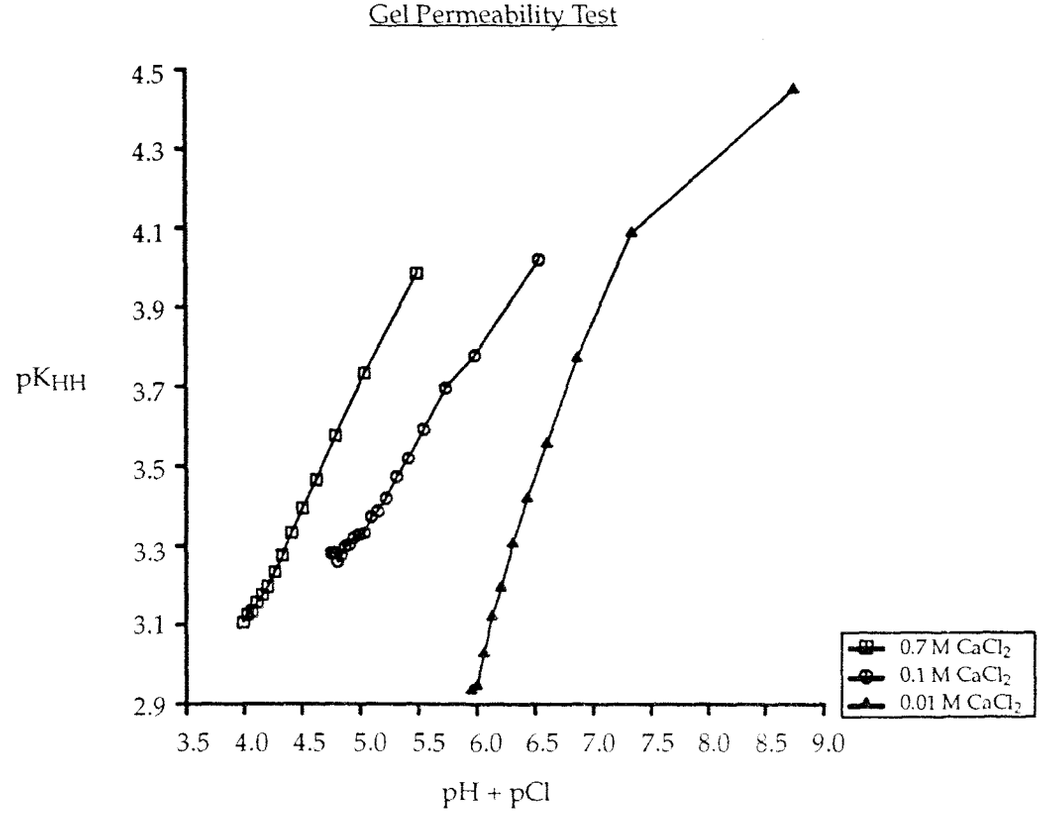

Figure 5.6 Plot to test for permeability of Tamar River fulvic acid to Ca^{2+} ions in $CaCl_2$ solutions (carboxylic acid sites only).

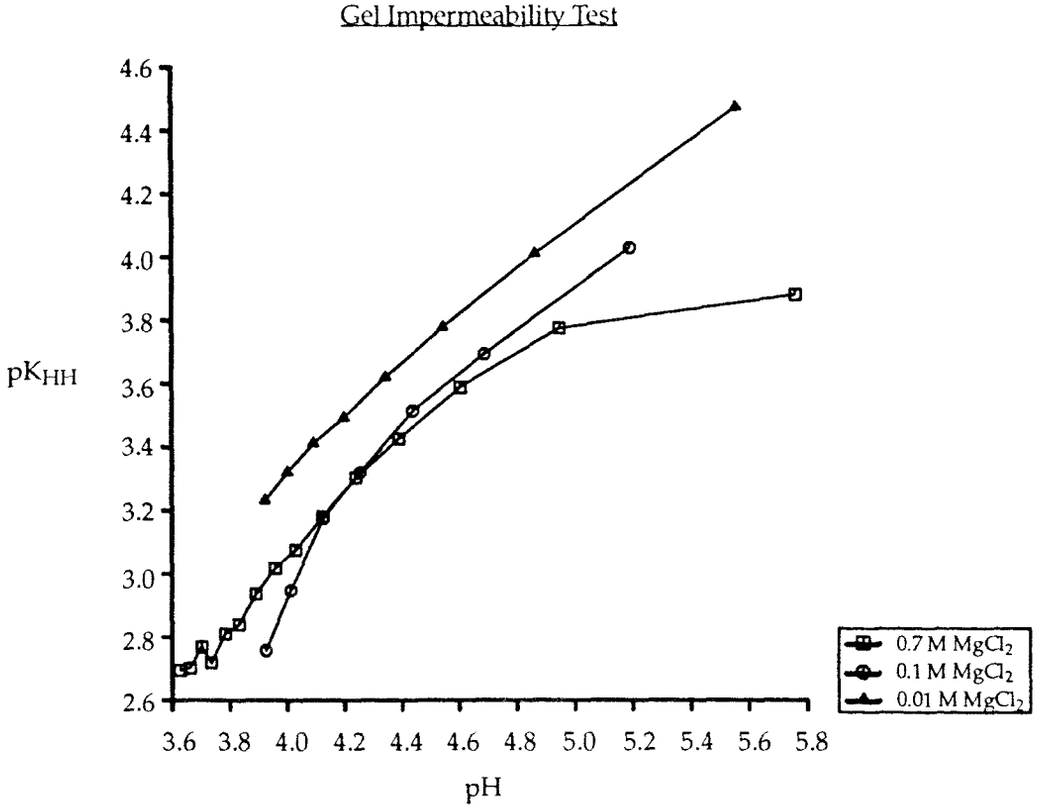

Figure 5.7 Plot to test for impermeability of Tamar River fulvic acid to Mg^{2+} ions in $MgCl_2$ solutions (carboxylic acid sites only).

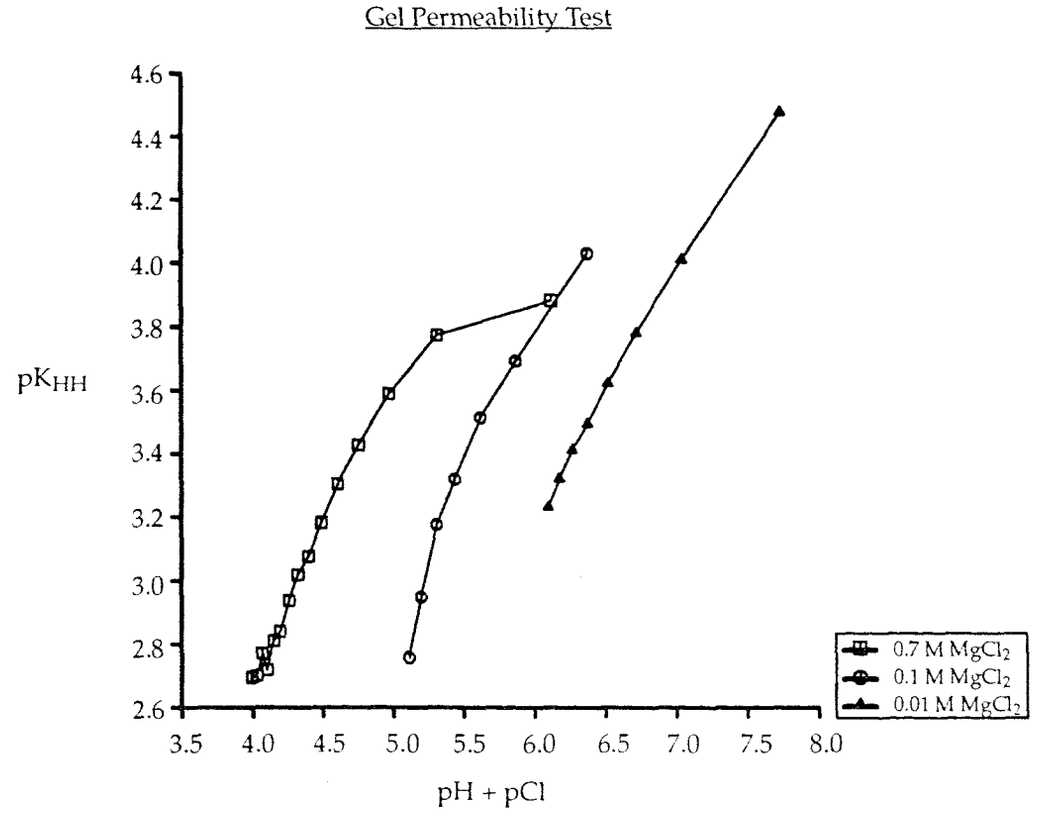

Figure 5.8 Plot to test for permeability of Tamar River fulvic acid to Mg^{2+} ions in $MgCl_2$ solutions (carboxylic acid sites only).

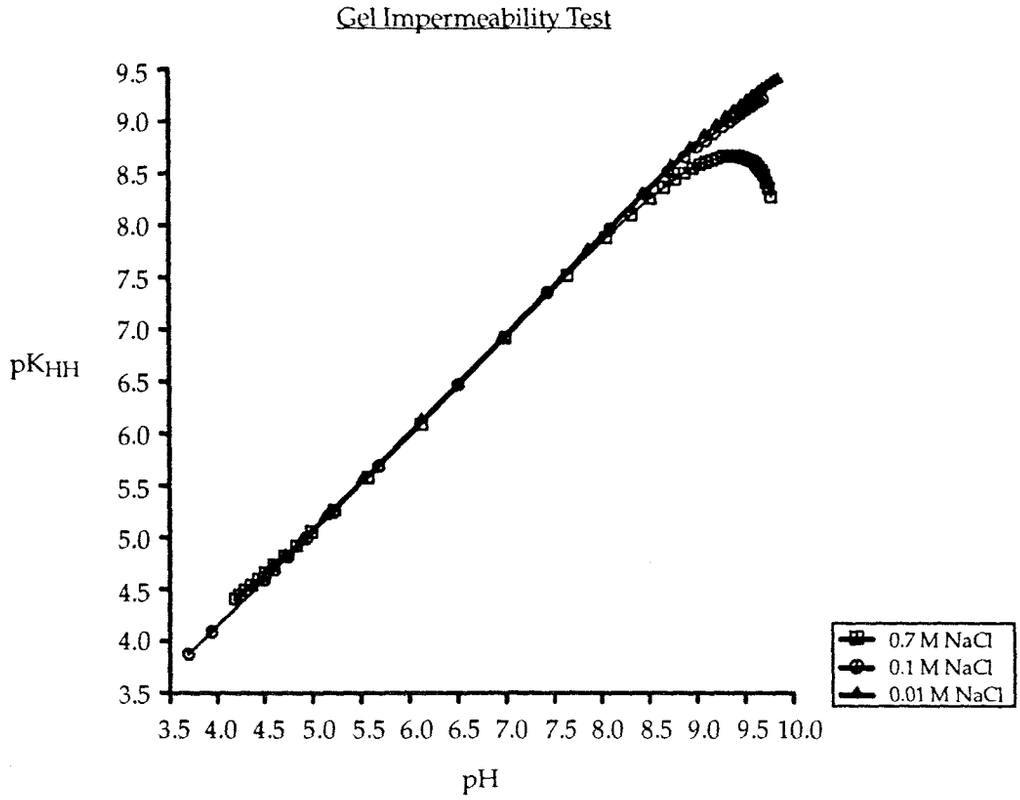

Figure 5.9 Plot to test for impermeability of Tamar River fulvic acid to Na^+ ions in NaCl solutions (all sites).

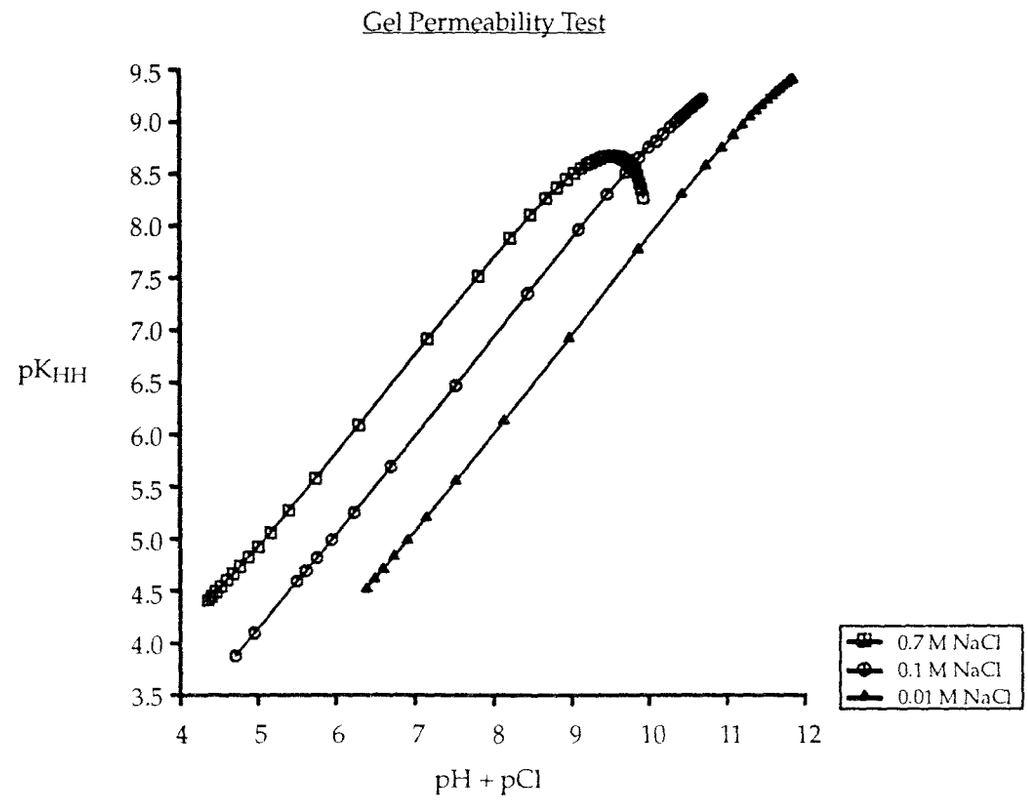

Figure 5.10 Plot to test for permeability of Tamar River fulvic acid to Na^+ ions in NaCl solutions (all sites).

5.3 Discussion

Figure 5.11 shows "Impermeability Test" and "Permeability Test" plots for a Suwannee River fulvic acid sample titrated in KNO_3 solutions (Ephraim *et al.*, 1986). These plots were taken to provide unambiguous proof that the sample existed in aqueous medium as a rigid, impermeable polymer by Ephraim and his co–workers.

There is a great deal of similarity between the plots of Figure 5.11 and those presented for the Tamar River sample (Figures 5.1 – 5.8), suggesting that this too has a rigid, impermeable structure. Gel filtration chromatography results for the Tamar River sample (Table 1.3) indicate that it undergoes a significant size change in the pH range 2.15 – 4.00. This is not, however, reflected in the pK_{HH} vs pH of Figures 5.1, 5.3, 5.5 & 5.7 (which are predicted to diverge if molecular expansion occurs), since these plots cover only a small part of this pH range.

The equations proposed by Marinsky to form the diagnostic tests (Section 2.4.2) of the polyelectrolyte gel model are only derived for 1:1 electrolyte solutions (Marinsky, 1985). However, the diagnostic plots appear to be equally effective for symmetric and asymmetric electrolytes. In particular, there is no apparent difference in the "Permeability Test" plots generated for NaCl and Na_2SO_4 solutions (Figures 5.2 & 5.4), despite the different charges of the anions in these solutions.

It is not particularly surprising that the fulvic acid appears to be impermeable to electrolyte ions, since its molecules are extremely small when compared to the synthetic polymers for which the polyelectrolyte gel model was developed.

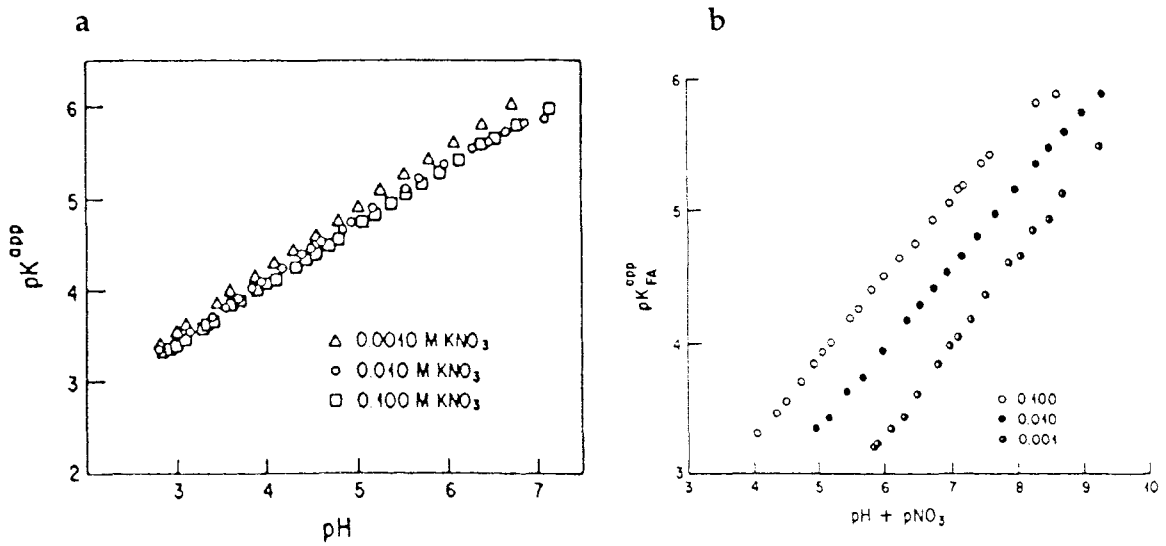

Figure 5.11 Impermeability Test (**a**) and Permeability Test (**b**) plots for Suwannee River fulvic acid. (Reprinted with permission from Ephraim *et al.*, 1986, Environ. Sci & Technol., 20, 354 – 366. Copyright (1986) American Chemical Society).

5.4 Conclusion

The results presented in Section 5.2 indicate that the Gel Invasion Analysis of Marinsky and co–workers is not applicable to the Tamar River fulvic acid sample used in this study.

The diagnostic plots presented in Section 5.2 exhibit the patterns predicted for substrates impermeable to the ions of the supporting electrolyte (Marinsky, 1985). This impermeability almost certainly arises as a result of the relatively small size of the fulvic acid molecules.

6. FULVIC ACID: GOUY CHAPMAN ANALYSIS

6.1 Introduction

The Gouy Chapman model (Section 2.2) has been used to describe surface charge development on humic substances (De Wit *et al.*, 1988; De Wit *et al.*, 1989). The model assumes that the charge on a fulvic acid molecule is stabilised by a diffuse layer of counterions in the solution around it (the distribution of the ions in the diffuse layer is described by the Poisson – Boltzmann equation).

The chemical conditions (i.e. aqueous phase concentrations) prevailing at the surface of the fulvic acid molecule can be calculated from bulk solution concentrations by taking the influence of the diffuse layer into account. The diffuse layer correction is dependent on the size of the molecule, large molecules ($r > 10nm$) are assumed to behave like planar surfaces (Eqn. 2.2.3, Section 2.2.2), while smaller molecules are assumed to be spherical (Eqn. 2.2.11, Section 2.2.3).

De Wit and co–workers propose that plots of the degree of protonation of a given site, i, on the substrate (θ_i) against its surface pH (pH_s) can be used to obtain intrinsic affinity constant ($\log_{10} K_{i,H}$) values. The molecular weight (M) of the substrate can be used as an adjustable parameter in the calculation of σ_0 (Eqns. 6.1.3 & 6.1.4) (and therefore θ_i (Eqn. 2.2.18)) in order to achieve coincidence of σ_0 (θ) vs pH_s curves for different ionic strength solutions and provide an unique value of $\log_{10} K_{i,H}$ (De Wit *et al.*, 1988; De Wit *et al.*, 1991a).

This approach is illustrated by use of the (highly simplified) assumption that the fulvic acid functional groups can be divided into only two site types (carboxylic and phenolic). These sites can be described by two degrees of protonation (θ_1 & θ_2) and two fractional abundances (f_1 & f_2). The fractional abundances of the carboxylic and phenolic sites can be estimated from the value of the formation function at pH_{infl} (3.5 $mmol.g^{-1}$) and the total acidity of the fulvic acid. ($f_1 = 3.5 / 6.5$, $f_2 = (6.5 - 3.5) / 6.5$). θ_1 and θ_2 can be calculated using rearrangements of Eqn. 2.2.18, assuming that for pH values below pH_{infl} the phenolic sites are completely protonated ($\theta_2 = 1$), and at pH_{infl} and above the carboxylic sites are completely deprotonated ($\theta_1 = 0$) (see Eqns. 6.1.1 & 6.1.2).

$$\theta_1 = 1 - \frac{|\sigma_0|}{f_1 D_s F} \qquad (6.1.1)$$

$$\theta_2 = 1 - \frac{1}{f_2}\left(\frac{|\sigma_0|}{D_s F} - f_1\right) \qquad (6.1.2)$$

6.1.1 Estimation of Fulvic Acid Surface Area

In order to calculate the charge density at the surface of the fulvic acid (σ_0), a value for its specific surface area (A) must be determined. However, the techniques available for

determination of surface areas of particulate samples (e.g. BET adsorption) are not applicable to fulvic acid, due to its organic nature and relatively small size.

The specific surface area of the Tamar River fulvic acid sample was therefore calculated by assuming it to be a sphere of radius r and molecular weight M (Eqn 6.1.3) (N is Avogadro's number).

$$A = \frac{4\pi r^2 N}{M} \qquad (6.1.3)$$

Calculation of A for σ_0 determination (e.g. Figures 6.1 – 6.5) was initially achieved by using Stokes' radius and molecular weight data at pH 1.15 (Varney, 1982 – see Section 1.5.1). The value obtained (~3500 m^2g^{-1}) is considerably larger than the values typically found experimentally for inorganic particles, ~100 m^2g^{-1}, as would be expected for smaller particles.

6.1.2 Surface Charge Correction

The surface charge on the fulvic acid at a given titration point can be calculated from the difference between the net number of moles of added acid and the net number of moles of free acid found in solution (Eqn. 6.1.4). (This is equivalent to the acid – base balance used to calculate the formation function (Eqn. 3.8.3), but is of opposite sign, since the formation function considers the consumption of hydroxyl ions, while surface charge is concerned with the production of charged sites (Eqn. 6.1.5)).

$$\sigma_0 = \frac{\{(H_a - H) - (OH_a - OH)\}F}{m_s A} \qquad (6.1.4)$$

$$\sigma_0 = \frac{-\delta n_{OH} F}{A} \qquad (6.1.5)$$

Correction of surface charge values was achieved, as for formation functions, by reference to the inflection point of the titration curves (see Sections 4.3.3 & 4.3.4). The surface charge on the fulvic acid at the inflection point was calculated from its equivalent formation function value (3.5 $mmol.g^{-1}$) using Eqn. 6.1.5.

Surface charge was calculated from experimental data using Eqn. 6.1.4 and a spline was then fitted to the experimental σ_0 – pH data, which was used to offset the surface charge values so that $\sigma_0(pH_{infl}) = -\{3.5F/A\}$ $\mu C.cm^{-2}$. The corrected surface charge values were then used to calculate pH_s according to the desired geometry (see Sections 6.2 & 6.3.1).

Plots of corrected surface charge (σ_0) vs pH for Tamar River fulvic acid in NaCl, Na_2SO_4, $CaCl_2$ and $MgCl_2$ solutions are shown in Figures 6.1 – 6.4. The effect of solution ionic strength on surface charge development, noted in Sections 4.2.1 and 4.3.4, can also be seen in these plots, with greater surface charges developing on the fulvic acid in the higher ionic strength solutions in each case.

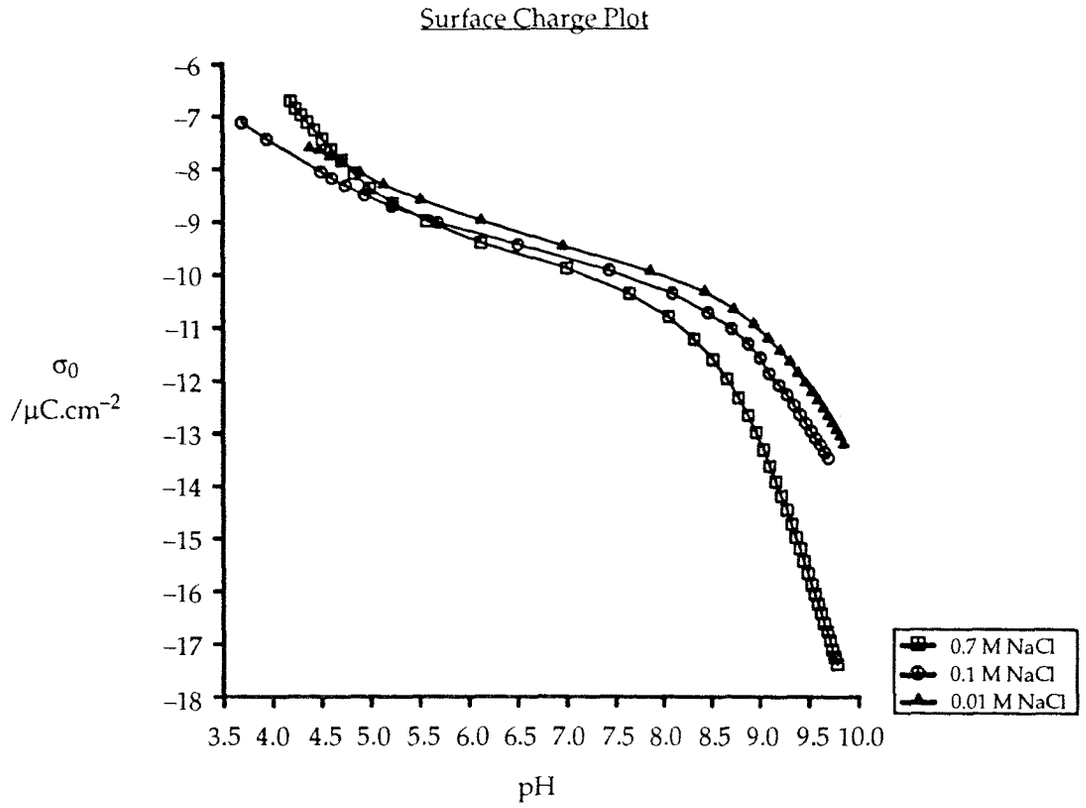

Figure 6.1 Plot of corrected surface charge (σ_0) against pH for Tamar River fulvic acid in NaCl solutions.

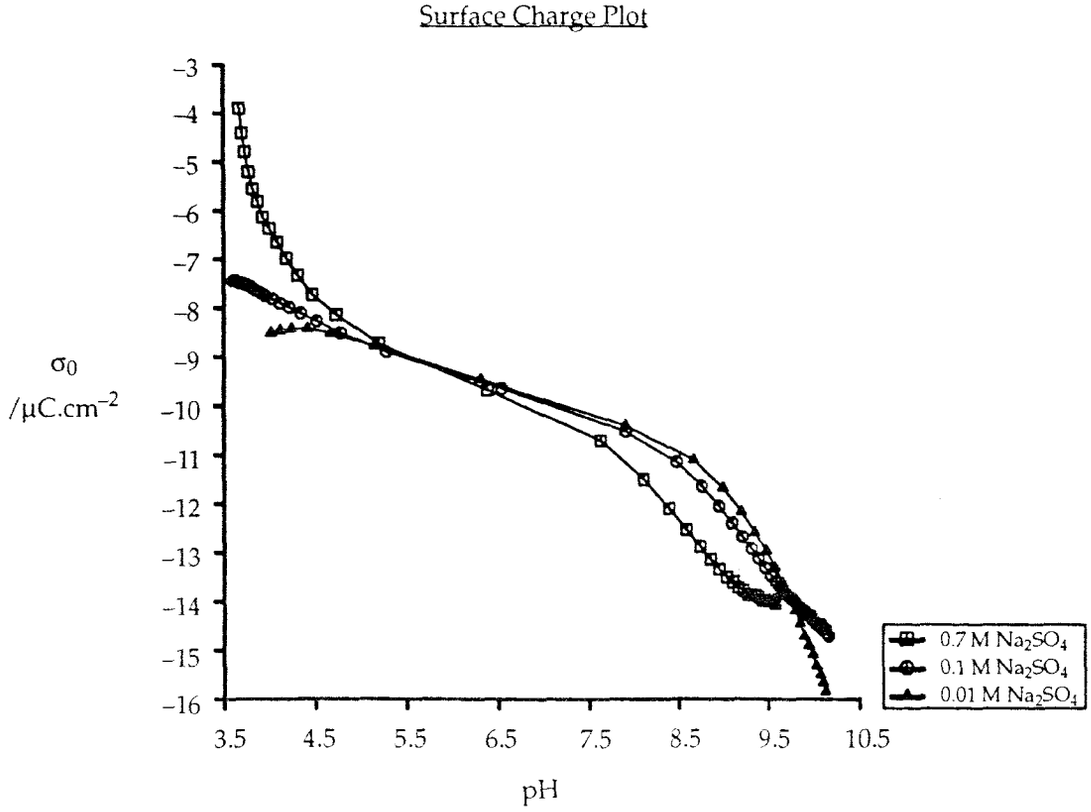

Figure 6.2 Plot of corrected surface charge (σ_0) against pH for Tamar River fulvic acid in Na_2SO_4 solutions.

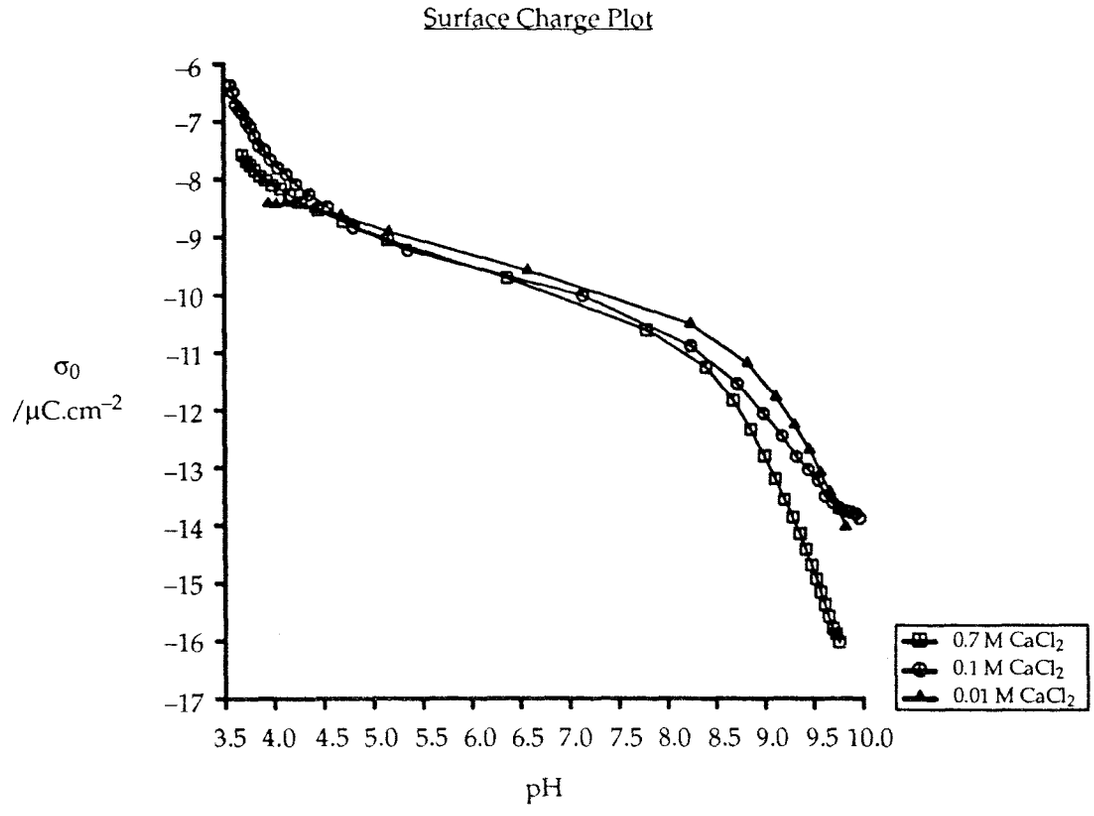

Figure 6.3 Plot of corrected surface charge (σ_0) against pH for Tamar River fulvic acid in $CaCl_2$ solutions.

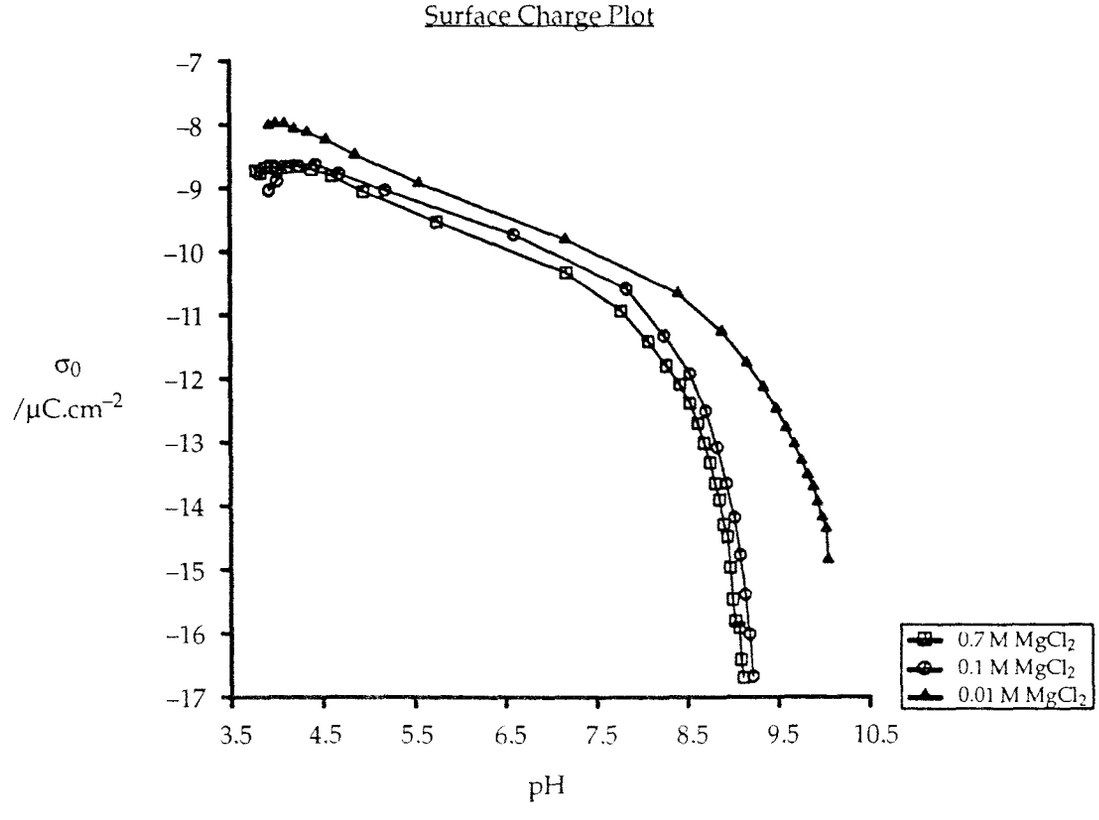

Figure 6.4 Plot of corrected surface charge (σ_0) against pH for Tamar River fulvic acid in $MgCl_2$ solutions.

6.2 Planar Surface

A plot of fulvic acid surface charge (σ_0) against pH_s calculated using planar geometry (Eqn. 2.2.4) for NaCl solutions is shown in Figure 6.5. This figure also includes an additional y–axis, indicating the degree of protonation (θ) of the fulvic acid. The separations of the σ_0 vs pH_s curves in Figure 6.5 are rather large (e.g. at $\sigma_0(pH_{infl})$; 0.01M – 0.1M ~2 pH_s units, 0.1M – 0.7M ~1pH_s unit), and, relative to the σ_0 vs pH curves of Figure 6.1, they appear to be over–corrected for ionic strength effects, since the curves are more widely separated following correction and the order in which the curves appear on the x–axis is reversed.

Variation of molecular weight, as a means of obtaining a θ vs pH_s mastercurve, was not attempted in this case, as the separations of the curves were too great for coincidence to be possible (see Section 6.3.1.2 for a discussion of the effects of molecular weight variation).

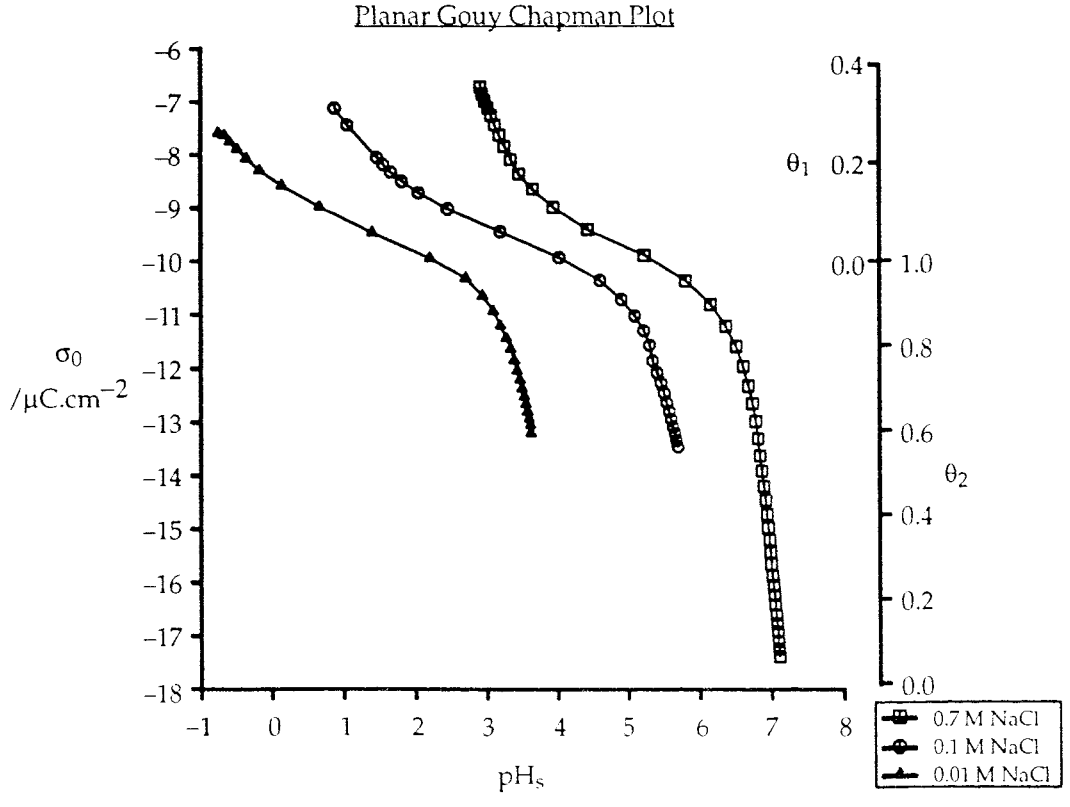

Figure 6.5 Plot of corrected surface charge against pH_s (planar) for Tamar River fulvic acid in NaCl solutions.

6.3 Spherical Colloid

6.3.1 σ_0 vs pH_s

Figures 6.6 – 6.10 show plots of surface charge against pH_s (spherical geometry) for Tamar River fulvic acid in simple salt solutions. The calculation of pH_s in these plots is based on use of Eqn. 2.2.11 (see Section 2.2.3). The NAG subroutine C05ADF was used to find the value of y_0 for which Eqn 6.3.1 (which is derived from Eqn. 2.2.11) was equal to zero, within the limits $1 < y_0 < 8$ (which define the range over which the coefficients B_{kl} are valid (Stigter, 1972)).

$$f(y_0) = \sigma_0 - \sigma_{DH}\left[1 + \left\{\frac{2}{y_0}\sinh\left(\frac{y_0}{2}\right) - 1\right\}\sum_{k=0}^{7}\sum_{l=0}^{6} B_{kl}x^k z^l\right] \qquad (6.3.1)$$

6.3.1.1 Determination of pH_s – Effect of Particle Radius

At a given surface charge and solution ionic strength, surface potential (ψ_0) (and therefore, y_0) will be lower on a small particle than on a large one (see, for example, Figure 1 of De Wit *et al.*, 1989). The effect of reducing particle radius on σ_0 vs pH_s curves for different ionic strengths is to decrease the separation between them, i.e. to reduce the degree of over–correction introduced by assuming the fulvic acid to be planar (see Figure 6.5 ($r \rightarrow \infty$)).

Figure 6.6 shows the σ_0 vs pH_s curves obtained for experiments carried out in NaCl solutions, using a value of 0.658 nm for the fulvic acid radius and 825 daltons for molecular weight. These are the lowest values of the sample's Stokes' radius and molecular weight reported by Varney (1982). While it is clear, from comparisons of Figures 6.5 & 6.6, that the over – correction introduced by assuming the fulvic acid to be planar is dramatically reduced, it is also apparent that the curves of Figure 6.6 are not coincident. Coincidence of the σ_0 vs pH_s curves could not be obtained for any of the simple salt solutions using this radius value and molecular weights within the range described by Eqn. 2.2.14 and the humic density range, 0.7 – 1.7 $g.cm^{-3}$, (De Wit *et al.*, 1991a).

Coincidence of the experimental curves was obtained at slightly smaller particle radii (< 0.6 nm). The curves of Figures 6.7 – 6.10 have been calculated using a value of 0.5 nm for the radius of the fulvic acid, this being the highest value of r for which coincidence could be achieved for all of the salt solutions within the molecular weight limits imposed by Eqn. 2.2.14. The molecular weights and fulvic acid densities used to obtain the mastercurves of Figures 6.7 – 6.10 are shown in Table 6.1.

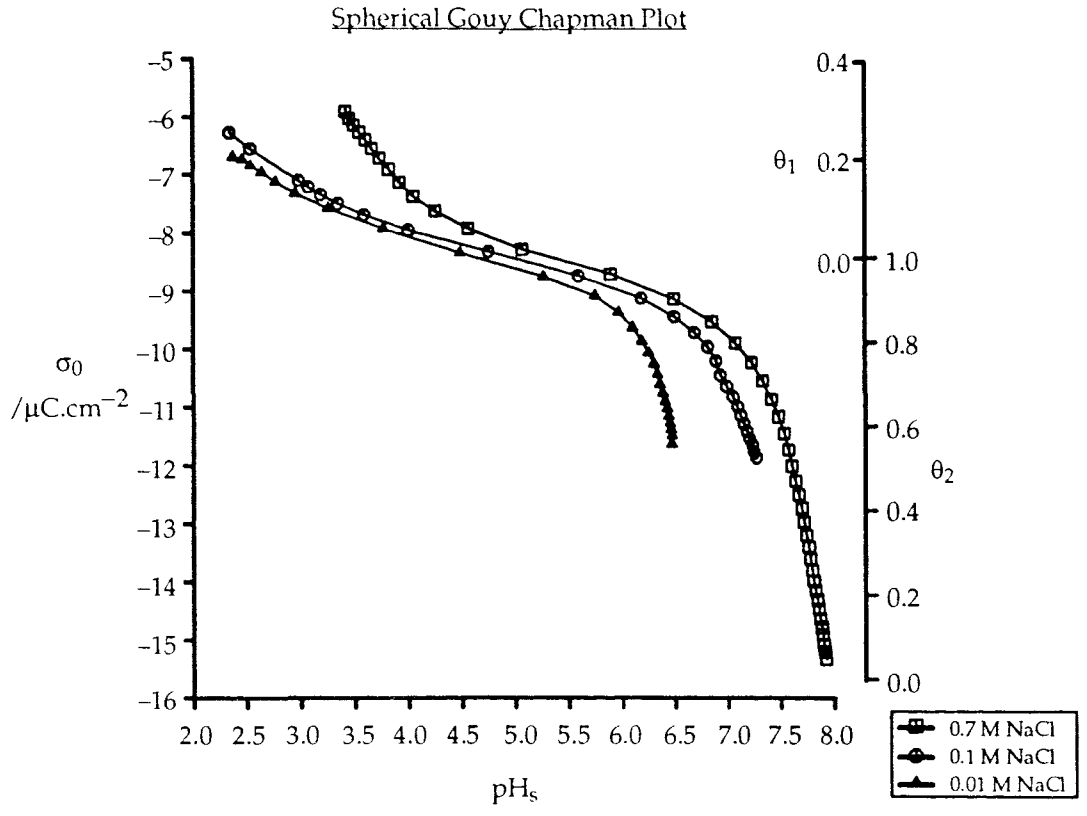

Figure 6.6 Plot of corrected surface charge against pH_s (spherical) for Tamar River fulvic acid in NaCl solutions (r = 0.658 nm, M = 825 daltons).

6.3.1.2 Determination of pH_s – Effect of Molecular Weight

The effect of molecular weight on the separations of σ_0 vs pH_s curves is rather modest compared to that of radius.

At a given particle radius the effect of reducing the value of M is to decrease the slope of each σ_0 vs pH_s curve. While this change in slope may be quite large (depending on the change in M), the change in curve separation is only slight and decreases with decreasing surface charge.

Changes in molecular weight have the greatest effect on the agreement of the curves in the high surface charge region.

6.3.1.3 Determination of pH_s – Effect of Ionic Strength

The computation of y_0 (and hence pH_s) is reliant on C05ADF being able to locate a root of Eqn. 6.3.1 within the specified limits. However, at high solution ionic strength (i.e. 0.7M) and low surface charge ($|\sigma_0| < \sim 6$ $\mu C.cm^{-2}$), the stabilising effect of the solution counterions was sufficient to give 'reduced potentials' (y_0) of less than 1, violating the programmed boundary conditions and causing the analysis to fail.

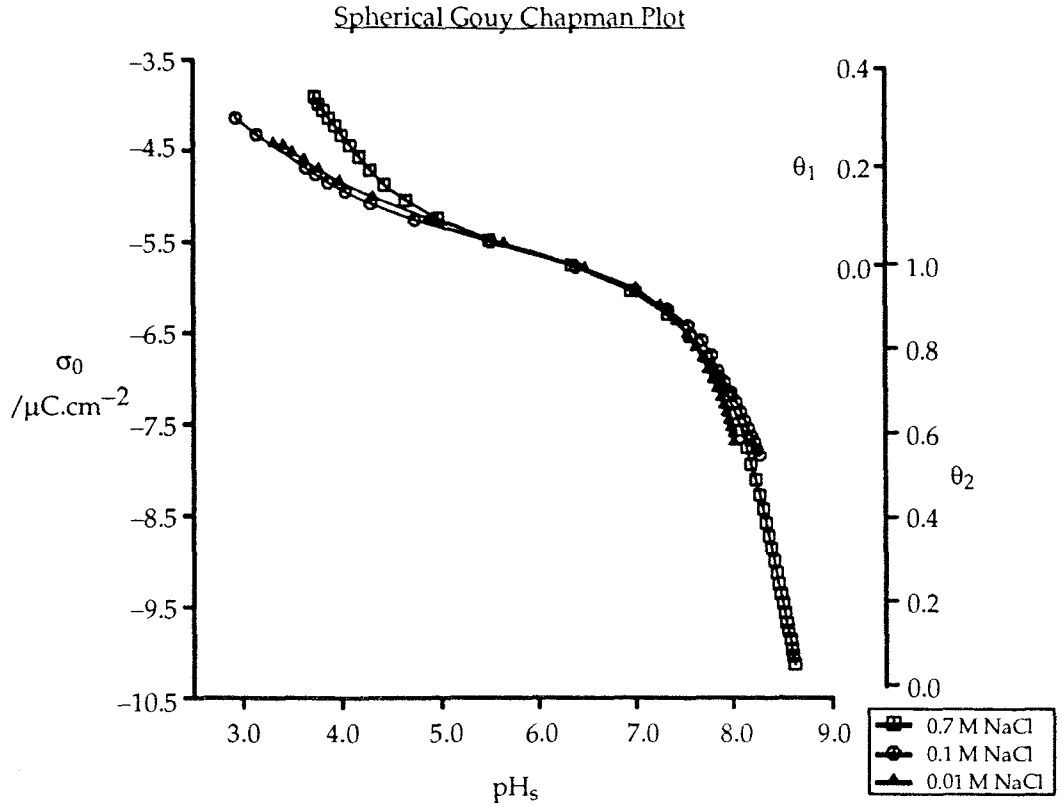

Figure 6.7 Plot of corrected surface charge against pH_s (spherical) for Tamar River fulvic acid in NaCl solutions (r = 0.5 nm, M = 315 daltons).

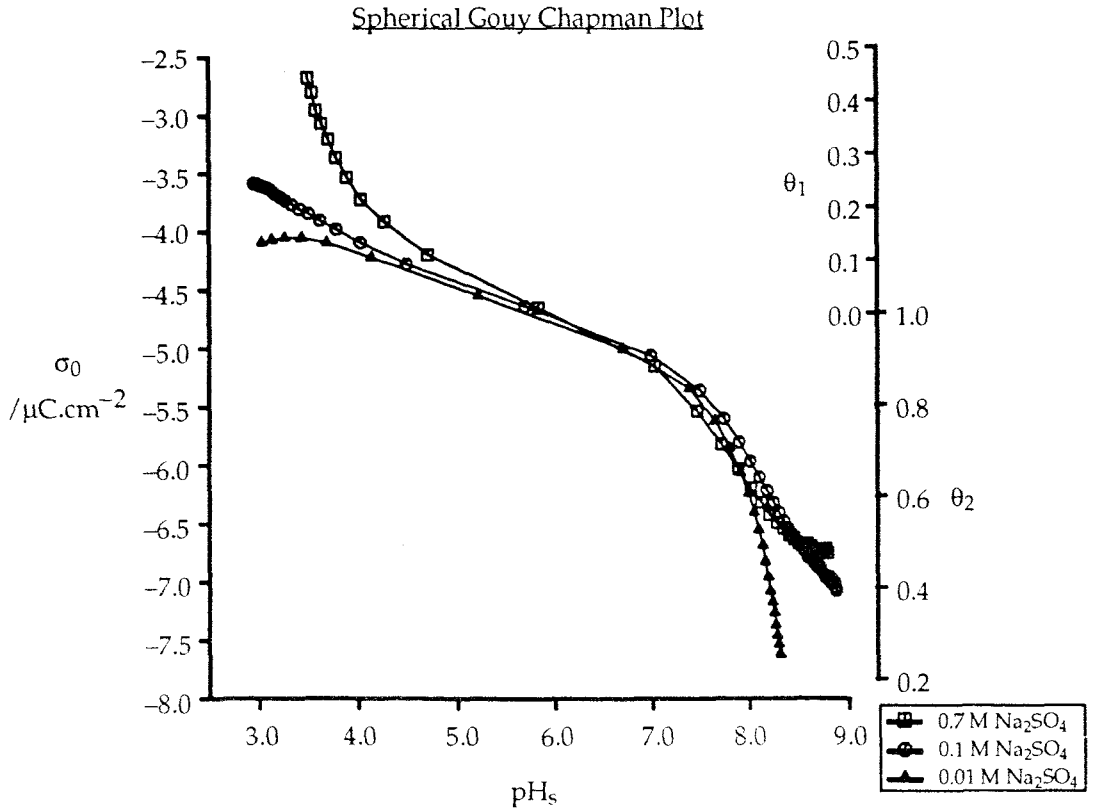

Figure 6.8 Plot of corrected surface charge against pH_s (spherical) for Tamar River fulvic acid in Na_2SO_4 solutions (r = 0.5 nm, M = 260 daltons).

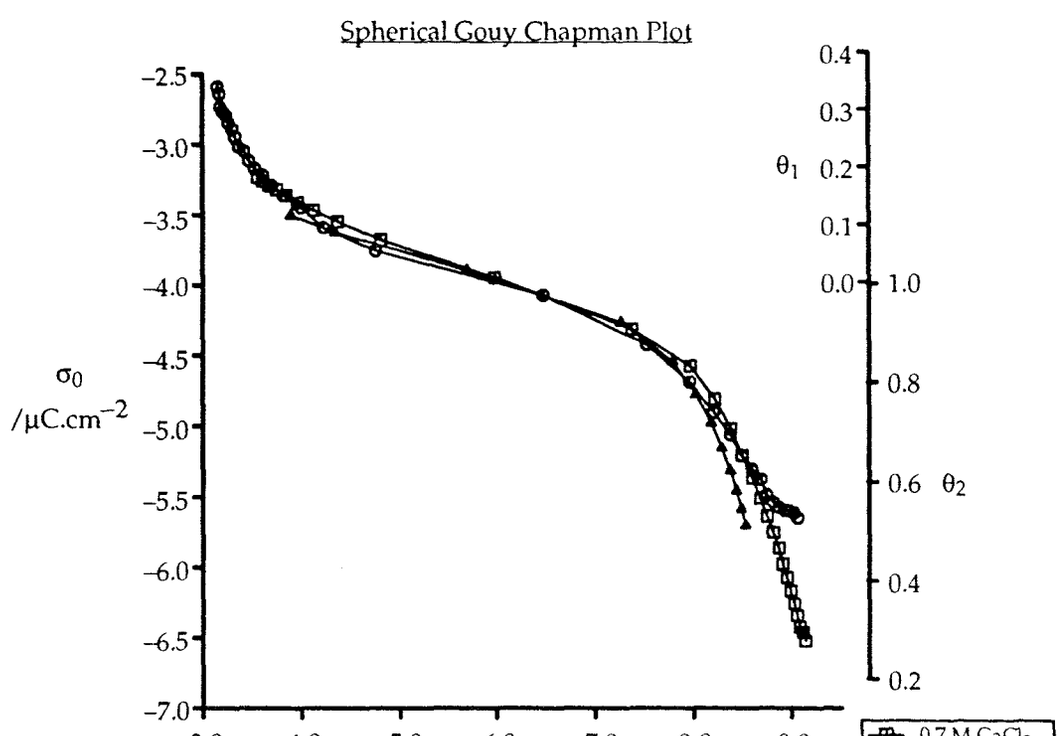

Figure 6.9 Plot of corrected surface charge against pH_s (spherical) for Tamar River fulvic acid in $CaCl_2$ solutions (r = 0.5 nm, M = 220 daltons).

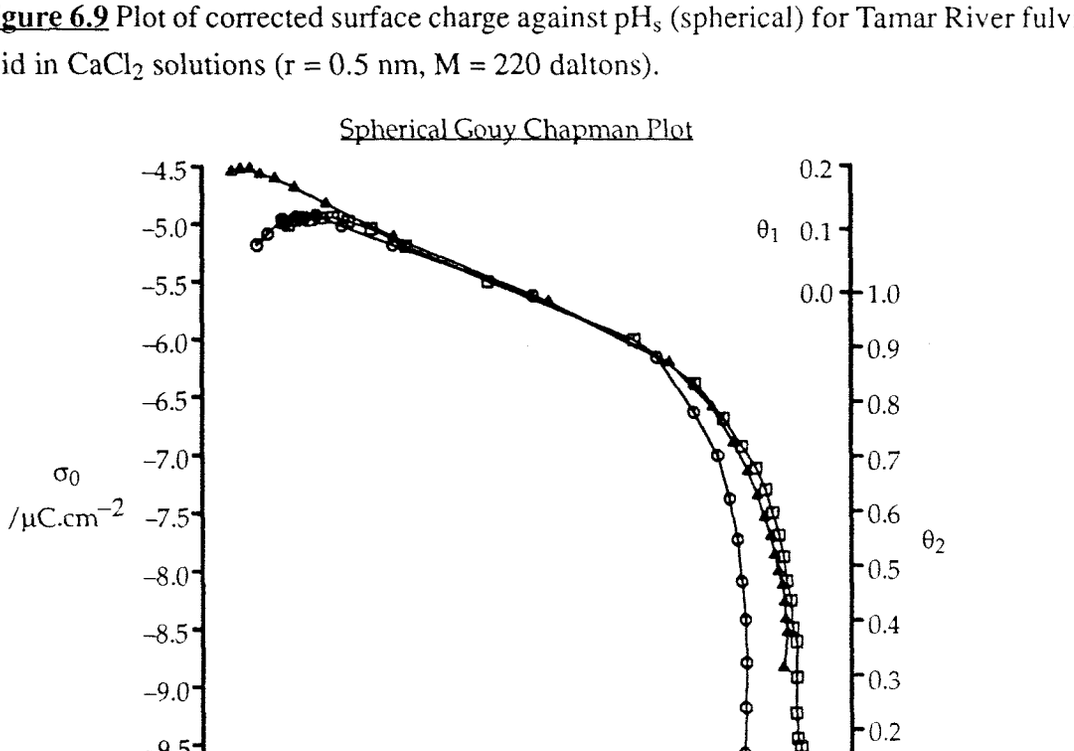

Figure 6.10 Plot of corrected surface charge against pH_s (spherical) for Tamar River fulvic acid in $MgCl_2$ solutions (r = 0.5 nm, M = 315 daltons).

Examination of the various terms of Eqn. 6.3.1 for y_0 values lower than 1 indicates that it may be used in this region with the introduction of only small errors. The $2/y_0.sinh(y_0/2)$ term tends to one for small values of y_0, so that (even assuming the summation term to be incorrect) an error of less than 4% is introduced into the value of σ_{DH}. This error decreases with decreasing y_0, and at $y_0 = 0.3$ the value of the square bracketed term of Eqn. 6.3.1 can be taken to be 1, with an error of less than 0.4%. (For small particles (< 0.5 nm) and low ionic strengths, the differences between Eqn. 6.3.1 and the Debye – Hückel approximation (Eqn. 2.2.9) are negligible (De Wit *et al.*, 1990)).

6.3.2 Intrinsic Affinity Constants

Figures 6.6 – 6.10 include an additional y–axis indicating the degree of protonation of the fulvic acid carboxylic acid groups (θ_1, Eqn. 6.1.1) and phenolic groups (θ_2, Eqn. 6.1.2).

It can be seen from the θ–axes of Figures 6.7 – 6.10 that none of the fulvic acid titration curves includes values of θ_1 higher than 0.5. It is not, therefore, possible to estimate $\log_{10} K_{1,H}$ (the intrinsic affinity constant for the fulvic acid carboxylic acid groups) from these plots. However, there is a wider range of θ_2 values in these plots, and $\log_{10} K_{2,H}$ (the affinity constant for the phenolic groups) values have been estimated according to Eqn. 6.3.2 (Table 6.1). (Eqn. 6.3.2 is taken from De Wit *et al.* (1989) and, as stated in Section 6.1, is included as an illustration of the use of the mastercurve for affinity constant determination).

$$\log_{10} K_{2,H} = pH_s \ (\theta_2 = 0.5) \qquad (6.3.2)$$

The values of $\log_{10} K_{2,H}$ obtained from Figures 6.7 – 6.10 are in broad agreement with one another, although there is some influence on them from molecular weight (M = 315 daltons, $7.7 < \log_{10} K_{2,H} < 8.2$; M = 220 daltons, $8.5 < \log_{10} K_{2,H} < 9.1$). The higher of these values are of similar magnitude to that of a second affinity distribution function peak ($\log_{10} K_H^{int} = 9$) obtained for a lakewater fulvic acid (De Wit *et al.*, 1991a).

Table 6.1 Molecular weights, particles densities and intrinsic affinity constants extracted for the phenolic sites of Tamar River fulvic acid using the spherical Gouy Chapman model, radius 0.5 nm.

Solution	M g.mol	ρ g.cm^{-3}	$\log_{10} K_{2,H}$
NaCl	315	1.0	8.2
Na_2SO_4	260	0.8	8.1 – 8.4
$CaCl_2$	220	0.7	8.5 – 9.1
$MgCl_2$	315	1.0	7.7 – 8.1

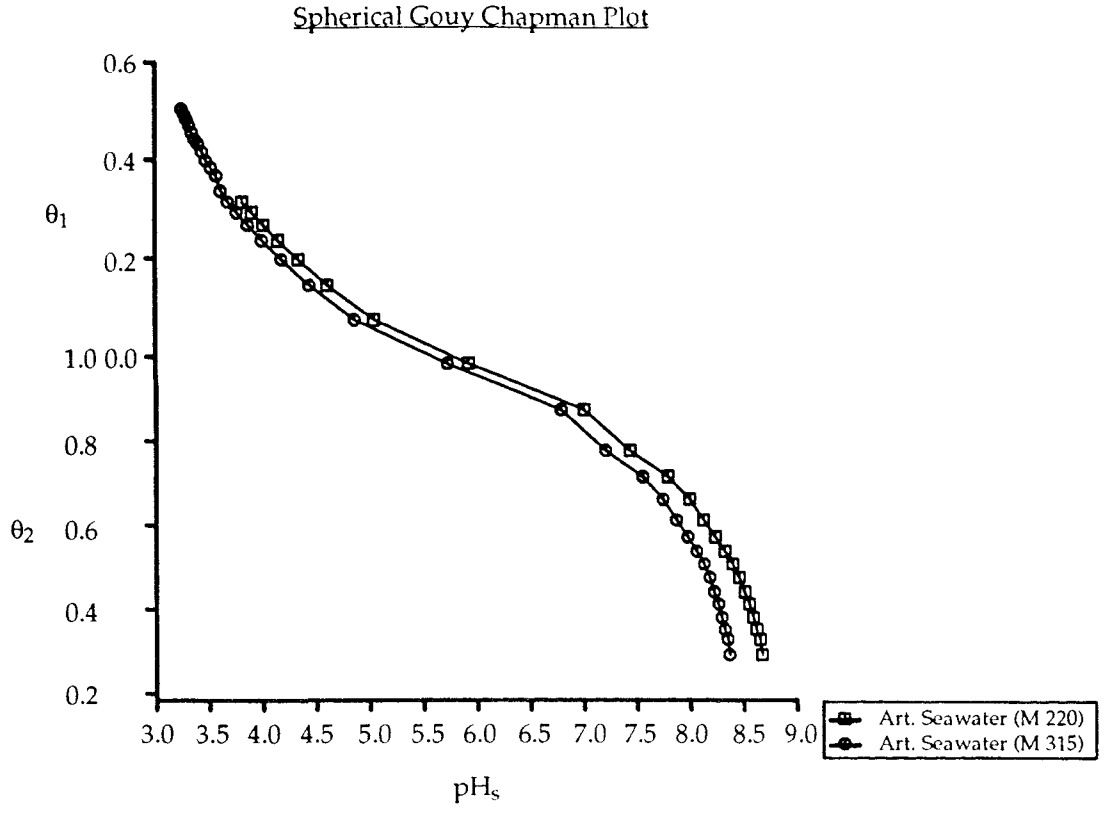

Figure 6.11 Plot of degree of protonation against pH_s (spherical) for Tamar River fulvic acid in artificial seawater solution (r = 0.5 nm).

Calculation of θ vs pH_s curves for Na_2SO_4 and $CaCl_2$ solutions using a molecular weight of 315 daltons produces $\log_{10} K_{2,H}$ values closer to those obtained for NaCl and $MgCl_2$ solutions, although there is a much greater spread in the values obtained (Na_2SO_4, $7.8 < \log_{10} K_{2,H} < 8.6$; $CaCl_2$, $8.0 < \log_{10} K_{2,H} < 8.7$) as these curves do not coincide particularly well.

Figure 6.11 shows θ vs pHs curves for the titration of Tamar River fulvic acid in artificial seawater solution, calculated using a radius of 0.5 nm and molecular weights of 220 and 315 daltons. (Eqn. 6.3.1 was solved for this solution by assuming the artificial seawater to be a 1:1 electrolyte with a concentration equal to its ionic strength, 0.726M). The values of $\log_{10} K_{2,H}$ obtained from these curves are –8.4 (220 daltons) and –8.1 (315 daltons), which are in agreement with the values quoted for the simple salt solutions at these molecular weights (Table 6.1).

6.4 Discussion

6.4.1 Planar Geometry

The large separations of the different ionic strength data in Figure 6.5 are evidence that the planar model is inappropriate for use with the Tamar River fulvic acid (Section 6.2). This is not surprising in view of its small size ($0.658 \text{ nm} < R_W < 1.321 \text{ nm}$; Varney, 1982) in comparison with the minimum particle size required to justify the use of planar geometry ($r > 10$ nm; De Wit *et al.*, 1989).

6.4.2 Spherical Geometry

The use of the spherical Gouy Chapman model with high ionic strength solutions proved to be slightly problematic (Section 6.3.1.3). The combination of high solution ionic strength and small particle radius leads to the development of surface potentials lower than those for which Eqn. 6.3.1 is considered to be valid (Stigter, 1972). Examination of Eqn. 6.3.1 however, suggests that it may be applied to small potentials (i.e. $y_0 < 1$) with the introduction of only a small error (< 4%) into the calculation.

Adjustment of the values of fulvic acid radius (r) and molecular weight (M) proved to be a successful means of producing mastercurves for the simple salt solution systems. Both of these parameters affect the calculated surface charge density (σ_0) through their influence on fulvic acid surface area. Particle radius is also taken into account explicitly in the numerical solution of the Poisson – Boltzmann equation. Of the two parameters r has considerably greater influence on the separations of the calculated σ_0 vs pH_s curves, variation in M producing only a small change in curve separation at relatively high surface charge values.

In the determination of intrinsic affinity constants by the mastercurve method however, both parameters are of considerable importance. The value of pH_s in the θ vs pH_s mastercurve is dependent on those of r and M and thus they will have a direct influence on the values of affinity constants determined by the method used here, or by an affinity distribution technique (e.g. LOGA–1, De Wit *et al.*, 1991a).

The value of r used to produce mastercurves for the fulvic acid titrations in simple salt solutions is a little lower than the sample's measured Stokes' radius, although a radius of 0.5 nm is not so low as to be physically unreasonable. De Wit and co–workers (1991a) have produced a mastercurve from the data of Ephraim *et al.* (1986) using similar parameter values (r = 0.55 nm, M = 450 daltons), see Figure 6.12.

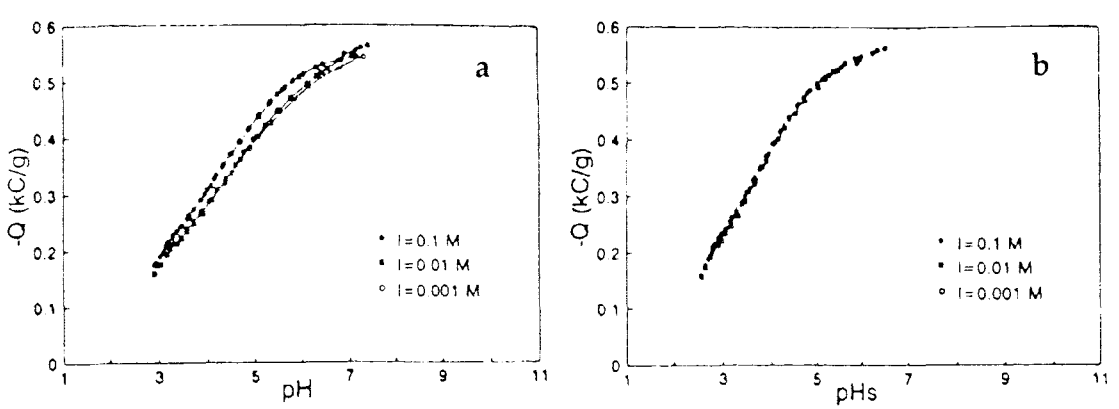

Figure 6.12 Surface charge (Q) vs pH (**a**) and pH_s (**b**) curves for Suwannee River fulvic acid (data of Ephraim *et al.*, 1986). (Reproduced by permission of Kluwer Academic Publishers from De Wit *et al.*, 1991a).

The assumption of spherical geometry for the fulvic acid represents a limiting case of surface charge density, since a sphere has a lower surface area to volume ratio (and therefore higher charge density) than a similar volume (molecular weight) molecule of a different geometry. A cylindrical double layer model has been used to obtain a mastercurve for the data of Tipping *et al.* (1988), using cylinder radius (r = 0.32 nm) and surface area (A = 6250 m^2g^{-1}) as adjustable parameters (De Wit *et al.*, 1991b).

Figure 6.13 shows the uncorrected data of Tipping *et al.*, together with the spherical and cylindrical geometry mastercurves reported for it (De Wit *et al.*, 1990; De Wit *et al.*, 1991b). (Spherical adjustable parameters, radius (1 nm) and site density (0.7 sites.nm^{-2}) (De Wit *et al.*, 1990)). Comparison of the two mastercurves (**b** & **c**) indicates that the scatter of their data points varies little with changing geometry, although the cylindrical model generally gives rise to slightly higher surface pH values.

Without some independent assessment of the molecular shape of humic substances it is difficult to differentiate between these two means of determining the mastercurve. In practise it is unlikely that humic substances maintain either geometry rigidly and the geometry of the double layer can be treated to some extent as a further adjustable parameter of this model.

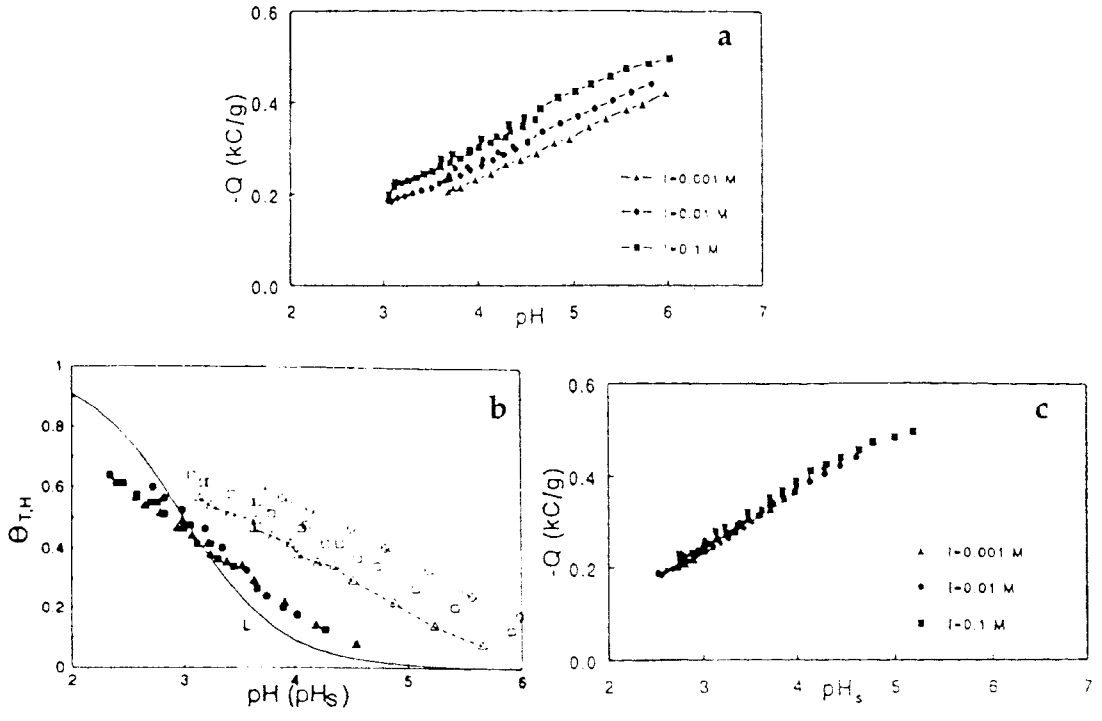

Figure 6.13 Surface charge (Q) vs pH (**a**) and pH_s (**b** & **c**) curves for Lochard Forest humic substance (data of Tipping *et al.*, 1988). Curve **b** was calculated using spherical geometry, curve **c** using cylindrical geometry (solid line in **b** represents a mono–component Langmuir isotherm calculated about $\theta = 0.5$). (Reproduced with permission from De Wit *et al.*, 1991b (**a** & **c**) and De Wit *et al.*, 1990 (**b**)).

6.5 Conclusions

Solution of the spherical Gouy Chapman equation (Eqn. 6.3.1) allows affinity constant values to be obtained for the Tamar River fulvic acid, although use of a slight approximation is necessary for high ionic strength solutions (Section 6.3.1.3).

Many combinations of the adjustable parameters r and M lead to production of "mastercurves", although consideration of the density of humic substances in solution restricts the realistic range of these values. In the case of the Tamar River fulvic acid sample the radius value used was the largest (i.e. the closest to the measured value) for which mastercurves could be determined for all of the simple salt solutions.

The values of r and M used to produce mastercurves for the fulvic acid are significantly different from the measured values of these parameters. However, the use of M and r as adjustable parameters in this case should not be taken as an indication of their true values, the adjusted values simply define the mastercurve.

A simplified reaction scheme has been used to demonstrate the extraction of intrinsic affinity constants from the mastercurve. De Wit and co–workers (1988, 1989, 1990 & 1991 a & b) recommend the use of affinity distribution functions for this purpose, although other methods, such as a multisite model (Paxéus & Wedborg, 1985), may be equally applicable.

7. FULVIC ACID: SURFACE COMPLEXATION ANALYSIS

7.1 Introduction

The surface complexation models consider the interface between charged substrate and solution to consist of one or more planes of adsorbed ions immediately adjacent to the surface, with a diffuse layer of charge extending further into the solution (see Section 2.3). The constant capacitance model confines all adsorbed ions to one layer (Morel *et al.*, 1981), while the triple layer model provides for two adsorption layers, H^+ / OH^- ions in the inner, complexing ions (e.g. Na^+, Cl^-) in the outer (Davis *et al.*, 1978).

The reactions occurring at the surface of the substrate can be described in terms of "one pK" or "two pK" protonation / deprotonation processes (see Sections 2.1.3.1 & 2.1.3.2). The "two pK" process has been applied previously to potentiometric titration data (e.g. Davis *et al.*, 1978; Lövgren *et al.*, 1990), and provides a means of extracting intrinsic stability constants from the experimental data obtained for the Tamar River fulvic acid sample (Section 7.2).

7.1.1 HALTAFALL Speciation Routine

Parameters specific to the constant capacitance and triple layer interface models (e.g. capacitances) were determined by use of a modified version of the HALTAFALL speciation routine.

HALTAFALL is capable of determining the chemical speciation of an aqueous system from data describing the concentrations and activity coefficients of the dissolved species, together with stability constants for their interactions with one another. The modified version used here is also able to include the interactions of the surface sites of particulate species (with constant capacitance or triple layer type interfaces) in speciation calculations (Turner *et al.*, 1991).

Inclusion of a subroutine version of this program within a non–linear least sum of squares regression analysis allowed stability constant and capacitance values to be fitted to experimentally determined surface charge – pH data. Non–linear regression was carried out using NAG subroutines in a procedure similar to that employed for analysis of calibration experiments (Section 3.6.1). (Thanks to Snr. Fransisco Penedo of the University of Santiago, Spain for supplying the original version of this program).

The results of stability constant and model parameter determinations for each salt solution were then used to predict the acid – base behaviour of the fulvic acid in artificial seawater (Section 7.3.2).

7.2 pK Extrapolation

Intrinsic stability constants (for use as initial estimates in the non–linear fitting) for deprotonation and cation "complex ionisation" reactions of the fulvic acid can be estimated from plots based on Eqn. 2.3.18 (Section 2.3.3.1) and Eqn. 2.3.21 (Section 2.3.3.2) against

α_- (Eqn. 2.3.15) (Davis *et al.*, 1978). The reactions of Ca and Mg with fulvic acid are assumed to occur through complexation of hydroxo ions, e.g. Eqn. 7.2.1.

$$SOH + Ca^{2+} + H_2O \Leftrightarrow SO^-\text{–}CaOH^+ + 2H^+ \ , \ {}^*K_{CaOH}{}^{int} \qquad (7.2.1)$$

Plots showing the variation of the apparent stability constants, $pK_2{}^{app}$, $p^*K_{Na}{}^{app}$, $p^*K_{CaOH}{}^{app}$ and $p^*K_{MgOH}{}^{app}$, with the overall degree of dissociation of the fulvic acid are shown in Figures 7.1 – 7.4 respectively.

Each of these plots shows two regions of relatively shallow slope (at low and high α_- values), linked by a region of steeper slope. This pattern reflects the division of the fulvic acid functional groups into two types (i.e. carboxylic and phenolic), the regions of shallow slope indicating two pK^{int} values. However, as the overall degree of dissociation of the sample has been used to calculate pK^{app} in these plots (rather than α_- for each site) they cannot be used to extrapolate intrinsic stability constant values.

pK^{int} values for the fulvic acid carboxylic acid site could potentially be obtained from similar plots calculated for its degree of dissociation. In this case however, the number of data points in such a plot would be rather low and the length of extrapolation necessary rather high ($\alpha_- > 0.7$ to $\alpha_- = 0$) and this has not been attempted. Extrapolation of pK^{int} values for the phenolic site is complicated by the fact that the fulvic acid is already charged at the point when these sites are completely undissociated.

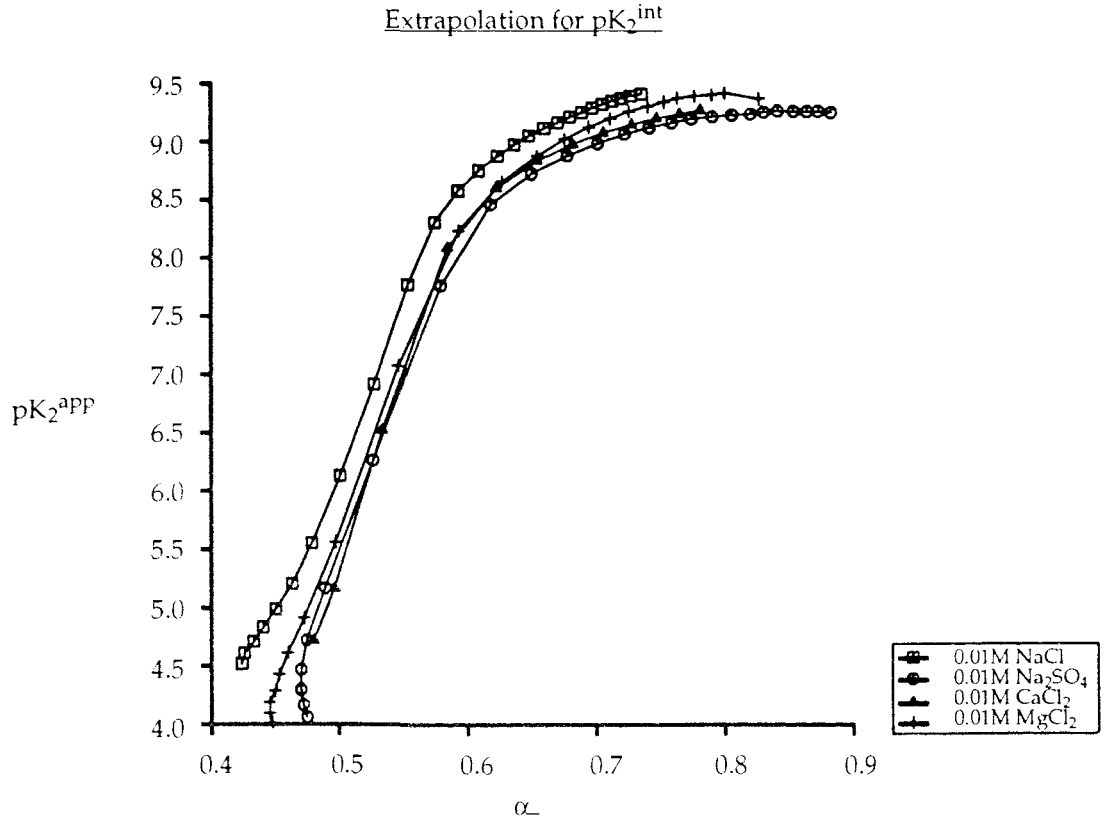

Figure 7.1 Plot of $pK_2{}^{app}$ against degree of dissociation of fulvic acid in 0.01M solutions of NaCl, Na_2SO_4, $CaCl_2$ and $MgCl_2$.

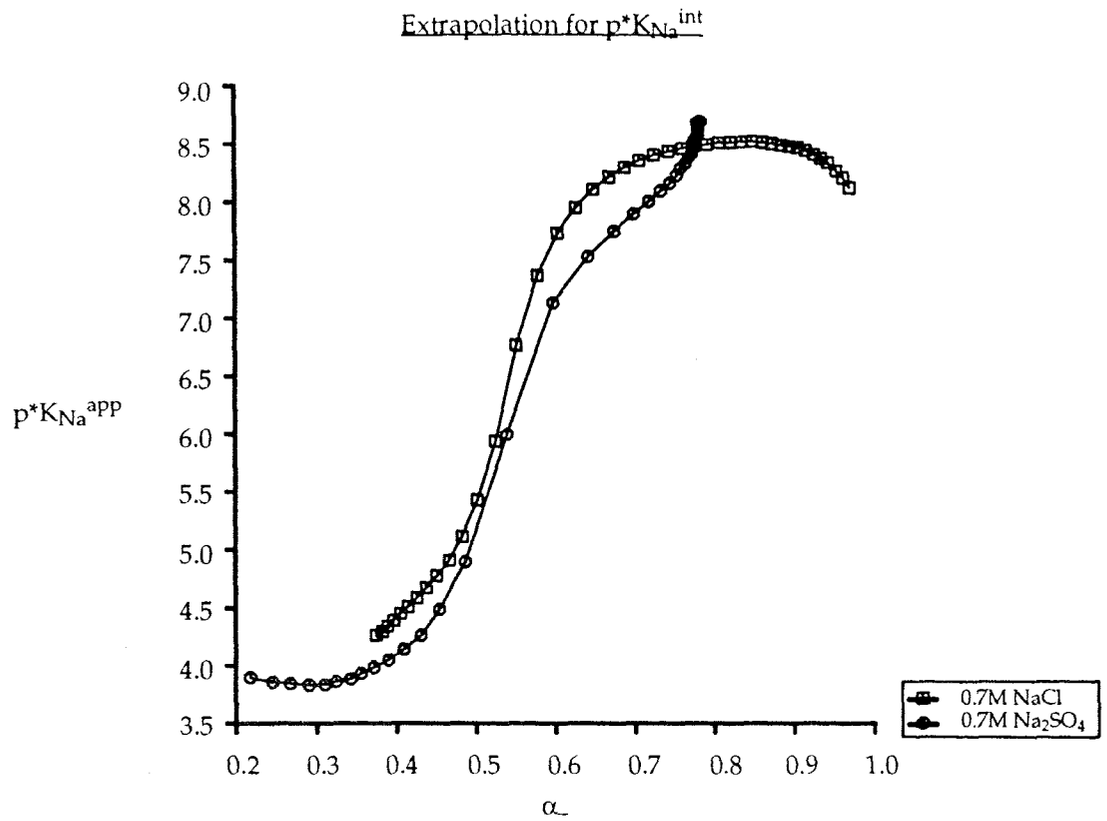

Figure 7.2 Plot of p*K_{Na}^{app} against degree of dissociation of fulvic acid in 0.7M solutions of NaCl and Na_2SO_4.

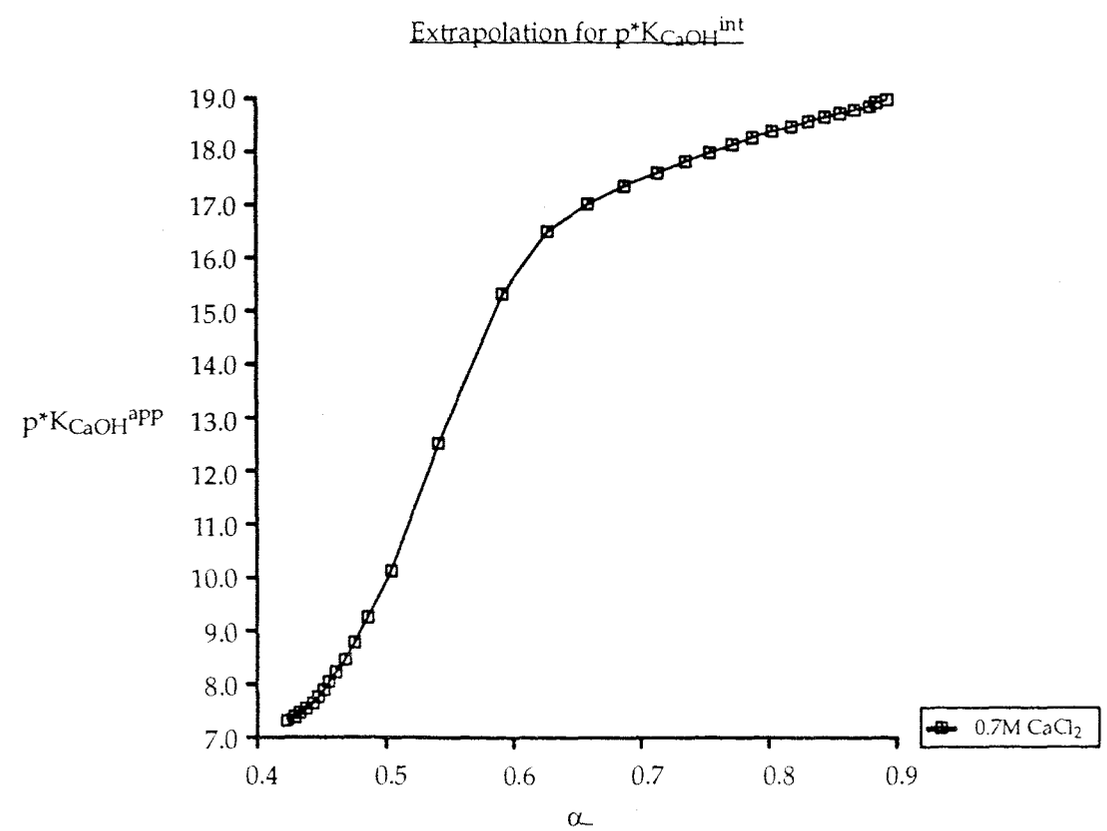

Figure 7.3 Plot of p*K_{CaOH}^{app} against degree of dissociation of fulvic acid in 0.7M $CaCl_2$ solution.

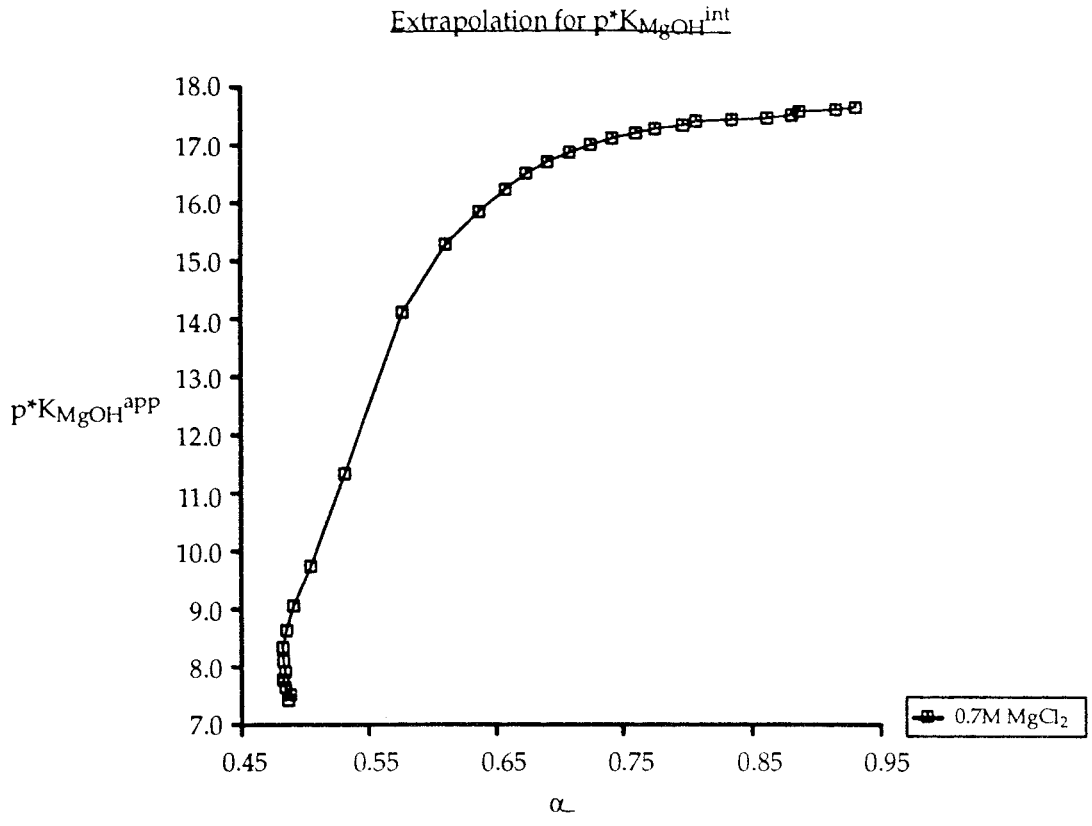

Figure 7.4 Plot of $p^*K_{MgOH}^{app}$ against degree of dissociation of fulvic acid in 0.7M $MgCl_2$ solution.

7.3 Stability Constant and Capacitance Fitting

Fitting of stability constants for the more acidic of the fulvic acid surface sites and capacitance values was attempted using the constant capacitance model (the simpler of the two interface models). As the fulvic acid carries a negative charge over the whole of the titration range (and in natural systems), only surface species including negatively charged sites (i.e. SO^-, SO^-–M^+ and SO^-–MOH^+) were included in the fitting procedure.

The aim of the fitting procedure was to obtain a set of ionic strength independent stability constants for the reactions of protons and sodium, calcium and magnesium ions with the Tamar River fulvic acid sample. These stability constants should then allow prediction of those ions' effects on the surface charge of the sample in artificial seawater to be made.

Two schemes for parameter fitting were adopted. Initially fitting was attempted using individual data files to optimise different parameters (e.g. pK_2 values fitted from 0.01M titration data, since surface charge development in these solutions should be principally due to proton dissociation) (Section 7.3.1.1). Parameters were also obtained from fittings of high ionic strength data only (0.7M), since the results were required for use in a high ionic strength situation (artificial seawater) (Section 7.3.1.2).

Simple metal complexation stability constants (e.g. pK_{Na}, Eqn. 2.1.6) were used as fitting parameters rather than the complex ionisation constants p*K, since the complex

ionisation constants include the deprotonation constants and there would be covariance between them.

7.3.1 Fitting Procedure

7.3.1.1 Parameter Optimisation using Individual Data Files

Stability constant (pK_2 and pK_M) and capacitance values were initially determined by a two stage process. Firstly, pK values were fitted to the experimental σ_0 vs pH curves for all ionic strength solutions of a particular electrolyte simultaneously. Capacitance values were varied manually during this process in order to reproduce the slope of the experimental curves. This yielded general parameter estimates (pK_2, pK_M & C), which could be refined by fitting of individual experiments. pK_2 was determined from the 0.01M titration, then pK_M from the 0.7M titration and finally C was fitted for each titration.

This approach provided good fits (i.e. low standard deviations) to experimental data, but the parameters obtained lacked chemical reasonableness. (See Table 7.1 and Figure 7.5, which show the results obtained for NaCl solutions by this method). The carboxylic acid stability constant fitted for NaCl solutions ($pK_2 = 0.74$) is rather unrealistic when compared to the dissociation constants reported for simple carboxylic acids ($3.88 < pK < 5.04$ @ 25°C & zero ionic strength; Martell & Smith, 1977).

The capacitance values shown in Table 7.1 are rather lower than those reported for particulate samples by other workers (1.28 $F.m^{-2}$, Lövgren *et al.*, 1990; 0.89 $F.m^{-2}$, Turner *et al.*, 1991). During the fitting procedure a high degree of covariance was noted between pK_2 and C. This covariance prevented these parameters from being fitted simultaneously (e.g. for 0.01M experiments), as the results of the fitting were highly dependent on the initial estimates of their values. The poor quality of the chemical parameters obtained by this method is probably due to this covariance, since it effectively allows several combinations of pK_2 and C values to be fitted to a data set without significant differences in the standard deviations of the fits.

Table 7.1 Fitted parameters, standard errors and standard deviations of fits for Tamar River fulvic acid in NaCl solutions (Individual file method).

Parameter	Value		
	0.7M	0.1M	0.01M
pK_2		0.74±0.04	
pK_{Na}		4.85±0.16	($p^*K_{Na} = 5.59$)
C / $F.m^{-2}$	0.37±0.01	0.44±0.01	0.40±0.01
σ_{fit} / $\mu C.cm^{-2}$	0.27	0.22	0.23

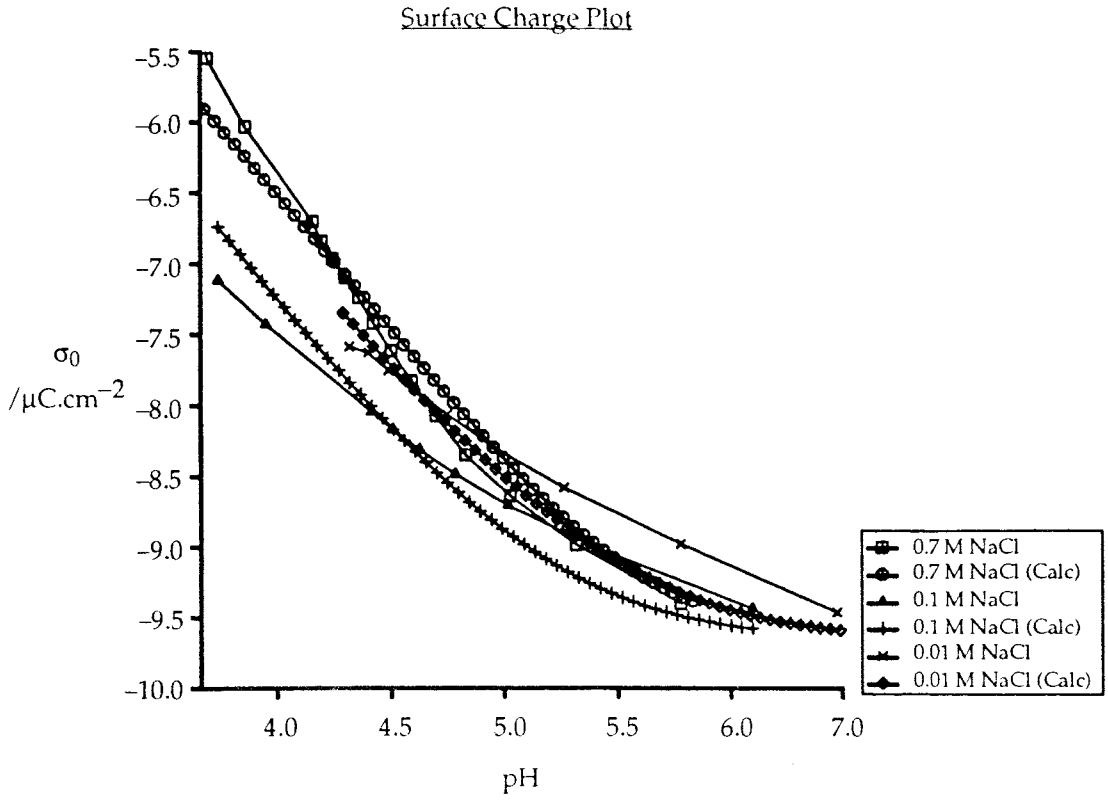

Figure 7.5 Calculated and observed surface charge plots for Tamar River fulvic acid in NaCl solutions (fittings of individual data files).

7.3.1.2 Parameter Fitting from High Ionic Strength Data

Since it was found to be difficult to obtain chemically realistic values for fulvic acid stability constants by optimising parameters individually (Section 7.3.1.1), fitting of all parameters (pK_2, pK_M & C) was attempted simultaneously. This was accomplished using the 0.7M data file for each electrolyte.

By including pK_M in the fitting procedure the number of degrees of freedom of the fit were reduced and the covariant parameters pK_2 and C appeared to be forced to take their optimum values. The results of these fits were essentially independent of the initial estimates of the values of pK_2 and C.

Table 7.2 shows the values of the parameters fitted, their standard errors and the standard deviations of the fits. (Standard errors for $CaCl_2$ and $MgCl_2$ fitting parameters are not included in Table 7.2 as the fitting routine was unable to reach complete convergence for these files. The inclusion of these values is justified by the low standard deviations of the fits). Calculated σ_0 vs pH curves for these fits are shown in Figure 7.6.

The pK_2 values fitted in this way are much closer to the dissociation constants reported for simple carboxylic acids, while pK_M (and p^*K_M) values show the strength of metal ion interactions with the sample to increase in the order Na << Ca < Mg. The fitted capacitance values (0.65 $F.m^{-2}$ – 1.37 $F.m^{-2}$) are also closer to those reported by other workers than were those obtained in Section 7.3.1.1. The value of pK_{Na} obtained for NaCl

solution is rather large compared to values reported for other sodium – carboxylic acid interactions ($-0.18 < pK_{Na} < 0.83$ @ 25°C & zero ionic strength; Martell & Smith, 1977).

Fitting of pK_{CaOH} and pK_{MgOH} was also attempted with the values of pK_2 and C held constant at those fitted for Na_2SO_4 solution. While the fitting routine was able to reach convergence in this way, the quality of the fit was significantly worse than the results quoted in Table 7.2 (standard deviations of fits were approximately an order of magnitude greater).

Table 7.2 Fitted stability constant and capacitance values, standard errors and standard deviations of fits for Tamar River fulvic acid (0.7M data).

Salt	pK_2	pK_M	C /F.m^{-2}	σ_{fit} /μC.cm^{-2}	p^*K_M
NaCl	2.05±0.08	4.35±0.75	0.65±0.03	0.05	6.40
Na_2SO_4	3.12±0.32	0.94±0.51	1.37±0.47	0.49	4.06
$CaCl_2$	1.7	8.3	0.90	0.26	10.0
$MgCl_2$	1.5	10.5	0.77	0.22	12.0

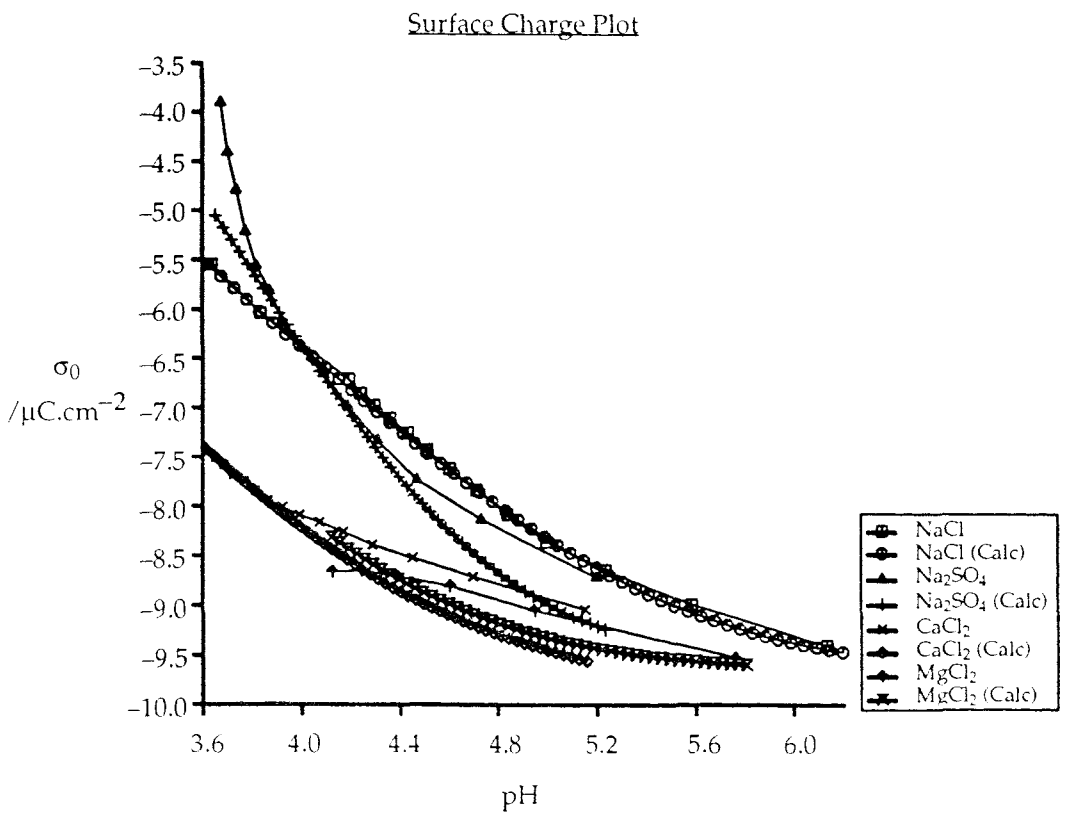

Figure 7.6 Calculated and observed surface charge plots for Tamar River fulvic acid in 0.7M NaCl, Na_2SO_4, $CaCl_2$ and $MgCl_2$ solutions.

7.3.1.3 Variation of Capacitance with Ionic Strength

The capacitance of the adsorbed layer is predicted by theory to be proportional to the square root of solution ionic strength (Section 2.3.4.1), i.e. capacitance should vary according to Eqn. 7.3.1 (a is a constant) (Dzombak & Morel, 1990).

$$C = a.\sqrt{I} \qquad (7.3.1)$$

It can be seen from Table 7.1 that capacitance values fitted to the surface charge data in NaCl solutions for a given set of stability constants do not show this relationship. Results presented in this work (Section 9.4.2) and elsewhere (Turner *et al.*, 1991) suggest that capacitance actually varies with a lower power of ionic strength ($C \alpha I^{\sim 0.1}$).

Figures 7.7 – 7.10 show surface charge curves for 0.1M and 0.01M data calculated using stability constant values from Table 7.2 and capacitance values which vary according to $I^{0.1}$ (the results of the fits for the 0.7M data were used to determine appropriate values of a). These curves generally reproduce the experimental curves very poorly, although there is good agreement between experimental and calculated curves for the 0.1M $CaCl_2$ experiment (Figure 7.9) and the separations of the curves at pH_{infl} is mimiced in all cases.

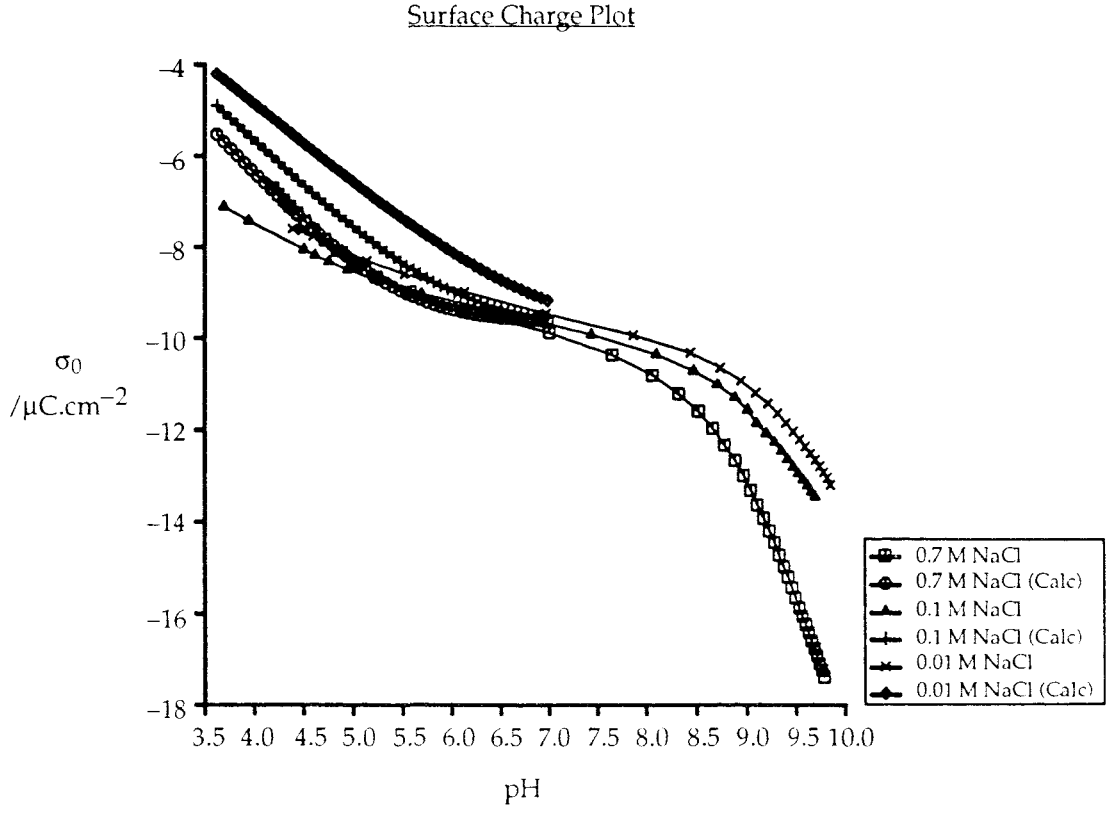

Figure 7.7 Calculated and observed surface charge plots for Tamar River fulvic acid in NaCl solutions.

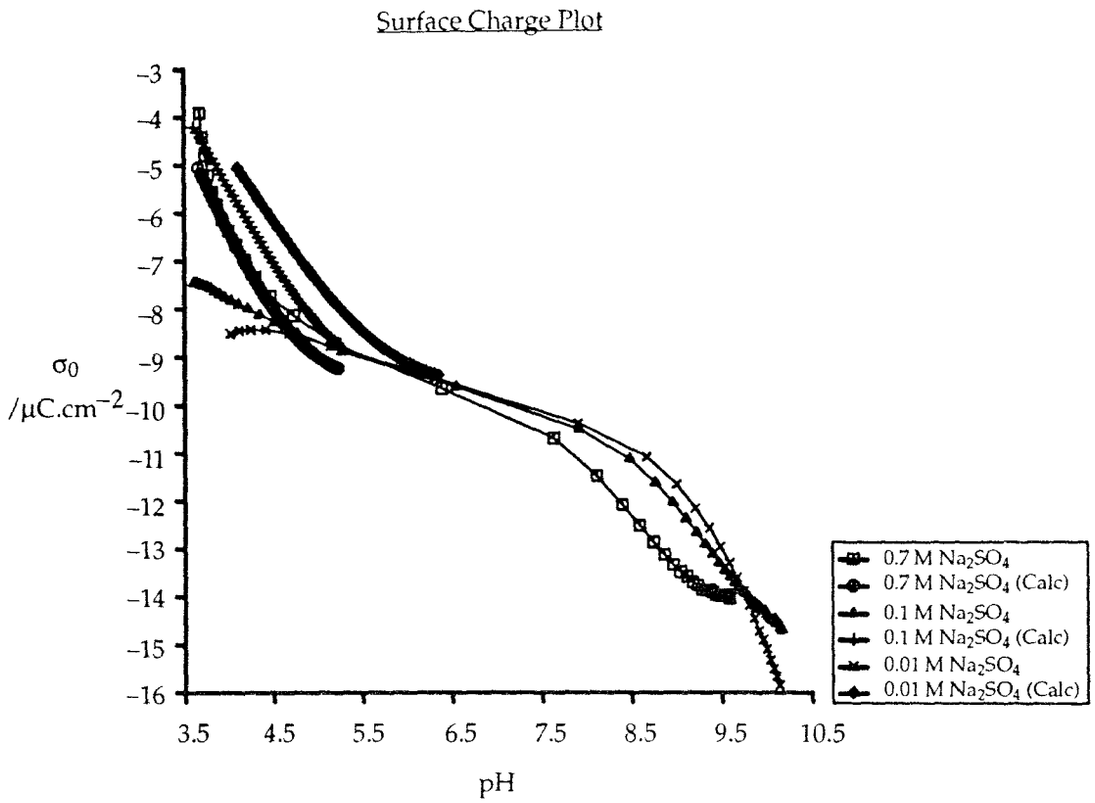

Figure 7.8 Calculated and observed surface charge plots for Tamar River fulvic acid in Na_2SO_4 solutions.

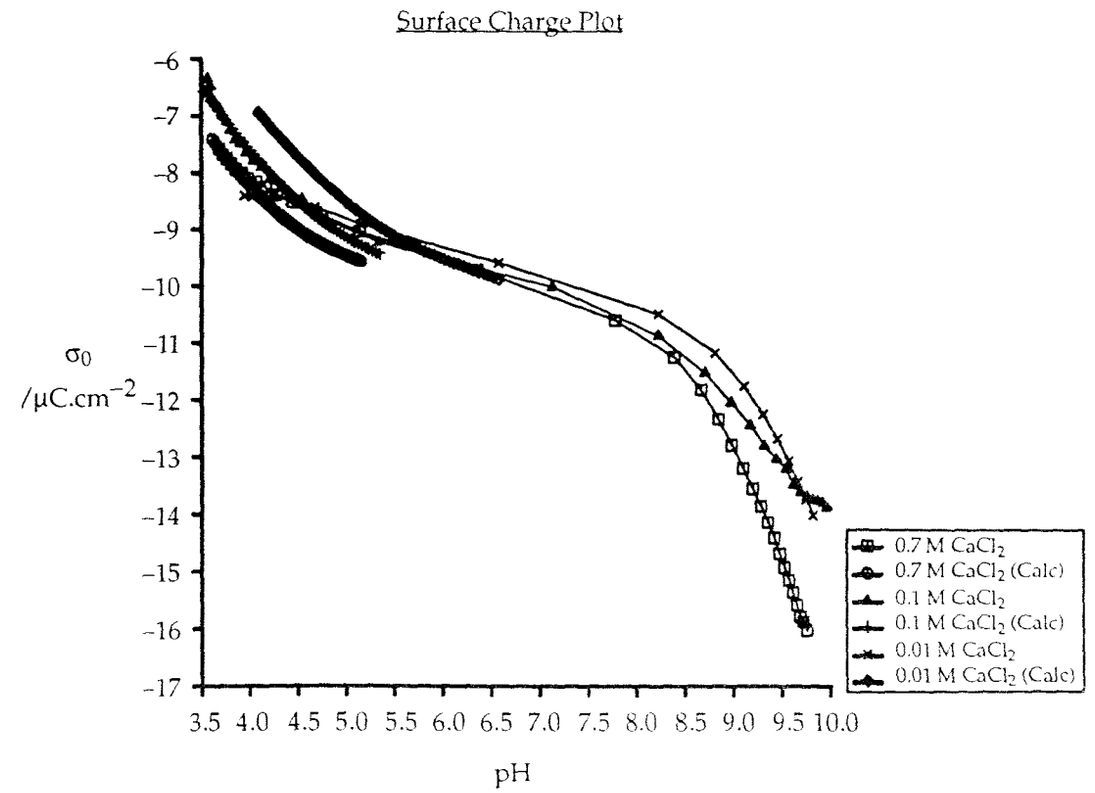

Figure 7.9 Calculated and observed surface charge plots for Tamar River fulvic acid in $CaCl_2$ solutions.

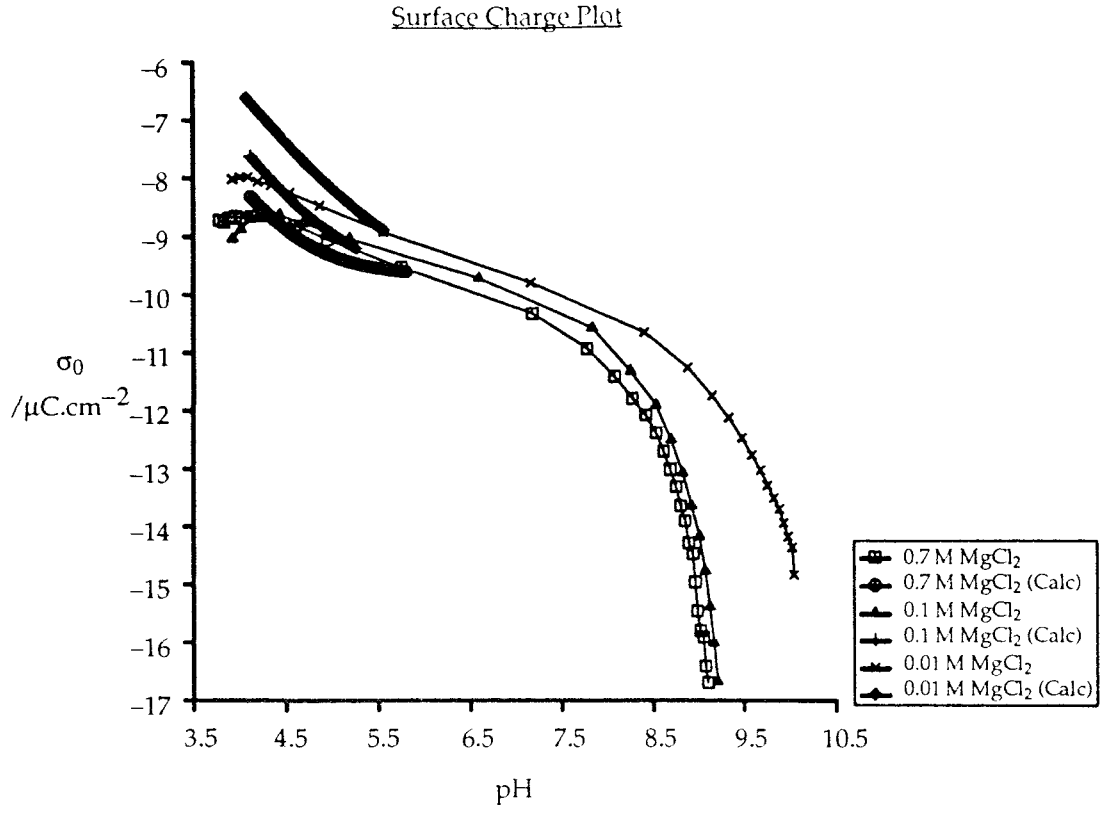

Figure 7.10 Calculated and observed surface charge plots for Tamar River fulvic acid in $MgCl_2$ solutions.

7.3.2 Prediction of Fulvic Acid Surface Charge in Artificial Seawater

The stability constant and capacitance data fitted for fulvic acid in high ionic strength (0.7M) solutions of NaCl, Na_2SO_4, $CaCl_2$ and $MgCl_2$ (Section 7.3.1.2) were used as input to the HALTAFALL speciation routine. Together with the concentrations of its components, they were used to predict the surface charge developing on the fulvic acid in an artificial seawater solution.

A predicted σ_0 vs pH curve was calculated using the stability constant values listed in Table 7.2 (pK_2 & p^*K_{Na} from Na_2SO_4; p^*K_{CaOH} from $CaCl_2$; p^*K_{MgOH} from $MgCl_2$) and the mean of the fitted capacitance values for 0.7M experiments (0.92 $F.m^{-2}$). This curve is shown, together with the experimentally determined curve in Figure 7.11.

The agreement between the observed and predicted surface charge curves in Figure 7.11 is extremely good considering that the prediction has been based on the results of only four experiments. The slope of the observed curve has not been completely matched in the predicted, but variation in the capacitance value within the range obtained in Table 7.2 should enable the slope to be reproduced.

(HALTAFALL input files used in the fitting procedure (Section 7.3.1) and in the determination of surface charge in artificial seawater solution can be found in Appendix 2.A).

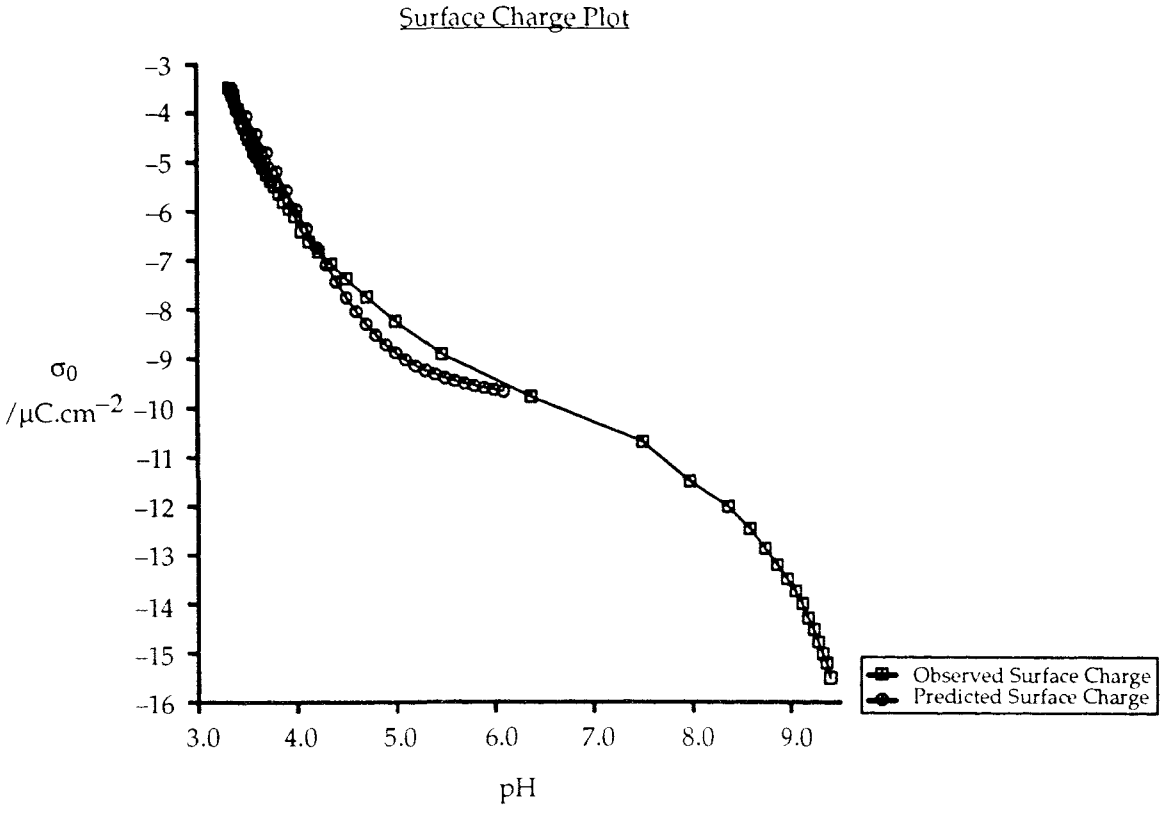

Figure 7.11 Observed and predicted surface charge plots for Tamar River fulvic acid in artificial seawater solution.

7.4 Discussion

The pK extrapolation procedure of Davis and co–workers (Davis *et al.*, 1978) showed plots consistent with a two site system when applied to the entire fulvic acid data set (Figures 7.1 – 7.4). However, truncation of the data in order to obtain pK values for only one surface site was not possible as there was too little data for the carboxylic acid site and the nature of the sample precludes extrapolation of the phenolic site data to a state of zero charge (Section 7.2).

In the absence of suitable extrapolated values, it was necessary to rely on the HALTAFALL fitting to provide pK values for the fulvic acid.

A fitting procedure in which the values of individual parameters were optimised by fittings of individual data files proved to produce good agreement between observed and calculated data, but the parameters were chemically unrealistic (Figure 7.5; Table 7.1).

An alternative procedure in which all of the parameters were fitted simultaneously to the 0.7M data file of each salt solution produced more realistic stability constant values (Table 7.2) and better agreement between observed and calculated data for the 0.7M experiments only. Curves calculated for the lower ionic strength data using the fitted stability constants and assuming capacitance to vary as a function of $I^{0.1}$ did not reproduce the experimental data at all well, although the displacement of the experimental curves at high pH values was reproduced.

The results of the latter fitting procedure provided a reasonably good prediction of the fulvic acid surface charge development in artificial seawater (Section 7.3.2). The stability constant values used in the predictive exercise were obtained from data at only one ionic strength (and have been applied to a similar ionic strength). They are unlikely to provide adequate descriptions of surface charge development on the sample at the lower salinities of estuarine waters.

The triple layer model has not been applied to the Tamar River fulvic acid titration data as the increased complexity of this model makes fittings of the type used with the constant capacitance model extremely difficult.

7.5 Conclusions

Combination of the constant capacitance interface model with the surface complexation reaction scheme provides a basis for determination of fulvic acid stability constant data at high solution ionic strengths (Section 7.3.1.2).

When fitting was attempted using individual data files the quality of the fit was dependent on the value chosen for the capacitance of the adsorbed layer (C) and it was found that this parameter was best fixed semi–manually. However, this method could not provide a consistent set of parameters for any of the electrolyte solutions, nor were the results realistic.

Model parameters could also be determined from fittings of high ionic strength data only, and the stability constant values obtained appeared chemically realistic, despite the narrow range of α_- values available for the carboxylic acid site examined. Stability constant determination (by extrapolation or fitting) for the fulvic acid phenolic site is not possible without some modification of the procedures to take account of the charge on the fulvic acid at the point when dissociation of these groups begins.

Use of this scheme for prediction of the acid – base behaviour of the fulvic acid sample in an artificial seawater solution by speciation modelling was quite successful, although the stability constants obtained were probably not applicable to lower ionic strength solutions.

8. ALUMINA AND ALUMINA / FULVIC ACID: FORMATION FUNCTIONS & SURFACE AREAS

8.1 Introduction

The results of the investigations carried out on suspensions of γ–alumina (concentration 0.48 $g.l^{-1}$) and mixtures of γ–alumina with the Tamar River fulvic acid sample (concentration (0.48 g Al_2O_3 + 50 mg FA).l^{-1}) are summarised below. Both of these systems were subject to potentiometric acid – base titrations in NaCl solutions and surface area determination. Experiments were also conducted to determine the effects of pH and ionic strength on adsorption of the fulvic acid onto the alumina.

Electrode calibration data for the potentiometric titrations described in this chapter are included in Appendix 1.B.

8.2 Alumina Suspensions

8.2.1 Acid – Base Titrations

The data obtained from acid – base titrations of the washed γ–Al_2O_3 are shown as 'pH vs net base added' plots in Figure 8.1. The titration curves of the alumina at each ionic strength take the form of two sigmoidal regions, the boundary between which occurs at approximately pH 5.3.

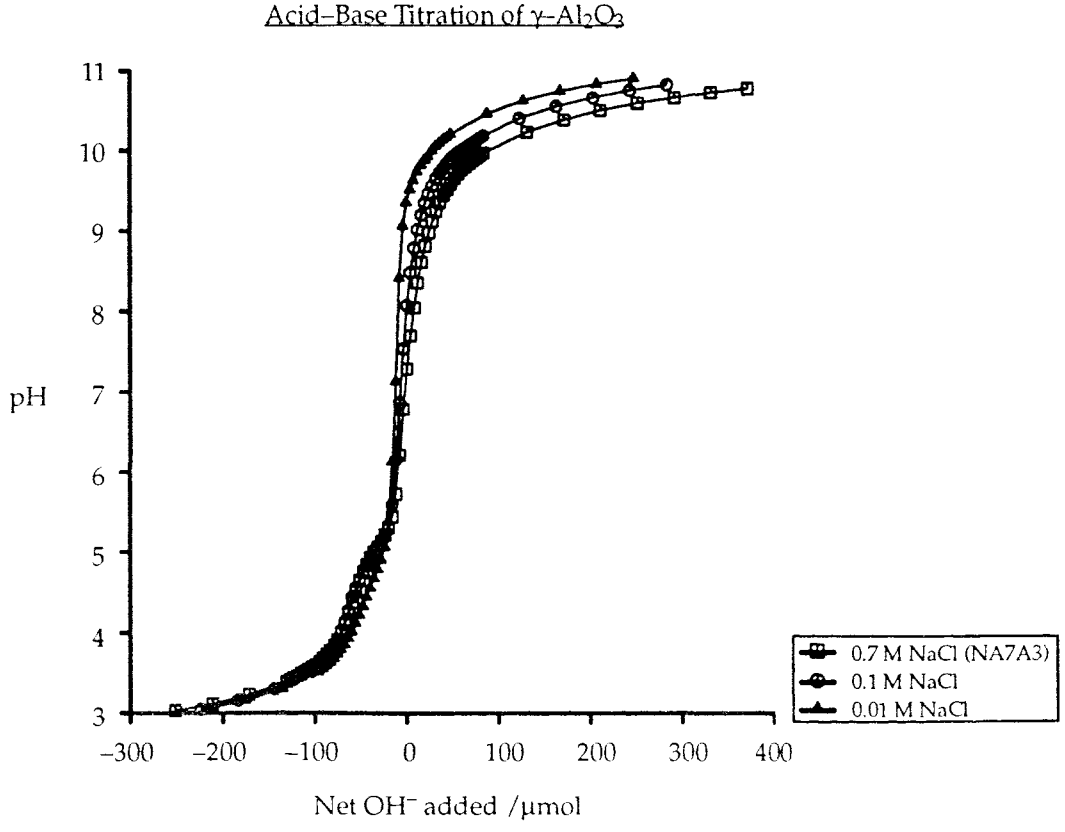

Figure 8.1 Titration data for γ–Al_2O_3 in NaCl solutions at various ionic strengths.

8.2.1.1 Point of Zero Charge pH of Alumina

Titration of an amphoteric oxyhydroxide with acid or base results in changes in its protonic surface charge, as can be seen from Eqns. 8.2.1 & 8.2.2 (from Eqns. 2.1.4 & 2.1.5, Section 2.1.3.2).

$$SOH_2^+ \Leftrightarrow SOH + H_s^+ \qquad (8.2.1)$$

$$SOH \Leftrightarrow SO^- + H_s^+ \qquad (8.2.2)$$

At some pH the contributions to surface charge from the reactions depicted in Eqns. 8.2.1 & 8.2.2 exactly equal one another and the net protonic charge of the substrate is zero. This pH is termed the point of zero charge pH (pH_{PZC}).

However, in solutions containing electrolyte ions (e.g. NaCl) there is also a contribution to the overall surface charge by ion–pair formation (e.g. Eqns. 8.2.3 & 8.2.4).

$$SOH_2^+ + Cl_s^- \Leftrightarrow SOH_2^+\text{–}Cl^- \qquad (8.2.3)$$

$$SO^- + Na_s^+ \Leftrightarrow SO^-\text{–}Na^+ \qquad (8.2.4)$$

Plots of calculated substrate surface charge (Eqn. 6.1.3) against pH for titrations carried out at different electrolyte concentrations allow the point of zero overall surface charge (i.e. that due to Eqns. 8.2.1 – 8.2.4) to be determined. As the charge on the substrate is reduced, the interactions of electrolyte ions with the surface are reduced, so that at zero overall charge the differences between titrations due to reactions of Na^+ and Cl^- become zero, and the surface charge plots converge (Turner *et al.*, 1987a; Hawkins 1987).

This point of zero overall surface charge may also represent the pH_{PZC} of the substrate, if the affinities of the electrolyte anion and cation for the surface are equal (Hawkins, 1987). Equivalent anion and cation adsorption has been reported previously for Na^+ and Br^- (on γ–Al_2O_3 (Sprycha, 1983)) and Na^+ and Cl^- (on TiO_2 (Sprycha, 1984) and α–Al_2O_3 (Ballion & Jeffrezic–Renault, 1985)), and this has lead other workers to assume that equivalent adsorption also occurs in the NaCl / γ–Al_2O_3 system (Hawkins, 1987).

Figure 8.2 shows a plot of surface charge (calculated using Eqn 6.1.3) against pH for the γ–alumina / NaCl system. There is a very clear intersection of the 0.7M, 0.1M and 0.01M surface charge curves at pH 5.27 in this plot. This pH also corresponds to the boundary between the two sigmoidal regions of Figure 8.1. Assuming equivalent adsorption of Na^+ and Cl^- on γ–Al_2O_3, it seems probable that this pH represents the pH_{PZC} of the γ–alumina used in this study.

The sigmoidal regions of Figure 8.1 therefore correspond to the reactions of the alumina when positively charged (Eqns. 8.2.1 & 8.2.3) at pH values below 5.27, and when negatively charged (Eqns. 8.2.2 & 8.2.4) at pH values above 5.27.

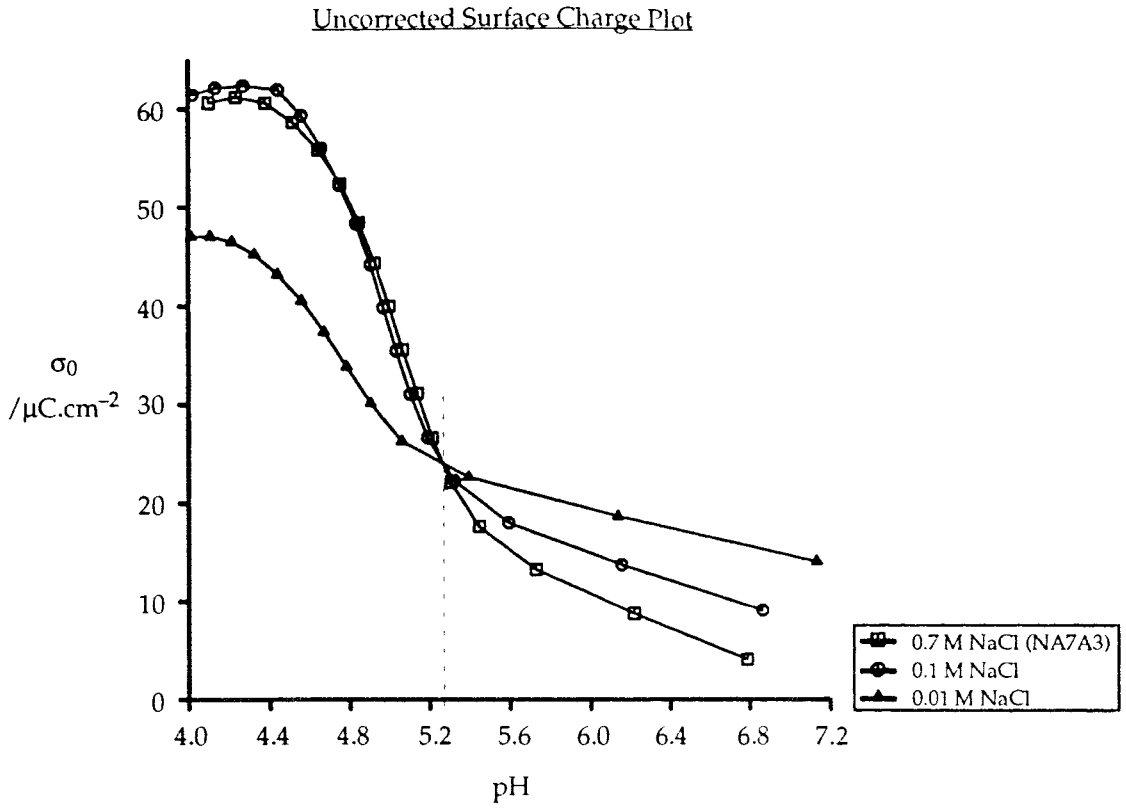

Figure 8.2 Plot of uncorrected surface charge against pH for γ–alumina in NaCl solutions.

However, this value of pH_{PZC} is rather lower than those quoted by other workers for γ–alumina (see Table 8.1). Specific adsorption of SeO_3^- ions has been found to lower the isoelectric point of α–Al_2O_3 from pH 8.5 to 5.2 (Ballion & Jaffrezic–Renualt, 1985). It seems likely therefore, that contamination of the sample by a specifically adsorbing anion would have the effect of lowering the sample's apparent pH_{PZC} (Breeuwsma & Lylkema, 1973). Titration curves of the unwashed sample are very similar to those of Figure 8.1, showing two sigmoidal regions either side of pH ~5.3. It seems probable that anion contamination was present on the untreated alumina, and that the washing procedure was unable to remove it.

Table 8.1 Point of zero charge pH values for γ–alumina.

pH_{PZC}	Reference
8.3	Westall & Hohl, 1980
8.7	Kummert & Stumm, 1980
8.5	Huang & Stumm, 1972

8.2.1.2 Formation Functions

Figure 8.3 shows formation functions (δn_{OH}) for the alumina sample, which have been corrected to zero at the calculated pH_{PZC} of the material (Section 8.2.1.1).

The effect of solution ionic strength on surface charge development, discussed in Sections 4.2.1 & 4.3.4 with regard to fulvic acids, can be seen very clearly in Figure 8.3. A total of 0.20 $mmol.g^{-1}$ of surface sites were titrated in 0.01M NaCl over the pH range 5.27 – 10, while, over the same pH range in 0.7M NaCl, 0.65 $mmol.g^{-1}$ of surface sites were titrated. However, at pH values below pH_{PZC} there is no apparent difference between the alumina titration curves in 0.1M and 0.7M solutions, while the separation of these curves from that of the 0.01M experiment is similar to the 0.01M – 0.7M separation above pH_{PZC}.

The numbers of titrateable functional groups appears to be different either side of pH_{PZC} (0.3 $mmol.g^{-1}$ below, 0.65 $mmol.g^{-1}$ above in 0.7M solution), although the surface complexation reaction scheme (Eqns. 2.1.4 & 2.1.5) implies that this should not be so. This may due to the different pH ranges either side of pH_{PZC} (~1.5 and 5 pH units) and the rather low accuracy of the formation function at low pH values.

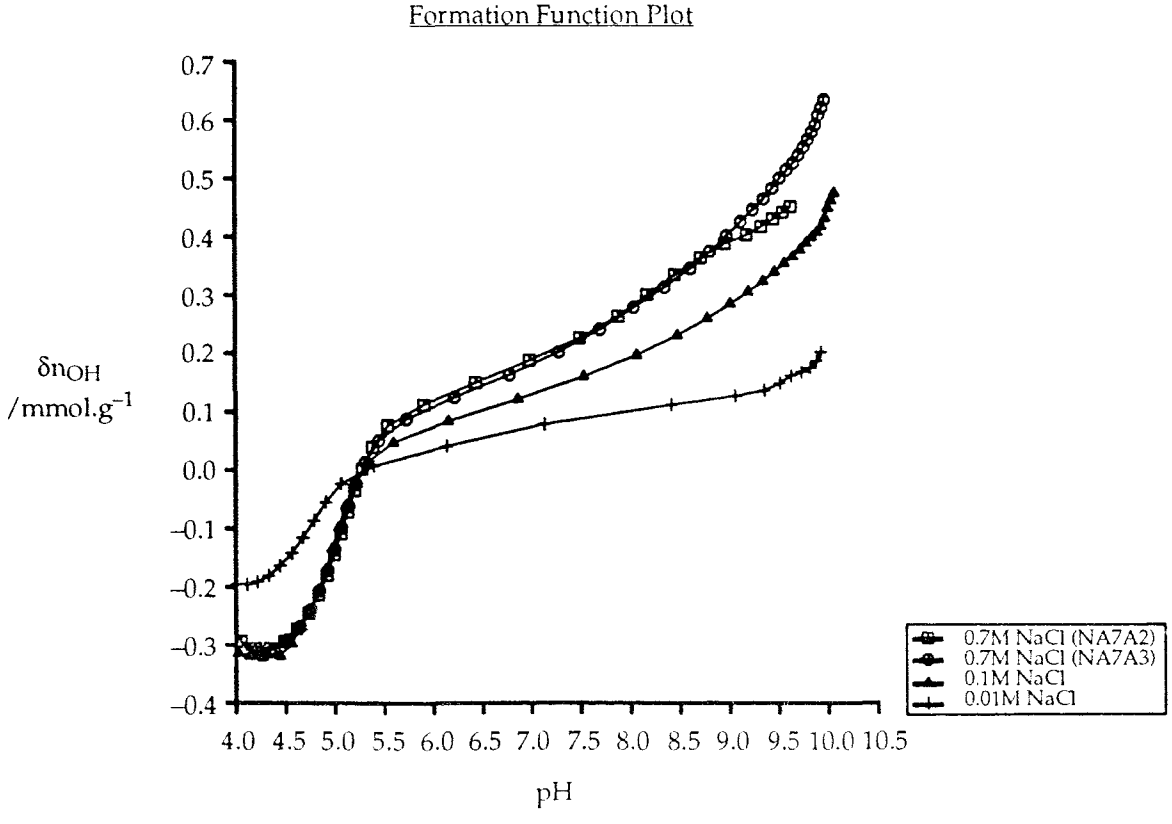

Figure 8.3 Plot of formation function (δn_{OH}) against pH for γ–Al_2O_3 in NaCl solutions (δn_{OH} corrected to zero at pH_{PZC}).

Figure 8.3 includes δn_{OH} vs pH curves for two experiments carried out on the alumina in 0.7M NaCl solutions (Experiments NA7A2 & NA7A3). At pH < 9, these illustrate the very good reproducibility obtainable using the experimental regime described in Chapter 3. (Experiment NA7A2 was conducted on 101.8 mg of γ–Al_2O_3, using calibration data from experiment NA7B43 to calculate pH, while experiment NA7A3 used 100.2 mg of γ–Al_2O_3 and calibration experiment NA7B51.) At pH > 9 the plots diverge, probably as a result of a failure of the titration apparatus which occurred towards the end of experiment NA7A2 (there is a sharp increase in electrode drift rate at the point of divergence in this titration).

8.2.2 Surface Area

The specific surface area of 47.4 mg of NaOH washed γ–alumina (Section 3.1.2) was determined by BET adsorption (Section 3.5) to be 3.80 m^2, giving a specific surface area for the sample of 80.2 m^2g^{-1}. (The specific surface area of γ–Al_2O_3 from another source (Cabot Corp., Boston, Mass., USA) has been determined to be 129 m^2g^{-1} (Huang & Stumm, 1972)).

8.3 Alumina – Fulvic Acid Mixtures

8.3.1 Adsorption of Fulvic Acid on Alumina

The results obtained from investigation of the adsorption of the Tamar River fulvic acid onto alumina (Section 3.4) at the concentrations of fulvic acid and alumina used in potentiometric titrations are shown in Table 8.2 and Figure 8.4.

Table 8.2 lists the concentrations of organic carbon found to remain in solution after equilibration of portions of fulvic acid with γ–alumina, together with the equilibrium pH of each suspension. Percentage adsorption figures in Table 8.2 are calculated using the "fulvic acid blank" (see Section 3.4.1) for each ionic strength to represent 0% adsorption. Figure 8.4 shows the percentage adsorption for each experiment as a function of pH.

8.3.1.1 Effect of pH and Ionic Strength

As discussed in Section 1.1.4.3, adsorption is thought to be brought about by ligand exchange of alumina surface hydroxyls and protonated hydroxyls with the negatively charged functional groups of the fulvic acid (Parfitt *et al.*, 1977), while repulsive forces between adsorbed molecules are reduced by protonation or cation complexation of non – adsorbing functional groups (Tipping, 1981). In the absence of complexing cations, the number of potential ligand exchange sites (SOH & SOH^+) decreases with increasing pH, while the negative charge on the fulvic acid increases. This leads to a maximum in adsorption at relatively low pH and decreasing adsorption with increasing pH thereafter. (See, for example, Figure 8.5a, which is reproduced from Davis, 1980, and represents adsorption of a lake sediment organic extract (USOM) on γ–alumina in NaCl solutions).

Table 8.2 Concentrations of organic carbon remaining in solution and percentage adsorption after equilibration of fulvic acid with γ–Al_2O_3 at various pH values and at different ionic strengths of NaCl.

(Figures in italics are for fulvic acid free experiments, those in bold are for alumina free experiments.)

pH	[org. C] /μM	% Adsorption
I = 0.7M		
3.21	702.6±38.9	66.0±4.2
5.00	307.9±17.1	85.1±1.8
6.23	411.2±22.8	80.1±2.2
6.60	627.7±34.4	69.6±3.2
7.23	364.2±19.8	82.4±1.9
7.36	786.0±43.2	62.0±4.2
7.95	480.7±26.3	76.7±2.6
10.07	794.5±43.7	61.5±4.2
3.08	*323.3±17.5*	
4.32	*294.8±12.4*	
10.30	*118.9±8.2*	
6.03	**2066.3±114.3**	
I = 0.1M		
3.28	271.2±14.6	84.9±1.7
5.94	202.0±10.7	88.7±1.2
6.64	571.1±31.2	68.2±3.5
8.21	792.4±43.5	56.0±4.9
10.36	671.5±36.9	62.7±4.2
6.71	*153.3±8.0*	
6.65	**1800.0±99.6**	
I = 0.01M		
3.18	163.6±8.6	86.8±1.4
6.75	515.8±28.2	58.6±4.5
7.76	1025.0±56.5	17.8±9.1
9.96	703.8±38.7	43.6±6.2
6.50	*348.3±18.5*	
6.59	**1247.5±68.8**	

While the adsorption curves of Figure 8.4 all show an adsorption maximum at low pH (in the range pH 3 – 6), adsorption does not decrease to zero as it does in Figure 8.5a, and there is an increase in adsorption at pH values above 8. The effect of solution ionic strength on adsorption of Tamar River fulvic acid (Figure 8.4) and USOM (Figure 8.5a) is also quite different. Adsorption of USOM was reduced at ionic strengths above 0.01M, while increasing ionic strength appears to reduce the variability in percentage adsorption of Tamar River fulvic acid, without significant variation in its maximum value (see Table 8.2).

It can also be seen, by comparison of Figures 8.4 & 8.5a, that a greater proportion of Tamar River fulvic acid is adsorbed on γ–alumina than was USOM. It was observed that the adsorbing and non – adsorbing fractions of USOM differed in their acidity contents, with the adsorbing fraction having a higher proportion of weakly acidic functional groups (Davis, 1982). Davis proposed that the adsorbing fraction was more likely to contain functional groups in *ortho* arrangements than the non – adsorbing fraction, and that this would enhance its adsorption (see Section 1.1.4.3). The potentiometric titration curves of Tamar River fulvic acid (Section 4.3) and USOM (Davis, 1982) indicate that the Tamar sample has proportionally more weakly acidic groups than USOM, and this may, therefore, explain its greater extent of adsorption.

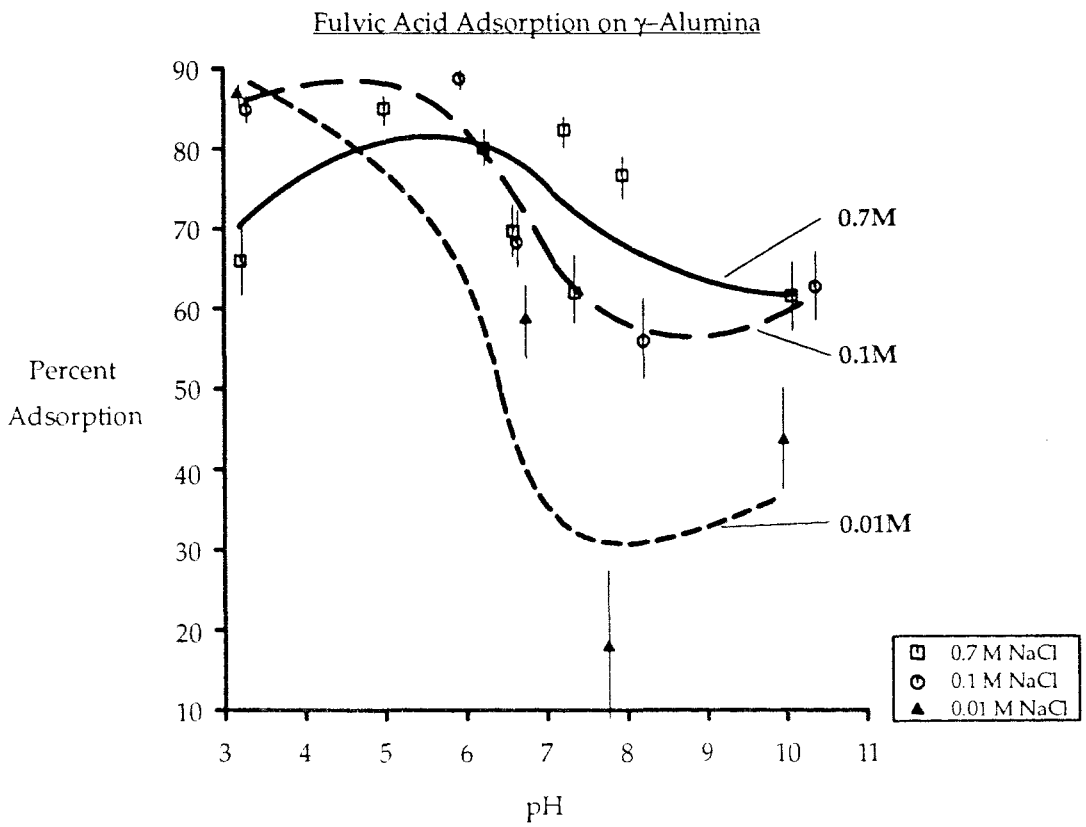

Figure 8.4 Plot of percentage adsorption of fulvic acid on γ–alumina against pH at various ionic strengths of NaCl.

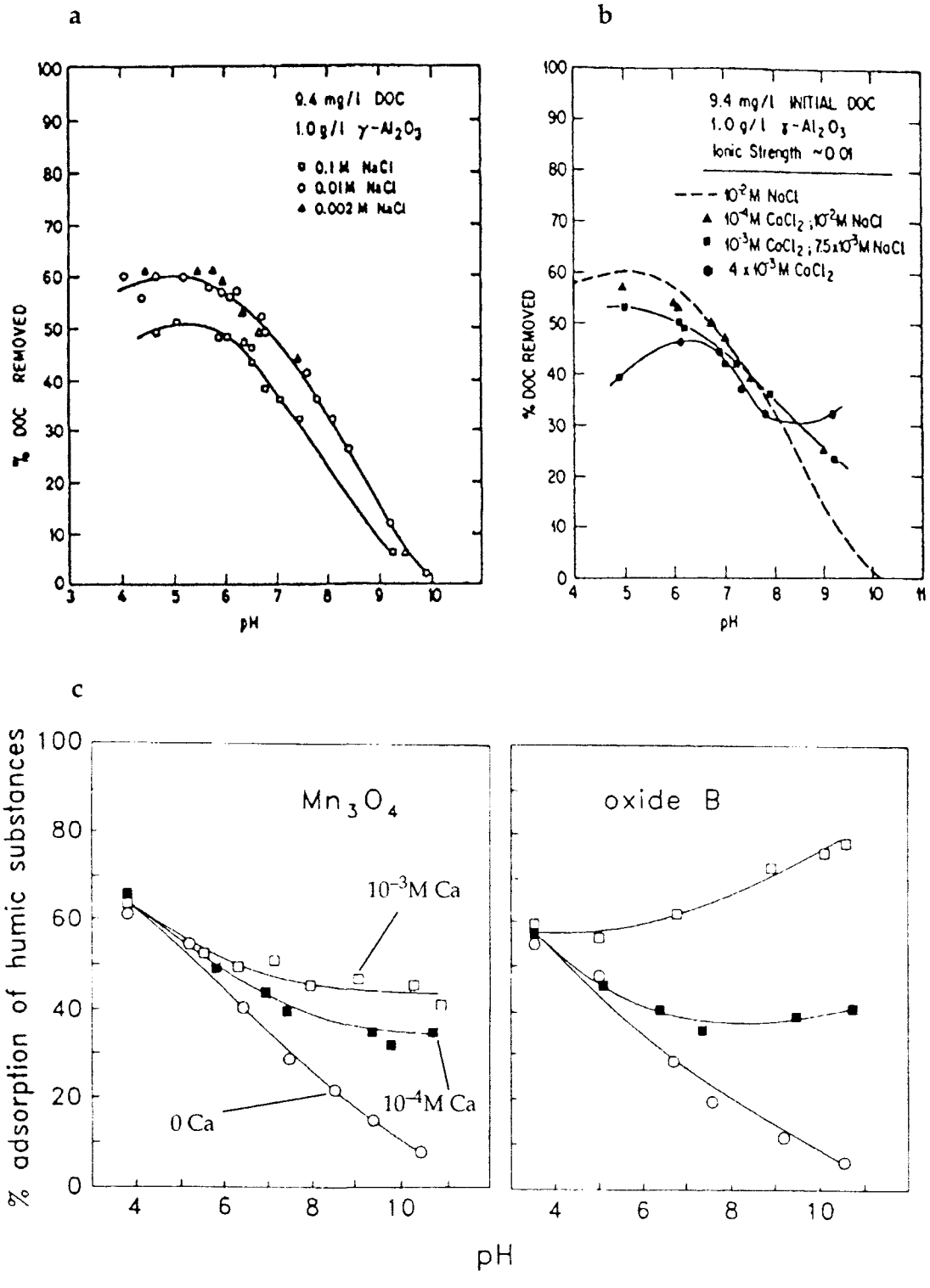

Figure 8.5 Adsorption of natural aquatic organics on oxide particles against pH at various ionic strengths of NaCl and $CaCl_2$.

Lake sediment organic extract (USOM) on γ–Al_2O_3 in NaCl solutions (**a**) and in solutions of NaCl and $CaCl_2$ (**b**). (Reproduced with permission from Davis, 1980, and Davis, 1982, Geochim. Cosmochim. Acta, 46, 2381 respectively). Penwhirn Reservoir humic substances on Mn oxides in 0.01M NaCl solutions with 0, 10^{-4}M & 10^{-3}M $CaCl_2$ (**c**). (Reproduced with permission from Tipping, 1990).

8.3.1.2 Effect of Calcium

It has been shown in Section 4.2.2 that the Tamar River fulvic acid sample under study contains a significant amount of calcium (1.7 $mmol.g^{-1}$). Complete dissociation of this calcium from the fulvic acid would result in a total concentration of calcium of $\sim 10^{-4}M$ at the fulvic acid concentration in use.

The effect of similar concentrations of calcium on organic matter adsorption has been studied previously (onto γ–alumina (Davis, 1982) and onto manganese oxides (Tipping, 1990)). Both of these workers reported increased adsorption in the presence of calcium, especially at high pH values, Davis at $[Ca] = 4 \times 10^{-3}M$, Tipping at $[Ca] = 10^{-4}M$. (Figure 8.5c shows the adsorption curves obtained for Penwhirn Reservoir humic substances with Mn oxides (Tipping, 1990)).

The curves of Figure 8.4 are qualitatively similar to those reported for organic adsorption in the presence of calcium (see Figure 8.5b & c) (Davis, 1982; Tipping, 1990), and it therefore seems probable that the calcium present in the fulvic acid sample modifies its adsorption behaviour by the formation of Al_2O_3 – Ca – FA bonds, or by neutralisation of adsorbed fulvic acid charge (Tipping, 1990). The increase in organic adsorption at high pH in Figures 8.4 & 8.5b & c may be due to a process similar to Eqn. 8.3.1, which would be favoured in the high pH range because the concentrations of SO^- and FA^- would both be high.

$$SO^- + Ca^{2+} + FA^- \Leftrightarrow SO\text{–}Ca\text{–}FA \qquad (8.3.1)$$

8.3.2 Acid – Base Titrations

Titration data, in the form of 'pH vs net base added' and formation function plots, for mixtures of fulvic acid and γ–alumina are shown in Figures 8.6 & 8.7. The formation function curves of Figure 8.7 have been corrected to zero at the point of zero charge pH of γ–alumina, as point of zero charge data are unavailable for this mixture. (The nature of the fulvic acid – alumina mixture does not allow an unique (i.e. ionic strength independent) point of zero charge pH to be determined – see Sections 8.3.2.1 & 8.3.2.2).

In contrast to Figures 8.1 & 8.3, there appears to be very little influence of solution ionic strength on the proton exchange behaviour of this mixture. Both the pH curves of Figure 8.6 and the δn_{OH} curves of Figure 8.7 are almost coincident with one another. Figure 8.7 indicates that the number of functional groups being titrated are essentially the same at all ionic strengths. Comparison of the low pH regions of Figures 8.3 & 8.7 shows that, even at the pH of maximum fulvic acid adsorption (Section 8.3.1), the mixture still exhibits some of the titration characteristics of alumina. This implies that the ratio of fulvic acid to alumina used in this study is not sufficient to produce total coverage of the alumina particles with fulvic acid.

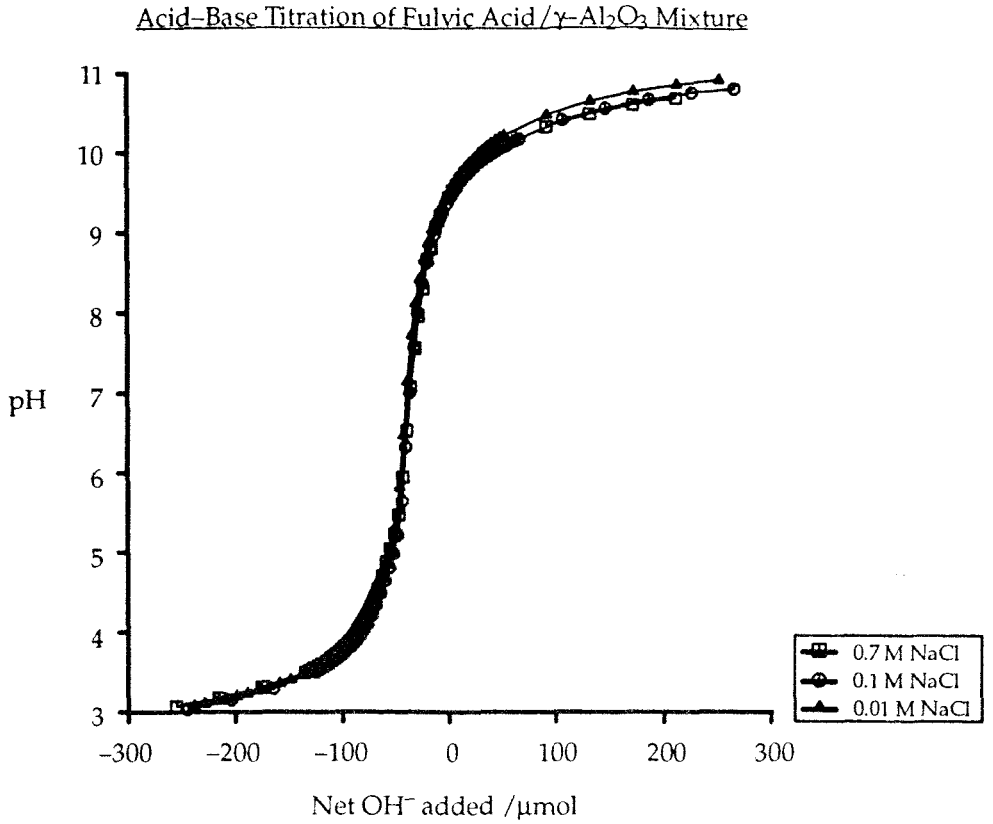

Figure 8.6 Titration data for fulvic acid / γ–Al_2O_3 mixtures in NaCl solutions at various ionic strengths.

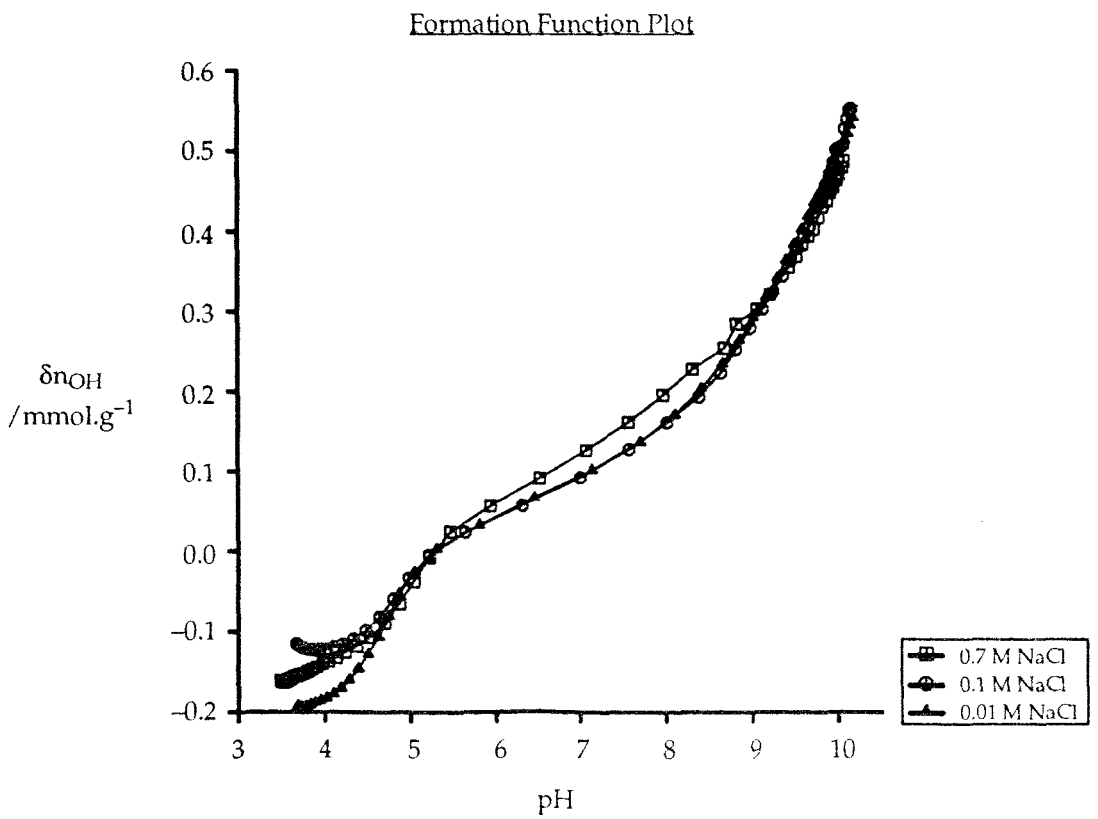

Figure 8.7 Plot of formation function (δn_{OH}) against pH for fulvic acid / γ–Al_2O_3 mixtures in NaCl solutions (δn_{OH} corrected to zero at $pH_{PZC}(Al_2O_3)$).

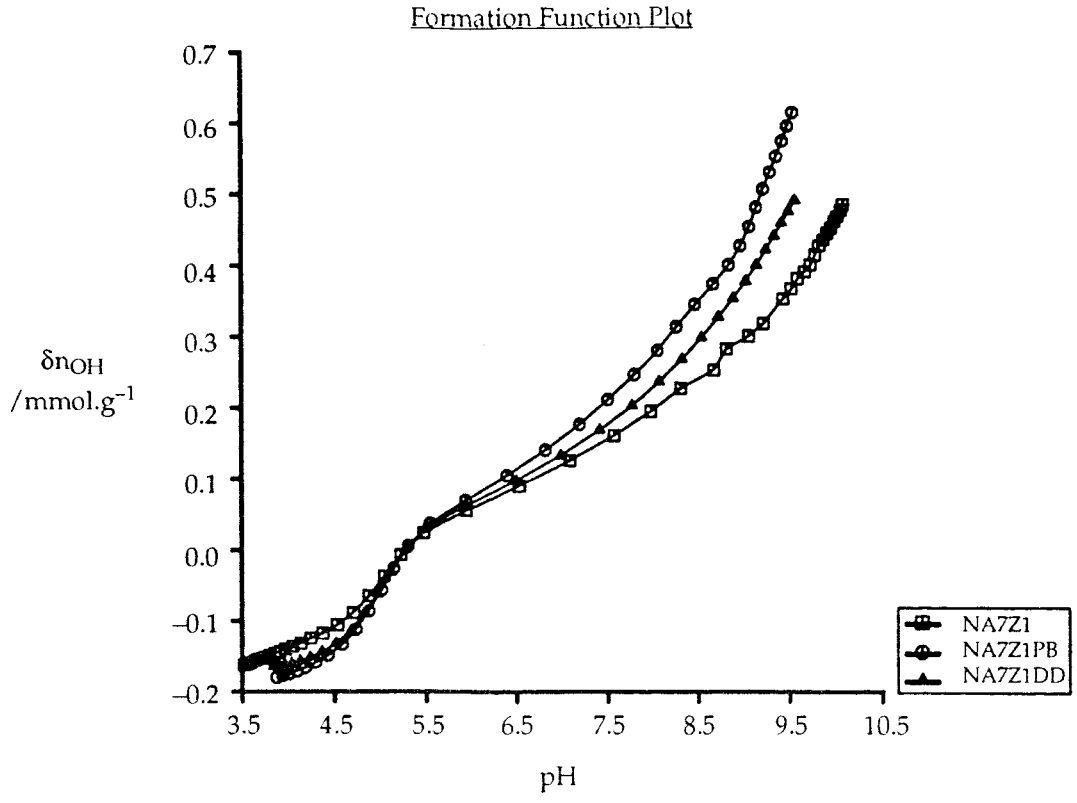

Figure 8.8 Plot of formation function against pH for fulvic acid / γ–Al_2O_3 mixtures in 0.7M NaCl solution.

Figure 8.8 shows formation functions for several fulvic acid / alumina mixtures titrated in 0.7M NaCl solution (NA7Z1 – Figure 8.7, NA7Z1PB & NA7Z1DD). The latter of these (NA7Z1PB & NA7Z1DD) show a greater number of titrateable functional groups than do the experiments reported in Figure 8.7. The most likely cause of this increase in titrateable group numbers is that there is a lower degree of fulvic acid – alumina interaction in these experiments.

It is unclear what may have caused this change as the fulvic acid : alumina ratio is the same in all cases and the experimental regimes of the titrations were also kept as constant as possible.

8.3.2.1 Fulvic Acid – Alumina Interactions

The extent to which fulvic acid and alumina titrateable functional groups are involved in adsorption reactions can be assessed by comparing the observed formation function curves of the mixture with those of its individual components.

Figures 8.9 – 8.11 show δn_{OH} curves for fulvic acid (from Figure 4.9), alumina (Figure 8.3), the fulvic acid – alumina mixture (Figure 8.7) and 'fulvic acid + alumina' for each of the solution ionic strengths studied. The 'fulvic acid + alumina' curve in each plot represents the expected δn_{OH} curve of the mixture were there no functional group interactions between the fulvic acid and alumina. All curves in these plots have been corrected to zero at $pH_{PZC}(Al_2O_3)$, as this pH marks the transition from net positive to net

negative charge on the alumina. (The formation functions are expressed as mmoles of active sites per litre of solution for ease of comparison).

The differences between the δn_{OH} curves of the actual and 'non–interacting' fulvic acid – alumina mixtures over the pH range of the titrations and with ionic strength are quite noticeable. Figures 8.9 – 8.11 all indicate that the total number of titrateable functional groups increases with increasing pH, i.e. the fractional difference between the observed and 'non–interacting' curves decreases. Also, the magnitude of the increase in titrateable group numbers with pH increases with decreasing ionic strength. Table 8.3 lists the fractions of theoretical total sites ('fulvic acid + alumina') which were actually titrated at a number of pH values for these experiments.

The changes in numbers of titrateable functional groups with pH and ionic strength indicated by Figures 8.9 – 8.11 and Table 8.3 appear to be a reflection of the fulvic acid adsorption data presented in Table 8.2 and Figure 8.4. These experiments indicated that fulvic acid adsorption was greatest at low pH and that the range of percentage fulvic acid adsorption values was greatest at low ionic strength.

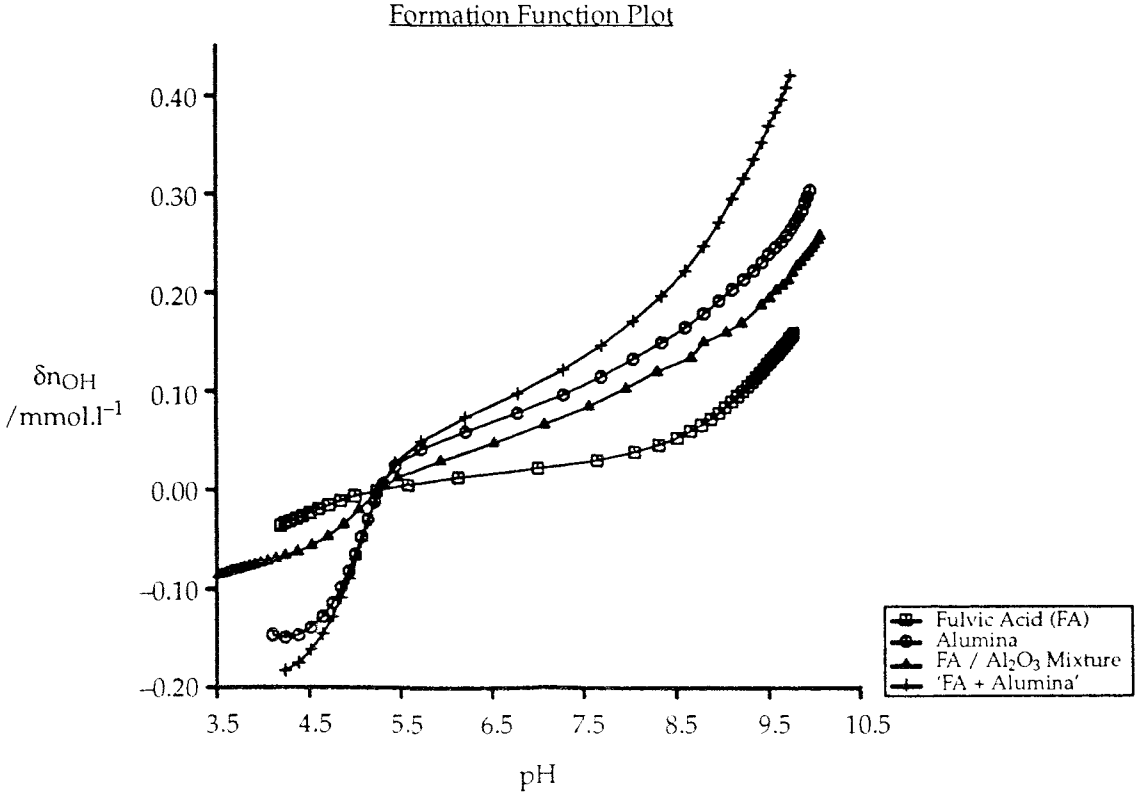

Figure 8.9 Formation functions ($mmol.l^{-1}$) for fulvic acid, γ–alumina, fulvic acid / alumina mixture and "fulvic acid + alumina" in 0.7M NaCl solution.

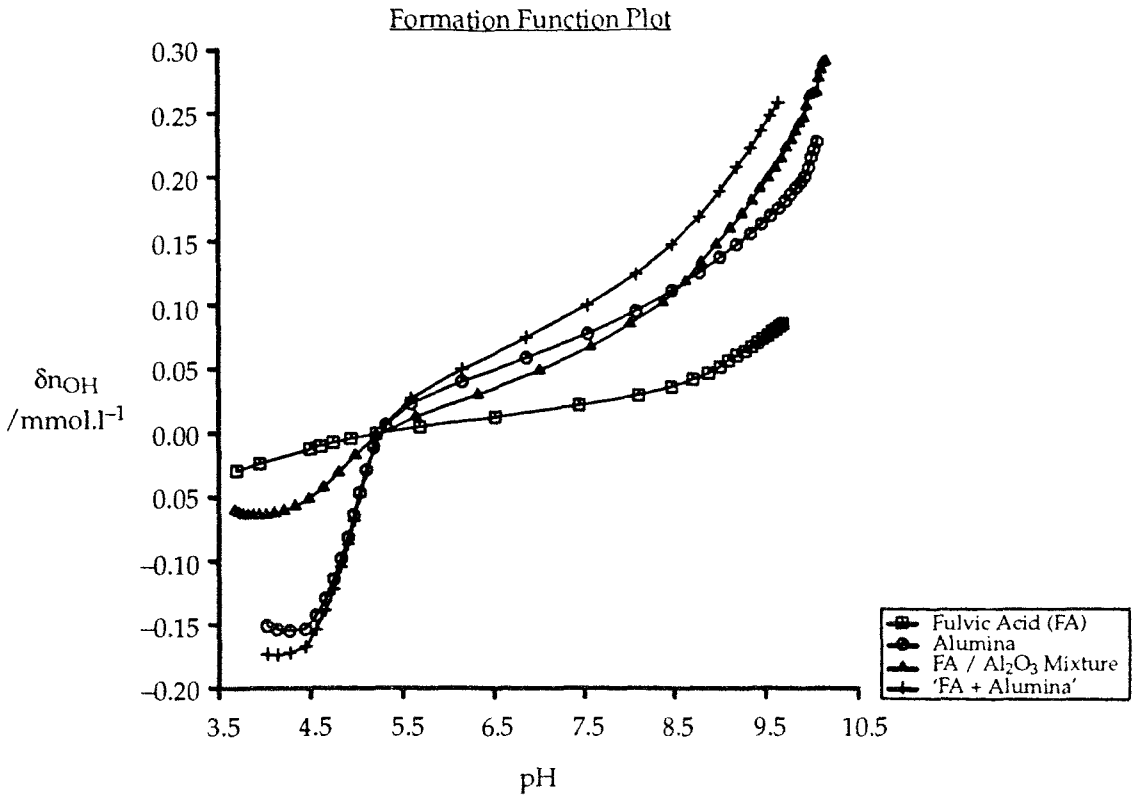

Figure 8.10 Formation functions (mmol.l^{-1}) for fulvic acid, γ–alumina, fulvic acid / alumina mixture and "fulvic acid + alumina" in 0.1M NaCl solution.

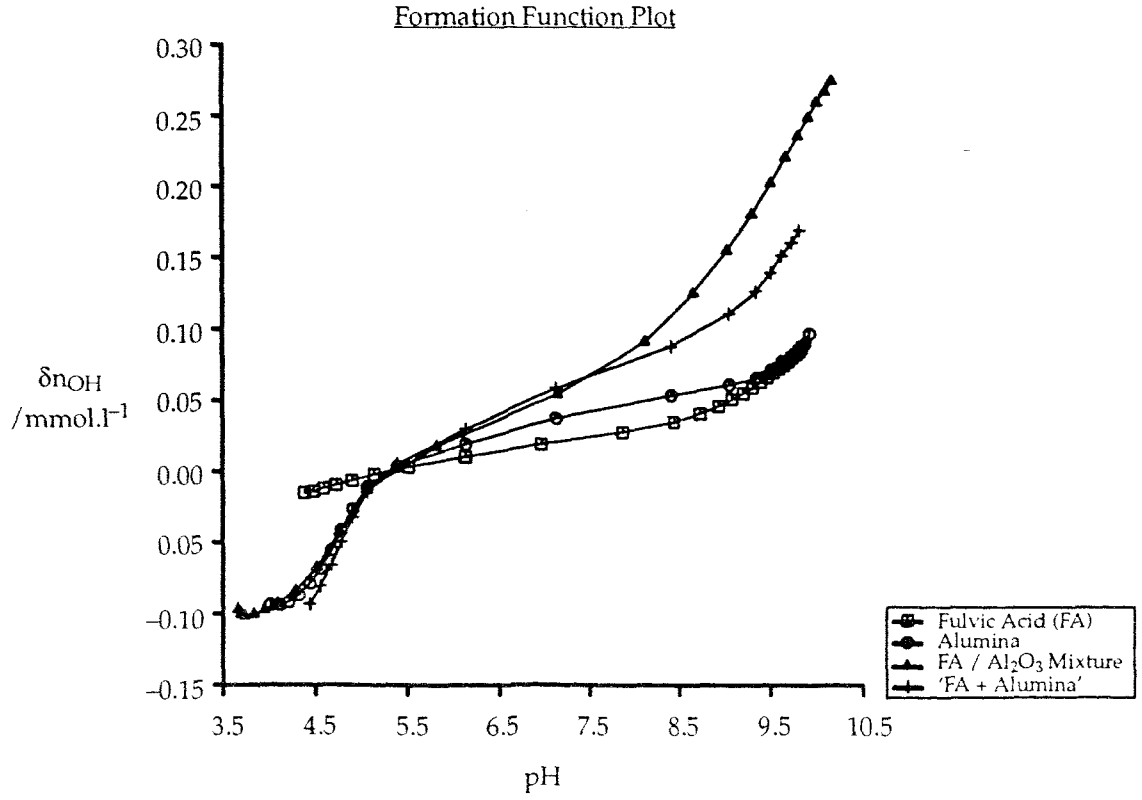

Figure 8.11 Formation functions (mmol.l^{-1}) for fulvic acid, γ–alumina, fulvic acid / alumina mixture and "fulvic acid + alumina" in 0.01M NaCl solution.

Table 8.3 Fractions of sum total available fulvic acid and alumina functional groups titrated in fulvic acid – alumina titrations.

(All fractions are calculated relative to $\delta n_{OH} = 0$ in each of Figures 8.9 – 8.11, those in parentheses are calculated using Eqn. 8.3.2).

pH	Ionic Strength ($mol.l^{-1}$)					
	0.7		**0.1**		**0.01**	
4.5	0.34	(0.78)	0.31	(0.86)	0.81	(0.75)
6.0	0.52	(0.74)	0.50	(0.70)	0.86	(0.56)
7.5	0.60	(0.71)	0.65	(0.73)	1.00	(0.77)
9.0	0.55	(0.62)	0.80	(0.69)	1.35	(0.70)

Also included in Table 8.3 are values of the fraction of total sites titrated (F), which have been calculated using Eqn. 8.3.2.

$$F = \frac{C_{FA} + C_{Al} - 2\beta C_{FA}}{C_{FA} + C_{Al}} \qquad (8.3.2)$$

Eqn. 8.3.2 represents the fraction of sites remaining after a fraction β of the fulvic acid adsorbs on alumina, assuming that two sites (one fulvic, one alumina) are involved in the adsorption reaction (see Eqns. 1.1.5 & 8.3.1). C_{FA} and C_{Al} are the concentrations of fulvic acid and alumina functional groups at a given pH (from Figures 8.9 – 8.11) and β has been estimated from the curves of Figure 8.4. The calculated values of F are in good agreement with those measured from Figures 8.9 – 8.11 considering that Eqn. 8.3.2 does not take account of any reduction in titrateable sites due to steric effects and the general nature of the curves of Figure 8.4 from which β was estimated.

It can be seen from Figure 8.11 that the number of mixture sites titrated in 0.01M NaCl solution appears to exceed the total available at high pH values (see also Table 8.3). This may be due to an underestimation of the total numbers of fulvic acid sites, caused by the correction of the fulvic acid formation function to zero at pH 5.27, and also to a combination of the errors in the formation function calculation at high pH values.

From the above it would appear that the apparent lack of ionic strength dependence of the fulvic acid – alumina titration data can be explained if there is desorption of fulvic acid from the alumina when the solution pH is raised and if this desorption is greatest in low ionic strength solutions. In this way, the greater (counterion promoted) proton exchange capacity of the mixture in high ionic strength solutions (as seen for fulvic acid and alumina alone) is roughly balanced by the greater increase in the number of titrateable groups caused by desorption of fulvic acid from alumina in low ionic strength solutions.

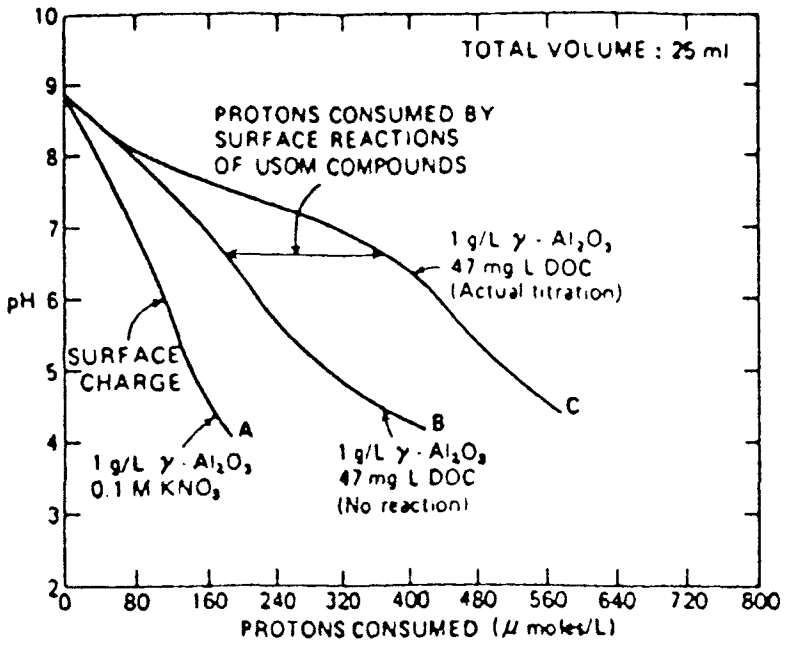

Figure 8.12 Plot showing the pH dependence of proton consumption for alumina and interacting and non–interacting mixed alumina – USOM systems (Reproduced with permission from Davis, 1982, Geochim. Cosmochim. Acta, 46, 2381).

Although no desorption experiments were conducted in this work, desorption of natural organics from alumina and iron oxides upon pH increase has been reported previously (Davis, 1980; Tipping *et al.*, 1989).

Figure 8.12 shows the variation in proton consumption with pH for the USOM – alumina system (Davis, 1982). This plot shows the titration in the base to acid direction and reveals a clear extra consumption of protons of the mixed system over the sum of its components. This extra proton consumption is consistent with the release of surface hydroxyls due to organic matter adsorption and their subsequent titration.

8.3.2.2 Point of Zero Charge pH of Fulvic Acid – Alumina Mixture

It has been shown in Section 8.3.1 that the proportion of fulvic acid which is adsorbed to alumina at a given pH can vary quite markedly with solution ionic strength. The result of this variation in adsorption is that the proportions of fulvic acid, alumina and fulvic acid coated alumina functional groups are also different at different ionic strengths.

Given that the point of zero charge pH (pH_{PZC}) of a material arises as a balance of its proton and major ion equilibria (Section 8.2.1.1), it is therefore unlikely that an ionic strength independent pH_{PZC} can be measured (or calculated) for this system.

Since it also appears that fulvic acid desorbs from alumina when solution pH is raised (Section 8.3.2.1), and that a change in the proportions of free and adsorbed species would result from such desorption, it would appear that a point of zero charge pH cannot be determined for the fulvic acid – alumina mixture, even at constant ionic strength.

8.3.3 Surface Area

A sample of fulvic acid contacted alumina was prepared by a similar procedure to that used in Sections 8.3.1 & 8.3.2. In order to avoid the need to wash NaCl from the particulate material, alumina (50 mg) was suspended in double distilled water and allowed to equilibrate for 30 minutes. The pH of the suspension was adjusted to bring about maximum adsorption of the fulvic acid (pH ~4.5, Section 8.3.1), and 5 ml of fulvic acid stock solution was then added.

Adsorption appeared to be extremely rapid, the white alumina particles turning brown within a few minutes. However, the suspension was allowed to stand in the dark for a period of 24 hours to ensure that equilibrium was reached. After this time, the particulate matter was removed from suspension by centrifugation (5,000 rpm, 30 minutes) and freeze–dried.

The specific surface area of the material recovered by this process (40.3 mg) was determined to be 78.2 m^2g^{-1} by BET adsorption (Section 3.5). Comparison of this value with the specific surface area determined for organic–free alumina (80.2 m^2g^{-1}, Section 8.2.2) implies that there is very little influence of the organic material on the surface of the alumina. This is in contrast to the changes in acid – base chemistry brought about by adsorption of the fulvic acid onto alumina (Sections 8.2.1 & 8.3.2), and indicates that there is a poor correlation between BET surface areas and chemical properties in this respect.

9. ALUMINA AND ALUMINA / FULVIC ACID: ADSORPTION MODELS

9.1 Introduction

Potentiometric titration data have been obtained for samples of alumina and fulvic acid / alumina mixtures in NaCl solutions at several ionic strengths (Sections 8.2 & 8.3). These data are used below to assess the applicability of the polyelectrolyte gel (Section 2.4), Gouy Chapman (Section 2.2) and surface complexation (Section 2.3) models to these systems.

9.1.1 Correction of Fulvic Acid / Alumina Mixture Titration Data

The difficulties in determining a point of zero charge pH (which could be used to correct the data) for the fulvic acid / alumina mixture have been discussed in Sections 8.3.2.1 & 8.3.2.2. In Section 4.3.3.2 the initial pH of a fulvic acid solution was used (together with a charge balance equation) to determine a common charge for a series of fulvic acid titrations. However, the variation in fulvic acid adsorption (and probable desorption) with ionic strength and pH (Sections 8.3.1 & 8.3.2), as well as the probable role of Ca^{2+} ions in the fulvic acid – alumina interaction (Section 8.3.1.2), make this approach impractical for use with the fulvic acid / alumina mixture. Initial solution pH values are not available for all of the mixture titrations and the extent of fulvic acid – Ca – alumina interaction is unknown.

The fulvic acid / alumina mixture data have therefore been corrected to zero at the pH_{PZC} of γ–Al_2O_3. This is justified by the facts that the titration curves of the mixture retain much of the character of those of alumina and that this pH represents the point at which one of the components of the mixture (the alumina) is uncharged. This correction also allows a direct assessment of the effect of fulvic acid on the acid – base chemistry of the alumina to be made.

9.2 Polyelectrolyte Gel Analysis

This analysis consists of a diagnostic test for invasion of salt ions into a substrate matrix and a quantitative model for such salt ion invasion (these are described in more detail in Section 2.4). Briefly, the diagnostic test employs plots of the Henderson – Hasselbalch pK (pK_{HH}, Eqn. 2.4.1) against pH and pH+pX to indicate whether or not a substrate is permeable to the ions of its supporting electrolyte. Where the substrate is permeable, the model offers a means of obtaining intrinsic stability constants ($p\overline{K}_{HA}^{int}$) from titration data by extrapolation (Marinsky, 1985).

9.2.1 Determination of α

As in Section 5.1.1, the degree of dissociation (α) of the alumina and alumina / fulvic acid mixtures has been determined by reference to the zero point of the formation function ($\alpha = 0$) and its maximum value, the total titrateable acidity of each substrate ($\alpha = 1$). The

total acidities of the alumina and mixture samples are ~0.7 mmol.g^{-1} (Figure 8.3) and ~0.65 mmol.g^{-1} (Figure 8.7) respectively.

9.2.2 Permeability Test

"Impermeability Test" and "Permeability Test" plots for alumina and alumina / fulvic acid mixtures are shown in Figures 9.1 & 9.2 and 9.3 & 9.4. The degree of dissociation used to determine pK_{HH} in these plots was calculated for negatively charged surfaces (i.e. pH > pH_{PZC}) using Eqn. 5.1.1.

There is a marked difference in the ionic strength dependence of pK_{HH} between alumina and the mixture. The curves of Figures 9.3 & 9.4 exhibit the behaviour of a salt ion impermeable substrate (cf. Figures 5.1 – 5.11), while neither set of pK_{HH} vs pH or pK_{HH} vs pH+pCl curves in Figures 9.1 & 9.2 coincides with one another and thus do not give a clear indication of the permeability characteristics of the alumina. The separations of the curves in Figures 9.1 & 9.2 are close to half a log unit per ten fold change in ionic strength, with the curves of Figure 9.1 being only slightly closer together than those of Figure 9.2.

A plot of pK_{HH} vs α for the alumina titrations is shown in Figure 9.5. This is very similar to a pK_{HH} vs α plot reported for a sample of SiO_2 (Figure 9.6) (Marinsky *et al.*, 1983). This sample was classified as being impermeable by these authors, although no pK_{HH} vs pH or pK_{HH} vs pH+pX plots were reported for the sample.

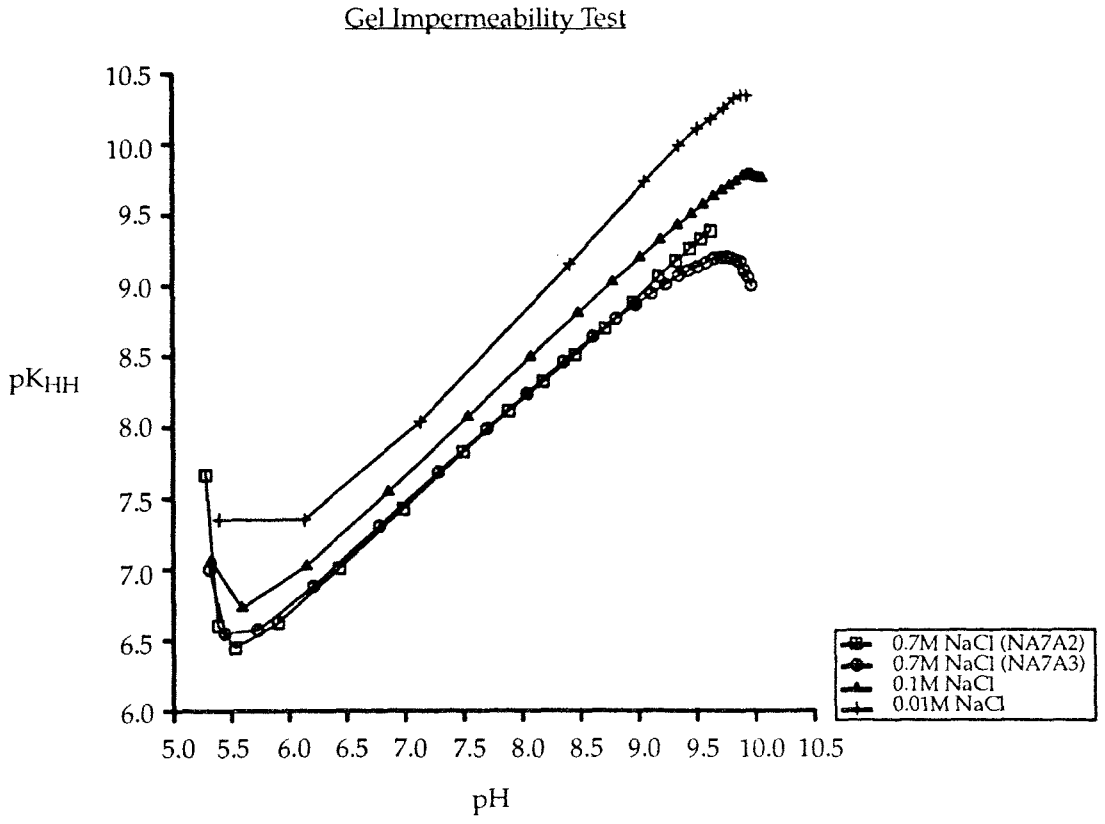

Figure 9.1 Plot to test for impermeability of γ–alumina to Na^+ ions in NaCl solutions.

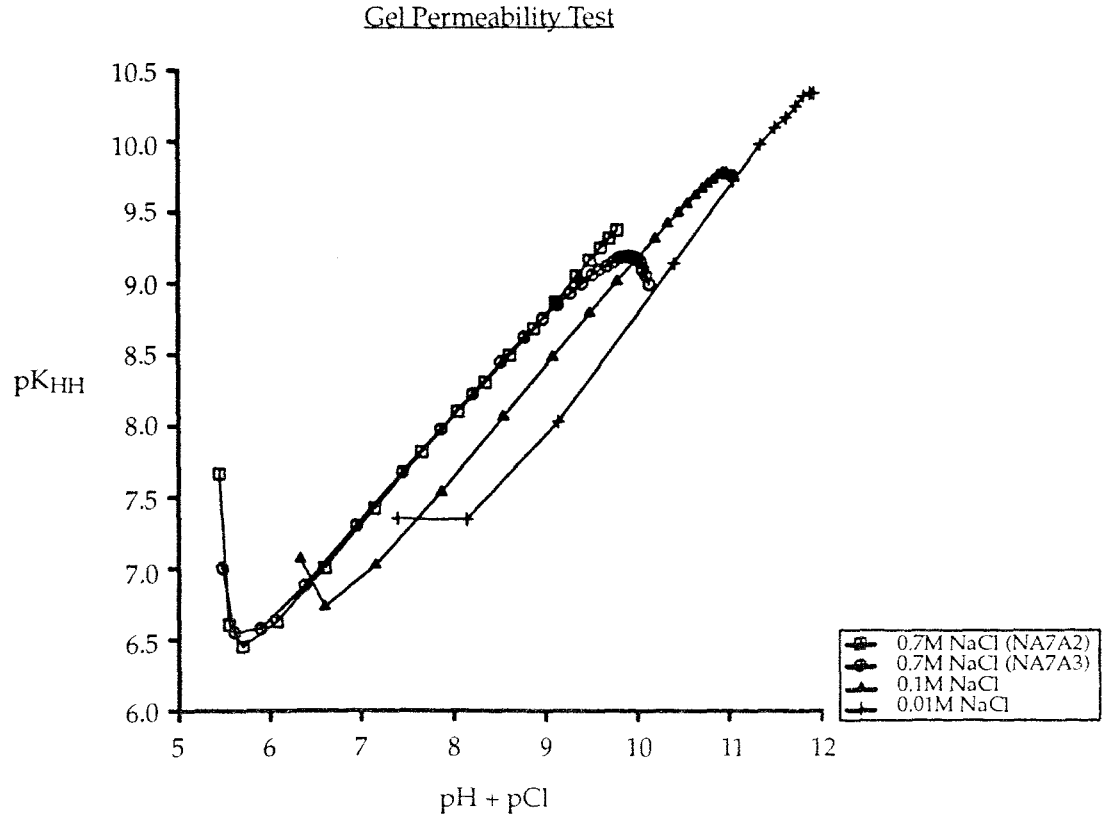

Figure 9.2 Plot to test for permeability of γ–alumina to Na^+ ions in NaCl solutions.

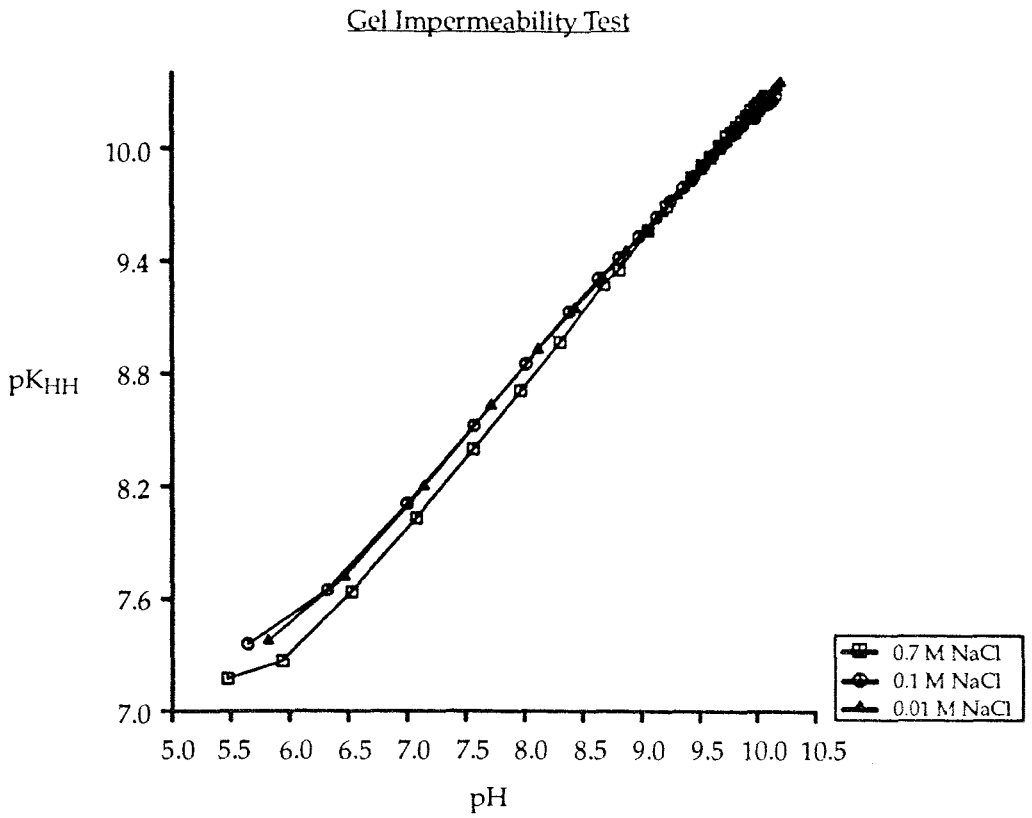

Figure 9.3 Plot to test for impermeability of fulvic acid / γ–alumina mixture to Na^+ ions in NaCl solutions.

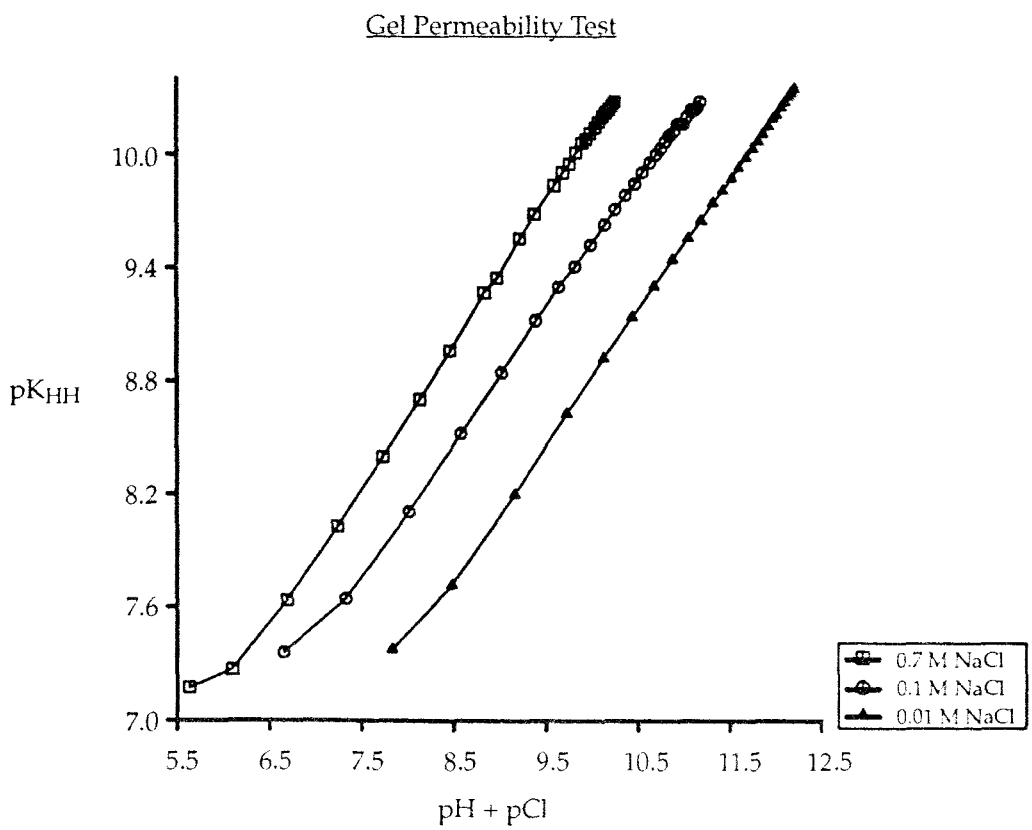

Figure 9.4 Plot to test for permeability of fulvic acid / γ–alumina mixture to Na^+ ions in NaCl solutions.

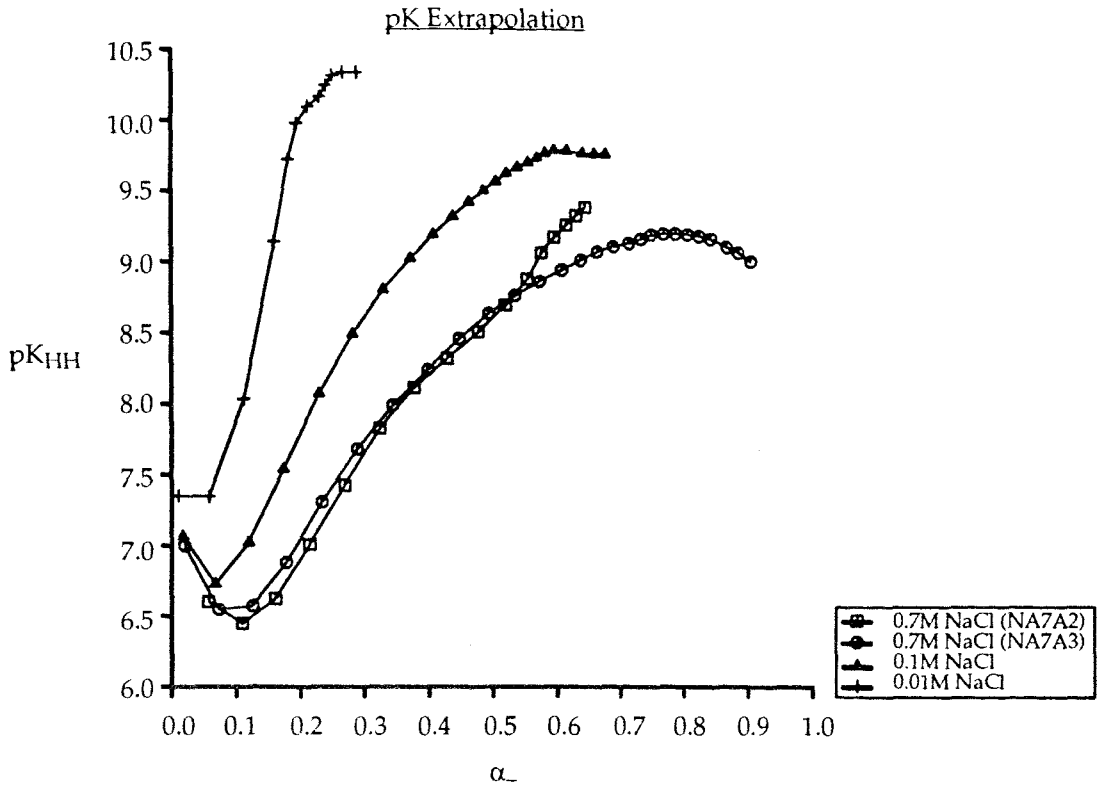

Figure 9.5 Plot of Henderson – Hasselbalch pK (pK_{HH}) against degree of dissociation of negative sites of alumina (α_-).

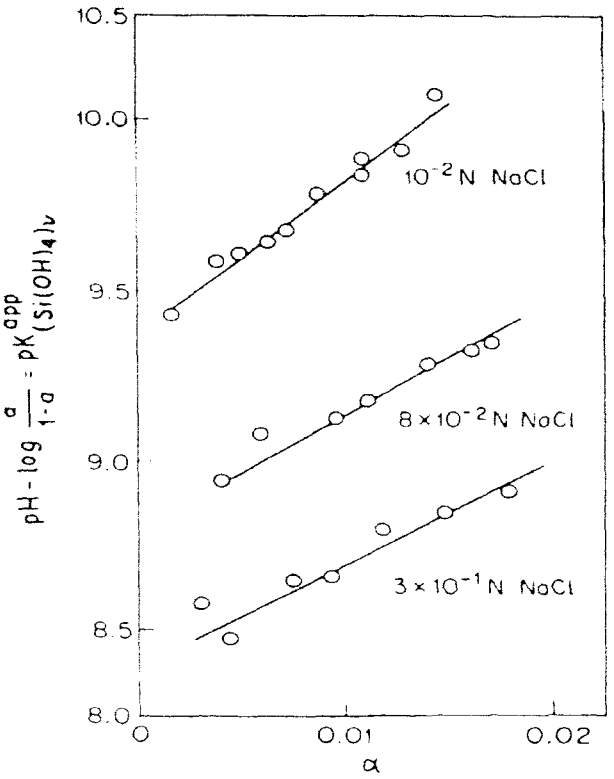

Figure 9.6 Plot of Henderson – Hasselbalch pK (pK_{HH}) against degree of dissociation of SiO_2. (Reproduced with permission from Marinsky *et al.*, 1983 Copyright (1983) American Chemical Society).).

9.3 Gouy Chapman Analysis

The Gouy Chapman – Stern model (Section 2.2) considers the interface between a charged substrate and its surrounding electrolyte to consist of a layer of adsorbed ions (the Stern layer) at the substrate surface with a diffuse layer of charge extending further into the solution (Bockris & Reddy, 1970; Westall & Hohl, 1980). When the substrate surface is organic in nature the Stern layer may collapse, leaving a diffuse layer alone (De Wit *et al.*, 1988).

9.3.1 Surface Charge

Figures 9.7 & 9.8 show the variation of surface charge (σ_0) with pH of the γ–alumina and fulvic acid / alumina mixtures at several ionic strength values. Surface charges have been calculated using Eqn. 6.1.2 and corrected to zero at $pH_{PZC}(Al_2O_3)$ by the procedure described in Section 6.1.2.

9.3.2 Surface pH Calculation

Surface pH (pH_s) for the alumina and mixed fulvic acid / alumina suspensions has been determined using planar geometry (Section 2.2.2), since the alumina particles are too large to be considered spherical (i.e. r > 10nm, De Wit *et al.*, 1989).

Figures 9.9 & 9.11 show σ_0 vs pH_s plots for these samples, in which pH_s has been calculated using Eqns. 2.2.1 & 2.2.2 (C_1 = 3 $F.m^{-2}$). Both plots show a gross over – correction of the σ_0 vs pH plots, i.e. low bulk pH appears to lead to high surface pH and *vice versa*.

This over – correction is due to the high surface charge density of the alumina (e.g. relative to that of fulvic acid, see Figure 6.5), which causes the pH correction term (from Eqn. 2.2.2) to become greater than pH. The surface charge density of the substrates may be over – estimated if their surface area values are too low.

The technique employed to determine the surface areas of the alumina and fulvic acid / alumina samples was BET adsorption (Sections 8.2.2 & 8.3.3). This has been noted to give lower surface areas than other techniques (e.g. ethylene glycol adsorption (Turner *et al.*, 1991; Dzombak & Morel, 1990)), and BET values have therefore been taken by other workers as a lower limit of particulate sample surface areas (Dzombak & Morel, 1990).

Sample surface area has therefore been treated as an adjustable parameter in order to aid in mastercurve determination. Increasing the surface area (A) of the alumina sample was found to increase the over – correction of the experimental curves when the Stern layer was included in the pH_s calculation.

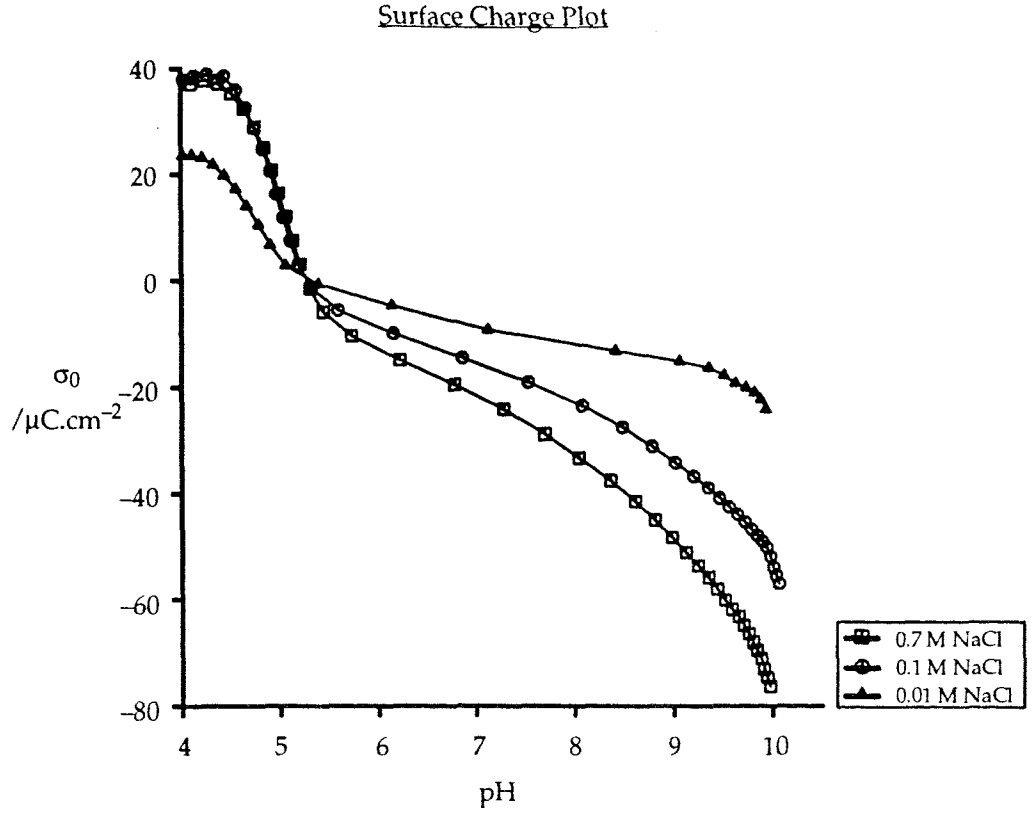

Figure 9.7 Plot of corrected surface charge (σ_0) against pH for γ–alumina suspended in NaCl solutions of various ionic strengths.

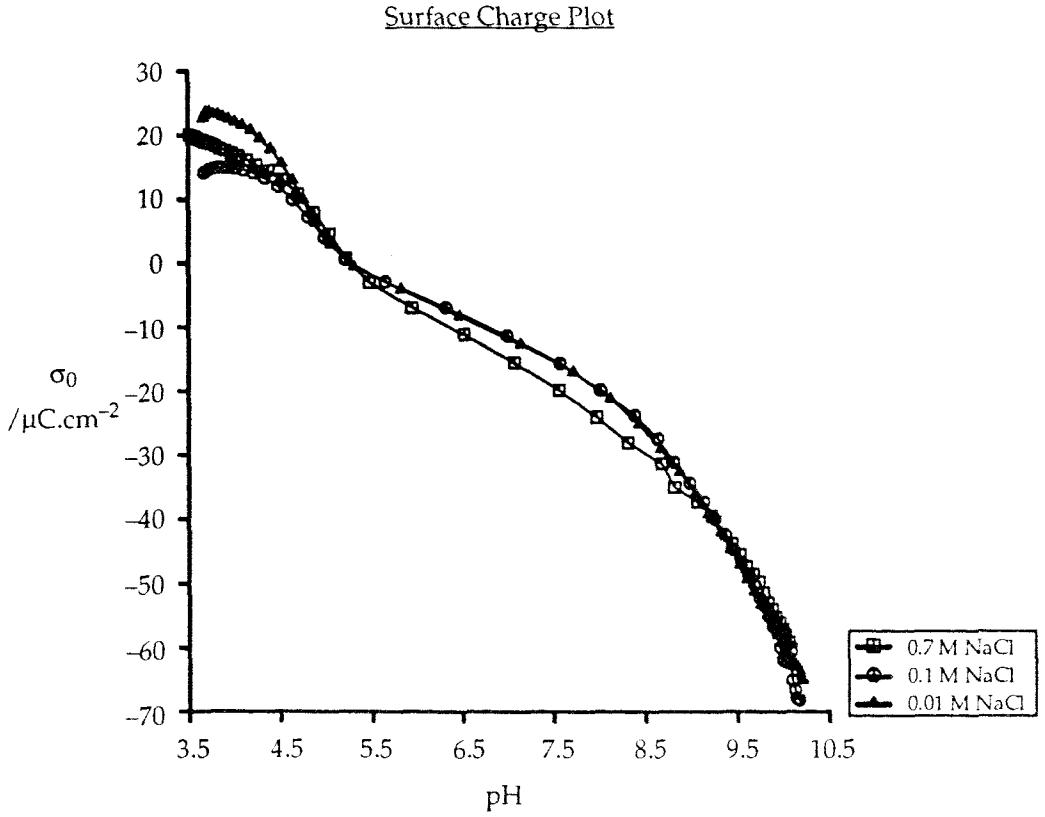

Figure 9.8 Plot of corrected surface charge (σ_0) against pH for fulvic acid / γ–alumina mixtures in NaCl solutions of various ionic strengths.

The curves of Figure 9.10 have therefore been calculated assuming a diffuse layer interface only (Eqn. 2.2.4), using a value of 600 m^2g^{-1} for the alumina surface area. This plot shows near agreement of the σ_0 vs pH_s curves at negative surface charge values, although they are still greatly over – corrected at positive surface charge values. Variation of A (600 – 800 m^2g^{-1}) gave coincidence of parts of the (negative) σ_0 vs pH_s curves for alumina, although a mastercurve was not obtained. The curves in the positive surface charge region were found to be widely separated even at 1000 m^2g^{-1}.

This procedure has not been attempted for the fulvic acid / alumina mixture data, as there is very little apparent effect of ionic strength on its surface charge development (see Figure 9.8). Calculation of surface pH for this system using Eqns 2.2.2 – 2.2.4 therefore inevitably produces non – coincident curves.

9.3.3 Discussion

The use of the Gouy Chapman – Stern model to calculate surface pH for alumina results in a very large over – correction of the effect of solution ionic strength (Figure 9.9). By treating the alumina – solution interface as a simple diffuse layer and using alumina surface area as an adjustable parameter this over – correction is reduced.

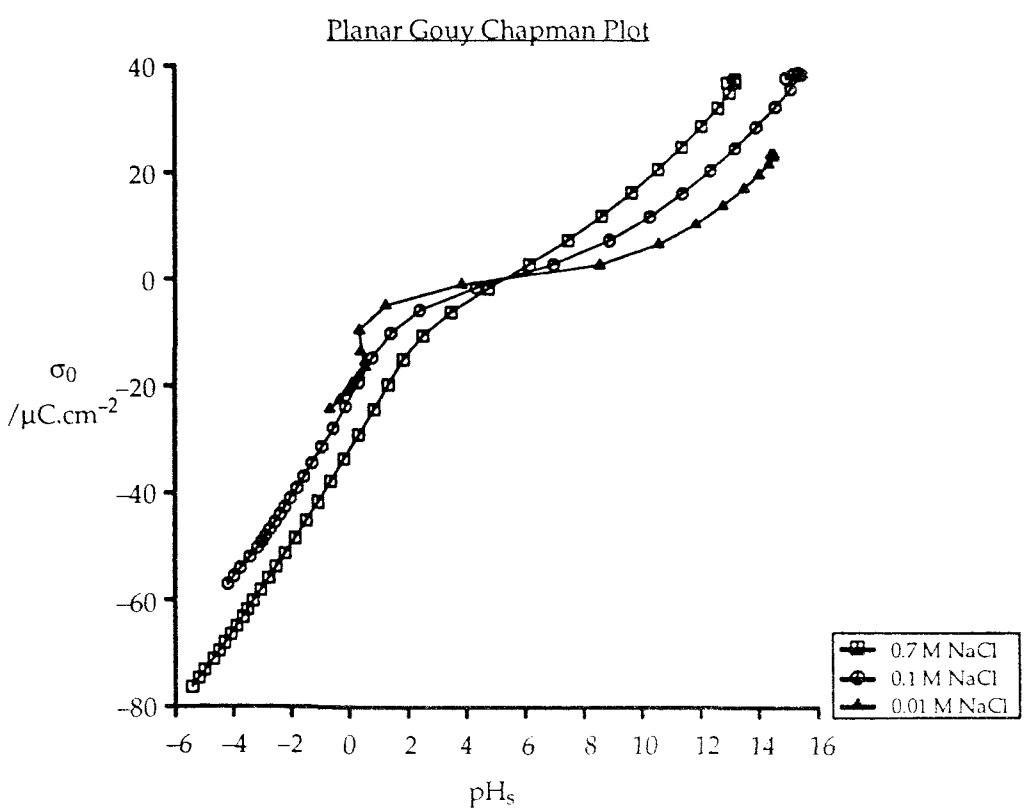

Figure 9.9 Plot of corrected surface charge against (planar) surface pH (pH_s) for γ–alumina suspended in NaCl solutions (Stern layer capacitance, C_1 = 3 $F.m^{-2}$).

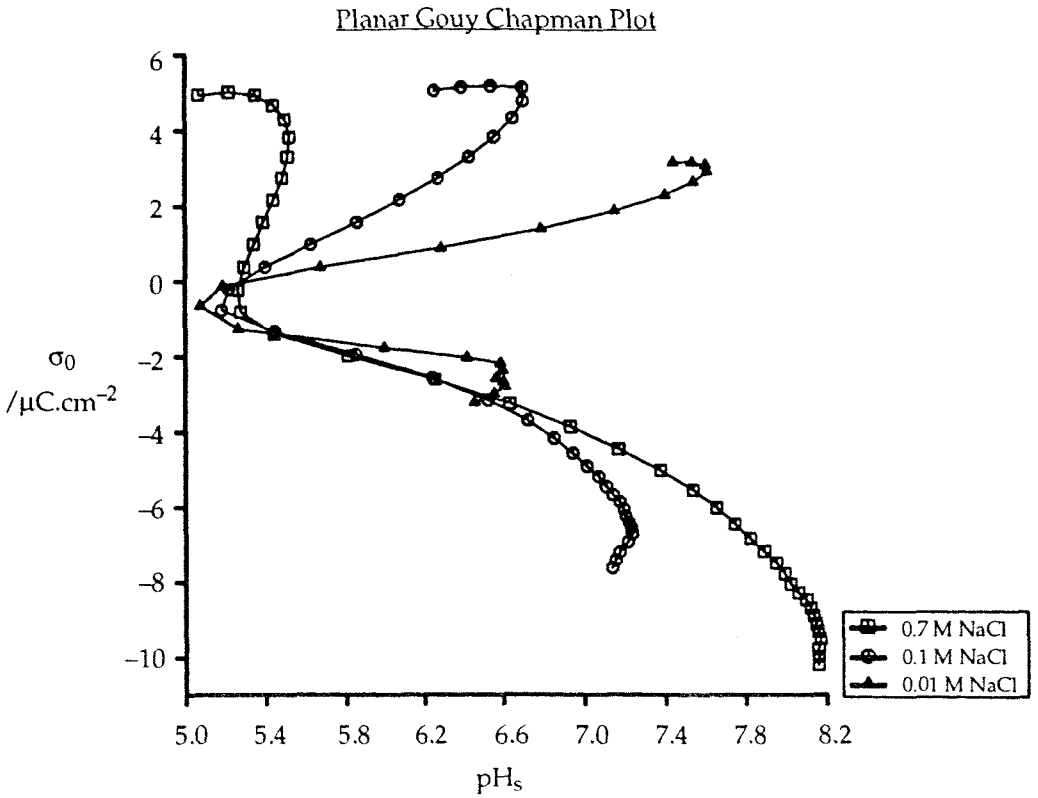

Figure 9.10 Plot of corrected surface charge against (planar) surface pH (pH_s) for γ–alumina in NaCl solutions (no Stern layer, A = 600 m^2g^{-1}).

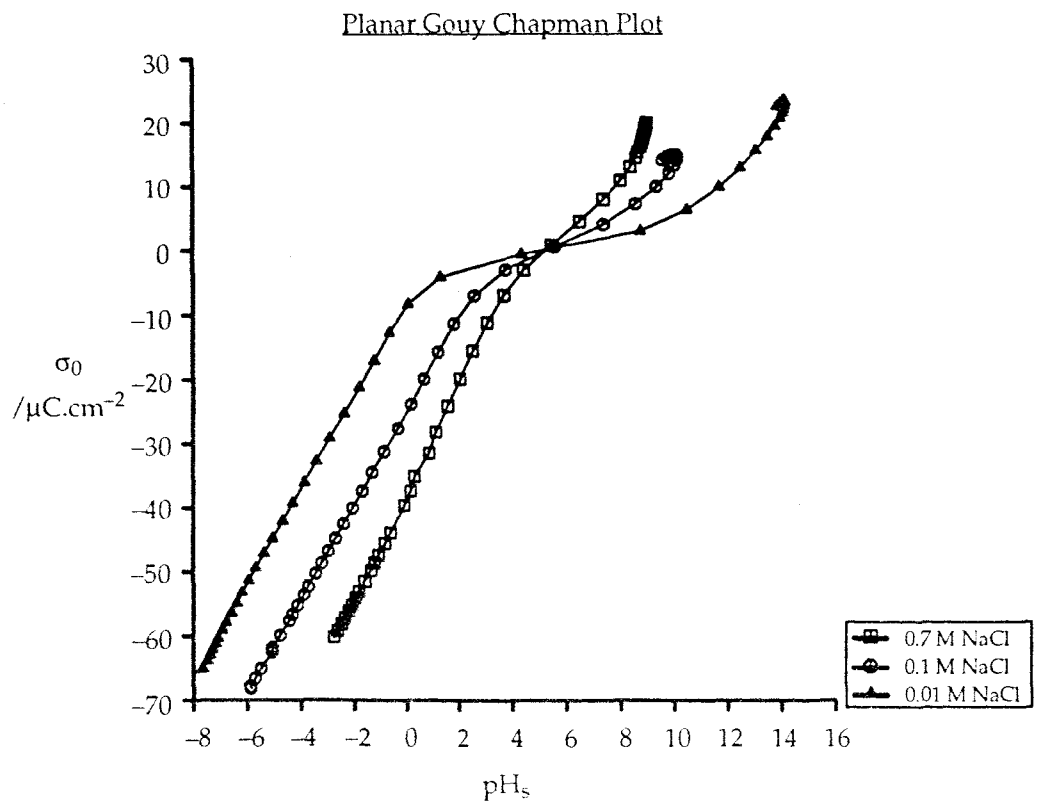

Figure 9.11 Plot of corrected surface charge against (planar) surface pH (pH_s) for fulvic acid / γ–alumina mixtures in NaCl solutions (Stern layer capacitance, C_1 = 3 $F.m^{-2}$).

Surface area values very much higher than that obtained by BET adsorption (600 – 800 m^2g^{-1}) are required to produce appropriate ionic strength corrections for the negatively charged alumina surface (Figure 9.10). Even so, a mastercurve of the type described by De Wit *et al.* (1988) cannot be obtained.

Surface charge – surface pH curves for the positively charged sites of alumina are still over – corrected at A = 1000 m^2g^{-1}. These sites are titrated over a rather narrow pH range, in a region of greater error in the proton balance calculation than the majority of negatively charged sites and the over – correction may be a result of this greater error.

The values of alumina surface area which produce appropriate ionic strength corrections are extremely high. Ethylene glycol adsorption generally gives values of A two to three times those of BET adsorption (Dzombak & Morel, 1990), whereas areas eight to ten times the BET value are required for this data set. The equations of the Gouy Chapman model in use do not take account of the reduction in surface charge brought about by specific adsorption of electrolyte ions. The inclusion of these reactions in the model may allow ionic strength effects to be corrected more effectively.

This data correction method would seem to be inappropriate to the fulvic acid / alumina system, which shows very little ionic strength dependency in its acid – base reactions.

9.4 Surface Complexation Analysis

The surface complexation models combine a reaction scheme, describing the development of charge on a substrate surface, with descriptions of the substrate – solution interface (constant capacitance or triple layer models) (Section 2.3). The reaction scheme chosen allows stability constants for ion – substrate reactions to be determined by extrapolation (Davis *et al.*, 1978), and these and other model parameters may also be determined by non–linear least squares analysis.

9.4.1 pK Extrapolation

Plots showing extrapolations for the intrinsic stability constants of alumina and fulvic acid / alumina mixtures are shown in Figures 9.12 (pK_1 & p^*K_{Cl}) and 9.13 (pK_2 & p^*K_{Na}). ($\alpha = 0$ in these plots is defined by the point of zero charge of the substrates, i.e. pH 5.27). The values obtained for pK_2 and p^*K_{Na} are given in Table 9.1, while the extrapolation curves for pK_1 and p^*K_{Cl} do not show linear regions amenable to extrapolation.

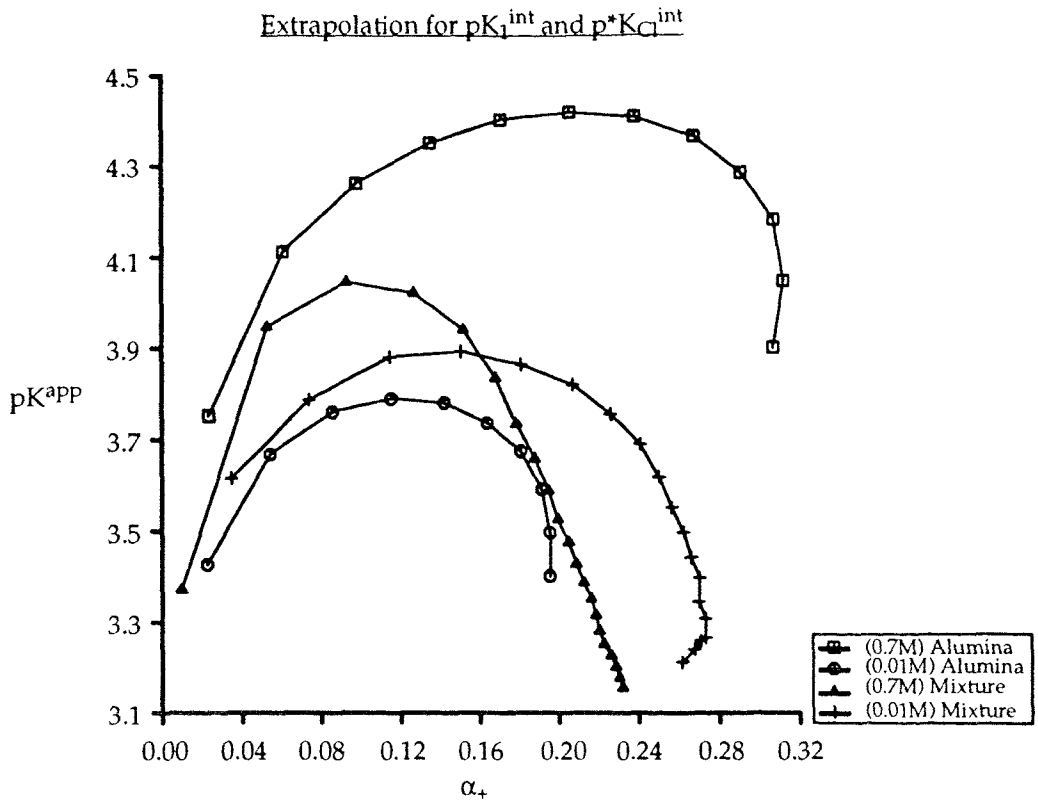

Figure 9.12 Extrapolation plot to determine pK_1 and p^*K_{Cl} for alumina and a fulvic acid / alumina mixture in NaCl solutions.

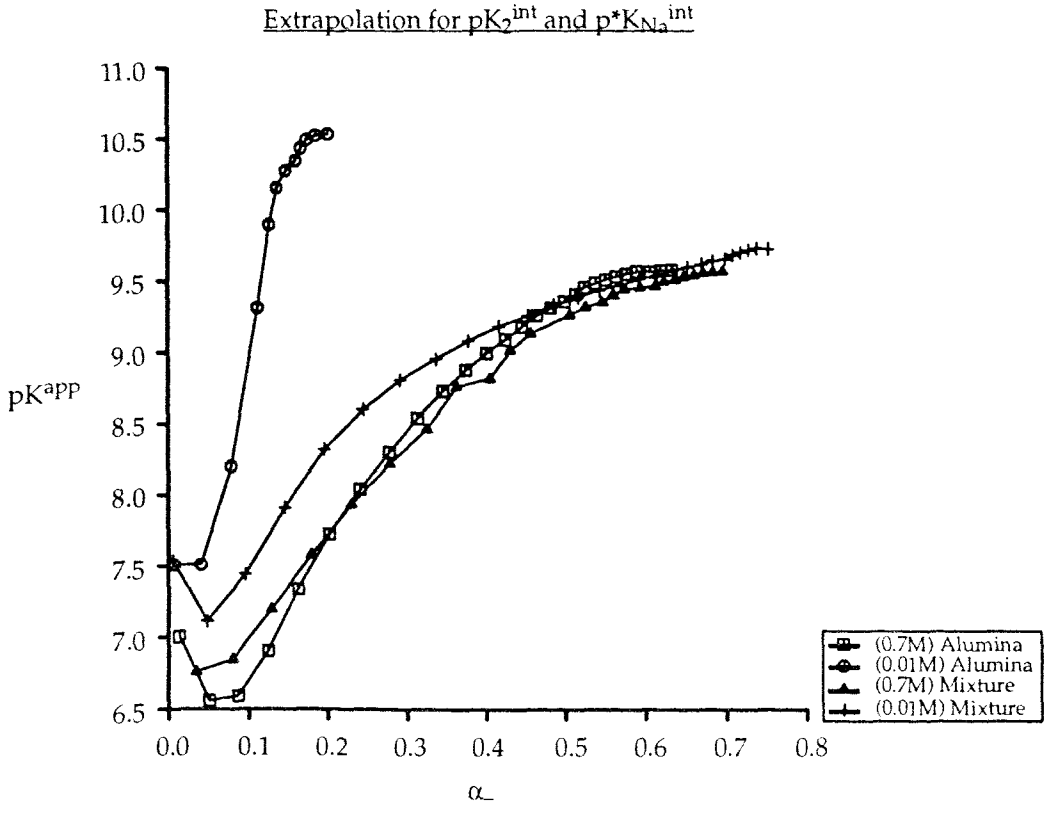

Figure 9.13 Extrapolation plot to determine pK_2 and p^*K_{Na} for alumina and a fulvic acid / alumina mixture in NaCl solutions.

Table 9.1 Extrapolated values of stability constants for acid – base and complexation reactions of alumina and fulvic acid / alumina mixtures.

Stability Constant	Substrate	
	Alumina	Mixture
pK_2	5.53±0.08	6.69±0.10
p^*K_{Na}	5.60±0.20	6.40±0.20

9.4.2 Stability Constant and Capacitance Fitting

Fitting of alumina and fulvic acid / alumina stability constants and capacitances was carried out by a similar procedure to that employed for fulvic acid data (Section 7.3) (HALTAFALL input files relevant to this work can be found in Appendix 2.B).

9.4.2.1 Constant Capacitance Model – Alumina

All surface species (i.e. SOH_2^+, SO^-, SOH_2^+–Cl^- & SO^-–Na^+) were initially included in the fitting procedure, initial values for pK_2 and p^*K_{Na} being taken from the extrapolation data (Table 9.1), pK_1 being set to define pH_{PZC} according to Eqn. 9.4.1 (Dzombak & Morel, 1990) ($pK_1 = -5.01$) and p^*K_{Cl} being estimated from the literature ($pK_{Cl} = -1.0$, Davis *et al.*, 1978 ($p^*K_{Cl} = -4.0$)).

$$pH_{PZC} = (pK_2 - pK_1)/2 \qquad (9.4.1)$$

However, the fitting procedure was unable to reproduce the very different slopes of the surface charge curves either side of the point of zero charge of the alumina (see Figure 9.7). The slope of the surface charge plot is largely governed by the capacitance of the adsorbed layer and this in turn is related to the thickness of this layer (Section 2.3.4.1).

Bousse & Meindl (1986) used different capacitance values either side of pH_{PZC}, relating this to the size of the adsorbing ions (anions for $pH < pH_{PZC}$, cations for $pH > pH_{PZC}$). However, this approach would not aid in the fitting of the curves of Figure 9.7 as the relative sizes of the Na^+ and Cl^- ions would imply a lower capacitance for $pH < pH_{PZC}$, whereas a higher capacitance is required to reproduce the experimental curves.

The fitting procedure was therefore confined to the negatively charged surface species SO^- and SO^-–Na^+, whose reactions cover the greater pH range. Stability constants for the reactions of the positively charged species were retained in the speciation calculations as their values (especially pK_1) affect the calculated surface charge in the negative region at pH values close to pH_{PZC}.

As in Section 7.3.1.3, the fitted capacitance of the adsorbed layer was allowed to vary with solution ionic strength (Dzombak & Morel, 1990). This variation is represented by Eqn. 9.4.2, in which C1 is the capacitance in a 1M solution.

$$C = C1.I^{p} \qquad (9.4.2)$$

The ionic strength exponent, p, was varied manually, while pK_2, pK_{Na} and C1 were fitted simultaneously to alumina titration data at all three ionic strengths of NaCl. Variation in p changes the separations between the fitted σ_0 – pH curves at different ionic strengths. Its value was fixed at 0.2 for the alumina – NaCl system, this corresponding to the upper limit of p values found for Esk sediment titrations (Kleinot, pers. comm., 1992). Fitted values are listed in Table 9.2 and surface charge curves calculated using these parameters are shown in Figure 9.14.

The extrapolated and fitted values of pK_2 are in good agreement with one another, while the values of p^*K_{Na} are considerably different (Tables 9.1 & 9.2). The difference in the extrapolated and fitted values of p^*K_{Na} is not particularly surprising as the extrapolation equation (Eqn. 2.3.21) is strictly only applicable to the triple layer model (Section 2.3.3.2). The fitted value of pK_{Na} is also rather high compared to values reported for sodium binding with carboxylic acids ($-0.18 < pK_{Na} < 0.83$ @ 25°C & zero ionic strength; Martell & Smith, 1977), although some differences in the strength of ion interactions of carboxylic acids and the alumina surface are to be expected.

The fitted value of C1 is in quite close agreement with its theoretical value (2.5, Dzombak & Morel, 1990).

The agreement between the fitted and observed curves in Figure 9.14 is generally good, although the increase in slope of the observed curves near pH_{PZC} cannot be reproduced. This increase in slope may be due to some influence of the positively charged surface sites (see Figure 9.7), and it is apparent that it could be removed from Figure 9.14 by selecting a slightly higher value for the point of zero charge pH of the alumina (e.g. $pH_{PZC} = 5.5$). However, there is no justification (other than the consequent improvement in the quality of the fit to the data set) for using an alternative pH_{PZC} value.

Table 9.2 Fitted stability constant and capacitance values, standard errors and standard deviations of fit for interactions of alumina in NaCl solutions ($pK_1 = -5.01$, $p^*K_{Cl} = -4.0$, $p = 0.2$).

pK_2	5.34±0.20	
pK_{Na}	3.99±0.17	($p^*K_{Na} = 9.33$)
C1 / $F.m^{-2}$	2.32±0.11	
σ_{fit} / $\mu C.cm^{-2}$	3.27	

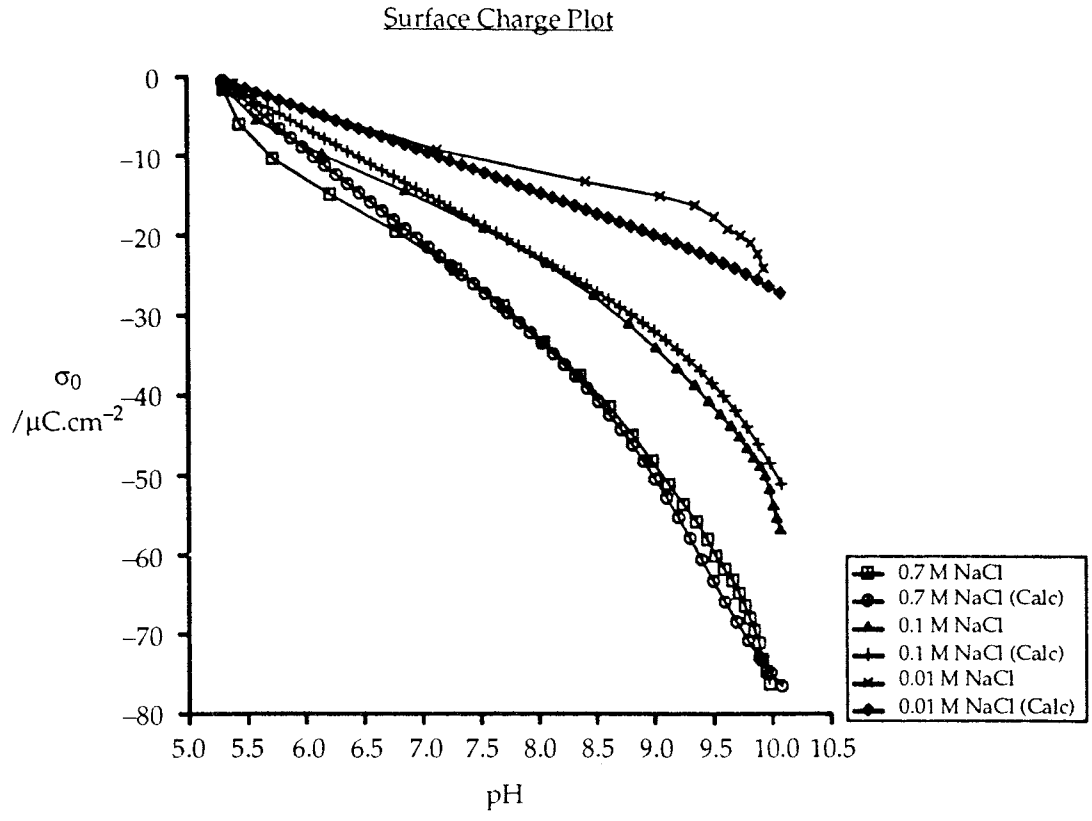

Figure 9.14 Calculated and observed surface charge plots for alumina in NaCl solutions (constant capacitance model, fitted pK values).

9.4.2.2 Constant Capacitance Model – Fulvic Acid / Alumina Mixture

As stated in Section 9.1.1, the fulvic acid / alumina mixture titration data is treated here as an alumina sample (i.e. $pH_{PZC} = 5.27$) in order to assess the effect of the fulvic acid on the acid – base chemistry of the alumina.

However, since the extent of the fulvic acid – alumina interaction appears to differ in different ionic strength solutions (Section 8.3.1), the titration data of the mixture at each ionic strength are treated separately. The capacitance of the adsorbed layer at each ionic strength was calculated using Eqn. 9.4.2 ($C1 = 2.32\ F.m^{-2}$, $p = 0.2$ – Table 9.2). Fitting was therefore carried out for pK_2 and pK_{Na} only at each ionic strength.

Table 9.3 shows the fitted values of pK_2 and pK_{Na} for each ionic strength, together with their calculated capacitance values. The values of pK_1 and p^*K_{Cl} used in these fittings were the same as those employed in Section 9.4.2.1. Calculated and observed σ_0 vs pH curves for 0.7M, 0.1M and 0.01M mixture titration data are shown in Figures 9.15 – 9.17.

Examination of Table 9.3 shows that the fitted values of pK_2 (and p^*K_{Na}) decrease with decreasing ionic strength. The decrease in the value of p^*K_{Na} can largely be accounted for by the decrease in pK_2. Thus the fitting procedure would appear to account for the changes in numbers of titrateable groups with ionic strength (due to fulvic acid desorption, Section 8.3.2.1) by altering the acidity of the mixture functional groups. (The version of

HALTAFALL in use is unable to take account of organic – particle adsorption / desorption reactions specifically).

It can be seen from Figures 9.15 & 9.17 that the fitted curves for 0.7M and 0.01M solutions do not pass through zero surface charge at the pH defined for the alumina (pH 5.27). This is because the values of pK_2 fitted for these experiments vary significantly from the equivalent value for alumina (see Tables 9.2 & 9.3), and these values appear to define a new pH_{PZC} for the material (Eqn. 9.4.1).

This effect can also be seen for the replicate titrations of the mixture in 0.7M NaCl solutions reported in Figure 8.8 (NA7Z1PB & NA7Z1DD). These experiments showed significantly greater numbers of titrateable groups than those shown in Figures 9.15 – 9.17 (NA7Z1PB > NA7Z1DD) presumably as a result of decreased fulvic acid adsorption. Analysis of this data showed that the fitting procedure increased the acidity and decreased the strength of the sodium ion interaction of the mixture to account for this change in adsorption (NA7Z1PB – pK_2 = 5.51, pK_{Na} = 3.50, σ_{fit} = 1.82 $\mu C.cm^{-2}$; NA7Z1DD – pK_2 = 5.86, pK_{Na} = 3.70, σ_{fit} = 1.61 $\mu C.cm^{-2}$; and see Table 9.3).

Table 9.3 Calculated capacitance values and fitted stability constants for the deprotonation and sodium ion complexation reactions of fulvic acid / alumina mixtures (pK_1 = –5.01, p^*K_{Cl} = –4.0).

0.7M	pK_2	6.24±0.07	
	pK_{Na}	4.04±0.11	(p^*K_{Na} = 10.28)
	C	2.16 $F.m^{-2}$	
	σ_{fit}	1.79 $\mu C.cm^{-2}$	
0.1M	pK_2	5.72±0.09	
	pK_{Na}	3.17±0.09	(p^*K_{Na} = 8.89)
	C	1.46 $F.m^{-2}$	
	σ_{fit}	1.40 $\mu C.cm^{-2}$	
0.01M	pK_2	3.27±0.44	
	pK_{Na}	3.67±0.27	(p^*K_{Na} = 6.94)
	C	0.92 $F.m^{-2}$	
	σ_{fit}	3.51 $\mu C.cm^{-2}$	

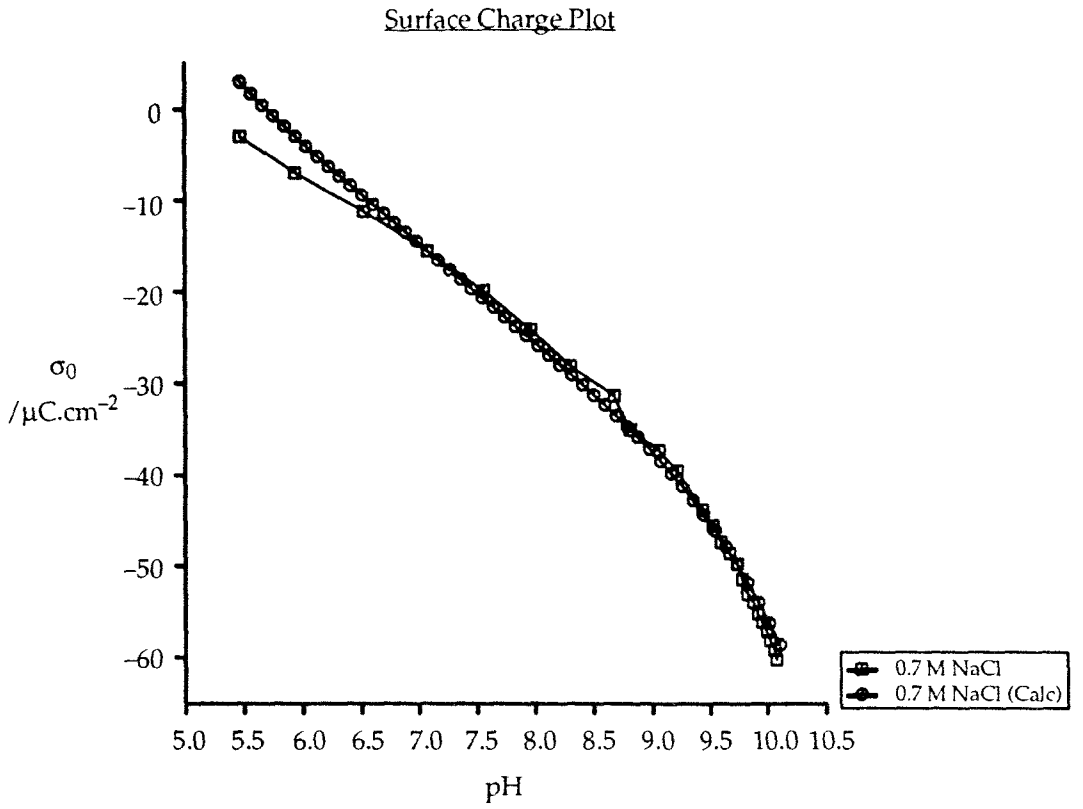

Figure 9.15 Calculated and observed surface charge plots for a fulvic acid / alumina mixture in 0.7M NaCl solution (constant capacitance model, fitted pK values).

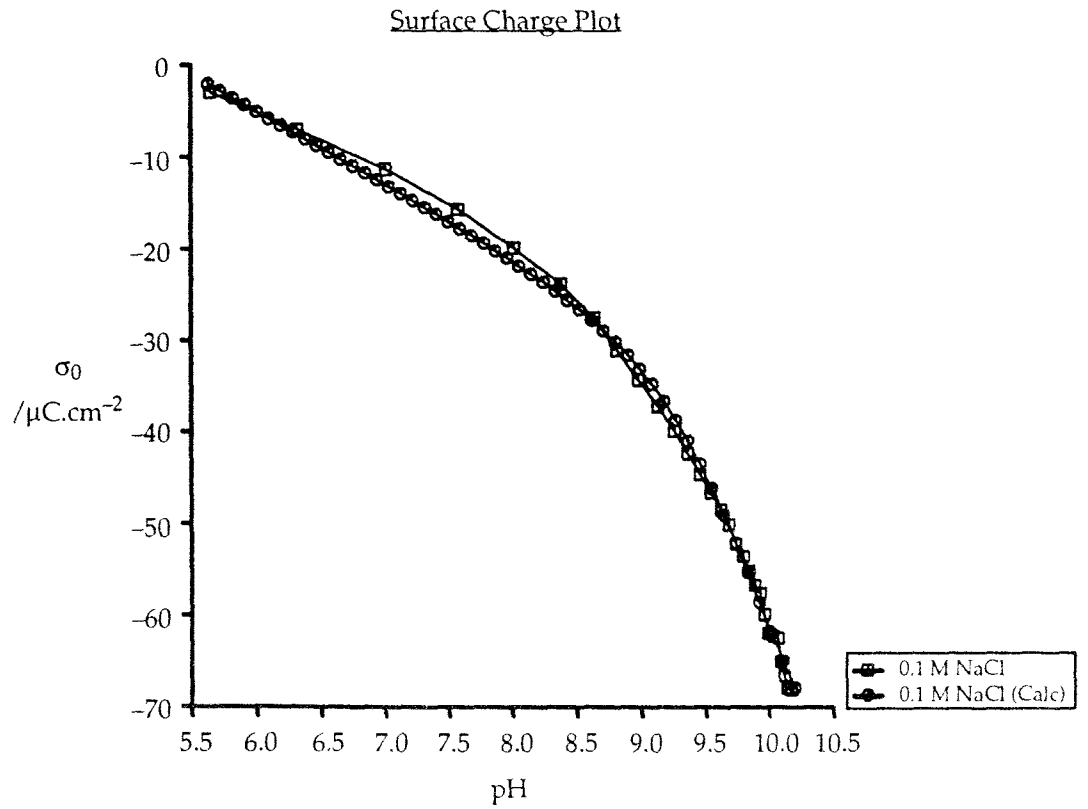

Figure 9.16 Calculated and observed surface charge plots for a fulvic acid / alumina mixture in 0.1M NaCl solution (constant capacitance model, fitted pK values).

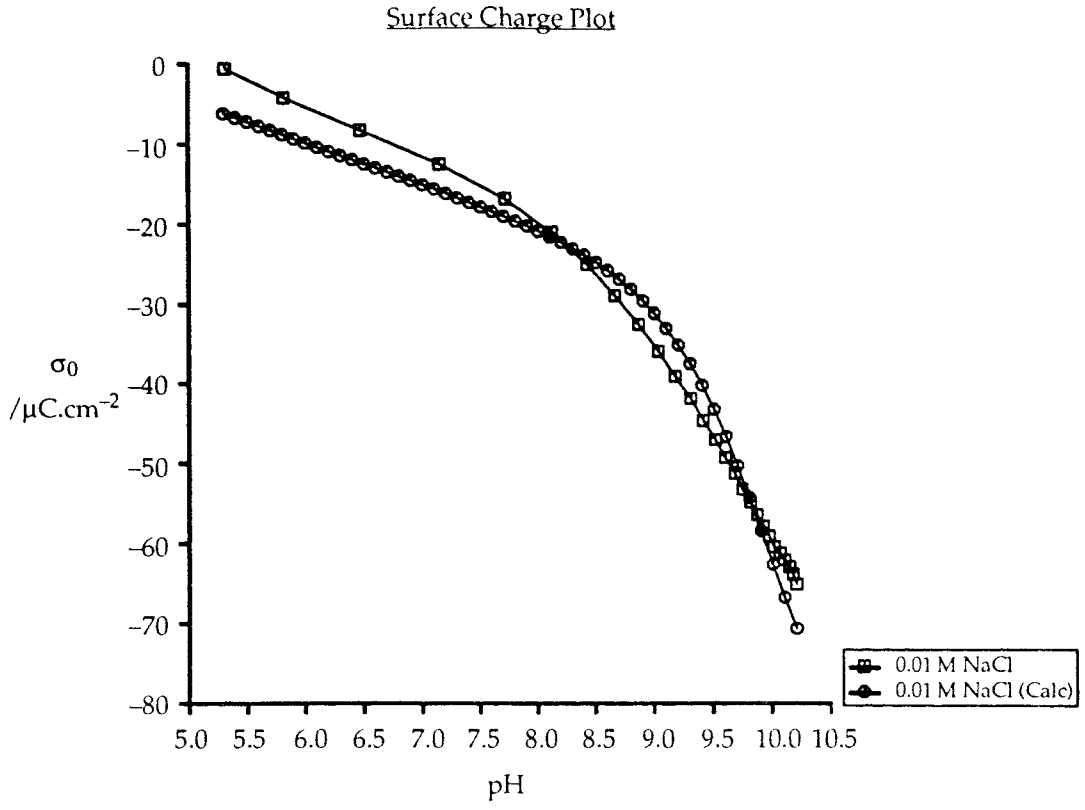

Figure 9.17 Calculated and observed surface charge plots for a fulvic acid / alumina mixture in 0.01M NaCl solution (constant capacitance model, fitted pK values).

9.4.2.3 Triple Layer Model

Attempts to fit stability constants and inner layer capacitance (C_1) for the alumina using a triple layer interface model (outer layer capacitance, $C_2 = 0.2$ F.m^{-2} (Davis *et al.*, 1978)) proved to be unsuccessful. The increased complexity of the model (relative to the constant capacitance model) appeared to overwhelm the fitting program and convergence of the non–linear regression analysis could not be achieved.

The results of manual variation of C_1 (within the reported range for its value, 1 – 1.4 F.m^{-2} (Davis *et al.*, 1978)) are shown in Figure 9.18. Calculated curves in this plot were produced by the HALTAFALL speciation routine, using the stability constant values obtained by extrapolation (Table 9.1) and a value for C_1 of 1.4 F.m^{-2}.

The triple layer model was not applied to the fulvic acid / alumina mixture.

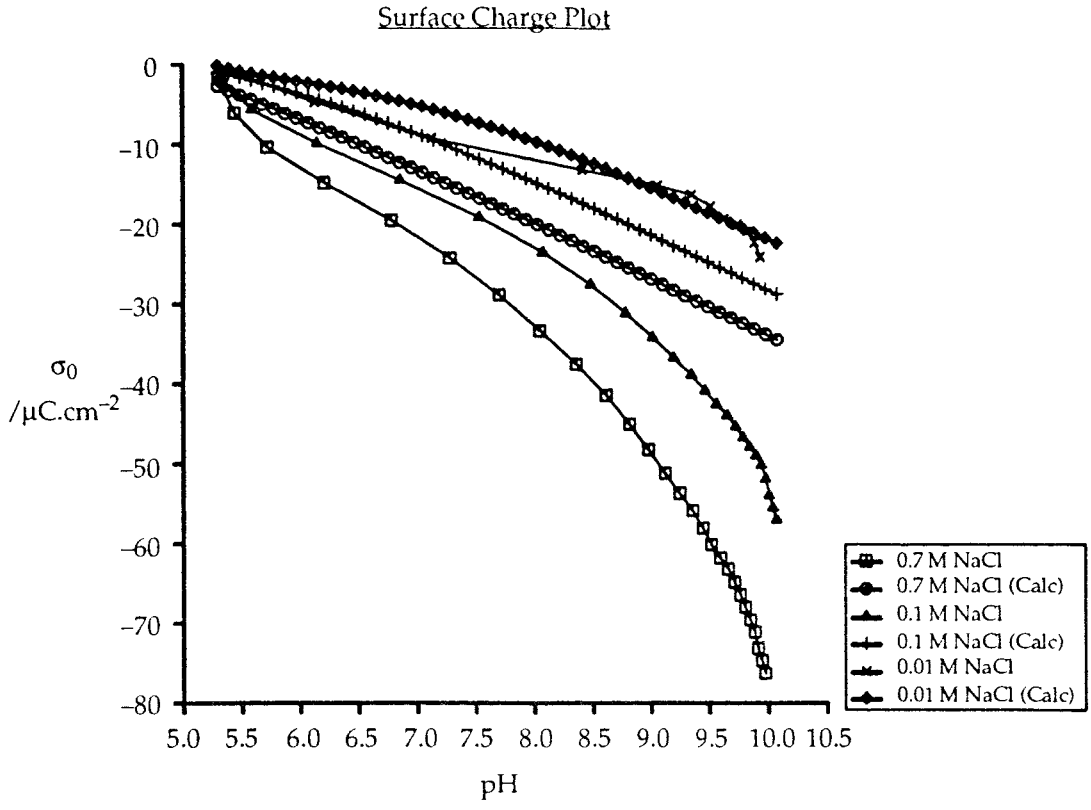

Figure 9.18 Calculated and observed surface charge plots for alumina in NaCl solutions (triple layer model, extrapolated pK values).

9.4.3 Discussion

Application of the surface complexation approach to the alumina and fulvic acid / alumina mixture data appears to be quite successful. The pK extrapolation scheme of Davis and co-workers (Davis *et al.*, 1978) produces well defined plots for the alumina and mixture at negative surface charge values, although the data at positive surface charge are confined to too narrow a pH (and α_+) range for extrapolation to be possible.

The values of pK_2 for alumina obtained by extrapolation and non-linear least squares analysis are in good agreement with one another (Tables 9.1 & 9.2). Other extrapolated pK values do not agree with their fitted equivalents. p^*K_{Na} values are determined for different models by extrapolation and fitting procedures, while pK_2 values for the fulvic acid / alumina mixture must include some contribution from fulvic acid adsorption / desorption reactions.

A set of consistent stability constant values has been determined for alumina by allowing the capacitance of the adsorbed layer to vary with solution ionic strength. There is however, no justification in theory for the ionic strength exponent (p = 0.2) which was found to reproduce the separations of the σ_0 vs pH curves.

The ionic strength dependency of fulvic acid – alumina interactions (Section 8.3.1.1) necessitated treatment of the mixture titration data as separate systems at each ionic

strength. The fitting procedure was then able to model each data set fairly well (Table 9.3). However, since the extent of fulvic acid adsorption on alumina also varies with pH (Section 8.3.1.1), the stability constants quoted in Table 9.3 must represent a combination of acid – base and adsorption reactions. Thus it is apparent that a complete description of this system cannot be obtained without the variation in fulvic acid adsorption being taken into account explicitly.

The constant capacitance model shows a distinct advantage over the triple layer model in that its relative simplicity allows model parameters to be determined by iterative speciation modelling.

9.5 Conclusions

Application of the diagnostic tests of the polyelectrolyte gel model to the alumina and fulvic acid / alumina titration data indicates that neither system is permeable to electrolyte ions (although the plots for alumina (Figures 9.1 & 9.2) are rather ambiguous).

The mastercurve method of De Wit and co–workers (1988) is able to reduce the ionic strength dependency of a portion of the alumina titration data, although specific adsorption at the surface must be neglected and extremely high values of surface area are necessary to achieve this. The mastercurve method is not applicable to the fulvic acid / alumina data.

Iterative speciation modelling provides a means of determining a consistent set of stability constants for the interactions of alumina using the constant capacitance model. This was achieved by allowing the capacitance of the adsorbed layer to vary with ionic strength. The iterative speciation modelling approach was also able to reproduce the titration curves of the fulvic acid / alumina mixture, although the fulvic acid – alumina interaction was not explicitly included in the model. This interaction must be taken into account if the acid – base chemistry of the mixture is to be modelled on the same basis as the alumina.

10. CONCLUSIONS

The stated aim of this research work was to identify a general adsorption model (or models) capable of describing the interactions of natural organic matter and organic coated mineral particles in aqueous solutions (Section 1.2). To a large extent this has been achieved.

10.1 Fulvic Acid Modelling

10.1.1 Polyelectrolyte Gel Model

The polyelectrolyte gel model does not appear to be applicable to the Tamar River fulvic acid studied. Diagnostic plots based on the Henderson – Hasselbalch pK indicated that the fulvic acid was impermeable to electrolyte ions in each of the solutions examined (NaCl, Na_2SO_4, $CaCl_2$ & $MgCl_2$, Section 5.2). The Donnan potential for which this model corrects cannot therefore, be expected to arise in this system.

This conclusion was not unexpected as the fulvic acid is considerably smaller than the synthetic polymers for which the polyelectrolyte gel model was developed (molecular weights of ~825 daltons (Varney, 1982) and > 5000 daltons (Anspach & Marinsky, 1975) respectively).

10.1.2 Gouy Chapman Model

The assumption of planar geometry for the electric field around fulvic acid was found to lead to over – correction of the titration data (Section 6.2). The use of a spherical diffuse layer equation to account for the effects of ionic strength on the titration curves of the fulvic acid proved to be very successful (Section 6.3). Mastercurves of the type described by De Wit and co–workers (1988, 1989, 1990, 1991a & b) were obtained for all of the salt solutions studied.

However, the assumption of spherical geometry for fulvic acid molecules is probably not a reflection of reality. The change in the assumed shape of the electric field around the fulvic acid from planar to spherical symmetry does, however, result in a great improvement in the ionic strength correction (cf. Figures 6.5 & 6.7). Solutions of the Poisson – Boltzmann equation for other symmetries (e.g. cylindrical, De Wit *et al.*, 1991b) may also be used, but the difference between mastercurves obtained using spherical and cylindrical geometries does not appear to be great (Figure 6.13). In practice, the actual geometry of the electric field around charged humics is unlikely to conform to a simple geometric shape and cannot be reproduced by a simple mathematical function. The particular form of the Poisson – Boltzmann equation used to determine the mastercurve can therefore be regarded as an adjustable parameter of the model.

The other adjustable parameters of the model (in this case radius, r, and molecular weight, M) should not be taken as absolute values of the physical parameters that they represent. Thus the production of a mastercurve for the Tamar River fulvic acid in NaCl

solutions using a spherical geometry and radius and molecular weight values of 0.5 nm and 315 daltons does not imply that the fulvic acid exists in this form in NaCl solution. The adjustable parameters probably also include some contribution from specific interactions of electrolyte cations with the fulvic acid, as these interactions are neglected in this model.

10.1.3 Surface Complexation Models

The application of the surface complexation reaction scheme to the fulvic acid titration data was disadvantaged by the necessity of restricting the analysis to the carboxylic acid site of the sample only. A relatively narrow range of titration data (in terms of degree of dissociation of the site) was available, and the lower pH range of this data was subject to large errors due to the low fulvic acid concentration in use.

In terms of reproduction of the experimental data only, an approach in which parameters of the constant capacitance model were optimised individually for each data set proved most effective (Section 7.3.1.1). However, the stability constants derived by this method were unrealistic and adsorbed layer capacitances were inconsistent for each of the electrolytes studied.

More realistic stability constant values were obtained from fittings of the high ionic strength data for each electrolyte only (Section 7.3.1.2). Even so, these values were unable to reproduce the experimental data at lower ionic strengths when adsorbed layer capacitance was varied according to a low power of ionic strength (0.1). (Variation of capacitance with ionic strength according to Gouy Chapman theory ($C \alpha \sqrt{I}$) produces extremely large separation of calculated curves at different ionic strengths). Nor were the values of the fitting parameters which were common to all of the salts (pK_2 and C) found to be consistent.

The stability constant and capacitance values obtained by the latter method did provide a reasonable prediction of fulvic acid surface charge development in artificial seawater (Section 7.3.2), but they are not likely to be so effective in lower salinity estuarine waters as they were unable to reproduce the titration data of the lower ionic strengths of each salt.

10.2 Particulate Suspension Modelling

10.2.1 Alumina

The diagnostic plots of the polyelectrolyte gel model are rather ambiguous in their analysis of the permeability characteristics of the alumina sample (Figures 9.1 & 9.2). However, by analogy with results published for a sample of SiO_2 (Marinsky *et al.*, 1983), the sample was classified as being impermeable to electrolyte ions. The Donnan potential correction model was therefore not applied to this data.

The Gouy Chapman – Stern model was found to greatly over – correct the effect of ionic strength on the titration curves of alumina. This over – correction could only be

reduced by assuming a very large surface area for the sample (8 – 10 times that measured by BET adsorption) and treating the alumina – solution interface as a simple diffuse layer (Section 9.3.2). A "mastercurve" could not be obtained for this system and it is possible that ion pair formation at high ionic strength is sufficiently strong to prevent this.

A consistent set of stability constant values for the interactions of alumina in NaCl solutions have been obtained using the constant capacitance interface model and surface complexation reaction scheme (Section 9.4.2.1). The effect of solution ionic strength was accounted for by variation in adsorbed layer capacitance ($C \alpha I^{0.2}$). The ionic strength exponent (0.2) is significantly smaller than that predicted by Gouy Chapman theory for high ionic strength cases (0.5, Dzombak & Morel, 1990).

The small amount of data available for the positively charged sites of alumina made estimation of stability constants in this region by graphical means or by the fitting procedure unfeasible.

10.2.2 Fulvic Acid / Alumina Mixture

Plots of the Henderson – Hasselbalch pK for this system clearly show that it is impermeable (Figures 9.3 & 9.4), i.e. that the fulvic acid coating on the alumina particles does not form a three – dimensional phase into which electrolyte ions can penetrate.

The titration curves of the mixture do not show significant variation with ionic strength (Figure 9.8). According to the mastercurve approach, this implies that the bulk and surface pH are equal in this system (i.e. there is no surface – solution boundary layer). Examination of fulvic acid – alumina interactions at each ionic strength (Section 8.3.2.1) indicates that the apparent lack of ionic strength dependency is a result of desorption of the fulvic acid. Mastercurve determination using the Gouy Chapman model is probably therefore inappropriate for this system.

Surface complexation modelling on the same basis as alumina (fitting of stability constants using a constant capacitance type interface) does allow the surface charge curves of fulvic acid / alumina mixtures to be reproduced reasonably well with capacitance values fixed at those determined for alumina (Section 9.4.2.2). However, the variation in fulvic acid adsorption with ionic strength means that this can only be achieved by treating the titration data at each ionic strength separately. As adsorption also varies with pH, the stability constants obtained must include some contribution from fulvic acid adsorption / desorption reactions. This is borne out by the differing values of pK_2 and pK_{Na} fitted for several sets of data obtained at 0.7M, in which the extent of adsorption appears to be different.

10.3 Summary

The goal of investigations into the metal and proton binding of heterogeneous complexants, such as particulate and natural organic matter, is the inclusion of their interactions into chemical speciation models of aquatic environments.

The work undertaken here has highlighted some important aspects of the modelling of such systems.

a the non–planar surface geometry of natural organic matter (fulvic acid) must be taken into account when considering the effects of ionic strength on their interactions.

b desorption of organic matter from particle surfaces with increasing pH appears to have a marked effect on the acid – base behaviour of the particles. Similar desorption of organic matter from natural particles has been noted previously (Tipping *et al.*, 1989), and this effect should be taken into consideration when studying the acid – base chemistry of such particles. Organic matter desorption may also affect the distribution of pollutant metals between dissolved and particulate phases in the environment.

10.4 Suggestions for Further Work

10.4.1 Experimental

In order to include fulvic acid adsorption / desorption reactions with the speciation model, a further set of experiments should be conducted to quantify the effects of changing ionic strength and pH on fulvic acid / alumina mixtures. These should ideally yield ionic strength independent stability constants for the reactions described in Eqns. 10.4.1 & 10.4.2 and quantify the extent to which they are reversible.

$$SOH + FA^- \Leftrightarrow S\text{–}FA + OH^- \qquad (10.4.1)$$

$$SO^- + M^{2+} + FA^- \Leftrightarrow SO\text{–}M\text{–}FA \qquad (10.4.2)$$

The binding of metal ions by mixed organic – particulate systems at low pH has been shown to remove them from the dissolved phase (see Section 1.1.4.4). Experiments should also be conducted to determine whether a subsequent increase in pH causes desorption of metal – organic species and results in the reintroduction of bound metal to the dissolved phase.

Experiments investigating the metal binding of natural organics, particulates and their mixtures should be conducted in conjunction with acid – base experiments (similar to those carried out in this work), since protons and metal ions generally compete for binding sites in these systems. Identification of the metal binding reactions occurring (e.g. Eqns. 1.1.2 – 1.1.4) can be aided by carrying out experiments at fixed pH and measuring the number of protons released by metal binding (i.e. the number of protons / hydroxyl ions required to maintain the fixed pH) (De Wit *et al.*, 1991a). The ratio of protons released to metal ions bound can indicate which binding reactions are occurring. Eqns. 1.1.2 & 1.1.3 have similar proton release behaviour at high pH, while Eqns. 1.1.3 & 1.1.4 have the same proton release signal at low pH (De Wit *et al.*, 1989).

10.4.2 Modelling

The spherical Gouy Chapman model proved to be very successful at correcting the ionic strength effects on fulvic acid titration data (Section 6.3). The mastercurve resulting from this correction may be used to investigate the heterogeneity or otherwise of the sample. Distribution functions have been recommended for this purpose (e.g. De Wit *et al.*, 1991a), but the use of multisite models may also be appropriate.

The application of a multisite model to the mastercurve would have two advantages over its use with uncorrected data. Fewer fitting parameters (site stability constants and concentrations) would be required to describe the mastercurve, as one site is generally required to describe ~2 pH units (Perdue, 1990), and the range of pH_s values is smaller than that of pH. The fitted parameters describing the mastercurve would also be ionic strength independent.

The use of the surface complexation / constant capacitance model to describe fulvic acid interactions was only a partial success, with ionic strength effects particularly poorly reproduced. The success of the spherical Gouy Chapman approach implies that the combination of this interface model with the surface complexation reaction scheme in iterative speciation calculations may be more successful at providing stability constants which are valid over a wide range of estuarine conditions.

The constant capacitance model is able to provide a set of consistent stability constants for the interactions of alumina at several ionic strengths and is also able to reproduce the titration curves of fulvic acid / alumina mixtures at individual ionic strengths fairly well. However, the stability constants fitted for the mixtures inevitably contain contributions from the adsorption / desorption reactions of the fulvic acid. A more rigorous model of the mixture's acid – base chemistry should therefore take account of fulvic acid – alumina interactions, and their variation with pH and ionic strength, explicitly.

Theory predicts that the capacitance of the adsorbed layer in the constant capacitance model should vary according to the square root of solution ionic strength (Dzombak & Morel, 1990). However, the ionic strength exponent which was found to reproduce the separations of the surface charge plots of alumina was considerably lower than 0.5. This has also been found to be the case for titrations of estuarine sediment particles (Kleinot, pers. comm., 1992). The ionic strength effect of a spherical electric field has been shown to be rather lower than that of a planar field, and it is therefore possible that the spherical geometry (with comparatively large particle radii) could be employed in the modelling of these particles.

REFERENCES

Anspach W.M., Marinsky J.A., (1975). "Complexing of Nickel(II) and Cobalt(II) by a polymethacrylic acid gel and its linear polyelectrolyte analogue.", *J. Phys. Chem.*, 79, 433.

Ballion D., Jaffrezic–Renault N., (1985). "Study of the uptake of inorganic ions and organic acids at the α–alumina – electrolyte interface in a colloidal system by radiochemical techniques and microelectrophoresis.", *J. Radioanal. Nucl. Chem.*, 92, 133.

Benes P., Gjessing E.T., Steinnes E., (1975). "Interactions between humus and trace elements in fresh water.", *Water Res.*, 9, 1079.

Bockris J.O'M., Reddy A.K.N., (1970). "Modern electrochemistry", McDonald, London, Vol. 2, Ch. 7.

Bourg A.C.M., Joss S., Schindler P.W., (1979). "Ternary surface complexes. 2. Complex formation in the system silica – Cu(II) – 2,2' bipyridyl.", *Chimia*, 33, 19.

Bousse L., Meindl J.D., (1986). "Surface potential–pH characteristics in the theory of the oxide–electrolyte interface.", *In: "Geochemical processes at mineral surfaces.", Davis J.A., Hayes K.F., eds.*, Am. Chem. Soc. Symp. Ser. 323, Ch. 5, 79.

Breeuwsma A., Lyklema J., (1973). "Physical and chemical adsorption of ions in the electrical double layer on haematite (α–Fe_2O_3).", *J. Colloid Interf. Sci.*, 43, 437.

Brunauer S., Emmett P.H., Teller E., (1938). "Adsorption of gases in multimolecular layers.", *J. Am. Chem. Soc.*, 60, 309.

Buffle J., (1988). "Complexation reactions in aqueous systems: An analytical approach.", Ellis Horwood, Chichester, Ch. 4, 146.

Buffle J., Altmann R.S., Filella M., Tessier A., (1990). "Complexation by natural heterogeneous compounds: Site occupation distribution functions, a normalized description of metal complexation.", *Geochim. Cosmochim. Acta*, 54, 1535.

Buffle J., Greter F.L., Haerdi W., (1977). "Measurement of complexation properties of humic and fulvic acids in natural waters with lead and copper ion–selective electrodes.", *Anal. Chem.*, 49, 216.

Cabaniss S.E., (1991). "Carboxylic acid content of a fulvic acid determined by potentiometry and aqueous Fourier transform infrared spectrometry.", *Anal. Chim. Acta*, 255, 23.

Cabaniss S.E., Shuman M.S., (1988). "Copper binding by dissolved organic matter: I. Suwanee River fulvic acid equilibria.", *Geochim. Cosmochim. Acta*, 52, 185.

Cabaniss S.E., Shuman M.S., Collins B.J., (1984). "Metal–organic binding – a comparison of models.", *In: "Complexation of trace metals in natural waters", Kramer C.J.M., Duinker J.C., eds.*, Martinus Nijhoff/W. Junk, The Hague, 165.

Cosovic B., Kozarac Z., (1985). "Metal studies of physico–chemical interaction of cadmium with organic coatings at interfaces.", *In:* "Commission Internationale Pour L'exploration Scientifique de la Mer Mediteranee. VII. Journes d'etudes sur les pollutions marines em Mediteranee", Monaco, C.I.E.S.M., 181.

Davis J.A., (1980). "Adsorption of natural organic matter from freshwater environments by aluminum oxide.", *In:* "Contaminants and Sediments", 2, *Baker R.A., ed.*, Ann Arbor Science, 279.

Davis J.A., (1982). "Adsorption of natural dissolved organic matter at the oxide/water interface.", *Geochim. Cosmochim. Acta*, 46, 2381.

Davis J.A., (1984). "Complexation of trace metals by adsorbed natural organic matter.", *Geochim. Cosmochim. Acta*, 48, 679.

Davis J.A., Gloor R., (1981). "Adsorption of dissolved organics in lake water by aluminum oxide. Effect of molecular weight.", *Environ. Sci. Tech.*, 15, 1223.

Davis J.A., Hayes K.F., (1986). "Geochemical processes at mineral surfaces: An overview.", *In:* "Geochemical processes at mineral surfaces", *Davis J.A., Hayes K.F. eds.*, Am. Chem. Soc. Symp. 323, 2.

Davis J.A., Hem J.D., (1989). "The surface chemistry of aluminum oxides and hydroxides.", *In:* "The environmental chemistry of aluminum", CRC Press, Ch.7, 185.

Davis J.A., James R.O., Leckie J.O., (1978). "Surface ionisation and complexation at the oxide/water interface. I. Computation of electrical double layer properties in simple electrolytes.", *J. Coll. Interf. Sci.*, 63, 480.

Davis J.A., Leckie J.O., (1978). "Surface ionisation and complexation at the oxide/water interface. II. Surface properties of amorphous iron oxyhydroxide and adsorption of metal ions.", *J. Coll. Interf. Sci.*, 67, 90.

Dempsey B.A., (1981). "The protonation, calcium complexation and adsorption of a fractionated aquatic fulvic acid.", Ph.D. Thesis, University of North Carolina.

Dempsey B.A., O'Melia C.R., (1983). "Proton and calcium complexation of four fulvic acid fractions.", *In:* "Aquatic and terrestrial humic materials.", *Christman R.F., Gjessing E.T., eds.*, Ann Arbor Science, Mich., Ch. 12, 239.

De Wit J.C.M., Nederlof M.M., Van Riemsdijk W.H., Koopal L.K., (1991a). "Determination of H^+ and metal ion affinity distributions for humic substances.", *Water, Air, Soil Poll.*, 57–58, 339.

De Wit J.C.M., Van Riemsdijk W.H., Koopal L.K., (1988). "Proton and metal ion binding on homogeneous and heterogeneous colloids.", *In:* "Heavy metals in the hydrological cycle", *Astruc M., Lester J.N., eds.*, London, 369.

De Wit J.C.M., Van Riemsdijk W.H., Koopal L.K., (1989). "Proton and metal ion binding on humic substances.", *In: "Metals speciation, separation and recovery"., Vol. 2, Patterson J.W., Passino R., eds.*, Lewis Publishers.

De Wit J.C.M., Van Riemsdijk W.H., Koopal L.K., (1991b). "Analysis of the functional group distribution of humic substances.", *Finnish Humus News*, 3, 139.

De Wit J.C.M., Van Riemsdijk W.H., Nederlof M.M., Kinniburgh D.G., Koopal L.K., (1990). "Analysis of ion binding on humic substances and the determination of intrinsic affinity distributions.", *Anal. Chim. Acta*, 232, 189.

Dickson A.G., Whitfield M., (1981). "An ion–association model for estimating acidity constants (at 25°C and 1 atm total pressure) in electrolyte mixtures related to seawater (ionic strength < 1 mol kg^{-1} H_2O).", *Mar. Chem.*, 10, 315.

Dzombak D.A., Morel F.M.M., (1990). "Surface complexation modelling: Hydrous ferric oxide.", Wiley, NY.

Eisenman G., (1967). "Glass electrodes for hydrogen and other cations.", Marcel Dekker, NY.

Ephraim J.H., Boren H., Pettersson C., Arsenie I., Allard B., (1989). "A novel description of the acid – base properties of an aquatic fulvic acid.", *Environ. Sci. Technol.*, 23, 356.

Ephraim J., Alegret S., Mathuthu A., Bicking M., Malcolm R.L., Marinsky J.A., (1986). "A unified physicochemical description of the protonation and metal ion complexation equilibria of natural organic acids (humic and fulvic acids). 2. Influence of polyelectrolyte properties and functional group heterogeneity on the protonation equilibria of fulvic acids.", *Environ. Sci. Technol.*, 20, 354.

Ephraim J., Marinsky J.A., (1986). "A unified physicochemical description of the protonation and metal ion complexation equilibria of natural organic acids (humic and fulvic acids). 3. Influence of polyelectrolyte properties and functional group heterogeneity on the copper ion binding equilibria in an Armadale horizons Bh fulvic acid sample.", *Environ. Sci. Technol.*, 20, 367.

Fish W., Morel F.M.M., (1984). "Modelling the interactions of trace metals and aquatic humic materials.", Project Report 346, Int. Copper Res. Assoc. Inc., NY, 150.

Florence T.M., (1983). "Trace metal speciation and aquatic toxicology.", *Trends Anal. Chem.*, 2, 162.

Forsling W., Hietanen S., Sillen L.G., (1952). "Studies on the hydrolysis of metal ions. III. The hydrolysis of the mercury (I) ion, Hg_2^{2+}.", *Acta Chem. Scand.*, 6, 901.

Gibbs R.J., (1983). "Effect of natural organic coatings on the coagulation of particles.", *Environ. Sci. Technol.*, 17, 237.

Gran G., (1952). "Determination of the equivalence point in potentiometric titrations: II.", *Analyst*, 77, 661.

Harvie C.E., Moller N., Weare J.H., (1984). "Prediction of mineral solubilities in natural waters: Na–K–Mg–Ca–H–Cl–SO_4–OH–HCO_3–CO_3–H_2O system to high ionic strength at 25°C.", *Geochim. Cosmochim. Acta*, 48, 723.

Hawkins S.J., (1987). "Interactions of metal and organic acid species with oxide surfaces.", Ph.D. Thesis, University of Bristol, UK.

Hayes M.H.B., MacCarty P., Malcolm R.L., Swift R.S., (1989). "The search for structure: Setting the scene.", *In: "Humic substances. II. In search of structure", Hayes M.H.B., MacCarty P., Malcolm R.L., Swift R.S., eds.*, Wiley, Ch. 1, 3.

Healy T.W., White L.R., (1978). "Ionisable surface group models of aqueous interfaces.", *Adv. Colloid Interf. Sci.*, 9, 303.

Hiemstra T., Van Riemsdijk W.H., Bolt G.H., (1989). "Multisite proton adsorption modelling at the solid / solution interface of (hydr)oxides: A new approach. I. Model description and evaluation of intrinsic reaction constants.", *J. Coll. Interf. Sci.*, 133, 105.

Ho C.H., Miller N.H., (1985). "Effect of humic acid on Uranium uptake by hematite particles.", *J. Coll. Interf. Sci.*, 106, 281.

Hohl H., Stumm W., (1976). "Interaction of Pb^{2+} with hydrous γ–Al_2O_3.", *J. Coll. Interf. Sci.*, 55, 281.

Huang C.P., Stumm W., (1972). "The specific surface area of γ–Al_2O_3.", *Surf. Sci.*, 32, 287.

Hunston D.L., (1975). "Two techniques for evaluating small molecule–macromolecule binding in complex systems.", *Anal. Biochem.*, 63, 99.

Hunter K.A., Liss P.S., (1979). "The surface charge of suspended particles in estuarine and coastal waters.", *Nature*, 282, 823.

Hunter R.J., (1981). "Zeta potential in colloid science. Principles and applications.", Academic Press, Ch. 2.

Ingri N., Kakolowicz W., Sillén L.G., Warnqvist B., (1967). "High speed computers as a supplement to graphical methods. V. HALTAFALL, a general program for calculating the composition of equilibrium mixtures.", *Talanta*, 14, 1261.

Kummert R., Stumm W., (1980). "The surface complexation of organic acids on hydrous γ–Al_2O_3.", *J. Colloid Interf. Sci.*, 75, 373.

Linder P.W., Murray K., (1987). "Statistical determination of the molecular structure and the metal binding sites of fulvic acids.", *Sci. Tot. Environ.*, 64, 149.

Loeb A.L., Overbeck J.Th.G., Wiersema P.H., (1961). "The electrical double layer around a spherical colloid.", Cambridge, M.I.T. Press.

Lövgren L., Sjöberg S., Schindler P.W., (1990). "Acid/base reactions and Al(III) complexation at the surface of goethite.", *Geochim. Cosmochim. Acta*, 54, 1301.

Marinsky J.A., (1985). "An interpretation of the sensitivity of weakly acidic (basic) polyelectrolyte (cross–linked and linear) equilibria to excess neutral salt.", *J. Phys. Chem.*, 89, 5294.

Marinsky J.A., (1987). "A two phase model for the interpretation of proton and metal ion interaction with charged polyelectrolyte gels and their linear analogs.", *In: "Aquatic surface chemistry", Stumm W. ed.*, Ch. 3, Wiley.

Marinsky J.A., Anspach W.M., (1975). "Complexation of copper(II) by a polymethacrylic acid gel.", *J. Phys. Chem.*, 79, 439.

Marinsky J.A., Baldwin R., Reddy M.M., (1985). "Interpretation with a Donnan–based concept of the influence of simple salt concentration on the apparent binding of divalent ions to the polyelectrolytes Polystyrenesulfonate and Dextran Sulfate.", *J. Phys. Chem.*, 89, 5303.

Marinsky J.A., Ephraim J., (1986). "A unified physicochemical description of the protonation and metal ion complexation equilibria of natural organic acids (Humic and Fulvic Acids). 1. Analysis of the influence of polyelectrolyte properties on protonation equilibria in ionic media: Fundamental concepts.", *Environ. Sci. Technol.*, 20, 349.

Marinsky J.A., Gupta S., Schindler P., (1982a). "A unified physicochemical description of the equilibria encountered in humic acid gels.", *J. Coll. Interf. Sci.*, 89, 412.

Marinsky J.A., Gupta S., Schindler P., (1982b). "The interactions of Cu(II) ion with humic acid.", *J. Coll. Interf. Sci.*, 89, 401.

Marinsky J.A., Lin F.G., Chung K–S., (1983). "A simple method for classification of the physical state of colloidal and particulate suspensions encountered in practice.", *J. Phys. Chem.*, 87, 3139.

Marinsky J.A., Wolf A., Bunzl K., (1980). "The binding of trace amounts of Pb(II), Cu(II), Cd(II), Zn(II) and Ca(II) to soil organic matter.", *Talanta*, 27, 461.

Martell A.E., Smith R.M., (1977), "Critical stability constants. Volume 3: Other organic ligands.", Plenum, NY, 329.

Morel F.M.M., Westall J.C., Yeasted J.G., (1981). "Adsorption models: a mathematical analysis in the framework of general equilibrium calculations.", *In: "Adsorption of inorganics at solid–liquid interfaces", Anderson M.A., Rubin A.J., eds.*, Ann Arbor Sci., Ch.7, 263.

Nederlof M.M., Van Riemsdijk W.H., Koopal L.K., (1988). "Methods to determine affinity distributions for metal ion binding in heterogeneous systems.", *In: "Heavy metals in the hydrological cycle", Astruc M., Lester J.N. eds.*, London, 361.

Nederlof M.M., Van Riemsdijk W.H., Koopal L.K., (1990). "Determination of adsorption affinity distributions: A general framework for methods related to local isotherm approximations.", *J. Coll. Interf. Sci.*, 135, 410.

Neihof R.A., Loeb G.I., (1972). "The surface charge of particulate matter in seawater.", *Limnol. Oceanogr.*, 17, 7.

Parfitt R.L., Fraser A.R., Farmer V.C., (1977). "Adsorption of hydrous oxides. III. Fulvic acid and humic acid on geothite, gibbsite and imogolite.", *J. Soil Sci.*, 28, 289.

Paterson R., Rahman H., (1984). "The ion exchange properties of crystalline inorganic oxide – oxyhydroxides. II. Exclusion of perchlorate from β–FeOOH by an ion sieve mechanism.", *J. Coll. Interf. Sci.*, 97, 423.

Paxéus N. (Plechanov N.), Josefsson B., Dyrssen D., Lundquist K., (1983). "Investigations on humic substances in natural waters.", *In: "Aquatic and terrestrial humic materials.", Christman R.F., Gjessing E.T., eds.*, Ann Arbor Science, Mich., Ch. 15, 387.

Paxéus N., Wedborg M., (1985). "Acid – base properties of aquatic fulvic acid.", *Anal. Chim. Acta*, 169, 87.

Perdue E.M., (1985). "Acidic functional groups of humic substances.", *In: "Humic substances in soil, sediment, and water.", Aiken G.R., McKnight D.M., Wershaw R.L., MacCarthy P., eds.*, Wiley, NY, Ch. 20, 493.

Perdue E.M., (1990). "Modelling the acid – base chemistry of organic acids in laboratory experiments and in freshwaters.", *In: "Organic acids in aquatic ecosystems.", Perdue E.M., Gjessing E.T., eds.*, J. Wiley & Son, 111.

Perdue E.M., Lytle C.R., (1983). "Distribution model for binding of protons and metal ions by humic substances.", *Environ. Sci. Technol.*, 17, 654.

Plavsic M., Kozar S., Krznaric D., Bilinski H., Branica M., (1980). "The influence of organics on the adsorption of Cu(II) on γ–Al_2O_3 in seawater. Model studies with EDTA.", *Mar. Chem.*, 9, 175.

Raspor B., (1989). "Adsorption of humic substances from seawater at differently charged surfaces.", *Sci. Tot. Environ.*, 81/82, 319.

Reuter J.H., Perdue E.M., (1977). "Importance of heavy metal–organic matter interaction in natural water.", *Geochim. Cosmochim. Acta*, 41, 326.

Rodbard D., (1973). "Mathematics of hormone–receptor interaction. I. Basic principles.", *Adv. Exp. Biol.*, 36, 289.

Schnitzer M., Khan S.U., (1972). Humic Substances in the Environment., Dekker, New York.

Sholkovitz E.R., (1976). "Flocculation of dissolved organic and inorganic matter during the mixing of river water and seawater.", *Geochim. Cosmochim. Acta*, 40, 831.

Sholkovitz E.R., Copland D., (1981). "The coagulation, solubility and adsorption properties of Fe, Mn, Cu, Ni, Cd, Co and humic acids in a river water.", *Geochim. Cosmochim. Acta*, 45, 181.

Shuman M.S., Calmano W., De Haan H., Fredrickson H.L., Henriksen A., Kramer J.R., Mannio J.Y., Morel F.M.M., Niemeyer J., Ohman L.–O., Perdue E.M., Weis M., (1990). "How are acid – base properties of "DOC" measured and how do they affect aquatic ecosystems?", *In: "Organic acids in aquatic ecosystems.", Perdue E.M., Gjessing E.T., eds.*, J. Wiley & Son, 141.

Slavek J., Pickering W.F., (1981). "The effect of pH on the retention of Cu, Pb, Cd and Zn by clay–fulvic acid mixtures.", *Water Air Soil Poll.*, 16, 209.

Slota P., Marinsky J.A., (1980). "An electrochemical method for the determination of the effective volume of charged polymers in solution.", *In: "Ions in polymers", Eisenberg A., ed.*, Adv. Chem. Series 187, Am. Chem. Soc., 311.

Sposito G., Holtzclaw K.M., (1977). "Titration studies on the polynuclear, polyacidic nature of fulvic acid extracted from sewage sludge–soil mixtures.", *Soil Sci. Soc. Am. J.*, 41, 330.

Sprycha R., (1983). "Attempt to estimate sb charge components on oxides from anion and cation adsorption measurements.", *J. Colloid Interf. Sci.*, 96, 551.

Sprycha R., (1984). "Surface charge and adsorption of background electrolyte ions at anatase / electrolyte interface.", *J. Colloid Interf. Sci.*, 102, 173.

Stevenson F.J., (1976). "Stability constants of Cu^{2+}, Pb^{2+} and Cd^{2+} complexes with humic acids.", *Soil Sci. Soc. Am. J.*, 40, 665.

Stigter D., (1972). "Functional representations of properties of the electrical double layer around a spherical colloid particle.", *J. Electroanal. Chem.*, 37, 61.

Stumm W., Morgan J.J., (1970). "Aquatic Chemistry. An introduction emphasizing chemical equilibria in natural waters.", Wiley, NY, 476.

Suffet I.H., MacCarthy P., eds., (1989). "Aquatic humic substances: Influence on fate and treatment of pollutants.", Adv. Chem. Series 219.

Sugimura Y., Suzuki Y., (1988). "A high temperature catalytic oxidation method for the determination of non–volatile dissolved organic carbon in seawater by direct injection of a liquid sample.", *Mar. Chem.*, 24, 105.

Tanford C., (1961). "Physical chemistry of macromolecules", Wiley, NY, 710.

Thakur A.K., Munson P.J., Hunston D.L., Rodbard D., (1980). "Characterisation of ligand–binding systems by continuous affinity distributions of arbitrary shape.", *Anal. Biochem.*, 103, 240.

Tipping E., (1981). "The adsorption of aquatic humic substances by iron oxides.", *Geochim. Cosmochim. Acta*, 45, 191.

Tipping E., (1990). "Interactions of organic acids with inorganic and organic surfaces.", *In: "Organic acids in aquatic ecosystems.", Perdue E.M., Gjessing E.T., eds.*, J. Wiley & Son, 209.

Tipping E., Backes C.A., Hurley M.A., (1988). "The complexation of protons, aluminium and calcium by aquatic humic substances: A model incorporating binding site heterogeneity and macroionic effects.", *Water Res.*, 22, 597.

Tipping E., Thompson D.W., Woof C., (1989). "Iron oxide particulates formed by the oxygenation of natural and model lakewaters containing Fe(II).", *Arch. Hydrobiol.*, 115, 59.

Tomaic J., Zutic V., (1988). "Humic material polydispersity in adsorption at hydrous alumina / seawater interface.", *J. Coll. Interf. Sci.*, 126, 482.

Travers C., Marinsky J.A., (1974). "The complexing of Ca(II), Co(II) and Zn(II) by polymethacrylic and polyacrylic acid.", *J. Polymer Sci.*, Symposium No. 47, 285.

Turner D.R., (1990). "The chemistry of metal pollutants in water.", *In: "Pollution: Causes, effects and control.", Harrison R.M., ed.*, Royal Society of Chemistry, Second Edition, Ch. 2, 19.

Turner D.R., Knox S., Titley J.G., Hamilton–Taylor J., Kelly M., Williams G.L., (1991). "Application of a surface complexation model to the interactions of Pu and Am with Esk estuary sediments.", Report on contract PECD/7/9/429, submitted to DOE, Plymouth Marine Laboratory, 156.

Turner D.R., Knox S., Whitfield M., Higgo J.J.W., Rees L.V.C., Cole T.G., (1987a). "Development of a surface complexation model for adsorption of neptunium and plutonium on marine sediments.", Report on contract DOE/RW/88.004, submitted to DOE, Marine Biological Association of the UK, 21.

Turner D. R., Varney M.S., Whitfield M., Mantoura R.F.C., Riley J.P., (1986). "Electrochemical studies of copper and lead complexation by fulvic acid. I. Potentiometric measurements and a critical comparison of metal binding models.", *Geochim. Cosmochim. Acta*, 50, 289.

Turner D. R., Varney M.S., Whitfield M., Mantoura R.F.C., Riley J.P., (1987b). "Electrochemical studies of copper and lead complexation by fulvic acid. II. A critical comparison of potentiometric and polarographic measurements.", *Sci. Tot. Environ.*, 60, 17.

Turner D.R., Whitfield M., (1983). "Inorganic controls on the biogeochemical cycling of the elements in the ocean.", *Ecol. Bull. (Stockholm)*, 35, 9.

Van Riemsdijk W.H., Bolt G.H., Koopal L.K., Blaakmeer J., (1986). "Electrolyte adsorption on heterogeneous surfaces: Adsorption models.", *J. Coll. Interf. Sci.*, 109, 219.

Varney M.S., (1982). "Organometallic interactions of fulvic acid extracted from natural waters.", Ph.D. Thesis, University of Liverpool, UK.

Varney M.S., Mantoura R.F.C., Whitfield M., Turner D. R., Riley J.P., (1983). "Potentiometric and conformational studies of the acid–base properties of fulvic acid from natural waters.", *In: "Trace metals in seawater", Wong C.S., Boyle E., Bruland K.W., Burton J.D., Goldberg E.D., eds.*, Plenum Press, NY, 751.

Westall J.C., (1987). "Adsorption mechanisms in aquatic surface chemistry.", *In: "Aquatic surface chemistry", Stumm W., ed.*, J. Wiley & Son, Ch. 1, 3.

Westall J., Hohl H., (1980). "A comparison of electrostatic models for the oxide/solution interface.", *Adv. Colloid Interf. Sci.*, 12, 265.

Westall J.C., Zachary J.L., Morel F.M.M., (1976). *Tech. Note 18, Water Quality Lab.*, Dept. Civil Eng., MIT, Cambridge, MA.

Whitfield M., Turner D.R., (1981). "Sea water as an electrochemical medium.", *In: "Marine electrochemistry", Whitfield M., Jagner D., eds.*, Wiley, Chichester, Ch. 1, 3.

Wilson D.E., Kinney P., (1977). "Effects of polymeric charge variations on the proton–metal ion equilibria of humic materials.", *Limnol. Oceanogr.*, 22, 281.

Winner R., (1985). "Bioaccumulation and toxicity of copper as affected by interactions between humic acid and water hardness.", *Water Res.*, 19, 449.

Wu Y., Chen C., Wang P., Zhen A., Huan P., (1985). "The effect of natural organic matters on the adsorption of heavy metals on suspended particulate matters.", *Coll. Oceanic Works*, 8, 37.

Xu H., Ephraim J., Ledin A., Allard B., (1989). "Effects of fulvic acid on the adsorption of Cd(II) on alumina.", *Sci., Tot. Environ.*, 81/82, 653.

Yates D.E., Levine S., Healy T.W., (1974). "Site–binding model of the electrical double layer at the oxide/water interface.", *J. Chem. Soc. Faraday Trans.*, 70, 1807.

Zamuda C., Sunda W., (1982). "Bioavailability of dissolved copper to the American oyster Crassostrea virginica. I. Importance of chemical speciation.", *Mar. Biol.*, 66, 77.

Zutic V., Tomaic J., (1988). "On the formation of organic coatings on marine particles: Interactions of organic matter at hydrous alumina/seawater interfaces.", *Mar. Chem.*, 23, 51.

APPENDIX 1: Electrode Calibration Data

Listed below are the calibration data obtained for electrodes used in the potentiometric acid–base titrations described in Section 3.3. The parameters shown are described in Section 3.6, with the exception of:

k_e* theoretical electrode slope (k_e* = RT/F)

pK_W* theoretical ionic product of water, calculated from Pitzer parameters for each solution

I solution ionic strength

Standard deviations for the acid and base region fits (σ_A & σ_B) are included with the fitted parameters, although standard errors for each of the parameters are not. The reader is directed to Table 3.5 in Chapter 3., which includes standard errors representative of those obtained for each parameter.

Where values of k_e or pK_W were not fitted for a particular experiment, their theoretical values (k_e* or pK_W*) were used in the calculation of pH (Section 3.7.1). Where liquid junction potentials (j_H or j_{OH}) were not fitted, their values were taken to be zero.

1.A Fulvic Acid Titrations

1.A.a NaCl Solutions

NA0B4 (NA0F1) I = 0.01M

K_H = 0 K_{OH} = 7 V_0 = 209.38 ml k_e* = 59.15mV pK_W* = 13.89

Electrodes		E^0	k_e	H_{init}	j_H	σ_A	pK_W	j_{OH}	σ_B
Glass	Ref	/mV	/mV	/μM	/V.M^{-1}	/mV		/V.M^{-1}	/mV
34	28	378.39	.	−17.14	−5.62	0.141	13.89	2.24	0.080
34	44	371.35	.	−17.21	−5.12	0.068	13.89	1.94	0.071
32	28	379.72	.	−17.25	−5.88	0.066	13.88	2.21	0.096
32	44	372.63	.	−17.28	−5.27	0.078	13.88	1.96	0.093

NA1B6 (NA1F1) I = 0.1M

K_H = 0 K_{OH} = 10 V_0 = 209.38ml k_e* = 59.16mV pK_W* = 13.77

Electrodes		E^0	k_e	H_{init}	j_H	σ_A	pK_W	j_{OH}	σ_B
Glass	Ref	/mV	/mV	/μM	/V.M^{-1}	/mV		/V.M^{-1}	/mV
11	40	381.97	.	−7.10	−0.13	0.059	13.76	−0.56	0.044
11	26	398.37	.	−8.03	−0.25	0.046	13.76	−0.59	0.045
33	40	385.11	.	−7.54	−0.23	0.031	13.75	−0.29	0.050
33	26	401.54	.	−7.97	−0.38	0.039	13.75	−0.30	0.051

NA7B28 (NA7F5) I = 0.7M

$K_H = 2$ $K_{OH} = 11$ $V_0 = 209.38ml$ $k_e^* = 59.15mV$ $pK_W^* = 13.68$

Electrodes		E^0	k_e	H_{init}	j_H	σ_A	pK_W	j_{OH}	σ_B
Glass	Ref	/mV	/mV	/μM	/V.M^{-1}	/mV		/V.M^{-1}	/mV
39	60	407.02	59.44	15.46	.	0.024	13.67	−0.33	0.028
39	46	402.07	59.38	15.27	.	0.034	13.68	−0.48	0.035
35	60	412.74	59.29	14.94	.	0.047	13.67	0.00	0.020
35	46	408.46	59.45	15.33	.	0.018	13.65	−0.01	0.044

NA7B80 (NA7F1CD) I = 0.7M

$K_H = 1$ $K_{OH} = 5$ $V_0 = 209.29ml$ $k_e^* = 59.17mV$ $pK_W^* = 13.68$

Electrodes		E^0	k_e	H_{init}	j_H	σ_A	pK_W	j_{OH}	σ_B
Glass	Ref	/mV	/mV	/μM	/V.M^{-1}	/mV		/V.M^{-1}	/mV
35	65	417.96	59.33	60.95	.	0.043	13.67	−0.09	0.071
35	2	418.34	59.11	60.63	.	0.022	13.69	−0.47	0.082
39	65	406.96	59.25	60.61	.	0.049	13.70	0.76	0.113
39	2	408.24	59.30	60.93	.	0.017	13.69	0.65	0.082

NA7B98 (NA7F1PB) I = 0.7M

$K_H = 1$ $K_{OH} = 5$ $V_0 = 209.29ml$ $k_e^* = 59.16mV$ $pK_W^* = 13.68$

Electrodes		E^0	k_e	H_{init}	j_H	σ_A	pK_W	j_{OH}	σ_B
Glass	Ref	/mV	/mV	/μM	/V.M^{-1}	/mV		/V.M^{-1}	/mV
36	69	401.36	59.01	54.35	.	0.032	13.72	−1.38	0.038
36	4	418.67	59.15	54.12	.	0.034	13.71	−1.29	0.036
51	69	397.53	58.94	54.14	.	0.036	13.72	−0.64	0.081
51	4	414.83	59.09	54.23	.	0.027	13.71	−0.52	0.078

NA7B113 (NA7F1DD) I = 0.7M

$K_H = 1$ $K_{OH} = 6$ $V_0 = 209.29ml$ $k_e^* = 59.16mV$ $pK_W^* = 13.68$

Electrodes		E^0	k_e	H_{init}	j_H	σ_A	pK_W	j_{OH}	σ_B
Glass	Ref	/mV	/mV	/μM	/V.M^{-1}	/mV		/V.M^{-1}	/mV
35	80	404.01	59.12	60.85	.	0.039	13.64	−1.56	0.117
35	68	420.26	59.04	60.71	.	0.026	13.65	−1.60	0.118
39	80	394.48	59.19	60.88	.	0.027	13.64	−1.24	0.076
39	68	411.19	59.26	61.11	.	0.028	13.63	−1.46	0.115

1.A.b Na_2SO_4 Solutions

NS0B6 (NS0F1) I = 0.01M

$K_H = 6$ $K_{OH} = 4$ $V_0 = 209.34ml$ $k_e^* = 59.16mV$ $pK_W^* = 13.78$

Electrodes		E^0	k_e	H_{init}	j_H	σ_A	pK_W	j_{OH}	σ_B
Glass	Ref	/mV	/mV	/μM	/V.M^{-1}	/mV		/V.M^{-1}	/mV
32	41	365.89	.	6.17	–4.82	0.099	13.79	3.632	0.110
32	44	382.34	.	2.20	–4.91	0.090	13.79	3.502	0.047
34	41	365.22	.	1.91	–4.91	0.084	13.80	3.330	0.013
34	44	381.49	.	1.72	–4.95	0.096	13.79	3.470	0.073

NS1B8 (NS1F1) I = 0.1M

$K_H = 1$ $K_{OH} = 14$ $V_0 = 209.38ml$ $k_e^* = 59.15mV$ $pK_W^* = 13.39$

Electrodes		E^0	k_e	H_{init}	j_H	σ_A	pK_W	j_{OH}	σ_B
Glass	Ref	/mV	/mV	/μM	/V.M^{-1}	/mV		/V.M^{-1}	/mV
33	40	379.89	.	–25.59	–0.44	0.044	13.48	0.42	0.044
33	26	386.75	.	–25.72	–0.42	0.033	13.48	0.44	0.044
11	40	375.02	.	–25.59	–0.44	0.029	13.48	0.39	0.042
11	26	381.89	.	–25.88	–0.42	0.032	13.48	0.41	0.030

NS7B8 (NS7F1) I = 0.7M

$K_H = 9$ $K_{OH} = 14$ $V_0 = 209.38ml$ $k_e^* = 59.16mV$ $pK_W^* = 12.92$

Electrodes		E^0	k_e	H_{init}	j_H	σ_A	pK_W	j_{OH}	σ_B
Glass	Ref	/mV	/mV	/μM	/V.M^{-1}	/mV		/V.M^{-1}	/mV
35	46	353.28	58.73	150.3	.	0.046	13.01	–0.09	0.046
35	60	366.82	58.98	154.4	.	0.037	12.99	–0.08	0.036
36	46	346.30	58.57	150.8	.	0.040	13.04	–0.30	0.075
36	60	359.58	58.71	152.3	.	0.033	13.04	–0.27	0.073

1.A.c $CaCl_2$ Solutions

CA0B5 (CA0F1) I = 0.01M

$K_H = 6$ $K_{OH} = 4$ $V_0 = 209.34ml$ $k_e^* = 59.16mV$ $pK_W^* = 13.87$

Electrodes		E^0	k_e	H_{init}	j_H	σ_A	pK_W	j_{OH}	σ_B
Glass	Ref	/mV	/mV	/μM	/V.M^{-1}	/mV		/V.M^{-1}	/mV
32	25	390.98	.	–37.18	–5.58	0.120	13.87	3.749	0.172
32	44	392.57	.	–41.53	–5.76	0.120	13.87	3.351	0.106
34	25	389.62	.	–42.00	–5.62	0.095	13.87	3.449	0.066
34	44	391.16	.	–45.34	–5.82	0.108	13.88	3.371	0.138

CA1B9 (CA1F1) I = 0.1M

$K_H = 1$ $K_{OH} = 6$ $V_0 = 209.34ml$ $k_e^* = 59.14mV$ $pK_W^* = 13.69$

Electrodes		E^0	k_e	H_{init}	j_H	σ_A	pK_W	j_{OH}	σ_B
Glass	Ref	/mV	/mV	/μM	/V.M^{-1}	/mV		/V.M^{-1}	/mV
14	40	390.90	.	38.14	–0.69	0.080	13.66	–0.48	0.100
14	42	402.85	.	38.29	–0.71	0.087	13.66	–0.47	0.100
33	40	386.23	.	36.99	–0.84	0.046	13.68	–0.42	0.100
33	42	398.25	.	37.50	–0.85	0.051	13.68	–0.36	0.093

CA7B3 (CA7F1) I = 0.7M

$K_H = 2$ $K_{OH} = 8$ $V_0 = 209.34ml$ $k_e^* = 59.16mV$ $pK_W^* = 13.41$

Electrodes		E^0	k_e	H_{init}	j_H	σ_A	pK_W	j_{OH}	σ_B
Glass	Ref	/mV	/mV	/μM	/V.M^{-1}	/mV		/V.M^{-1}	/mV
36	46	388.30	58.95	–75.02	.	0.094	13.42	0.05	0.087
36	60	402.66	59.14	–74.93	.	0.098	13.41	0.00	0.071
39	46	386.55	58.91	–76.37	.	0.090	13.43	0.00	0.084
39	60	400.84	59.07	–76.93	.	0.101	13.42	–0.01	0.082

1.A.d $MgCl_2$ Solutions

MG0B5 (MG0F1) I = 0.01M

$K_H = 4$ $K_{OH} = 4$ $V_0 = 209.29ml$ $k_e^* = 59.16mV$ $pK_W^* = 13.76$

Electrodes		E^0	k_e	H_{init}	j_H	σ_A	pK_W	j_{OH}	σ_B
Glass	Ref	/mV	/mV	/μM	/V.M^{-1}	/mV		/V.M^{-1}	/mV
32	25	398.25	.	–86.31	–5.98	0.140	13.81	5.32	0.091
32	41	409.68	.	–86.75	–5.96	0.129	13.81	4.92	0.108
34	25	397.12	.	–91.58	–6.27	0.101	13.81	3.72	0.042
34	41	408.50	.	–91.49	–6.23	0.093	13.82	3.12	0.073

MG1B2 (MG1F1) I = 0.1M

$K_H = 1$ $K_{OH} = 0$ $V_0 = 209.34ml$ $k_e^* = 59.16mV$ $pK_W^* = 13.30$

Electrodes		E^0	k_e	H_{init}	j_H	σ_A	pK_W	j_{OH}	σ_B
Glass	Ref	/mV	/mV	/μM	/V.M^{-1}	/mV		/V.M^{-1}	/mV
31	42	397.74	.	–131.1	–0.93	0.059	.	.	.
31	26	407.18	.	–132.1	–0.89	0.055	.	.	.
33	42	398.50	.	–132.6	–0.89	0.098	.	.	.
33	26	408.01	.	–133.7	–0.85	0.039	.	.	.

MG7B5 (MG7F1) I = 0.7M

$K_H = 4$ $K_{OH} = 0$ $V_0 = 209.34ml$ $k_e^* = 59.13mV$ $pK_W^* = 12.78$

Electrodes		E^0	k_e	H_{init}	j_H	σ_A	pK_W	j_{OH}	σ_B
Glass	Ref	/mV	/mV	/μM	/V.M^{-1}	/mV		/V.M^{-1}	/mV
36	46	391.00	59.05	–13.23	.	0.119	.	.	.
36	60	391.67	58.66	–16.05	.	0.045	.	.	.
39	46	389.22	58.87	–13.50	.	0.079	.	.	.
39	60	390.21	58.58	–16.21	.	0.048	.	.	.

1.A.e Artificial Seawater

SW7B6 (SW7F1) I = 0.726M

$K_H = 7$ $K_{OH} = 0$ $V_0 = 209.29ml$ $k_e^* = 59.16mV$ $pK_W^* = 13.15$

Electrodes		E^0	k_e	H_{init}	j_H	σ_A	pK_W	j_{OH}	σ_B
Glass	Ref	/mV	/mV	/μM	/V.M^{-1}	/mV		/V.M^{-1}	/mV
36	46	405.38	59.27	–41.81	.	0.057	.	.	.
36	60	404.69	59.39	–41.62	.	0.063	.	.	.
39	46	403.97	59.40	–39.18	.	0.055	.	.	.
39	60	403.11	59.46	–39.66	.	0.052	.	.	.

1.B Alumina and Mixed Fulvic Acid/Alumina Titrations

1.B.a Alumina (NaCl)

NA0B11 (NA0A1) I = 0.01M

$K_H = 1$ $K_{OH} = 5$ $V_0 = 209.29ml$ $k_e^* = 59.15mV$ $pK_W^* = 13.89$

Electrodes		E^0	k_e	H_{init}	j_H	σ_A	pK_W	j_{OH}	σ_B
Glass	Ref	/mV	/mV	/μM	/V.M^{-1}	/mV		/V.M^{-1}	/mV
34	64	402.98	.	−20.72	−5.49	0.048	13.90	2.13	0.024
34	66	403.03	.	−20.06	−5.27	0.057	13.90	2.43	0.042
17	64	401.63	.	−21.50	−5.59	0.087	13.89	2.09	0.045
17	66	401.60	.	−20.51	−5.30	0.061	13.89	2.30	0.038

NA1B27 (NA1A1) I = 0.1M

$K_H = 3$ $K_{OH} = 6$ $V_0 = 209.29ml$ $k_e^* = 59.16mV$ $pK_W^* = 13.77$

Electrodes		E^0	k_e	H_{init}	j_H	σ_A	pK_W	j_{OH}	σ_B
Glass	Ref	/mV	/mV	/μM	/V.M^{-1}	/mV		/V.M^{-1}	/mV
33	61	406.72	.	−29.72	−1.76	0.056	13.80	0.17	0.058
33	67	408.90	.	−31.82	−1.47	0.011	13.80	0.01	0.018
38	61	397.69	.	−30.58	−1.37	0.002	13.79	0.07	0.015
38	67	400.22	.	−33.05	−1.56	0.019	13.80	−0.01	0.069

NA7B43 (NA7A2) I = 0.7M

$K_H = 1$ $K_{OH} = 7$ $V_0 = 209.29ml$ $k_e^* = 59.16mV$ $pK_W^* = 13.68$

Electrodes		E^0	k_e	H_{init}	j_H	σ_A	pK_W	j_{OH}	σ_B
Glass	Ref	/mV	/mV	/μM	/V.M^{-1}	/mV		/V.M^{-1}	/mV
36	69	405.19	59.27	−4.89	.	0.076	13.69	−1.31	0.035
36	65	407.33	59.05	−5.01	.	0.042	13.72	−1.01	0.132
39	69	402.67	59.26	−5.51	.	0.067	13.69	−1.05	0.022
39	65	404.84	59.06	−5.45	.	0.067	13.72	−1.04	0.135

NA7B51 (NA7A3) I = 0.7M

$K_H = 1$ $K_{OH} = 6$ $V_0 = 209.29ml$ $k_e^* = 59.16mV$ $pK_W^* = 13.68$

Electrodes		E^0	k_e	H_{init}	j_H	σ_A	pK_W	j_{OH}	σ_B
Glass	Ref	/mV	/mV	/μM	/V.M^{-1}	/mV		/V.M^{-1}	/mV
36	69	407.24	59.41	8.13	.	0.074	13.68	0.80	0.040
36	65	408.80	59.39	7.62	.	0.058	13.69	0.76	0.113
39	69	405.13	59.26	7.21	.	0.063	13.69	1.36	0.084
39	65	406.70	59.25	6.71	.	0.053	13.69	1.32	0.086

1.B.b Fulvic Acid/Alumina (NaCl)

NA0B21 (NA0Z1) I = 0.01M

$K_H = 2$ $K_{OH} = 5$ $V_0 = 209.29ml$ $k_e^* = 59.15mV$ $pK_W^* = 13.89$

Electrodes		E^0	k_e	H_{init}	j_H	σ_A	pK_W	j_{OH}	σ_B
Glass	Ref	/mV	/mV	/μM	/V.M^{-1}	/mV		/V.M^{-1}	/mV
34	66	410.03	.	–7.65	–5.09	0.049	13.90	1.80	0.085
34	64	410.10	.	–6.16	–4.75	0.050	13.89	1.74	0.049
17	66	409.40	.	–7.09	–4.85	0.065	13.89	1.84	0.082
17	64	409.71	.	–6.76	–4.85	0.005	13.89	1.86	0.080

NA1B28 (NA1Z1) I = 0.1M

$K_H = 1$ $K_{OH} = 6$ $V_0 = 209.29ml$ $k_e^* = 59.13mV$ $pK_W^* = 13.77$

Electrodes		E^0	k_e	H_{init}	j_H	σ_A	pK_W	j_{OH}	σ_B
Glass	Ref	/mV	/mV	/μM	/V.M^{-1}	/mV		/V.M^{-1}	/mV
33	61	406.73	.	–2.63	–0.37	0.027	13.78	–0.29	0.053
33	67	409.71	.	–2.60	–0.46	0.035	13.79	–0.29	0.053
38	61	397.54	.	–2.65	–0.42	0.039	13.78	–0.51	0.050
38	67	400.51	.	–2.60	–0.46	0.035	13.79	–0.29	0.053

NA7B59 (NA7Z1) I = 0.7M

$K_H = 1$ $K_{OH} = 6$ $V_0 = 209.29ml$ $k_e^* = 59.16mV$ $pK_W^* = 13.68$

Electrodes		E^0	k_e	H_{init}	j_H	σ_A	pK_W	j_{OH}	σ_B
Glass	Ref	/mV	/mV	/μM	/V.M^{-1}	/mV		/V.M^{-1}	/mV
36	69	410.46	58.93	26.22	.	0.077	13.75	–0.27	0.088
36	65	410.75	58.94	25.90	.	0.058	13.74	–0.28	0.089
39	69	409.33	59.10	25.89	.	0.094	13.73	0.20	0.053
39	65	409.04	58.95	25.58	.	0.063	13.74	0.08	0.058

NA7B102 (NA7Z1PB) I = 0.7M

$K_H = 1$ $K_{OH} = 7$ $V_0 = 209.29ml$ $k_e^* = 59.16mV$ $pK_W^* = 13.68$

Electrodes		E^0	k_e	H_{init}	j_H	σ_A	pK_W	j_{OH}	σ_B
Glass	Ref	/mV	/mV	/µM	/V.M^{-1}	/mV		/V.M^{-1}	/mV
36	69	406.15	59.45	62.94	.	0.048	13.66	–0.30	0.059
36	4	416.80	58.92	61.99	.	0.032	13.71	–0.89	0.024
51	69	404.92	59.44	62.66	.	0.055	13.65	–0.04	0.018
51	4	415.95	59.02	61.96	.	0.034	13.69	–0.57	0.064

NA7B112 (NA7Z1DD) I = 0.7M

$K_H = 1$ $K_{OH} = 7$ $V_0 = 209.29ml$ $k_e^* = 59.15mV$ $pK_W^* = 13.68$

Electrodes		E^0	k_e	H_{init}	j_H	σ_A	pK_W	j_{OH}	σ_B
Glass	Ref	/mV	/mV	/µM	/V.M^{-1}	/mV		/V.M^{-1}	/mV
36	65	412.75	59.12	59.16	.	0.018	13.69	0.01	0.088
36	69	412.36	59.30	59.53	.	0.023	13.67	0.33	0.091
51	65	409.50	58.90	58.97	.	0.047	13.70	0.61	0.100
51	69	408.77	58.98	59.34	.	0.037	13.69	0.62	0.126

APPENDIX 2: HALTAFALL Input Files

Data files used in HALTAFALL speciation calculations are shown in Sections 2.A & 2.B. The structure of these files is desribed below:

Header Zone initiation and file heading

Activity Coefficients no. lines of data, heading and parameters (B, C & D) of an extended Debye–Hückel equation (Eqn. 2.A.i)

No. of System Components

No. of Complexes

Complex Data stability constants and stoichiometry of complex reaction with each component for each complex

Print & Calculation Orders

Component Data concentrations of major ions (e.g. Na^+, Cl^-) or concentration, surface site density, surface area and interface model parameters (e.g. capacitances) for solids

End Zone

Activity coefficients are calculated using Eqn 2.A.i, in which I represents the effective ionic strength. This was determined iteratively (by a modification to HALTAFALL) according to the method of Dickson & Whitfield (1981), and the values of B and C used were taken from the same paper.

$$\ln \gamma = -1.176\, z^2\sqrt{I} / (1 + B\sqrt{I}) + CI + D\sqrt{(I^3)} \qquad (2.A.i)$$

Where titrations were carried out at different ionic strengths of the same electrolyte, only one data file is listed for each substrate – interface model combination (the file used for 0.01M solutions). Files appropriate for the other ionic strengths of each solution were obtained by changing the major ion concentrations in the "Component Data" block.

2.A Fulvic Acid Modelling

2.A.a NaCl Solutions

```
0
1
Calc. of surface charge for 0.01M NaCl  FA titration, const. cap
8
ACTIVITY COEFFICIENTS BASED ON MACINNES CONVENTION
1   1.670   0.525   0.000 H
2   1.541   0.126   0.000 Na
7   1.265   0.014   0.000 Cl
9   0.988   0.475   0.000 OH
15  0.000  –0.300   0.000 1:1
16  1.265   0.014   0.000 1:2
17  0.000  –1.200   0.000 2:2
50  0.000   0.000   0.000 Blank
5
4
9   0.991 –14  –1   0   0   0   0  –1 OH
15  0.625 –14  –1   1   0   0   0   0 NaOH
50  8.710  –5  –1   1   0   1   0   0 SONa
50  1.000  –4  –1   0   0   1  –1  –1 SO
0
2
–1 2 –1 8
1
0.4
32
6  1  1 H
–4.3 –0.1
1 1  2 Na
–1 –1D–8
0.01
8 –1  7 Cl
0.01
0 0 50 SOH
–15 –1D–8
5.015D–5 3.50 3500000.
1.29 –1.0
–21 0 50 INNR
–3 –1D–8
–1
–1
–1
```

2.A.b Na_2SO_4 Solutions

```
0
1
Calc. of surface charge for 0.01M Na2SO4 FA titration, const. cap
9
ACTIVITY COEFFICIENTS BASED ON MACINNES CONVENTION
1   1.670   0.525   0.000 H
2   1.541   0.126   0.000 Na
9   0.988   0.475   0.000 OH
10  1.347  -0.088   0.000 HSO4
15  0.000  -0.300   0.000 1:1
16  1.265   0.014   0.000 1:2
17  0.000  -1.200   0.000 2:2
50  0.000   0.000   0.000 Blank
45  2.876  -0.598   0.000 SO4
5
7
9   0.991 -14  -1   0   0   0   0  -1 OH
15  0.625 -14  -1   1   0   0   0   0 NaOH
10  9.528   1   1   0   1   0   0  -1 HSO4
15  1.901   1   1   1   1   0   0   0 NaHSO4
16  6.607   0   0   1   1   0   0  -1 NaSO4
50  8.710  -5  -1   1   0   1   0   0 SONa
50  5.410  -8  -1   0   0   1  -1  -1 SO
0
2
-1 2 -1 8
1
0.4
31
6  1  1 H
-3.7 -0.1
1 1  2 Na
-1 -1D-4
0.0066
8 2 45 SO4
0.0033
0 0 50 SOH
-15 -1D-8
5.015D-5 3.50 3500000.
1.29 -1.0
-21 0 50 INNR
-3 -1D-8
-1
-1
-1
```

2.A.c $CaCl_2$ Solutions

```
0
1
Calc. of surface charge for 0.01M CaCl2 FA titration, const. cap
8
ACTIVITY COEFFICIENTS BASED ON MACINNES CONVENTION
1   1.670   0.525   0.000 H
4   1.729   0.321   0.000 Ca
7   1.265   0.014   0.000 Cl
9   0.988   0.475   0.000 OH
15  0.000  -0.300   0.000 1:1
16  1.265   0.014   0.000 1:2
17  0.000  -1.200   0.000 2:2
50  0.000   0.000   0.000 Blank
5
4
9   0.991 -14  -1   0   0   0   0  -1 OH
16  0.140 -12  -1   1   0   0   0   1 CaOH
50  1.000 -10  -2   1   0   1   0   0 SOCaOH
50  5.140  -4  -1   0   0   1  -1  -1 SO
0
2
-1 2 -1 8
1
0.4
31
6  1  1 H
-3.8 -0.1
1 2  4 Ca
-1 -1D-4
0.00333
8 -1  7 Cl
0.00666
0 0 50 SOH
-15 -1D-4
5.015D-5 3.50 3500000.
0.8 -1.0
-21 0 50 INNR
-3 -1D-6
-1
-1
-1
```

2.A.d $MgCl_2$ Solutions

```
0
1
Calc. of surface charge for 0.01M MgCl2 FA titration, const. cap
8
ACTIVITY COEFFICIENTS BASED ON MACINNES CONVENTION
1    1.670    0.525    0.000  H
3    1.790    0.454    0.000  Mg
7    1.265    0.014    0.000  Cl
9    0.988    0.475    0.000  OH
15   0.000   -0.300    0.000  1:1
16   1.265    0.014    0.000  1:2
17   0.000   -1.200    0.000  2:2
50   0.000    0.000    0.000  Blank
5
4
9   0.991 -14  -1   0   0   0   0  -1 OH
16  0.161 -11  -1   1   0   0   0   1 MgOH
50  7.000  -9  -2   1   0   1   0   0 SOMgOH
50  5.140  -8  -1   0   0   1  -1  -1 SO
0
2
-1 2 -1 8
1
0.4
33
6  1  1 H
-3.7 -0.11
 2  3 Mg
-1 -1D-4
0.00333
8 -1  7 Cl
0.00666
0 0 50 SOH
-15 -1D-4
5.015D-5 3.50 3500000.
0.8 -1.0
-21 0 50 INNR
-3 -1D-6
-1
-1
-1
```

2.A.e Artificial Seawater

```
0
1
FA–SW calculations
12
ACTIVITY COEFFICIENTS BASED ON MACINNES CONVENTION
1   1.670   0.525   0.000 H
2   1.541   0.126   0.000 Na
3   1.790   0.454   0.000 Mg
4   1.729   0.321   0.000 Ca
7   1.265   0.014   0.000 Cl
9   0.988   0.475   0.000 OH
10  1.347  –0.088   0.000 HSO4
15  0.000  –0.300   0.000 1:1
16  1.265   0.014   0.000 1:2
17  0.000  –1.200   0.000 2:2
50  0.000   0.000   0.000 Blank
45  2.876  –0.598   0.000 SO4
8
15
9   0.991 –14  –1   0   0   0   0   0   0   0  –1 OH
10  9.528   1   1   0   0   0   0   1   0   0  –1 HSO4
15  0.625 –14  –1   1   0   0   0   0   0   0   0 NaOH
15  1.901   1   1   1   0   0   0   1   0   0   0 NaHSO4
16  6.607   0   0   1   0   0   0   1   0   0  –1 NaSO4
16  0.161 –11  –1   0   1   0   0   0   0   0   1 MgOH
16  2.393   2   1   0   1   0   0   1   0   0   1 MgHSO4
17  1.778   2   0   0   1   0   0   1   0   0   0 MgSO4
16  0.140 –12  –1   0   0   1   0   0   0   0   1 CaOH
16  1.901   2   1   0   0   1   0   1   0   0   1 CaHSO4
17  2.042   2   0   0   0   1   0   1   0   0   0 CaSO4
50  3.741  –1  –1   0   0   0   0   0   1  –1  –1 SO
50  8.710  –5  –1   1   0   0   0   0   1   0   0 SONa
50  1.000 –10  –2   0   0   1   0   0   1   0   0 SOCaOH
50  1.000 –12  –2   0   1   0   0   0   1   0   0 SOMgOH
0
5
–1 2 –1 8 0 2 12 –7 13 –7
1
0.4
23
6  1  1 H
–4.0 –0.1
1 1  2 Na
–1 –1D–4
0.49821
1 2  3 Mg
–3 –1D–4
```

0.05530
1 2 4 Ca
–5 –1D–4
0.01072
8 –1 7 Cl
0.57175
1 –2 45 SO4
–3 –1D–4
0.02925
0 0 50 SOH
–15 –1D–8
5.015D–5 3.50 3500000.
0.25 –1.0
–21 0 50 INNR
–3 –1D–8
–1
–1
–1

2.B Particulate Suspension Modelling

2.B.a Alumina – Constant Capacitance Interface

```
0
1
Calc. of surface charge for 0.01M NaCl Al2O3 titration, const. cap
8
ACTIVITY COEFFICIENTS BASED ON MACINNES CONVENTION
1    1.670    0.525    0.000  H
2    1.541    0.126    0.000  Na
7    1.265    0.014    0.000  Cl
9    0.988    0.475    0.000  OH
15   0.000   -0.300    0.000  1:1
16   1.265    0.014    0.000  1:2
17   0.000   -1.200    0.000  2:2
50   0.000    0.000    0.000  Blank
5
6
9    0.991 -14  -1   0   0   0   0  -1 OH
15   0.625 -14  -1   1   0   0   0   0 NaOH
50   5.800  -6  -1   1   0   1   0   0 SONa
50   3.334   3   1   0   1   1   0   0 SOH2Cl
50   5.821   6   1   0   0   1   1   1 SOH2
50   3.334  -3  -1   0   0   1  -1  -1 SO
0
2
-1 2 -1 8
1
0.4
36
6  1  1 H
-3.5 -0.2
1 1  2 Na
-1 -1D-4
0.01
1 -1  7 Cl
-4 -1D-4
0.01
0 0 50 SOH
-15 -1D-8
4.778D-4 0.70 80170.
1.05 -1.0
-21 0 50 INNR
-3 -1D-8
-1
-1
-1
```

2.B.b Fulvic Acid / Alumina Mixture – Constant Capacitance Interface

```
0
1
Calc. of surface charge for 0.01M NaCl FA/Al2O3 titration, const. cap
8
ACTIVITY COEFFICIENTS BASED ON MACINNES CONVENTION
1   1.670   0.525   0.000 H
2   1.541   0.126   0.000 Na
7   1.265   0.014   0.000 Cl
9   0.988   0.475   0.000 OH
15  0.000  -0.300   0.000 1:1
16  1.265   0.014   0.000 1:2
17  0.000  -1.200   0.000 2:2
50  0.000   0.000   0.000 Blank
5
6
9   0.991 -14  -1   0   0   0   0  -1 OH
15  0.625 -14  -1   1   0   0   0   0 NaOH
50  5.800  -6  -1   1   0   1   0   0 SONa
50  3.334   3   1   0   1   1   0   0 SOH2Cl
50  5.821   6   1   0   0   1   1   1 SOH2
50  3.334  -3  -1   0   0   1  -1  -1 SO
0
2
-1 2 -1 8
1
0.4
36
6  1  1 H
-3.5 -0.2
1 1  2 Na
-1 -1D-4
0.01
1 -1  7 Cl
-4 -1D-4
0.01
0 0 50 SOH
-15 -1D-8
5.280D-4 0.70 78164.
1.05 -1.0
-21 0 50 INNR
-3 -1D-8
-1
-1
-1
```

2.B.c Alumina – Triple Layer Interface

```
0
1
Calc. of surface charge for 0.01M NaCl Al2O3 titration, triple layer
8
ACTIVITY COEFFICIENTS BASED ON MACINNES CONVENTION
1    1.670    0.525    0.000  H
2    1.541    0.126    0.000  Na
7    1.265    0.014    0.000  Cl
9    0.988    0.475    0.000  OH
15   0.000   -0.300    0.000  1:1
16   1.265    0.014    0.000  1:2
17   0.000   -1.200    0.000  2:2
50   0.000    0.000    0.000  Blank
6
6
9    0.991  -14  -1   0   0   0   0   0  -1  OH
15   0.625  -14  -1   1   0   0   0   0   0  NaOH
50   1.000   -9  -1   1   0   1  -1   1   0  SONa
50   6.310    7   1   0   1   1   1  -1   0  SOH2Cl
50   1.259    6   1   0   0   1   1   0   1  SOH2
50   7.943  -12  -1   0   0   1  -1   0  -1  SO
0
2
-1 2 0 6
1
0.4
51
6  1  1 H
-5.3 -0.1
1 1  2 Na
-1 -1D-4
0.01
1 -1  7 Cl
-4 -1D-4
0.01
0 0 50 SOH
-15 -1D-6
4.778D-4 0.70 80170.
1.40 0.2
0.01 1
-21 0 50 INNR
-3 -1D-6
-22 0 50 OUTR
-3 -1D-6
-1
-1
-1
```